The effects of radiation on CAR-T cell functionality against neuroblastoma, within the context of an intact immune system

Farah Masood Alam

Great Ormond Street

Institute of Child Health

University College London

This thesis is submitted for the degree of

Doctor of Philosophy

April 2025

Declaration

I, Farah Masood Alam, confirm that the work presented in this thesis is my own. Where information has been derived from other sources, I confirm that this has been indicated in this thesis.

Abstract

Despite the success of CAR-T cells in the treatment of haematological malignancies, similar success has not been achieved in solid tumours, such as neuroblastoma, where high-risk disease yields poor survival outcomes. The immunosuppressive tumour microenvironment in neuroblastoma impedes CAR-T cell trafficking and persistence for effective anti-tumour response. Radiotherapy, a standard cancer treatment, can potentially enhance CAR-T cell therapy against neuroblastoma via immune-mediated effects. These effects depend on a regulated form of cell death (immunogenic cell death), which requires an intact immune system for an effective anti-tumour response. This study aimed to assess the effect of radiation on CAR-T cell activity against neuroblastoma within an intact immune system.

An *in vitro* radiosensitivity screen of TH-MYCN transgenic mouse models of high-risk neuroblastoma showed varying radiosensitivity based on the expression of known immunogenic cell death markers and cell viability, making them suitable models for investigating radiotherapy and CAR-T cell combinations. The anti-B7-H3 ScFv 376.96, which targets B7-H3 expressing neuroblastoma and cross-reacts with human and mouse B7-H3, was evaluated as a CAR candidate. While optimisations improved initial CAR expression, lack of sustained expression and functionality made the 376.96 CAR unsuitable for this study. An alternative CAR, HuK666, targeting GD2, showed stable expression and sustained functionality *in vitro*. Irradiation of $GD2^+$ targets with 2Gy or 8Gy did not enhance CAR-T cell functionality compared to controls but induced T-cell subset changes within the CAR population. These results suggest that radiation affects HuK666 CAR functionality. Further studies are needed to optimise the radiation regimen to determine whether this improves CAR-T cell treatment efficacy against neuroblastoma.

Impact Statement

This thesis aimed to investigate the potential of radiation to improve CAR-T cell function against the solid tumour neuroblastoma. Neuroblastoma is the most common extracranial solid tumour, which has seen improved survival outcomes through advancements in treatments like anti-GD2 antibody therapy. Still, patients with high-risk disease have a poor prognosis, with disease relapse a common occurrence.

The results in chapter three describe determining the range of radiosensitivity of the widely used TH-MYCN mouse models of high-risk neuroblastoma, which has not been previously reported in the literature. The utilisation of these immunocompetent tumour models allows the immune-mediated effects of radiation on CAR efficacy to be thoroughly evaluated and for more effective assessment of on-target off-tumour treatment toxicities known for CAR therapy.

Effective evaluation of CAR therapy in an immunocompetent setting requires mouse CAR-T cells to prevent immune-mediated rejection by the host. The technical challenges in mouse CAR-T cell production have resulted in them not being widely used for preclinical evaluation of CAR therapies. The results in chapter four describe the optimisations performed to generate the anti-B7-H3 CAR 376.96, a CAR candidate to utilise within this project due to its reported cross-reactivity between mouse and human B7-H3. Optimisations performed improved CAR expression. However, the expression was transient, and CAR functionality was short-lived, making this CAR unsuitable for long-term evaluation of CAR therapy, which is imperative for CAR therapy success. These results contradict those of Du et al., who reported *in vitro* and *in vivo* efficacy of 376.96 mouse CAR-T cells (1).

The results in chapter five describe the evaluation of an alternative anti-GD2 CAR, Huk666, which showed stable CAR expression and sustained CAR functionality in response to $GD2^+$ targets. *In vitro,* evaluation of HuK666 mouse CAR-T cells against an irradiated $GD2^+$ 9464D TH-MYCN neuroblastoma model revealed no additive effect of radiation on CAR functionality compared with controls. As immune-mediated effects of radiation are dependent on factors such as dose strength and exposure time, further optimisations in radiation regimens may better elucidate the effects of radiation on CAR functionality against neuroblastoma and its potential to be translated into the clinic to improve survival outcomes for patients with high-risk disease.

Findings presented in this thesis have been communicated within the wider scientific community through poster presentations at national and international conferences. This has allowed increased awareness and support for the potential of radiotherapy in improving CAR-T cell success in solid tumours like neuroblastoma.

Acknowledgements

First and foremost, I would like to thank my primary supervisor, Prof. John Anderson and my secondary supervisors, Prof. Tony Ng and Dr Jane Sosabowski, for allowing me to undertake this PhD. I am grateful to Cancer Research UK (CRUK) for providing the funding to complete this work.

I am truly grateful for the guidance that John provided throughout this process. His open-door policy provided continuous support in listening to new ideas and advice where needed throughout our discussions over these last four years. I am grateful for his understanding of the personal issues that arose during my PhD and the support he provided for that.

I am grateful for the guidance provided by my thesis committee members, Dr. Gilbert Fruhwirth and Prof. Alan Melcher. My thesis committee meetings provided a source of great discussion and support throughout my PhD.

Thank you to Ben Draper, who became my postdoc by proximity! Thank you for the advice and support you gave me over these last four years and for helping me focus on the bigger picture. I am also grateful for the support and help received from members of John and Jane's groups, especially Courtney Himsworth, Sophie Munning-Tomes and Eva Bugallo Blanco.

The last four years have also led to challenging personal circumstances, and so this is also in remembrance of both my grandmothers and father, who aren't here today to see me complete my degree.

To my family, it is hard to describe how much your support has meant throughout my PhD. First, to my mum, who has been the best parent I could have asked for. Everything I have done and the person I am today is down to your upbringing and your prayers, and I am so grateful for that, and I don't think I say that enough to you. To my siblings (Bhaiya, Raniya, Rafeah, Hamed and Sarah) and my sister-in-law (Sana bhabi) and brother-in-laws (Maaz bhai and Mudassir bhai) and my nieces and nephews for your support, advice and encouragement throughout these four years.

Finally, thank you to my husband Taha for your endless support and encouragement, and that I won't be the only one with a PhD in this family.

Table of Contents

List of Tables

List of Figures

List of Abbreviations

123I - Iodine-123

131I - Iodine-131

177Lu - Lutetium-177

225Ac - Actinium-225

99mTCO$_4^-$ - Technetium-99m pertechnetate

ACK - Ammonium–Chloride–Potassium

ACT - Adoptive Cell Therapy

ADC - Antibody Drug Conjugate

ADCC - Antibody-Dependent Cellular Cytotoxicity

ADCP - Antibody dependent cellular phagocytosis

AHSCT - Autologous Haematological Stem Cell Transplantation

ALK - Anaplastic Lymphoma Kinase

ALL - Acute Lymphocytic Leukaemia

AML - Acute Myeloid Leukaemia

ANOVA - Analysis of Variance

Anti-His - Anti-Histidine

APC - Antigen Presenting Cell

ARDS - Acute Respiratory Distress Syndrome

BiTE - Bi-specific T-cell Engager

BLI - Bioluminescence

BSA - Bovine Serum Albumin

CAF - Cancer-Associated Fibroblast

CAR - Chimeric Antigen Receptor

CD3ζ - Cluster of Differentiation 3 Zeta

CDC - Complement Dependent Cytotoxicity

CEM - Carboplatin, Etoposide and Melphalan

CFSE - Carboxyfluorescein Succinimidyl Ester

CHOP - Cyclophosphamide, Doxorubicin, Vincristine and Prednisolone

CNS - Central Nervous System

COG - Children's Oncology Group

CR - Complete Response

CRS - Cytokine Release Syndrome

CRT - Calreticulin

Cs^{137} - Caesium-137

CTLA-4 - Cytotoxic T-Lymphocyte-Associated Protein 4

CTV - Cell Trace Violet

CXCL - Chemokine (C-X-C motif) Ligand

CXCR - CXC Chemokine Receptor

DAMP - Danger-Associated Molecular Pattern

DC - Dendritic Cell

DIPG - Diffuse Intrinsic Pontine Glioma

DLBCL - Diffuse Large B-cell Lymphoma

DMEM - Dulbecco's Modified Eagle Medium

DNA - Deoxyribonucleic Acid

EBRT - External Beam Radiotherapy

EC-ATP - Extracellular-ATP

ECM - Extracellular Matrix

EFS - Event Free Survival

ELISA - Enzyme-Linked Immunosorbent Assay

EphA2 - Ephrin Type-A Receptor 2

ER - Endoplasmic Reticulum

E:T - Effector:Target

FAP - Fibroblast Activation Protein

FBS - Foetal Bovine Serum

FcR - Fc Receptor

FDA - US Food and Drug Administration

FMO - Fluroescence Minus One

GEMM - Genetically Engineered Mouse Model

GFP - Green Fluorescent Protein

GM-CSF - Granulocyte-Macrophage Colony-Stimulating Factor

GPC2 - Glypican-2

GVHD - Graft-Versus-Host-Disease

Gy - Gray

hB7-H3 - Human B7-H3

hb-FGF - Human Basic Fibroblast Growth Factor

h-EGF - Human-Epidermal Growth Factor

HIF-1α - Hypoxia-Inducible Factor-1 Alpha

HMGB1 - High Mobility Group Box 1

hNIS - Human Sodium Iodide Symporter

HSC - Haematopoietic Stem Cell

HSP - Heat Shock Protein

HSV1tk - Herpes Simplex Virus Thymidine Kinase 1

IC_{50} - Half-Maximal Inhibitory Concentration

ICANS - Immune-Effector Cell Associated Neurotoxicity Syndrome

ICB - Immune Checkpoint Blockade

ICD - Immunogenic Cell Death

ICDR-index - ICD-related index

IDT - Integrated DNA Technologies

IFN - Interferon

Ig - Immunoglobulin

IL - Interleukin

IL-13Ra2 - IL-13 Receptor Subunit Alpha-2

IMDM - Iscove's Modified Dulbecco's Medium

IMRT - Intensity Modulated Radiation Therapy

INRGSS - International Neuroblastoma Risk Group Staging System

INSS - International Neuroblastoma Staging System

IT - Immunotherapy

IVM - Intravital Imaging

LAG-3 - Lymphocyte-Activation Gene-3

LB - Luria-Bertani

LET - Linear Energy Transfer

LNP - Lipid Nanoparticle

LTR - Long Terminal Repeats

Luc - Luciferase

mAb - Monoclonal Antibody

mB7-H3 - Mouse B7-H3

mCD3 - Mouse CD3

MCL - Mantle Cell Lymphoma

MDSC - Myeloid-Derived Suppressor Cell

MHC - Major Histocompatibility Complex

MIBG - Metaiodobenzylguanidine

MIP1α - Macrophage Inflammatory Protein-1 Alpha

MMLV - Moloney Murine Leukaemia Virus

mNIS - Mouse Sodium Iodide Symporter

MOA - Mechanism of action

MOI - Multiplicity of Infection

mRNA - Messenger RNA

mtDNA - Mitochondrial DNA

MTT - 3-(4,5-dimethylthiazol-2-yl)-2,5-diphenyltetrazolium bromide

$NaClO_4$ - Sodium Percholate

NEAA - Non-Essential Amino Acids

NET - Noradrenaline Transporter

NIS - Sodium Iodide Symporter

NK - Natural Killer

NMA - Non-Myeloablative

NSCLC - Non-Small Cell Lung Cancer

NSG - NOD Scid Gamma

ORF - Open Reading Frame

PBMC - Peripheral Blood Mononuclear Cell

PBS - Phosphate-Buffered Saline

PCR - Polymerase Chain Reaction

PD-1 - Programmed Death 1

PD-L1 - Programmed Death-Ligand 1

PDX - Patient-Derived Xenograft

PET - Positron Emission Tomography

PFS - Progression Free Survival

Pheonix.Eco - Pheonix Ecotropic

PHOX2B - Paired-Like Homeobox 2B

PT - Proton Therapy

RBC - Red Blood Cell

rhB7-H3 - Recombinant Human B7-H3

ROS - Reactive Oxygen Species

RPMI - Roswell Park Memorial Institute

RT - Radiotherapy

SARRP - Small Animal Radiation Research Platform

ScFv - Single-Chain Variable Fragment

SCID - Severe Combined Immunodeficiency Disease

sLeA - sialyl Lewis-A

SOC - Super Optimal Culture

SPECT - Single Photon Emission Computed Tomography

TA - Tumour Antigen

TAA - Tumour-Associated Antigen

TAM - Tumour-Associated Macrophage

TanCAR - Tandem CAR

TBE - Tris-Borate-EDTA

TBI - Total Body Irradiation

TCR - T-Cell Receptor

TCR-T - T-Cell Receptor-Engineered T-Cell

TGF - Transforming Growth Factor

TGFβ - Tumour Growth Factor Beta

TH-MYCN - Tyrosine-Hydroxylase-MYCN

TIGIT - T-cell Immunoreceptor with Ig and ITIM Domains

TIL - Tumour-Infiltrating Lymphocytes

TIM-3 - T-Cell Immunoglobulin and Mucin-Domain-Containing-3

TLR - Toll-Like Receptor

TME - Tumour Microenvironment

TNP - Anti-2,4,6-trinitrophenol

TRAIL - TNF-Related Apoptosis-Inducing Ligand

Treg - Regulatory T-Cell

TSA - Tumour-Specific Antigen

ULA - Ultra-Low Attachment

VAC - Vincristine Sulfate, Adriamycin and Cyclophosphamide

VEGF - Vascular Epidermal Growth Factor

Chapter 1 Introduction

1.1 Childhood Cancers

In the paediatric population, childhood cancers are rare, accounting for 2% of all cancer cases in Western countries (2). The majority of childhood cancers diagnosed are leukaemias, followed by solid tumours, of which the most prevalent include neuroblastoma, soft-tissue sarcoma, Wilms tumour, bone tumours, and retinoblastomas (2).

Advances in diagnosis and treatment have greatly improved survival rates for childhood cancers since the 1960s, with the five-year survival rate being greater than 75% (2,3). However, childhood solid tumours pose additional challenges that need to be overcome to improve patient survival. For instance, treating CNS malignancies can result in normal tissue damage due to proximity to the malignancy, resulting in major developmental impairments (2).

The treatment outcomes of childhood tumours differ greatly from those of adult cancers, which are mainly carcinomas. Adult cancers are more a product of the accumulation of somatic mutations paired with a decline in DNA repair mechanisms over time, resulting in cancers with a higher mutational burden (4,5). In contrast, childhood cancers occur mostly during development, resulting in dysregulation that can lead to tumorigenesis (6,7). Thus, childhood cancers have a lower mutational burden with fewer somatic mutations than adult cancers. This lower mutational burden of childhood cancers poses additional challenges for treatment, as it reduces the pool of targets available for developing new therapies, such as within the context of immunotherapies. Additionally, childhood cancers are defined as “immunologically cold” tumours which may impact the response to immunotherapy, which is an important avenue in cancer treatment, as discussed in section 1.3 in further detail (8).

1.2 Neuroblastoma

Neuroblastoma (neuroblastoma) is an extracranial tumour that is the most commonly found solid tumour in childhood. The prevalence of this disease accounts for 15% of all childhood cancer-related deaths (9). neuroblastoma is commonly diagnosed in children under 10 years of age, with a median age of 18 months at diagnosis (10). While there are no geographical variations that contribute to the global prevalence of neuroblastoma, the disease is more common in boys than in girls (9).

neuroblastoma is a heterogeneous neuroendocrine tumour that clinically arises as a primary tumour of the sympathetic nervous system, with most cases occurring in the adrenal glands, with additional sites of origin, including the neck, chest, and pelvis (9). neuroblastoma is a product of disordered development, in which aberrant expression and regulation of proteins involved in development drive the onset of malignancy (2). neuroblastoma originates from the neural-crest-derived precursor cells of the sympathoadrenal cell lineage (2). These cells are important for neural crest development, which is imperative for embryonic and adult development (2). The heterogeneity of the disease is mirrored in patient survival, with long-term survival in low-risk disease being greater than 95% but less than 50% in high-risk patients (10).

1.2.1 Genetic predisposition

There have been reports of familial neuroblastoma and the contribution of environmental factors (e.g. prenatal exposure to alcohol and phenobarbital) to disease risk; however, most neuroblastoma cases occur sporadically (9). Genetic abnormalities have also been associated with neuroblastoma. First, germline mutations have been reported in the anaplastic lymphoma kinase (ALK) gene, with gain-of-function mutations in this tyrosine kinase implicated in cases of hereditary neuroblastoma (11). Second, the paired-like homeobox 2B (PHOX2B) gene has also been implicated in familial cases of neuroblastoma. PHOX2B is imperative for the development of the autonomic nervous system, and germline mutations in this gene are linked to cases of familial neuroblastoma and in approximately 4% of spontaneous neuroblastoma cases (10,12). Additional chromosomal abnormalities, such as deletions on chromosomes 1p and 11q and gain-of-function mutations on chromosome 17q, have also been implicated in neuroblastoma (9,10).

The most notable genetic abnormality implicated in neuroblastoma is the amplification of the transcription factor MYCN, which has been found in 25-35% of neuroblastoma cases (9). MYCN belongs to a family of genes that function as key transcription factors for a range of cell processes, ranging from cell proliferation to differentiation, and has been implicated as an oncogenic driver in many cancer types, including neuroblastoma (13,14). In neuroblastoma, MYCN amplification has been associated with poor prognosis irrespective of age and disease stage (15).

1.2.2 Clinical Presentation and Diagnosis

The clinical presentation of neuroblastoma varies, as it is affected by the site of tumour origin, disease progression, and the occurrence of any paraneoplastic syndrome. Upon diagnosis, neuroblastoma can be staged using two different systems. First, the International Neuroblastoma Risk Group Staging System (INRGSS) stages the disease based on imaging tests (such as CT, MRI or MiBG scans), and the INRGSS stage can be determined before the start of treatment (16). Alternatively, the International Neuroblastoma Staging System (INSS) may be utilised to stage the disease based on the tumour resection performed surgically (9,17). The choice of either diagnostic criterion is dependent on disease progression, such as the use of INRGSS over INSS for staging for patients in whom surgery is not plausible.

The use of INRGSS and INSS and additional prognostic factors, such as genetic predisposition, allows patients to be risk stratified, ranging from low-, intermediate-, to high-risk disease (9). 50% of patients are found to have localised disease, and about 35% of patients are found to have metastatic disease that has spread to lymph nodes at the time of diagnosis (9). Patients with low-risk disease have an excellent prognosis with surgery alone, although additional chemotherapy may be used if required. Intermediate-risk disease is primarily treated with surgery and chemotherapy; however, prognosis is highly dependent on the histological and biological features of the tumour (9). Even though high-risk neuroblastoma patients are responsive to chemotherapy, long-term survival is less than 40% in this group, and considering that nearly 50% of diagnosed cases are high-risk, current work is ongoing to determine additional treatment options, such as the use of biologic agents (18).

1.2.3 High-Risk neuroblastoma

Patients with high-risk neuroblastoma show progressive metastatic disease, which requires a multimodal treatment approach. Currently, patients with high-risk disease receive induction chemotherapy followed by surgical resection and radiotherapy at the primary tumour site to achieve local control, with neuroblastoma being one of the most radiosensitive childhood solid tumours (9). Subsequently, myeloablative chemotherapy is administered concurrently with Autologous haematopoietic stem cell transplantation (AHSCT) (9,19). This treatment regimen results in increased survival in some patients; however, less than 40% of patients show long-term survival without relapse (20,21). The addition of maintenance therapy, which usually includes anti-GD2 monotherapy, has been found to improve survival; however,

disease relapse still occurs with this regimen, with less than 10% of patients surviving disease recurrence (9,19). The treatment regimen for surviving patients has severe side effects, including infertility, neurological toxicity, and secondary malignancy (9,19). Thus, there is a need for improved treatment options that can increase the quality of life for patients.

1.3 Cancer Immunotherapy

Cancer is a disease of the genome in which inherited or acquired initial variants in DNA are followed by further mutations that accumulate over time, resulting in tumour development and progression (22). Such mutations can give rise to tumour antigens that the immune system can recognise as “non-self” and lead to an anti-tumour immune response (23,24). This immune surveillance, carried out by both non-specific (innate immunity) and specific (adaptive immunity) immune cells, allows them to infiltrate into the tumour microenvironment (TME) and contribute to the modulation of tumour progression (25,26). Therefore, effective immune responses can eradicate cancer cells; however, cancer cells have evolved adaptations such as defects in antigen presentation machinery and recruitment of immunosuppressive cells to escape immune surveillance and diminish the anti-tumour immune response (27,28). Immunotherapy is a breakthrough that has revolutionised the field of cancer treatment by developing therapies that allow us to boost the natural defences of the immune system to eliminate these cancer cells.

1.3.1 Antibody Therapy

Our understanding of antibodies stems as early as 1890, when there was an understanding that the factors present in the serum protected against infections (29). The experiments performed by Nobel Prize winners Emil von Behring and Shibasaburo Kitasato resulted in the concept of humoral immunity, in which it was proposed that a mediator in the blood was capable of neutralising foreign antigens (30). These mediators were later identified as antibodies, followed by the identification of plasma B cells as the producers of antibodies (31). In 1957, Frank Burnet proposed the clonal selection theory, in which antibody specificity is a product of clonal selection and not B cells adapting to antigens (32,33). Gustav Nossal and Joshua Lederberg subsequently confirmed that antibodies produced by B-cells show antigen specificity (34).

Upon binding to target antigens, antibodies exert an array of effector functions. These functions can be exerted through direct antigen-antibody interactions, neutralising or

activating targets, and through effector mechanisms mediated by the Crystallisable Fraction (Fc) portion (35). Antibodies exist in five different isotypes, with Immunoglobulin G (IgG) being the most common in clinical use. Engagement of the Fc portion through cognate Fc receptors expressed on immune cells allows a host of effector functions to be exerted to remove cancer cells. Effector functions to remove cancer cells include antibody-dependent cellular cytotoxicity (ADCC), complement-dependent cytotoxicity (CDC), and antibody-dependent cellular phagocytosis (ADCP), amongst other effects (35). The antibody structure and examples of iterations currently being developed for cancer treatment are summarised in Figure 1.1.

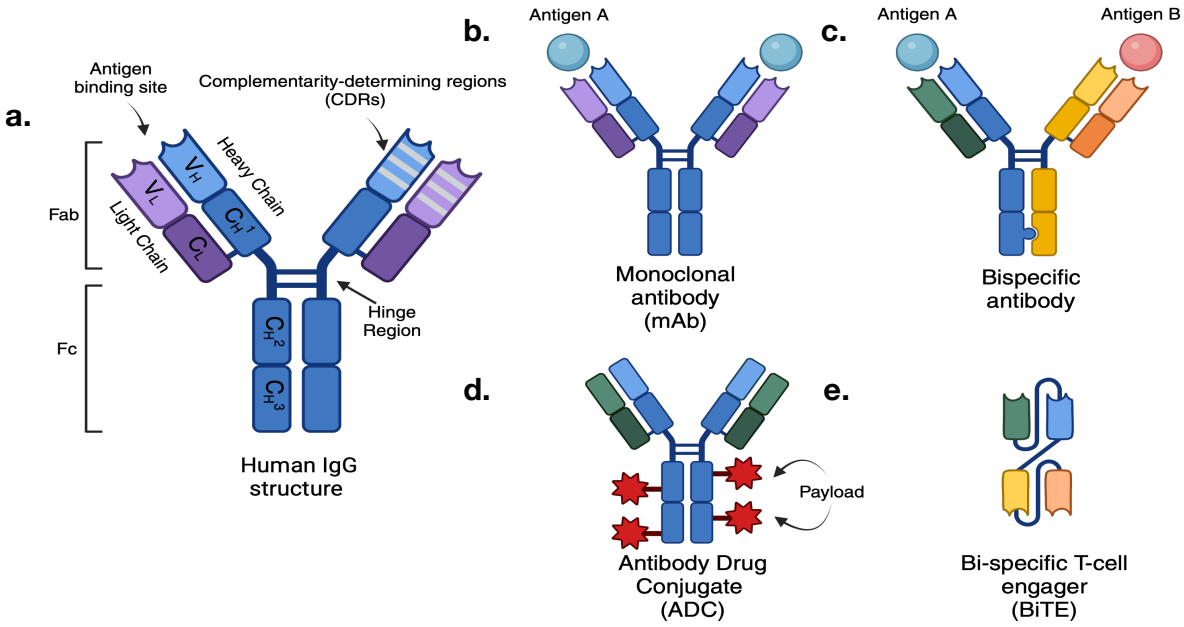

Figure 1.1 IgG Structure and derivatives

Antibody therapies mostly utilise the **a)** human IgG structure that consists of two pairs of identical light and heavy chains. The light chain consists of a variable (V_L) and a constant domain (C_L). The heavy chain is comprised of one variable (V_H) and three constant (C_H^{1-3}) domains. The antigen-binding fragment (Fab) is made up of two antigen-binding sites, of which complementarity-determining regions (CDRs) within the V_H and V_L chains confer antigen specificity to one antigen with high affinity. The hinge region joins the Fab region to the crystallisable fraction (Fc) region, which defines the Ig isotype based on the heavy chain isoforms (IgA, IgD, IgE, IgG, or IgM), and mediates Fc effector functions through Fc receptors expressed on effector cells, like immune cells. Antibodies have been engineered to confer specificity for one antigen, as **b)** monoclonal antibodies or multiple antigens, such as **c)** bispecific antibodies or **e**) BiTEs. Antibodies can also be conjugated to payloads such as anti-cancer agents to provide more targeted drug delivery, as **d)** ADCs. For a more comprehensive list of antibody engineering for oncology use, see Herrera et al (52). Figure created using Biorender.

1.3.2 Monoclonal Antibodies

Monoclonal Antibodies (mAbs) are produced by B cells and can detect specific antigens expressed on cells. In 1975, Köhler and Milstein introduced the hybridoma technique, which involves fusing B cells from an immunised animal with myeloma cells, and has allowed the large-scale production of pure mAbs (36). This has greatly enhanced mAb use in basic research through diagnostic techniques, such as immunohistochemistry and flow cytometry, and for clinical use (37,38). Initial development of mAbs was found to be immunogenic in humans due to their mouse origin. However, the progress in recombinant DNA techniques has enabled the generation of engineered antibodies that range from being chimeric (made of human and murine origins), humanised (human in nature except for the antigen-binding site), and fully human (39).

In 1997, the US Food and Drug Administration (FDA) approved the first mAb for cancer treatment, rituximab, which recognises the pan B cell antigen CD20. Rituximab was developed soon after findings showing treatment efficacy in targeting CD20 in lymphoma (40). Initial clinical trials revealed the promise of rituximab; however, it was later revealed that its efficacy as a monotherapy for front-line use was limited (41–43). That being said, the combination of rituximab with CHOP-based chemotherapy (cyclophosphamide, doxorubicin, vincristine, and prednisolone), and the use of rituximab as maintenance therapy have been found to greatly improve survival in patients with $CD20^{+}$ B cell lymphomas (44).

Antibody therapy has also been clinically evaluated against a range of targets in paediatric solid tumours. Examples of these targets include growth factors, growth factor receptors, and cell death receptors, such as vascular epidermal growth factor (VEGF) and TNF-related apoptosis-inducing ligand (TRAIL) (45–47). While these therapies have shown tolerability in patients, variable clinical responses have been observed with the use of antibody therapy alone. A great success of antibody therapy has been observed with anti-GD2, which has been used across a range of solid tumours that overexpress this antigen, including neuroblastoma and sarcoma (47,48). In neuroblastoma, anti-GD2 therapy has shown great success, as discussed further in section 1.6.

1.3.3 Bispecific Antibodies

Advancements in antibody engineering have resulted in the production of antibodies that target more than one antigen (bispecific antibodies). This allows for more mechanisms of action (MOA) beyond those of mAbs. Examples of these MOAs include antibodies that can simultaneously target two tumour antigens, which mitigates the risk of antigen escape (49). Bispecifics have also been developed to target receptor tyrosine kinases, such as HER2 and HER3, resulting in the inhibition of tumour signalling (50). Antibodies have also been developed to shuttle across the blood brain barrier by targeting receptors mediating transcytosis through one antigen binding site and utilising the other antigen binding site to bind to tumour antigens for brain tumours (51). However, the most promising use of bispecific antibodies comes from engineering them to have specificity for tumour antigens and immune-activating receptors, such as CD3 on T-cells and CD16 on natural killer (NK)-cells (51,52). This allows immune cells non-specific to cancer cells to be redirected to kill tumour cells. To date, ten have received regulatory approval for cancer treatment by the FDA, of which seven and four of them have received regulatory approval for haematological malignancies and solid cancers, respectively (53). Blinatumomab is an example of a bispecific antibody approved for paediatric and adult acute lymphocytic leukaemia (ALL) (53). It is composed of two single-chain variable fragments (ScFv) targeting CD3 (T-cell binder) and CD19 (B cell binder), which are joined by a linker and termed a bispecific T-cell engager (BiTE) (53,54). Ongoing research has evaluated anti-GD2-CD3 bispecific antibodies in neuroblastoma (53). A limited phase I/II trial of an anti-GD2-CD3 bispecific in patients with refractory/recurrent neuroblastoma and osteosarcoma [NCT02173093] revealed drug tolerability with evidence of post-treatment endogenous immune responses (55,56).

1.3.4 Antibody Drug Conjugates

Antibodies can be conjugated to cytotoxic drugs (payloads), such as chemotherapy agents or radioisotopes. These are termed as antibody drug conjugates (ADCs). ADCs provide a more targeted approach to the delivery of therapeutic drugs because of the targeted specificity provided by the antibody for target cells and the delivery of the toxic drug it is conjugated to (39). Typically, these are chemotherapeutic drugs such as DNA intercalators or microtubule disrupters (39). The cytotoxic payload is released from the ADC through

cleavage of the drug from the antibody after endocytosis (39). This minimises the risk of damage to non-target cells.

An important consideration in the development of ADCs is linking the drug conjugate to an antibody. This is because the choice of the linker determines the amount of drug that can be conjugated to the antibody. The most commonly used amino acid is lysine, which has over 80 sites on IgG (the most commonly used isoform for ADCs) (39). In contrast, the amino acid cysteine has 16 pairs in one IgG molecule (38). As a result, the choice of amino acid residues for conjugation will impact the drug-to-antibody ratio, which will influence the pharmacokinetic and pharmacodynamic properties of the drug.

Several ADCs are currently in clinical use for cancer treatment, with 13 approved by the FDA thus far, which target acute myeloid leukaemia (AML) and lymphomas, to solid tumours, such as breast and lung cancer, as shown in Table 1.1 (57). Gemtuzumab ozogamicin (Mylotarg) is a humanised anti-CD33 mAb conjugated to N-acetyl gamma calicheamicin, an enediyne antibiotic that induces double-stranded DNA (dsDNA) breaks resulting in cell death (57). This ADC is used in the treatment of adult and paediatric AML, in which improvements have been seen in event-free survival when used in combination with chemotherapy; however, toxicity has been observed, such as hepatotoxicity and myelosuppression (57,58). Another approved ADC example is inotuzumab ozogamicin (Besponsa) for adult and paediatric relapsed/refractory ALL. Besponsa consists of an anti-CD22 mAb targeting B cells and is conjugated to the chemotherapy drug N-acetyl gamma calicheamicin (57). Clinical evaluation of Besponsa has shown improved survival, but trials are ongoing to evaluate lower doses of the drug in reducing the treatment-associated hepatotoxicity observed (59,60).

The use of ADCs, in which radioisotopes are conjugated to mAbs, is also used for cancer treatment. There has been a clinical evaluation of the treatment efficacy of anti-tenascin and anti-chondroitin proteoglycan sulfate Me1 antibodies radiolabelled with Iodine-131 (^{131}I) against central nervous system (CNS) solid tumours and CNS metastases (61). Kramer et al. reported the use of ^{131}I-anti-GD2 and ^{131}I-anti-B7-H3 antibodies as part of a multimodal therapeutic approach in a phase I trial for patients with recurrent neuroblastoma metastatic to the CNS. Of the 21 patients treated, 17 were found to be disease-free at the end of the study (mean of 33 months since CNS relapse) and found the treatment to be well tolerated, suggesting the potential for improved survival and quality of life with this therapeutic approach (62). An anti-B7-H3 mAb, 8H9 conjugated to iodine 124 (^{124}I), was evaluated against diffuse intrinsic pontine glioma (DIPG) (63). Souweidance et al. evaluated the safety of ^{124}I-

omburtamab (^{124}I-8H9) therapy in 37 patients with DIPG (64). Although there was intratumoural targeted delivery of ^{124}I-8H9 with minimal systemic radiation exposure, no significant clinical improvement was observed (64).

Additional payloads are currently being evaluated for ADCs in neuroblastoma. Shusterman et al. evaluated the use of anti-GD2 mAb conjugated to IL-2 (hu14.18-IL2) in patients with relapsed/refractory neuroblastoma, showing a complete response (CR) rate of 21.7% in patients whose disease was evaluated by MiBG scan and/or bone marrow histology, whereas those with bulky disease did not show any response (65). A subsequent study performed by Shusterman et al. evaluated the use of hu14.18-IL2 in combination with GM-CSF and isotretinoin (13-cis retinoic acid) in patients with relapsed/refractory neuroblastoma and reported a similar response rate, suggesting no enhanced therapeutic efficacy of hu14.18-IL2 in multimodal treatment compared to that of a single agent (65).

Table 1.1 FDA-approved ADC drugs for cancer treatment

Name (Trade Name)	**Antibody Target (Antibody Trade Name)**	**Payload**	**Approved Use(s)**
Gemtuzumab Ozogamicin (Mylotarg)	CD33 (Gemtuzumab)	Calicheamicin	Acute Myeloid Leukaemia
Brentuximab Vedotin (Adcetris)	CD30 (Brentuximab)	Monomethyl auristatin E	Hodgkin's Lymphoma, Anaplastic Large Cell Lymphoma
Trastuzumab Emtansine (Kadcyla)	HER2 (Trastuzumab)	Mertansine	Breast Cancer
Inotuzumab Ozogamicin (Besponsa)	CD22 (Inotuzumab)	Calicheamicin	Acute Lymphoblastic Leukaemia

Moxetumomab Pasudotox (Lumoxiti)	CD22 (Moxetumomab)	Pseudomonas exotoxin A	Hairy Cell Leukaemia
Polatuzumab Vedotin (Polivy)	CD79b (Polatuzumab)	Monomethyl auristatin E	Diffuse Large B-cell Lymphoma
Enfortumab Vedotin (Padcev)	Nectin-4 (Enfortumab)	Monomethyl auristatin E	Urothelial Cancer
Trastuzumab Deruxtecan (Enhertu)	HER2 (Trastuzumab)	Deruxtecan	Breast Cancer
Sacituzumab Govitecan (Trodelvy)	TROP2 (Sacituzumab)	SN-38	Breast Cancer and Urothelial Cancer
Disitamab Vedotin (Aidixi)	HER2 (Disitamab)	Monomethyl auristatin E	Gastric Cancer and Urothelial Cancer
Loncastuximab Tesirine (Zynlonta)	CD19 (Loncastuximab)	PBD SG3199	Diffuse Large B-cell Lymphoma
Tisotumab Vedotin (Tivdak)	TF (Tisotumab)	Monomethyl auristatin E	Cervical Cancer

Mirvetuximab Soravtansine (Elahere)	FRα (Mirvetuximab)	DM4	Ovarian Cancer

1.3.5 Immune checkpoint therapy

Antibody technology has also been applied to target the immune system, rather than tumour antigens. The most prominent example is immune checkpoint blockade (ICB). T-cells in cancer often serve as useful prognostic biomarkers for assessing clinical outcomes in patients (66). However, T-cells infiltrating the tumour commonly exhibit a phenotype associated with exhaustion owing to the consistent antigen stimulation they receive (67). T-cell exhaustion is observed in chronic diseases such as cancer and viral infections (67). A key feature of exhausted T-cells is the expression of immunosuppressive receptors (68,69). Examples of immune checkpoints include programmed cell death 1/ligand-1 (PD-1/PD-L1), cytotoxic T-lymphocyte-associated protein 4 (CTLA-4) and Lymphocyte-activation gene 3 (LAG-3) (67,68). The expression of these markers in T-cells is associated with poor anti-tumour activity, lack of effector functionality, and proliferative capacity (70). Table 1.2 details the immune checkpoint inhibitors approved by the FDA for multiple cancer types (71)

Table 1.2 FDA-approved immune checkpoint inhibitors

Name (Trade Name)	**Target**
Ipilimumab (Yervoy)	CTLA-4
Nivolumab (Opdivo)	PD-1
Pembrolizumab (Keytruda)	PD-1
Atezolizumab (Tecentriq)	PD-L1
Avelumab (Bavencio)	PD-L1
Durvalumab (Imfinzi)	PD-L1

Cemiplimab (Libtayo)	PD-1
Dostarlimab (Jemperli)	PD-1
Tremelimumab (Imjudo)	CTLA-4
Relatlimab (Opdualag)	LAG-3
Toripalimab (Loqtorz)	PD-1
Retifanlimab (Zynyz)	PD-1
Tislelizumab (Tevimbra)	PD-1

1.3.5.1 PD-1

PD-1 is one of the most common immune checkpoints. It is a transmembrane protein receptor of the CD28 family with two ligands from the B7 family: PD-L1 (B7-H1/CD274) and PD-L2 (B7-DC/CD273) (67). Originally, PD-1 was considered a regulator of apoptosis, but it has now been identified as a key immunosuppressive receptor expressed on T-cells (72). In T-cells, PD-1 expression is induced and maintained by TCR stimulation, but modulation through cytokines and other signals also occurs (67). PD-1 plays a role in preventing immune system hyperactivation; however, tumour cells have evolved to hijack this mechanism to evade detection and inhibit antigen-specific tumour responses (67).

Anti-PD-1 targeted antibody therapy allows the reversal of PD-1 blockade, thus preventing its activation by its cognate ligands and reinvigorating exhausted T cell responses. PD-1 therapy has shown improved clinical outcomes in a range of cancers, with pembrolizumab being the first PD-1 inhibitor approved in 2014 for melanoma (73). This was based on the findings of the KEYNOTE-001 study, which revealed improved clinical outcomes in patients with advanced melanoma who had previously failed treatment with ipilimumab (anti-CTLA-4 mAb) and a BRAF inhibitor (74). Subsequent follow-ups of patients in this study revealed that the drug was well tolerated, with a median overall survival of 45% (75). Subsequently, additional anti-PD-1 therapies were developed and approved for a range of adult cancers (73). The discovery of PD-1 and CTLA-4 and their therapeutic potential resulted in James Allison and Tasuku Honjo receiving the Nobel Prize in Physiology and Medicine in 2018.

1.3.5.2 CTLA-4

CTLA-4 is an immune checkpoint molecule belonging to the Ig superfamily and is constitutively expressed on T-cells and regulatory T-cells (Tregs). While homologous to CD28 and binding to the same B7 ligands, B7-1 (CD80) and B7-2 (CD86), CTLA-4 inhibits T-cell activation upon binding to CD80/86. Compared to CD28, CTLA-4 has higher avidity and affinity for CD80/86, which causes its downregulation upon binding (76,77). Additionally, CTLA-4 switches off antigen-presenting cells once bound to its ligands to modulate the immune response (78). Reducing CD28-mediated signalling during antigen presentation increases the threshold for T-cell activation, thus preventing immune responses to weak antigens, such as tumour antigens (79).

Anti-CTLA-4 antibody therapies have shown success in treating solid tumours, with the first approved CTLA-4 inhibitor, ipilimumab, providing improved overall survival in metastatic melanoma. However, a phase III clinical trial comparing ipilimumab and anti-PD1 nivolumab revealed that nivolumab led to better survival (6.9 months Progression-Free Survival (PFS) and response rates (44%) than ipilimumab (19% response rate and 2.8 months PFS) in metastatic melanoma patients (80). Moreover, the combined use of both antibodies resulted in even higher response rates (58%) and survival (11.5 months PFS) (80). Additionally, anti-CTLA-4 blockade has shown increased patient survival compared to conventional chemotherapies in other cancers, including renal cell carcinoma, squamous cell carcinoma and non-small cell lung cancer.(79)

1.3.5.3 Additional Checkpoint inhibitors

While PD-1 and CTLA-4 are the main foci of immune checkpoint therapy, additional checkpoint molecules that contribute to T-cell exhaustion have been identified. Examples include Lymphocyte-activation gene-3 (LAG-3), T-cell immunoglobulin and mucin-domain-containing-3 (TIM-3), T-cell immunoreceptor with Ig and ITIM domains (TIGIT), and B7-H3 (CD276) (8,81) . The identification of these proteins and their contribution to T-cell dysfunction in the TME will improve treatment options to prevent T-cell exhaustion, either by introducing them as antibodies or by using adoptive cell therapy.

The success of immune checkpoint therapy highlights the importance of understanding the mechanics of the immune system and how better treatments can be developed to mount an effective anti-tumour immune response.

1.3.5.4 The use of ICB in paediatric cancer

The success of using ICB in adult cancers has not been recapitulated in paediatric diseases. The low mutational burden seen in paediatric cancers reduces the likelihood of the host immune system recognising “foreign” tumour antigens (82). Additionally, paediatric tumours are considered more “immunologically cold”, with lower numbers of tumour-infiltrating lymphocytes (TILs) and an immunosuppressive TME, which limits T-cell trafficking (83). Additionally, many paediatric tumours lack the expression of checkpoint markers such as PD-1, PD-L1, and PD-L2, hindering the success of ICB in paediatric cancers (84). Paediatric disease occurs in a young population with a less developed immune system, which may hinder the mounting of a robust anti-tumour immune response (83).

Studies have reported the overexpression of PD-L1 in tumour and metastatic bone marrow samples obtained from patients with high-risk neuroblastoma and its association with poor prognosis (82,85). Ehlert et al. reported that two high-risk neuroblastoma patients treated with a combination of nivolumab and dinutuximab after failing front-line therapy showed a good clinical response (86). Ongoing clinical trials are evaluating the use of ICB therapy (nivolumab and ipilimumab) in patients with neuroblastoma (82).

The use of anti-CTLA-4 therapy has been limited to paediatric cancers. In the first report published on the use of ipilimumab in solid tumours in paediatric patients, some durable tumour regression was observed, but no major clinical response was seen with immune-related toxicities similar to those seen in adults (87). The use of nivolumab in combination with ipilimumab was assessed in a phase I/II trial in paediatric patients with relapsed/refractory solid tumours of ewing sarcoma, rhabdomyosarcoma, and osteosarcoma. While the treatment was found to be tolerable, there was limited clinical response observed in patients; however, durable partial responses were observed in two patients that were maintained for 36 months after the end of the study (88).

1.3.6 Cancer Vaccines

Since the discovery of the smallpox vaccine by Edward Jenner in 1979, our understanding and utilisation of vaccines have greatly evolved in the field of immunology (89). Vaccines can induce an immune response to a foreign antigen, forming a memory response that leads to a faster secondary response upon antigen re-exposure. In the field of cancer immunotherapy, vaccines have been developed as an alternative way to boost the anti-tumour immune response to active immunotherapy options used for different cancer types (90).

Cancer vaccines utilise tumour antigens (TAs), which are either tumour-associated or tumour-specific. Tumour-associated antigens (TAAs) are expressed in both normal and tumour tissues; however, TAA expression tends to be higher in tumour tissues (90). Tumour-specific antigens (TSAs) or neoantigens are expressed only by cancer cells and are absent in normal tissues (90). TSAs were found to elicit a stronger immune response due to their restricted expression (91). Additionally, mutations in tumour cells can alter peptide amino acid sequences, leading to the formation of patient-specific neoantigens that can be utilised for cancer vaccine development (90). However, this vaccination method is associated with high production costs, which hinders its frequent use in cancer vaccine development (91).

1.3.6.1 Types of Cancer Vaccines

Cancer vaccines can be broadly grouped into three major types based on the antigens used: cellular, peptide/protein, and genetic.

Peptide/protein vaccines are composed of TAAs, TSAs, cancer germline antigens, or virus-specific antigens (90). The use of such antigens allows the generation of T-cells that are TAA-specific to mount an effective immune response. The limitation of epitopes for potential vaccine targets has been found to hinder the success of these vaccines, as well as the weaker immunogenicity of tumour antigens and the occurrence of immune evasion, such as downregulation of MHC expression (92). Peptide vaccines also allow the inclusion of synthetic peptides; however, this requires ensuring that the selected immunogens can elicit the desired immune response (92). Moreover, $CD8^+$ T-cells generated using protein-based vaccines are less effective than those generated using other vaccines (90,93).

Genetic vaccines consist of DNA and mRNA, which encode TAs from proteins and peptides to induce an anti-tumour immune response and a subsequent memory response (90). DNA

vaccines enter antigen-presenting cells (APCs), which are transcribed and translated into TAs, which then undergo antigen processing and are presented as peptide-MHC complexes, thereby activating a specific immune response (94). These vaccines can also deliver multiple genes simultaneously using this method of delivery, thus bolstering the immunogenicity of the generated anti-tumour immune response (90). mRNA vaccines work similarly to DNA vaccines, with the advantage that transcription is not necessary, and thus mRNA encoding TAs are further involved in the process of antigen presentation via MHC complexes (94). The biggest challenge for the use of DNA and mRNA vaccines is their delivery into the cell, with challenges such as penetrating the cell membrane and processing through endocytic pathways before being released into the cell for subsequent antigen presentation (95).

The delivery of DNA, mRNA, and peptides may also occur through the use of either lipid nanoparticles (LNPs) to directly stimulate the immune system, or through the use of a vector such as an attenuated virus or bacteria to prevent degradation and further stimulate the immune response (95).

Clinical trials evaluating DNA vaccines have not shown significant success owing to their poor immunogenicity (96). Attempts to overcome this obstacle through approaches such as codon optimisation and the development of multi-epitope sequences to increase immunogenicity have resulted in little success (96–98). The use of RNA- and peptide-based vaccines has shown similar results; thus, these continue to be great challenges in developing vaccines for cancer treatment (99).

Cellular vaccines involve the use of whole tumour cells and dendritic cell vaccines. The use of whole-tumour cell vaccines entails the use of killed cancer cells, with the target not needing to be identified beforehand and can be non-specific in cancer targeting (90). Dendritic cell (DC) vaccines utilise autologous patient-derived DCs preloaded with peptide antigens or transfected with antigen genes (100). DC vaccines have been shown to improve survival in AML patients (101). The clinical success of DC vaccines was observed with the approval of the first DC cancer vaccine, Sipuleucel-T (Provenge), in 2010 (90). The sipuleucel-T vaccine has been used to treat prostate cancer by pulsing patient DCs with TAA, prostatic acid phosphatase expressed in prostate cancer, and granulocyte-macrophage colony-stimulating factor (GM-CSF) (102). Treatment with sipuleucel-T showed an improved survival benefit of 25.8 months compared to 21.7 months with placebo (102). These results resulted in the approval of sipuleucel-T against hormone-refractory prostate cancer. However, whether the benefits provided are sufficient to outweigh the cost of production remains controversial (90).

While there have been developments in cancer vaccines, their use alone as monotherapy may not be sufficient to eradicate cancer. Recent studies have reported improved treatment responses by combining cancer vaccines with other therapies such as cytokines, radiotherapy, and ICB (103).

The evolution of cancer vaccines has largely focused on adult cancers, with a limited evolution in paediatric cancers (104). In a phase I trial, Krishnadas et al. evaluated the use of the chemotherapeutic agent decitabine to upregulate cancer-testis antigen expression, followed by administration of a DC vaccine targeting the cancer-testis antigens MAGE-A1, MAGE-A3, and NY-ESO in patients with refractory/relapsed neuroblastoma and sarcoma (105). Only one patient was reported to have a complete response with a disease-free survival of 3.5 years post-treatment (105). Moreover, there is currently an ongoing phase I trial evaluating the use of a GM-CSF based cell vaccine (GVAX) in combination with ICB for neuroblastoma (NCT04239040).

1.3.7 Adoptive T-cell therapy

While the use of antibody therapy, ICB, and cancer vaccines bolsters tumour-infiltrating lymphocytes (TILs) *in situ*, adoptive cell therapy (ACT) aims to do this through *ex vivo* expansion and/or genetic modification of immune cells, which are introduced into the patient to bolster the anti-tumour immune response. Clinically, several types of ACTs have been evaluated, including TILs, endogenous T-cell receptor-engineered T-cells (TCR-T), and chimeric antigen receptor (CAR) T-cells.

1.3.7.1 Tumour infiltrating lymphocytes

The first study that uncovered the therapeutic potential of TILs was performed by Rosenberg et al. in 1987. TILs were isolated from different murine tumours, expanded *in vitro* with the cytokine interleukin-2 (IL-2), and were shown to exhibit anti-tumour activity *in vivo* when infused back into tumour-bearing mice (106). Moreover, they found that the therapeutic effect of TILs was enhanced when administered in combination with IL-2 (107). Subsequently, the first clinical trial to evaluate TILs was performed in patients with metastatic melanoma. Tumour regression was observed in approximately 50% of patients with the combination therapy of TILs with IL-2. In this study the clinical response observed was short-lived, lasting for up to 13 months (108). However, the preconditioning of patients with a non-myeloablative

(NMA) lymphodepletion chemotherapy regimen of two days of cyclophosphamide (60 mg/kg) followed by five days of fludarabine (25 mg/m^2) before infusion of TIL therapy produced a more prolonged anti-tumour response, with over 50% of patients with metastatic melanoma showing a clinical response (109). Moreover, the clinical response could be further improved by the addition of total body irradiation (TBI) to the NMA chemotherapy regimen (110,111). The success of TIL therapy for melanoma has recently resulted in the approval of the first TIL therapy (Lifileucel) by the FDA in 2024 for patients with unresectable or metastatic melanoma (112). TIL therapy has also been evaluated in a range of other solid tumours such as cervical cancer, non-small cell lung cancer (NSCLC), breast cancer, and cholangiocarcinoma, with varied clinical benefits (113).

TIL therapy provides low toxicity because TILs come from the patients themselves without any gene modification. However, for a durable anti-tumour response to be achieved, effector T-cells with anti-tumour activity are required to be present within the tumour (113). As a result, differences between immunologically cold and hot tumours limit the feasibility of TIL therapy, with an immunosuppressive tumour microenvironment being the main obstacle to overcome (113). TILs are also found to have a short survival time *in vivo*, and thus work is ongoing to improve the survival and tumour-homing of TILs after reinfusion into patients. (113).

1.3.7.2 T-cell receptor engineered T-cells

The advent of genetic engineering of immune cells has allowed the development of additional ACT therapies that enhance T-cell tumour specificity and effector functions. One method is to engineer T-cells to express a new tumour antigen-specific TCR (TCR-T). This allows T-cells to be redirected against tumour-specific antigens (114). This provides an advantage over antibody therapies as TCRs are MHC-restricted and thus able to recognise intracellular antigens, increasing the range of tumour-specific antigens to target and limiting the risk of on-target off-tumour toxicity. However, antigen selection is imperative for targeted therapies to ensure therapeutic efficacy and safe treatment. Clinical trials evaluating TCR-T therapies against tumour antigens such as MART-1, gp100, and CEA showed some clinical benefit, but severe toxicity was reported because of low antigen expression in normal tissues (114). The first clinical trial evaluating MART-1-specific TCR-T cells in melanoma patients showed that the clinical response was only seen in two out of the 17 patients in the trial (115). Moreover, a recent clinical trial with a different TCR for MART-1 showed similar severe toxicities and patient death, resulting in the early termination of the study (116).

The occurrence of off-target off-tumour toxicities or cross-reactivity has also been a challenge in the development of effective TCR-T therapies. TCR-T cells targeting the cancer testis antigen MAGE-A3 were found to be cross-reactive, resulting in the death of four patients (117). Engineered TCR-T cells were also found to recognise a peptide from TITIN , a muscle protein, leading to fatal toxicity against cardiac tissue (117). Therefore, it is imperative to ensure that TCR cross-reactivity is assessed at the preclinical level, especially concerning TCR sequences modified to enhance affinity (114).

While some TCR-T therapies have shown the issues detailed above, there has been success with the use of other antigens, such as the cancer testis antigen, NY-ESO-1. Across five clinical trials assessing TCR-T cells targeting NY-ESO-1 in 107 patients, an average clinical response rate of 47% was observed, without any major toxicities (114). While the clinical response has been promising, antigen expression of NY-ESO-1 is still limited in metastatic cancers, and tumour expression tends to be heterogeneous (114). This seems to suggest that the affinity of these TCR-T cells has to be optimised to try and better address heterogeneous antigen expression in the tumour while minimising the occurrence of on-tumour off-target toxicity,

While the success of TCR-T therapies has been seen against solid tumours, MHC restriction constrains the use of this therapy, as TCRs need to be matched to the patient's MHC haplotype. Moreover, MHC downregulation is a common immunoevasion mechanism observed in tumours, resulting in the escape of tumour cells from TCR-T-engineered cells. The use of TCR-T therapies in combination with other therapeutic options, such as ICB, may address these obstacles (114).

1.3.8 CAR-T cells

Another method of genetically engineering T-cells is through the expression of chimeric antigen receptors (CARs) that allow the targeting of tumour antigens that are not MHC-resistant and can mimic TCR activation in an MHC-independent manner. Since its inception in the 1980s, CAR-T cell design has evolved into multiple generations and has been utilised for other immune cells as well.

1.3.8.1 Evolution of CAR-T cells

The concept of CARs emerged in 1987 by Kurosawa et al. who combined the variable regions of an anti-phosphorylcholine antibody with TCR-derived constant regions (118). The expression of these anti-phosphorylcholine chimeric receptors in murine T-cell lymphoma EL4 cells resulted in calcium influx upon exposure to phosphorylcholine-positive bacteria, suggesting that the generated chimeric receptor could lead to T-cell activation in response to antigens (118). Subsequent work performed in 1989 by Gross, Waks, and Eshhar involved generating a chimeric T-cell receptor like Kurosawa et al. against anti-2,4,6-trinitrophenol (TNP), which showed antigen recognition in an MHC-independent manner (119). Murine MD.45 cytotoxic T lymphocyte hybridoma cells were generated to express the anti-TNP chimeric TCR and were shown to bind to the TNP antigen, resulting in T-cell activation via production of IL-2 and killing of target cells (119).

To generate these double-chain heterodimeric TCRs, co-transduction was performed with two separate retroviral vectors, which resulted in a low transduction efficiency. To circumvent this issue, Eshhar et al. designed what is now known as a prototype for first-generation CARs. A single-chain chimeric receptor was developed in which a single-chain variable fragment (ScFv) was fused to a lymphocyte intracellular signalling domain from either CD3ζ or FcεRIγ (120). The ScFv is derived from a monoclonal antibody and shows the same binding affinity and specificity as the parental antibody. These chimeric antigen receptors could independently transduce T-cell signals in the absence of a conventional TCR complex, allowing non-MHC-restricted T-cell activation upon antigen binding. (120,121).

1.3.8.2 CAR Structure

The structure of a CAR comprises of an antigen binding domain (ScFv) followed by a linker or hinge region that is connected to intracellular domains consisting of co-stimulatory endodomains and a CD3ζ subunit. Intracellular domains of first-generation CARs comprise of only the CD3ζ subunit, whereas second- or third-generation CARs have the addition of one or two co-stimulatory domains, respectively. First-generation CARs exhibit evidence of signalling with the CD3ζ domain, providing an activation signal one. However, these CAR-T cells are found to become anergic, with failed persistence in the preclinical and clinical setting (121–123). The inclusion of a co-stimulatory endodomain (traditionally CD28 or 4-1BB) in second-generation CARs showed CAR-T cell persistence *in vivo* and clinical success due to

providing signal two as required in traditional TCR activation (121,124). The first-, second-, and third-generation CAR structures are shown in Figure 1.2.

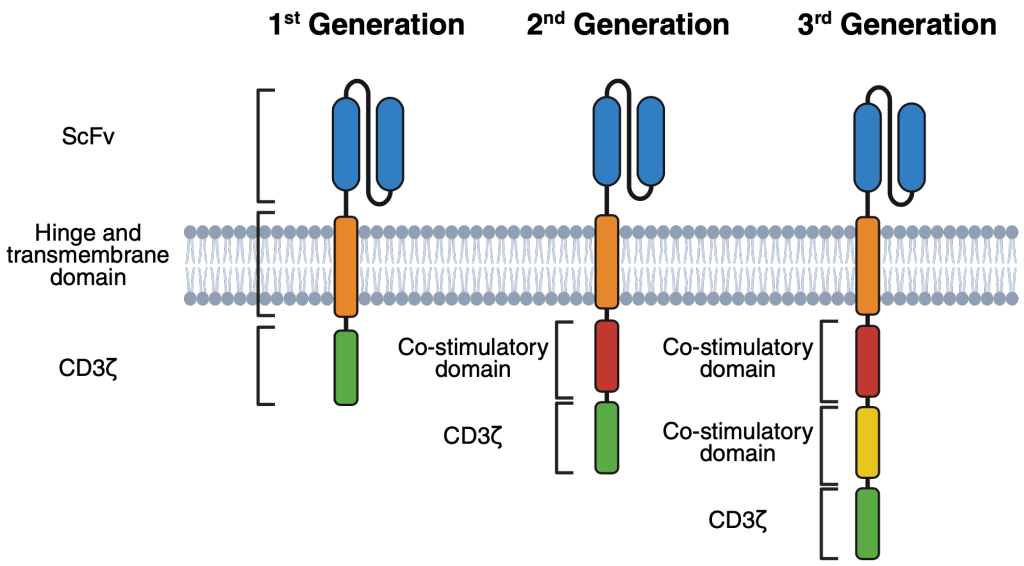

Figure 1.2 CAR Structure

Chimeric Antigen Receptors (CARs) have evolved into multiple generations since It's inception over the past 30 years. First generation CARs consist of an antigen binding domain, which consists of an SvFv (**blue**) targeting a specific antigen, which is fused to a hinge and transmembrane domain fused to a CD3ζ signalling domain (**green**). Second and third generation CARs have the same structure with the addition of co-stimulatory domains (for example, CD28 and 41-BB). Second generation CARs have one co-stimulatory domain (**red**), whilst third generation CARs have two co-stimulatory domains (**red and yellow**). Figure created using Biorender.

1.4 CAR-T cell success in haematological malignancies

CAR-T cell therapy has shown great success in treating haematological malignancies, such as leukaemia, lymphomas, and plasma cell malignancies. In haematological malignancies, T-cells being found in the circulatory system under homeostatic conditions means that trafficking to tumour cells does not pose as a challenge as it is in solid tumours. The use of anti-CD19 CAR-T cells has been successful in the field of CAR therapy. CD19 is a protein found to be expressed on B-lineage cells and identified to be an appropriate target for treating B-cell derived leukaemia, and the use of immunoglobulin replacement therapy to replace the non-malignant B-cell population mitigates the risk of therapy to patients (121,125). Second-generation CD19 CARs with either CD28 or 4-1BB costimulatory domains

have shown clinical success in patients with acute lymphoblastic leukaemia (ALL), diffuse large B-cell lymphoma (DLBCL), and mantle cell lymphoma (MCL) (126–131).

The use of anti-CD19 CAR therapy in three patients with chronic lymphocytic leukaemia (CLL) by Carl June and colleagues achieved a complete or partial response with CAR-T cell expansion in patients seen up to 1000 times, with functional CARs seen for at least six months post-infusion (132,133). The first paediatric patient to receive CAR-T cell therapy was in 2012, with CD19 CAR therapy being used to treat ALL (134). In response to treatment, one patient developed severe side effects such as cytokine release syndrome (CRS) and acute respiratory distress syndrome (ARDS) (134). However, treatment with the anti-IL6 antibody tocilizumab alleviated CRS, and the patient continued to be cancer-free 13 years after treatment, while the other patient relapsed with CD19 negative disease (134). The clinical success of CAR-T cell therapy has led to the approval of many CAR therapies by the FDA for the treatment of these diseases, as shown in Table 1.3 (135).

Table 1.3 FDA Approved CAR T-cell therapies

Name (Trade Name)	**Target**	**Approved Use(s)**
Idecabtagene vicleucel (Abecma)	BCMA	Multiple Myeloma
Obecabtagene autoleucel (Aucatzyl)	CD19	B-cell ALL
Lisocabtagene maraleucel (Breyanzi)	CD19	Follicular lymphoma, Large B-cell lymphoma, MCL and CLL
Ciltacabtagene autoleucel (Carvykti)	BCMA	Multiple myeloma
Tisagenlecleuce (Kymriah)	CD19	B-Cell ALL, DLBCL and follicular lymphoma
Brexucabtagene Autoleucel	CD19	B-Cell ALL and MCL

(Tecartus)		
Axicabtagene ciloleucel (Yescarta)	CD19	Large B-cell lymphoma and follicular lymphoma

Although CAR therapy has shown clinical success as a cancer treatment, patients undergoing this therapy are known to experience severe toxicities. The two most common side effects of this therapy are cytokine release syndrome (CRS) and immune-effector cell-associated neurotoxicity syndrome (ICANS).

CRS is driven by proinflammatory cytokines, such as IL-1 and IL-6, which result in a range of symptoms from fever and hypotension to other systemic symptoms (121). The approval of the anti-IL-6 antibody tocilizumab by the FDA mitigates the risk of CRS and neurotoxicity, along with other alternative treatments such as anakinra (IL-1 receptor antagonist) and siltuximab (anti-IL-6 mAb) (121,136). The occurrence of CRS has been suggested as likely due to the activation of monocytes and macrophages, which in murine models of CRS were found to be primary sources of IL-1 and IL-6 (137,138). Depletion of monocytes or IL-6 receptor blockade was found to prevent CRS; CRS and neurotoxicity were abrogated by the use of the IL-1 receptor antagonist anakinra (138). On-target off-tumour occurrence may contribute to CD19-CAR T cell therapy-associated neurotoxicity with CD19, which is also commonly expressed in brain mural cells (139). Additionally, other factors can also affect the severe side effects of CAR-T therapy, including pretreatment tumour burden, CAR-T cell dose administered, and intensity of the lymphodepletion regimen before CAR-T cell infusion (121).

Better mitigation of these side effects may occur with time as clinicians gain more experience. The use of biomarkers may allow better monitoring of clinical response and, in turn, better mitigate the risk of these severe toxicities with IFNγ, IL-13 and MIP1α having shown potential in predicting CRS in paediatric ALL patients treated with anti-CD19 CAR therapy (140). Moreover, improvements in CAR design are ongoing to identify factors that may block CRS-associated signalling, such as IL-6, IL-1, and GM-CSF, amongst other approaches (141).

1.5 Challenges hindering CAR-T cell success in solid tumours

To date, the success of haematological malignancies has yet to be seen against solid tumours. The challenges that CAR-T cell therapy needs to overcome in achieving success

against solid tumours are detailed below. Examples of these challenges include appropriate antigen selection, overcoming hostile TME, antigen escape, and immunosuppression.

1.5.1 Antigen selection and escape

Most solid tumours do not express tumour-specific antigens. As a result, antigen selection for targeted therapies, including CAR therapy, has focused on tumour-associated antigens, in which an antigen is highly expressed on tumour cells with restricted expression in normal tissues. However, this does lead to a potential risk of on-target off-tumour toxicity. Solid tumours also show a high degree of tumour antigen heterogeneity, and CAR-T cell susceptibility is dependent on targeting highly expressed antigens across most tumour cells. This poses an additional challenge for CAR-T therapy in paediatric cancers because of their low mutational burden, which restricts the antigens available to target using CAR therapy.

Antigen density is also found to be an important factor affecting CAR therapy, with CAR-T cells exposed to cells with lower antigen density resulting in diminished cytokine production and anti-tumour responses (142–144). Moreover, antigen escape has been reported in both preclinical and clinical settings. While CD19 CAR therapy has shown complete remission in many patients, patients relapse after treatment with the emergence of CD19 negative tumour cells, allowing tumours to evade CAR-mediated recognition and clearance even in the presence of CAR-T cell persistence (145,146). In solid tumours, antigen loss has been described as downregulation of the antigen EGFRvIII in five out of seven patients after one dose during a trial assessing an anti-EGFRvIII CAR against glioblastoma (147).

To overcome the hurdle of antigen heterogeneity and mitigate antigen escape, improvements in CAR design have been considered. Multi-specific CAR-T cell therapy, in which T-cells are engineered to express two CARs is being investigated and includes generating bicistronic CARs, tandem CARs (TanCAR), or LoopCARs (148). The development of TanCAR targeting IL-13 receptor subunit alpha-2 (IL-13Ra2) and ephrin type-A receptor 2 (EphA2) was found to be effective against both *in vitro* and *in vivo* models of glioblastoma with greater functionality than single CAR-T cells (149). Other CAR engineering methods that limit CAR-T cell activation to the tumour site have also been investigated. Examples of this include modifying the affinity of antigen binding of the CAR and using “switchable” CAR-T cells, which are found to only be active in the presence of an exogenous stimulus or “switch” (150). Examples of a “switch” may include small molecules that bind to the CAR’s costimulatory domain or an antibody that bridges the CAR to the antigen of interest (151–153). CARs may

also be designed to include an inhibitory peptide which reversibly blocks the ScFv, keeping the CAR in an off-state until reaching the TME, in which local conditions (e.g. hypoxic conditions or secreted proteases) lead to cleavage of the peptide, allowing CAR activation upon antigen binding (151).

There has also been targeting of cancer stem cells, which are closely related to tumour heterogeneity, thus potentially overcoming the hurdle of tumour heterogeneity. CD133 is a tumour stem cell marker found overexpressed in many solid tumours, with an association of $CD133^{+}$ tumour infiltrating cells driving intra-tumoural heterogeneity in multiple aggressive cancers, and thus being considered as a potential antigen target for CAR therapy for solid cancers (150,154,155).

1.5.2 T-cell trafficking

In haematological malignancies, tumour cells are easily targeted by CAR-T cells within the blood, lymph nodes, and bone marrow because immune cell migration normally occurs at these sites within the body. However, for solid tumours, CAR-T cells are required to migrate to the tumour sites, where they have to extravasate from blood vessels and infiltrate into the tumour itself to exert their anti-tumour activity (156,157). This is challenging, as many solid tumours tend to be sparse in tumour-infiltrating lymphocytes, and mechanisms of tumour exclusions are exerted by tumours, making it difficult for CAR-T cells to easily infiltrate into the tumour. Intra-tumoural infusion of CAR-T cells may circumvent this issue, but this is not widely used for metastatic tumour types, and responses seen with this method have been limited (156).

The tumour vasculature tends to be misaligned and disorderly as a result of being derived from mature vascular beds rather than from endothelial precursor cells that develop into normal vasculature (158,159). As a result, the poorly structured network of vessels surrounding the tumour tends to have suboptimal blood flow (160). Poor blood flow reaching the tumour through this vasculature creates a poorly oxygenated TME that may also be acidic and hypoxic. As a result, even if CAR T-cells can extravasate and infiltrate the TME, hostile conditions make CAR T-cell persistence difficult.

CAR strategies have addressed ways in which CAR-T cell trafficking can be promoted in the TME. Expression profiles of chemokines in the TME have been analysed to determine which chemokine axis can be exploited to promote T-cell infiltration (148). CXCR2-modified GDPC3

CAR-T cells were found to improve trafficking and anti-tumour efficacy compared to non-modified CAR-T cell controls in a hepatocellular carcinoma model (161). Other chemokine-modified CAR-T cells have been investigated in other solid tumours such as glioblastoma (CXCR1/CXCR2) and NSCLC (CCR2B) (162,163).

Fibroblast activation protein (FAP), a protease of cancer-associated fibroblasts (CAFs), is overexpressed in many solid tumours (164). FAP's role in remodelling the extracellular matrix (ECM) and promoting immunosuppression limits CAR-T cell tumour infiltration (165). The use of FAP-CAR-T cells has been evaluated against a range of solid tumours, showing increased homing and robust anti-tumour responses (165).

The poor trafficking of CAR-T cells into the tumour also creates a challenge in demonstrating CAR-T cell infiltration into the tumour site, as it requires the detection of both T-cells and CAR expression (156). Many approaches have been utilised to monitor CAR-T cell trafficking *in vivo*, such as radiolabeling CAR-T cells before injection and detecting CAR transgenes by quantitative polymerase chain reaction (qPCR) with varying success (156). However, these methods of detection do not adequately address the issues of cellular density and localisation of CAR-T cells within the tumour microenvironment, which is important for better assessment of clinical response (156). The co-expression of imaging reporter genes, such as the human sodium iodide symporter (hNIS) and herpes simplex virus thymidine kinase 1 (HSV1tk), by CAR-T cells, may provide a non-invasive method for CAR-T cell imaging in preclinical and clinical settings to better assess CAR-T cell trafficking and therapy response, especially in metastatic disease (166,167). These imaging reporter genes are compatible with commonly used clinical radiotracers, such as technetium-99m pertechnetate ($^{99m}TcO_4^-$), allowing high-resolution SPECT/CT imaging, which is routinely used in clinics (166,167).

1.5.3 Hostile TME

Even if CAR-T cells are successfully trafficked into solid tumours, CAR-T cells encounter a hostile TME, which diminishes their ability to function and persist. Solid tumours are strongly infiltrated by a mix of different cell types, which support tumour cell survival and growth while inhibiting the anti-tumour immune response (168). Prominent types of immune suppressor cells are found in the TME, including Tregs, myeloid-derived suppressor cells (MDSCs), and tumour-associated macrophages (TAMs), which facilitate tumour growth and proliferation by producing growth factors, cytokines, and chemokines, including VEGF, IL-4, IL-10, and TGFβ, and immune checkpoint molecules, such as CTLA-4 and PD-1, to promote tumour cell

survival while diminishing anti-tumour immunity (169–171). Solid tumours are also known to have high adenosine levels and reactive oxygen species (ROS), which are known to disrupt T-cell responses (170). Cancer-associated fibroblasts (CAFs) are commonly found in the TME, and their expression of FAP greatly influences the immunosuppressive TME and release of ECM proteins, making T-cell infiltration more challenging (171).

Paediatric solid tumours are "immunologically cold" with an immunosuppressive TME, creating barriers to successful CAR-T cell functionality and persistence. Various strategies have been proposed to overcome these limitations. Examples include CAR-T cells engineered to express enzymes that degrade the ECM or secrete proinflammatory cytokines to modify the TME and improve proinflammatory immune cell recruitment and function (170). The combined use of CAR-T cells and TME modulators has also been investigated, including checkpoint inhibitors in combination with CAR-T cells (170).

1.6 Immunotherapy for neuroblastoma

Neuroblastoma has shown success in immunotherapy for childhood solid tumours. Disialoganglioside GD2 is commonly expressed in neuroblastoma cells, making it a promising therapeutic target for immunotherapy (172). Moreover, the restricted expression of GD2 in healthy tissues, which is limited to peripheral nerves and melanocytes, also limits the potential toxicity of on-target off-tumour effects (48). The function of GD2 in neuroblastoma is unclear, but it may play a regulatory role in cell proliferation, adhesion, and invasion (48).

Before any development of immunotherapy intervention, treatment for high-risk neuroblastoma was focused largely on a multimodal approach consisting of surgery, radiotherapy, and chemotherapy (20,21). AHSCT was also utilised based on the aggressiveness of the chemotherapy regimen administered to the patients (20,21). While this approach improved survival outcomes, 40% of patients had a 5-year survival rate without relapse, with relapsed disease rarely being cured (20,21). During the 1980s, two murine anti-GD2 mAbs were identified: 14.18 and 3F8 (48,172) . These mAbs recognise GD2 in a range of cancers, including neuroblastoma (48). Preclinical studies have revealed that anti-GD2 antibodies are effective with antibody-dependent cytotoxicity (ADCC) and complement-dependent cytotoxicity (CDC), proposed as major mechanisms of action (48). Subsequent clinical evaluation of these antibodies and humanised versions generated showed clinical response in non-bulky disease (48,173,174). Following this, a large randomised trial by The

Children's Oncology Group (COG) evaluated the anti-GD2 mAb, dinituximab (chimeric version of the 14.18 mAb), in combination with GM-CSF, IL-2, and cis-retinoic acid compared to cis-retinoic treatment alone. These treatment options were evaluated in children with high-risk neuroblastoma as a maintenance therapy after receiving induction chemotherapy and AHSCT. Patients receiving anti-GD2 therapy showed a better clinical response with improved event-free survival (EFS) and overall survival after study completion and after almost a ten-year follow-up (175,176). This study resulted in the approval of dinituximab for use in childhood cancer by the FDA and became the first mAb approved specifically for paediatric solid tumours (20). Similar anti-GD2 antibodies have been used clinically. Dinituximab-beta has been approved for clinical use in Europe, and naxitamab (humanised mAb of 3F8) was recently approved by the FDA for relapsed or refractory neuroblastoma disease limited to the bone or bone marrow (20).

The exact mechanisms of action of anti-GD2 antibodies are not thoroughly understood, with ADCC and CDC demonstrated *in vitro,* and may also have some direct anti-tumour effects (48,177). In clinical use, the use of anti-GD2 mAbs has shown neurotoxicity to be a common occurrence, in which neuropathic pain occurs due to on-target off-tumour effects against GD2 expressed on peripheral nerves (173,174). In the anti-tumour response, ADCC is considered to be the main mechanism of action, with neurotoxicity considered to occur through CDC (48). Maintaining an anti-tumour response while reducing neuropathic pain can occur through changes in the Fc group, resulting in an attenuated CDC response (48,178).

Clinical evaluation of anti-GD2 antibodies against neuroblastoma continues. Evaluation of anti-GD2 mAb in combination with chemotherapy in a COG trial against relapsed, refractory neuroblastoma revealed that chemoimmunotherapy was effective in patients, especially those with chemorefractory disease, with significant disease regression (179). Therefore, the use of anti-GD2 mAb in combination with chemotherapy has become a standard therapeutic approach for patients with relapsed or refractory disease, and as part of induction chemotherapy for patients with newly diagnosed disease (180,181). Anti-GD2 antibodies are also being evaluated in other forms, such as radiolabelled antibodies or conjugated with IL-2, with varied clinical responses (48,62,182).

Even with the advent of anti-GD2 antibody therapy in neuroblastoma treatment improving clinical outcomes in patients, disease relapse still occurs even after receiving this therapy (175,176,179,181). Patients with relapse also show decreased GD2 expression, suggesting mechanisms of antigen escape by the tumour cells in response to anti-GD2 therapy

(176,183). As mentioned above, the use of anti-GD2 treatment can cause severe neurotoxicity with neuropathic pain due to the binding of anti-GD2 mAb on GD2 expressed on nerve fibres (178,184). As a result, anti-GD2 mAb is administered at much lower doses than those approved for antibody therapies for other cancers (20). Even at low doses, patients require narcotics and analgesics to mitigate neurotoxicity (20). Due to these challenges, additional TAA are required to target neuroblastoma through immunotherapy as well as to develop better anti-GD2 therapies such as CAR-T cells that may overcome the challenges of tumour cell resistance, antigen escape, and reducing neurotoxicity, as seen with anti-GD2 antibody therapies.

Adoptive cell therapies, such as CAR-T cell therapy, have been explored for use in relapsed and refractory disease, with most neuroblastoma trials focusing on targeting GD2. The first trial targeting paediatric cancers with CAR-T cell therapy was performed using a first-generation anti-GD2 CAR against neuroblastoma (185,186). The anti-GD2 CAR used in this trial had the same ScFv as dinituximab with no costimulatory endodomains (185,186). In patients with high-risk neuroblastoma, the CAR was found to mediate several clinical responses, with persistence beyond six weeks associated with improved clinical outcomes (186). Moreover, no on-target off-tumour neurotoxicity was reported even though patients had peripheral nerves positive for GD2 (186). However, preclinical evaluation of the same anti-GD2 binder as a second-generation has revealed less promising results with the occurrence of tonic signalling and T-cell exhaustion augmented with a CD28 endodomain compared to a 41-BB endodomain (187). Heczey et al. evaluated the use of a third-generation anti-GD2 CAR with a 14.18 binder and CD28/OX40 costimulation in relapsed/refractory neuroblastoma patients and showed poor clinical response even in combination with PD-1 blockade (188). The use of alternative anti-GD2 binders has shown improved clinical outcomes. The evaluation of a second-generation anti-GD2 CAR, which used K666 ScFv in a phase one trial against relapsed/refractory neuroblastoma showed more favourable clinical responses with dose-dependent anti-tumour activity and no occurrence of neuropathy (189). The evaluation of a third-generation anti-GD2 CAR with the 14.18 ScFv, CD28, and 41-BB endodomains was evaluated in a phase one trial in 27 patients with high-risk disease and showed promising clinical outcomes with no dose-limiting toxic effects reported and nine patients having a complete response (190).

1.6.1 Other immunotherapy targets in neuroblastoma

Beyond GD2, other targets have been identified for developing new immunotherapies against neuroblastoma that may improve clinical outcomes for patients. B7-H3 (CD276) is a checkpoint molecule overexpressed in neuroblastoma and other paediatric solid tumours, with restricted expression in normal tissues. It is a member of the B7 family, with PD-L1 being its closest relative, based on 30% homology (191). The role of B7-H3 is poorly understood and has been implicated in immunomodulation and pro-tumoural effects (191). Targeting of B7-H3 dates back to 2001 with the development of a mAb named 8H9 before the identification of its target being B7-H3 (192,193). This antibody is now being developed as a radio-conjugate (omburtomab) for use in neuroblastoma patients where the disease has spread to the CNS alongside other primary CNS malignancies (62,64,194). MGA271 (enoblituzumab) is an anti-B7-H3 mAb that has been developed and is currently under clinical evaluation for solid tumours, including neuroblastoma [NCT02982941] (195). Anti-B7-H3 CAR-T cells have shown promise in preclinical models of paediatric cancer and reached clinical evaluation for patients with neuroblastoma amongst other non-CNS solid tumours [NCT04483778] (1,196)

Anaplastic lymphoma kinase (ALK) is a receptor tyrosine kinase that is either mutated or overexpressed in some neuroblastoma patients. ALK is expressed in neuroblastoma cells, resulting in the development of anti-ALK ADCs and CAR-T cells, which have been evaluated in preclinical studies (143,197). Glypican-2 (GPC2) is a glycoprotein that plays a varied role in growth factor signalling and cancer growth and is highly expressed in neuroblastoma, with restricted expression in normal tissues (198). Anti-GPC2 CARs have shown anti-tumour activity in a human xenograft mouse model (199). However, for both GPC2 and ALK, low antigen density is a challenge in developing effective therapies against these targets; thus, the response to these therapies may not be as effective as that with highly expressed antigens such as GD2. Other additional targets that have been identified in neuroblastoma for immunotherapy development include NCAM, L1CAM and cancer testis antigens, including NY-ESO-1 and PRAME (20).

Preclinical evaluation of immunotherapies, including CAR-T cells, has largely focused on the use of immunodeficient mice, which do not reveal the cross-talk between immune cells and tumour cells, a factor that greatly influences the treatment efficacy of CAR-T cells. Moreover, within these models, the evaluation of known CAR toxicities such as CRS is limited. As a result, better preclinical *in vivo* evaluation is required for CAR-T cells, especially in the context

of how the use of other therapies in combination with CAR-T cells, such as radiation, may address the hurdles facing CAR-T cell success in solid tumours such as T-cell infiltration and persistence within the TME.

1.7 Animal models for neuroblastoma immunotherapy evaluation

The successful clinical translation of immunotherapy, including CAR-T cell therapy, requires the use of preclinical animal models consisting of established tumours, as observed in patients with both tumour and immune cells known to be found in the TME. CAR-T cell evaluation using *in vivo* models allows us to better address the clinical challenges of CAR-T cell therapy by assessing important parameters that currently limit CAR-T cell success in solid tumours, such as CAR-T cell trafficking and persistence within the TME and therapy-related toxicity. Two main types of animal models are utilised for CAR-T cell evaluation: immunocompromised (xenograft) and immunocompetent models.

In mice, haematological malignancies are usually modelled by injecting tumour cells systematically (intravenous or intracardiac injection). However, for solid tumours, tumour cells may be injected subcutaneously (allowing easy harvest of tumour tissues), orthotopically (for a more representative environment for tumour engraftment), or systemically (to model tumour invasion or metastatic disease). Figure 1.3 describes the four commonly used murine cancer models for immunotherapy evaluation.

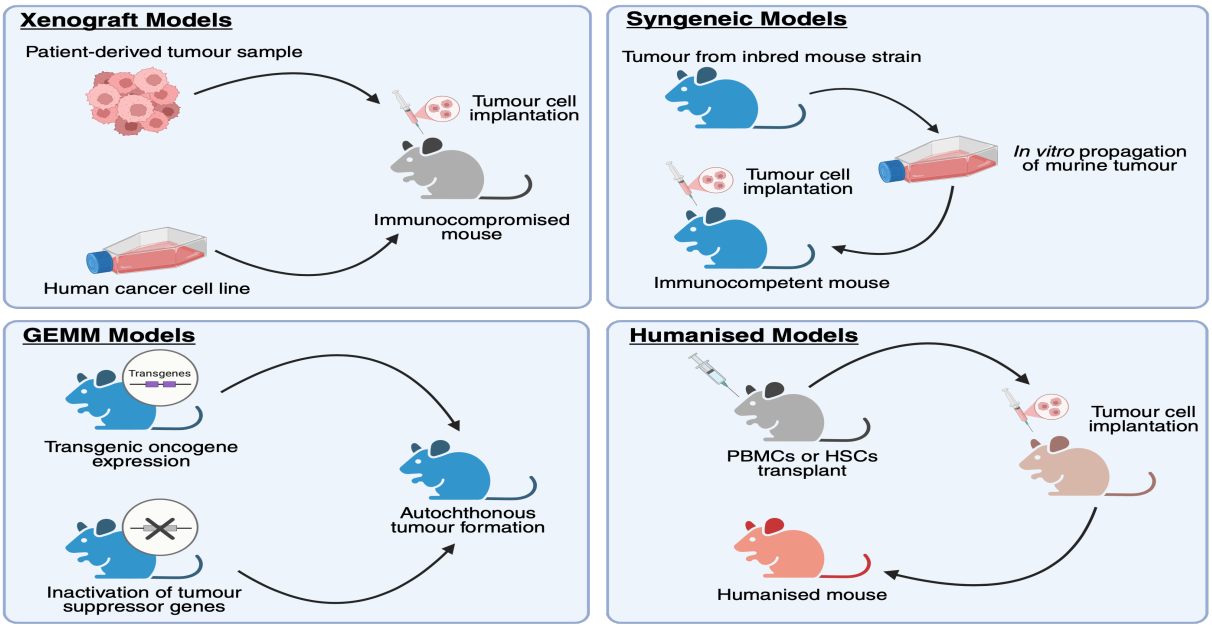

Figure 1.3 Preclinical Murine Cancer Models

Preclinical murine models used for cancer research broadly exist as four main types. First, xenograft mouse models involve the use of patient-derived tumour samples or human cancer cell line models, which are engrafted into immunocompromised (**grey**) mice. Second, syngeneic mouse models involve the use of tumours that have developed from immunocompetent (**blue**) inbred mouse strains, which are grown *in vitro,* followed by the implantation of these tumour cells into genetically identical immunocompetent inbred mouse strains. Third, genetically engineered mouse models (GEMMs) are established through typically genetically controlled expression of oncogenic drivers or inactivation of tumour suppressor genes in immunocompetent mice, leading to the generation of spontaneous tumour formation. Finally, humanised mouse models involve establishing aspects of the human immune system in immunocompromised mice through a PBMC or HSC transplant, followed by tumour cell implantation in these mice, leading to the generation of humanised (**red**) mice. Figure created using Biorender.

1.7.1 Immunocompromised (xenograft) models

Xenograft models are most commonly utilised in the preclinical evaluation of CAR-T cells. Many CAR-T cell products undergoing clinical evaluation have been preclinically evaluated in immunocompromised models, reporting *in vivo* tumour efficacy, including CARs targeting haematological malignancies (for example, CD19) and solid tumours (e.g. EGFRvIII, and mesothelin). Typically, most *in vivo* studies are performed using NOD/Scid/Gamma (NSG) mice, which lack functional T-, B-, and NK cells and have diminished DC function (200). Athymic nude mice with defects in T-cell development have also been used for CAR-T cell evaluation (201). Immunocompromised mice are typically engrafted with either a human

cancer cell line or patient-derived xenograft (PDX) models derived from clinical tumour samples (202). Once established, tumours are treated with human T-cells transduced with CARs to determine the efficacy of *in viv*o CAR-T cells. The advantage of utilising these models is that human tumours can be established without the risk of rejection of non-autologous tumours by the murine host, allowing for better understanding of the biology of human tumours (202). Immunocompromised mice are not depleted of all immune cells, allowing the presence of an endogenous immune response. MDSCs were found to expand in response to LPS stimulation and tumours in nude mice, suggesting some tumour-induced immunity is mediated by the myeloid compartment (203). After CAR infusion, myeloid cells in SCID-beige mice were found to produce IL-1, IL-6, and nitric oxide, leading to tumour-unrelated activity reduction, weight loss, and mortality, thus serving as a model for CRS, which is a known CAR-T cell toxicity (137). The targeting of MDSCs in these models enhances CAR T-cell anti-tumour activity, as reported by Long et al. using all-trans retinoic acid in sarcomas (204). However, the presence of these immune compartments is not sufficient for thorough CAR-T cell evaluation, considering that an intact immune system plays a role in tumour development and CAR-T cell function regulation.

Immunocompromised models are commonly used to evaluate CAR-T cells in neuroblastoma. CAR-T cell evaluation typically occurs in a subcutaneous or orthotopic tumour model in athymic nude or severe combined immunodeficiency disease (SCID) mice. The use of the orthotopic model requires tumoural injection into the adrenal gland fat pad, which can be technically challenging with the need for surgery to inject into the adrenal gland. Examples of commonly used human neuroblastoma cell line models for preclinical evaluation using NSG mice include SK-N-SH, SH-SY5Y, LAN-1 and LAN-5 (205).

1.7.2 Immunocompetent models

In contrast to immunocompromised models, immunocompetent models provide a more representative approach to immunotherapy evaluation. This is because of the presence of an intact immune system within these models, which is important considering the crosstalk between immune cells and the TME. Moreover, immunotherapeutic applications, including CAR-T cells, are also influenced by the immune system and, in turn, affect the anti-tumour immune response. These models also allow preconditioning regimens to be used clinically for immunotherapy, such as lymphodepletion with radiation or chemotherapy, and evaluation of combination therapy to be recapitulated in preclinical settings (202). Immunocompetent

models tend to exist in three main types: syngeneic, humanised, and genetically engineered mouse models (GEMMs), which are discussed further below.

1.7.3 Syngeneic tumour models

Syngeneic tumour models are immunocompetent models established by injecting histocompatible (syngeneic) tumour cells into an immunocompetent host, which typically includes common mouse strains such as C57BL/6 (202). In these models, solid tumours are typically established subcutaneously, or orthotopically using tumour implantation into a relevant organ to produce a more representative TME (202).

The first syngeneic model for neuroblastoma, C1300-NB, was established from spontaneously occurring spinal cord tumours in A/J mice, and showed more local disease (206). Subsequent clonal models from C1300-NB have also been derived, such as TBJ-NB and NSX2, which display more rapid tumour growth and metastatic disease (206–208). These models have immune and histological characteristics that are similar to those of human neuroblastoma, resulting in their use in the evaluation of immune-based therapeutic approaches (205,208–210). Moreover, syngeneic mouse models are highly reproducible and affordable for preclinical evaluations (205). However, these models are not representative of human neuroblastoma because of their differing biological and genetic alterations, and because they do not arise from embryogenesis as human neuroblastoma does (207).

1.7.4 Genetically engineered mouse models

Genetically engineered mouse models (GEMM) have an advantage over syngeneic mouse models because they provide a system of *in situ* tumour growth, allowing us to see how the endogenous anti-tumour response co-evolves with tumour progression. Tumour GEMMs are typically established through the genetically controlled expression of oncogenic drivers or disabling tumour suppressor genes in target tissues under specific conditions (202,211). GEMMs provide the ability to study endogenous anti-tumour T-cells, including the effects of T-cell exhaustion as a result of continuous antigen exposure starting from early tumour initiation (202). This allows a better understanding of the endogenous anti-tumour response before any immunotherapeutic intervention for preclinical evaluation.

In neuroblastoma, the best-defined GEMM is the TH-MYCN GEMM model. The importance of MYCN as an oncogenic driver in neuroblastoma development led to the creation of transgenic mice overexpressing N-myc neural crest cell lineage cells under the control of the rat tyrosine hydroxylase (TH) gene promoter (212,213). Subsequently, TH-MYCN transgenic mice developed spontaneous neuroblastoma tumours that closely resembled human neuroblastoma in histology, pathology, and tumour localisation (213). Moreover, the heterogeneity observed in human neuroblastoma is also present in these tumours, with a tumour consisting of both adrenergic and mesenchymal cell populations (205). However, the tumours were absent in the adrenal glands of TH-MYCN (a common location of human neuroblastoma tumours). Moreover, MYCN overexpression in this model did not lead to metastatic disease, as seen in human neuroblastoma, with no metastases observed in typical neuroblastoma metastatic sites, such as bones, bone marrow, or liver (205,214). Tumour penetrance in the TH-MYCN transgenic mouse has been found to show some strain differences, with a higher frequency of tumours arising from the 129/SvJ background compared to other genetic strains such as C57BL/6, with no clear understanding of these strain-specific differences (213,214). Nonetheless, the close modelling of human neuroblastoma achieved using this GEM model has resulted in its widespread use in the field of neuroblastoma, including for evaluating immunotherapeutic approaches (205).

For immunotherapy evaluation using the TH-MYCN GEMM model, 9464D is widely used for this purpose (215–217). The 9464D tumour model was generated from spontaneous tumours arising in TH-MYCN transgenic mice on a C57BL/6 background and now exists as an immortalised cell line (218). The characteristics of this model are similar to those of human neuroblastoma, with endogenous GD2 expression and low MHC-I levels (219). However, prolonged *in vitro* culture results in loss of GD2 expression (220). Orthotopic 9464D tumours are more aggressive than those in conventional subcutaneous models (221). Moreover, recently reported clonal cell lines have been derived from 9464D, which shows metastatic disease with organ-specific metastasis, such as in the bone and liver, which is frequently reported in high-risk neuroblastoma patients (222). This allows greater translational value from these models as primary tumours in many patients with neuroblastoma are located within the adrenal glands (18).

Activating mutations in the ALK oncogene and the overexpression of the epigenetic regulator LIN28B are also associated with neuroblastoma development. Attempts have been made to generate mouse models expressing ALK F1174L (the most common ALK mutation in neuroblastoma) or overexpressing LIN42B in the sympathetic lineage, resulting in

neuroblastoma tumour formation (223,224). However, studies have indicated that these mutations alone are not enough to model neuroblastoma, with increased tumourigenicity seen when overexpression of ALK mutants or LIN28B is combined with MYCN overexpression, as seen with the generation of TH-MYCN/ALK^{F1174} mice (205,225,226). Similar to the TH-MYCN model, the metastatic spread of the disease, as observed in patients, was absent in this model (205).

Recent progress made by Louis Chesler et al. at the Institute of Cancer Research, London, has resulted in the generation of TH-MYCN allograft lines of neuroblastoma. On the 129/SvJ background, TH-MYCN alone did not lead to penetrant tumours. The crossing of TH-MYCN mice with TH-ALK^{1174} mice led to potentiation of the oncogenic effects of MYCN, leading to TH-MYCN-ALK transgenic 129/SvJ mice that develop highly aggressive and penetrant tumours (225). A chemo-naive allograft line, 129NS1, was produced through generational *in vivo* passages of a spontaneous tumour arising from TH-MYCN-ALK transgenic mice in the 129/SvJ genetic background. This serial *in vivo* passaging of this tumour generated a neurosphere cell line, which recapitulates the histological and pathological aspects of human neuroblastoma. To model a treatment-refractory state of the disease, the TAM6 allograft line was generated using the same process as that used for the 129NS1 line (227). However, the mice underwent multiple cycles of vincristine sulfate, adriamycin, and cyclophosphamide (VAC) treatment, resulting in the development of chemoresistance (227). This study builds on the initial work by Yogev et al., who demonstrated that the administration of cyclophosphamide to TH-MYCN transgenic mice on a 129/SvJ background produced *in vivo* modelling of chemoresistance with genomic changes characteristic of chemoresistant human neuroblastoma (228). Figure 1.4 describes the generation of murine allograft models of neuroblastoma.

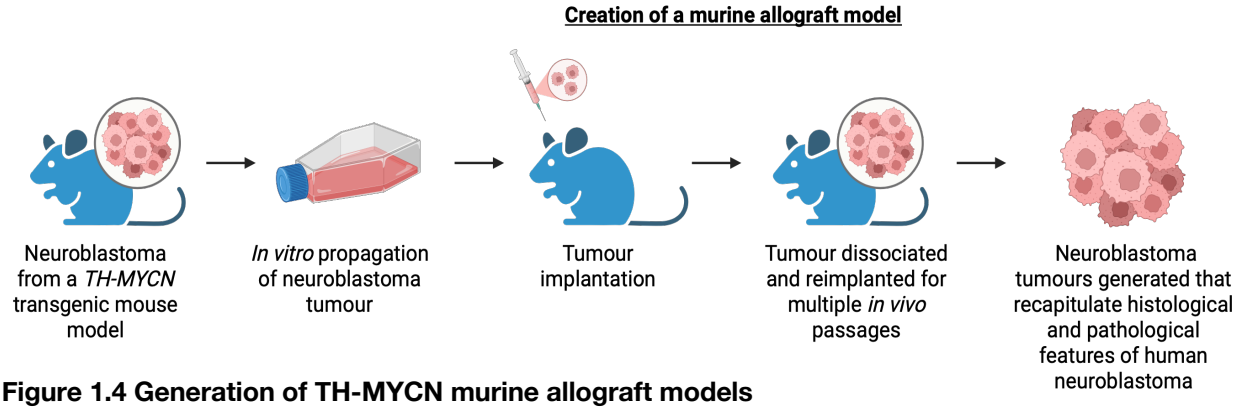

Figure 1.4 Generation of TH-MYCN murine allograft models

The TH-MYCN transgenic mouse model is a widely used model for high-risk neuroblastoma and has been used to generate murine allograft tumour models that recapitulate features of human neuroblastoma. The murine allograft models are generated through *in vitro* propagation of spontaneous neuroblastoma tumours that arise in TH-MYCN transgenic mice. The tumour cells propagated *in vitro* are then implanted into immunocompetent mice. The developed tumour is then dissociated and reimplanted for multiple *in vivo* passages. This leads to the generation of a murine allograft model in which neuroblastoma tumours generated recapitulate histological and pathological aspects of human neuroblastoma. Figure created using Biorender.

1.7.5 Humanised mouse models

The use of PDXs to model human-originated cancers relies on the use of immunocompromised models. To circumvent this hurdle, mice with humanised immune systems have been investigated as potential cancer models. Generating humanised models requires that mice be injected with human peripheral blood mononuclear cells (PBMCs) or haematopoietic stem cells (HSCs) into immunodeficient mice to reconstitute the human immune system (229). An alternative approach may involve the implantation of the foetal thymus, foetal liver, and foetal liver HSCs that promote the development of human lymphocytes (229). Mouse strains can also be engineered with MHC molecules and human cytokines (e.g. GM-CSF, and M-CSF) to support the engraftment of human haematopoietic cells (e.g. mouse strains such as NSG/NRG-SGM3) (229).

Although some success has been reported in generating humanised models for CAR-T cell evaluation of targets such as CD19, to date, no reports have been published on the successful generation of humanised models of neuroblastoma (202,205). Cohn et al. reported the generation of a mouse-human neural crest chimaera as an neuroblastoma model. In this model, human neural crest cells carrying the associated genetically altered neuroblastoma oncogenes MYCN and ALK were injected into a mouse embryo (230). This resulted in the

development of human neuroblastoma in immunocompetent mice, which had more heterogeneous cell populations resembling the primary tumours observed in patients with neuroblastoma (230). Developed human neuroblastoma tumours are infiltrated by mouse immune cells, resulting in a potent anti-tumour host response (230). However, tumours have been found to exert immunosuppressive effects, such as promoting Treg infiltration and expressing immunosuppressive molecules such as PD-L1, as immunoevasion methods (230).

1.8 Radiotherapy

1.8.1 History of Radiotherapy

The use of ionising radiation in cancer treatment dates back to the 19th century, soon after the description of X-rays by Wilhelm Conrad Roentgen in 1895 (231). Following this discovery, the use of X-rays in cancer treatment was shortly followed by clinical reports of treatment success for cancers ranging from gastric carcinoma to skin cancers and sarcomas (231). However, the limited penetration of these early X-rays limited their curative success in most tumours.

Following the discovery of X-rays, the field of radiotherapy grew exponentially by the end of the 19th century with the discovery of radium by Marie and Pierre Curie in 1898, and into the 20th century, Antoine-Henri Becquerel discovered that uranium salts emitted radioactivity (231). This led to the notion that radioactive elements could be used to treat cancers, which in turn led to the advent of internal radiation therapy or brachytherapy. Brachytherapy causes less damage to the skin and surrounding tissues and better penetration into the tumour than externally applied X-rays. The subsequent use of radium was expedited for oncology; however, the hazards of radioactivity were slow to gain worldwide traction, with known examples of radiation toxicity such as the death of Marie Curie and her daughter Irene from secondary haematopoietic disorders due to radiation poisoning (231).

In the modern age, the field of radiation oncology has developed significantly, serving as a cornerstone in cancer treatment (231). X-rays, gamma rays, and charged particles are widely used in cancer treatment (232). The mode of delivery may also differ between external beam therapy, brachytherapy, and systemic radiation therapy using radioactive substances (232).

1.8.2 Radiotherapy dose-fractionation

Radiotherapy aims to kill cancer cells while limiting damage to surrounding normal tissues. The doses of radiotherapy used to treat cancers vary greatly, from 20-50 Gy in childhood cancers to 60–80 Gy in adult cancers, such as prostate cancer (233–235). Considering this large range of radiation dose, if patients were to receive this one large dose, this would lead to substantial damage to the surrounding tissues and risk of life for the patient. However, if the total dose the patient receives is divided into smaller doses given over time, then normal tissues can recover between doses, while cancer cells are found to recover less quickly and die. As a result, fractionated radiotherapy has become standard clinical practice (236,237).

The process of dividing the total dose into smaller doses is known as dose fractionation, where each small dose provided by the total dose is referred to as a fraction. The dose of radiotherapy is measured in gray units (Gy), with one Gy representing the absorption of one joule of ionising radiation per kilogram of matter (238). In addition to determining the dose fractionation for treatment, the time between fractions is also important, as cancer cells may recover and repopulate quickly if radiotherapy is not delivered within sufficient time (239). Additionally, the time between fraction delivery must ensure that while cancer cells do not recover, normal cells do so (73). As a result, a major challenge in utilising RT in the clinic is determining the optimal total dose, dose per fraction, and treatment time that is optimal for cancer treatment efficacy.

1.8.3 The Six “R’s” of Radiotherapy

The effective use of radiotherapy for cancer treatment, especially concerning fractionation, is defined by the guiding principles known as the “R’s” of radiotherapy (Figure 1.5). These principles emphasise the key factors that need to be considered when determining the optimal treatment plan for the patient. Five “R’s” were initially proposed: repair, repopulation, reoxygenation, reassortment, and radiosensitivity (240,241). Moreover, a sixth “R” has been proposed: reactivation of the host immune response (242).

First, repair refers to the ability of irradiated cells to recover from radiation-induced DNA damage, which is central to the way RT works (see Section 1.8.6) (240,241). Repopulation refers to the ability of cells to recover and proliferate between fractionation doses (240,241). Third, reoxygenation refers to how radiosensitivity increases in well-oxygenated tissues, with radiotherapy found to kill cells that are well-oxygenated most effectively (240,241). Fourth,

reassortment refers to how the cell stage during the cell cycle affects radiosensitivity. Cells undergoing mitosis are the most radiosensitive, whereas cells in S phase are radioresistant (240,241). With multiple doses, the ability of radiation to kill more cells increases as the cells progress through the cell cycle. Fifth, radiosensitivity refers to how the response to radiation differs based on tumour cell heterogeneity and thus helps to determine which tumours would show therapeutic benefit with radiation (240,241). Owing to the growing number of reports on how radiation induces immunogenicity, a sixth R of radiotherapy, which reactivates the host immune response has been proposed (242). The efficacy of radiation is influenced by the potency of the anti-tumour immune response induced by radiation (discussed in further detail in Section 1.8.7). Therefore, it is important to consider the effect of the radiation regimen utilised in the clinic on the induced anti-tumour immune response and its effect on therapeutic efficacy.

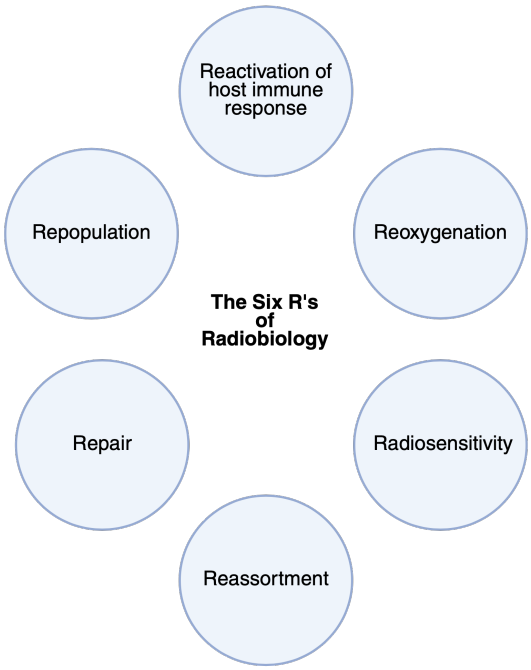

Figure 1.5 The Six R's of Radiotherapy

The effective use of radiotherapy in cancer treatment is defined by six guiding principles which need to be considered to determine the optimal treatment plan for patients.

1.8.4 Paediatric Radiotherapy

Advances in planning systems, imaging tools, and protocols for radiation treatment have broadened the techniques for delivering radiotherapy in a more targeted format across

different delivery modes, as mentioned above. Historically, radiotherapy has focused on adult cancer treatments; it has also become an important standard of care for the treatment of childhood cancers. Great achievements have empowered the use of radiotherapy for childhood cancers. In 1919, Dr. Harvey Cushing pioneered the use of postoperative radiotherapy for medulloblastoma (243). This was followed by the recognition of the need for craniospinal irradiation in medulloblastoma (244). RT is the standard treatment for paediatric cancers, with approximately one-third of paediatric cancer patients receiving radiotherapy (245). However, the use of RT varies based on tumour type and risk category.

Compared to the treatment of adult cancers, the use of RT in children requires additional measures to be considered. Examples include interventions required to obtain guardian consent by addressing parental fear and anxiety (246). Reproducible delivery of RT to the child is dependent on the child's willingness to cooperate with treatment or to be anaesthetised and immobilised during treatment. This may be done using immobilisation techniques such as playing music during treatment to soothe the child (246).

1.8.5 RT use in neuroblastoma

Historically, RT has been a widely used treatment for neuroblastoma, with studies in the early 1990s showing the benefit of RT in providing tumour control in high-risk neuroblastoma due to the tumour cells being radiosensitive (247). However, the occurrence of late toxicities observed with treatment, including growth and developmental failures, has since diminished its use from 60% in 1973-1976 to 25% in 2005-2008 (245,248).

External Beam radiotherapy (EBRT) is an important component in the treatment of neuroblastoma, with its use now typically focusing on the treatment of any residual primary tumour present after surgical resection and any metastatic sites that persist after chemotherapy for high-risk neuroblastoma (249). Several studies have confirmed that the use of RT in neuroblastoma is beneficial for local disease control and the prevention of relapse (249–254). Effective local disease control was seen by Gatcombe et al. in 34 high-risk neuroblastoma patients who underwent radiation dose escalation between 2001-2007 (253). The total dose that was used in these patients ranged between 21-24Gy at 1.5-1.8 Gy per day after induction chemotherapy and surgery and revealed excellent local disease control with a 3-year local control rate of 94% (253).

Casey et al. reported effective local disease control in 246 high-risk neuroblastoma patients that received a total dose of 21Gy (1.5Gy twice per day) to the primary tumour between 2000-2014 (254). This RT regimen reduced local relapse rates to 7.1% and 9.8% at two and five years post treatment, respectively (254). These studies have shown that RT can provide therapeutic benefits to high-risk neuroblastoma patients at a dose of ≥ 21 Gy at the primary tumour to produce favourable disease control outcomes. This is also in line with the dose recommended by the International Society of Pediatric Oncology-Pediatric Oncology in Developing Countries (SIOP-PODC) of 21Gy for both the primary tumour and residual bone metastases at the end of consolidation therapy (255). However, it is important to note that this proposal of a fixed dose (21Gy) for all patients is not a consensus across the field, with proposals of higher doses (36-40Gy) for patients with residual disease only and a two-part treatment in which 21Gy is delivered before tumour resection, followed by another course of RT (up to 36Gy) to target the residual tumour (256).

Previously, RT treatment regimens included total body irradiation (TBI), which was shown to cause serious toxicities later on, resulting in limited use in neuroblastoma treatment; largely now the focus is on the use of external beam therapy. The advances made in RT techniques have opened an avenue for the greater use of RT within neuroblastoma treatment in providing more targeted doses to the tumour while reducing RT exposure to normal tissues and subsequent treatment toxicity.

1.8.5.1 Intensity Modulated Radiation Therapy

Intensity modulated radiation therapy (IMRT) is a radiotherapy technique that, with the aid of computer programs, calculates and delivers radiation directly to the tumour from different angles due to the ability of a radiation beam to be separated into multiple smaller beams (257). This provides patients with the ability to receive higher radiation doses that more effectively target cancer cells while limiting radiation damage to surrounding healthy tissues and organs. The use of IMRT in neuroblastoma treatment has been shown to improve the distribution of the radiation dose provided and protect surrounding organs more effectively than conformal 3D dimensional based RT (252,258).

1.8.5.2 Proton Therapy

Proton therapy (PT) is a recently developed radiation therapy modality which utilises protons rather than traditional photon-based radiation, such as X-rays and γ-radiation (259). A comparison between PT and IMRT in high-risk neuroblastoma patients treated between 2005-2010 by Hattangadi et al. showed that, while IMRT and PT showed comparable targeting of the tumour, PT was more effective in sparing the surrounding normal tissue (260). Moreover, 45 high-risk neuroblastoma patients retrospectively studied by Hill-Kayser et al., who between 2010-2015 received PT to the primary tumour or metastatic sites, saw a 5-year local disease control of up to 97% and a 5-year survival rate of up to 80% without any long-term hepatic or renal toxicity (261). A similar study by Bagley et al. revealed that 18 high-risk neuroblastoma patients treated with PT had a 5-year local disease control rate of 87% and a 5-year overall survival rate of 94% (262).

1.8.5.3 Metaiodobenzylguanidine

Metaiodobenzylguanidine (MIBG) has become a staple for neuroblastoma diagnosis and therapy. MIBG is a functional analogue of the neurotransmitter noradrenaline with high affinity and specificity for the noradrenaline transporter (NET) (263,264). As neuroblastoma originates from the sympathoadrenal cells of the adrenal medulla and the sympathetic nervous system, neuroblastoma tumours express NET receptors and are naturally expressed in the developed sympathetic nervous system throughout the body (263,264). MIBG can utilise these NET receptors, allowing them to accumulate in neuroblastoma tumours and other normal tissues expressing NET receptors when labelled with radioisotopes such as Iodine-123 (^{123}I) and Iodine-131 (^{131}I) (265–267).

MIBG was originally developed in 1980 for imaging of adrenal medullary tissues and tumours associated with it, such as pheochromocytoma (268–270). However, by 1984, it was shown to be an effective imaging modality for neuroblastoma (266,267). MIBG's ability to be labelled with ^{123}I has established its use in becoming essential for radionucleotide diagnostic imaging in neuroblastoma from initial diagnosis, assessing treatment response and monitoring for disease progression or recurrence, with over 90% of neuroblastoma tumours exhibiting visible uptake of MIBG (263). The use of MIBG treatment allows a more concentrated dose of radiation to be delivered with limited toxicity to surrounding tissues compared with the use of EBRT (263). For non-MIBG-avid tumours, alternative nucleotide imaging techniques, such

as fluorine 18 (18F) and technetium 99m-methylene diphosphonate (99mTc-MDP), are used (271).

MIBG is also found to be radiolabelled with ^{131}I and shown to be of therapeutic benefit for patients with refractory or relapsed and high-risk neuroblastoma. A phase II trial of ^{131}I-MIBG treatment in 164 patients with refractory neuroblastoma showed an overall response rate of 36% (272). Moreover, it helped identify additional patients who would benefit most from ^{131}I-MIBG treatment based on age, previous treatment history, and disease being local to only soft tissue or bone marrow (272). Additional studies have evaluated the therapeutic benefits of multiple doses of ^{131}I-MIBG. This is because single-dose ^{131}I-MIBG treatment was found to be dose dependent, suggesting that multiple doses of ^{131}I-MIBG may increase the tolerated dose in the patient while still reducing side effects and maximising therapeutic benefit (264). Several studies have shown that multiple doses of ^{131}I-MIBG have the highest response rate with the first dose, which then varies with subsequent doses, with an overall response rate of up to 39% (273–275). Thus, it is still unclear whether high-risk neuroblastoma patients would benefit more from the use of multiple doses of ^{131}I-MIBG than from a single dose.

Due to the variable response observed with ^{131}I-MIBG as a monotherapy, studies have also looked at increasing therapeutic benefits in combination with chemotherapy regimens and AHSCT. It has been reported that the use of ^{131}I-MIBG in combination with cisplatin, cyclophosphamide, topotecan, and melphalan has shown varying clinical response rates from 27% to 80%, with side effects reported to be similar to that of chemotherapy treatment alone (264). A phase II study of 50 patients evaluated the use of ^{131}I-MIBG in combination therapy that included carboplatin, etoposide, melphalan (CEM), AHSCT, and EBRT. Even with this aggressive therapy regimen, the response rate was 10% in patients with refractory and relapsed neuroblastoma disease, with a 20% 3-year event-free survival (EFS) (276). Moreover, a higher response rate was observed in patients who underwent this treatment after showing a response to induction therapy (276). This potentially suggests that ^{131}I-MIBG may be more effective as early treatment in high-risk neuroblastoma compared to being utilised at the end as salvage therapy after poor response to prior treatment. A high response rate was observed with ^{131}I-MIBG treatment before chemotherapy in treatment-naïve patients with high-risk neuroblastoma, suggesting that the early use of 131I-MIBG may have a greater effect on disease control (277,278).

1.8.6 The Biological Effects of Radiation

Radiation therapy uses low and high linear energy transfer (LET) radiation to kill cancer cells while minimising off-target effects and toxicity. LET is a unit of measurement that describes the energy transmitted by a radiation source to tissues as it passes through (279). X-rays and gamma rays are examples of low LET radiation, which are widely used in cancer treatment and lead to relatively less biological damage, especially to the surrounding normal tissues, compared to high LET radiation, such as alpha particles and heavy ions, such as carbon (279,280). Therefore, low LETs radiation continues to be the most commonly used treatment for cancer because high LET radiation can lead to lower cell survival and long-term health risks by inducing greater genomic instability and significant inflammatory responses (281). In addition to LET, the effectiveness of radiation therapy depends on the total dose, dose fractionation, and radiosensitivity of the targeted cancer. Thus, the use of this therapy differs greatly across the field of radio-oncology (279).

Radiation induces DNA damage through double- and single-strand DNA breaks, leading to cell death if not repaired. This occurs either through the direct induction of DNA breaks or indirectly via cell stress, resulting in the release of free radicals, which subsequently cause DNA damage (279). For low LETs such as gamma rays, cell death is mostly induced via indirect effects. Compared to normal cells, cancer cells have compromised DNA repair mechanisms due to genetic instability and thus are less able to repair DNA breaks in response to radiation, leading to cell death (282,283). Moreover, the ability of ionising radiation to induce additional chromosomal instability increases cancer cell sensitisation, which may lead to cell death (284).

The downstream effects of radiation on DNA damage influence its therapeutic efficacy based on the type of induced cell death and its downstream effects. Ionising radiation is commonly found to induce cell death that is programmed (apoptosis), or a product of aberrant cell division (mitotic catastrophe) (285). Ionising radiation may cause other types of cell death. First, necrosis may occur, in which cell swelling occurs because of breakdown of the cell membrane (285). Second, senescence may occur, in which cell cycle arrest occurs with cells remaining viable but unable to proliferate (285). Finally, autophagy occurs in the form of cellular self-digestion via autophagic/lysosomal compartments of the cell (285).

1.8.7 Radiation induces immunogenicity

In 1979, radiation was reported to activate the immune response, in which the anti-tumour response to radiotherapy diminished in the absence of T-cells in a murine fibrosarcoma model (286). Over the last two decades, it has been clarified that the effects of radiation on inducing cell death are not the only mechanisms in achieving treatment efficacy. The ability of radiation to induce an anti-tumour immune response not only at the local irradiated site but also at non-irradiated distant lesions (the abscopal effect) indicates that radiation has multifaceted effects (287,288).

Extensive preclinical studies have demonstrated that oxidative stressors, such as reactive oxygen species (ROS) generated by radiation, can induce an endoplasmic reticulum (ER) stress response that can induce a regulated form of cell death known as Immunogenic Cell Death (ICD), which results in the activation of the immune response (289–291). ICD is induced not only by radiotherapy but also by certain chemotherapeutic agents, oncolytic viruses, among others (292,293). ICD induction occurs via certain cell death pathways known to elicit immunogenicity (Apoptosis, Necroptosis and Pyroptosis) (294,295). However, not all anticancer therapies induce cell death that elicits ICD. There is evidence that radiotherapy can elicit cell death, such as apoptosis, in an immunogenic manner, resulting in ICD induction (296). When cells succumb to ICD in response to radiation, this is characterised by the release of key danger-associated molecular patterns (DAMPs) that lead to the subsequent activation of the anti-tumour immune response, as shown in Figure 1.6.

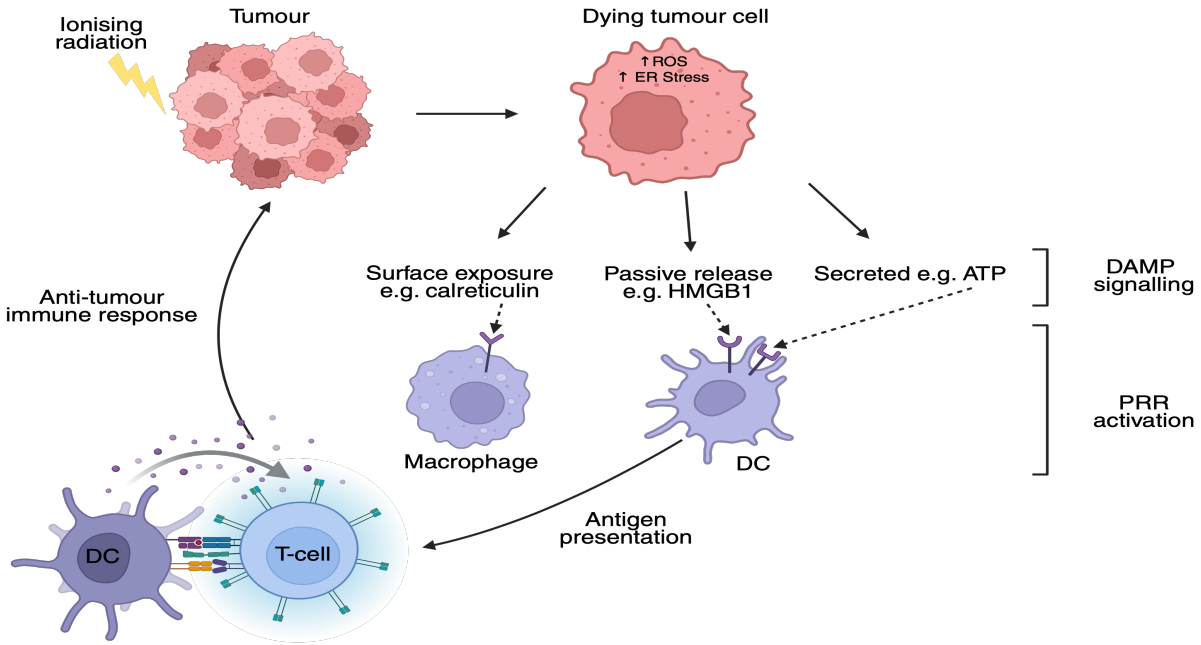

Figure 1.6 Immune mediated effects of radiation

Radiotherapy leads to cell death in tumour cells, in which cell stress occurs, mediated by increased levels of reactive oxygen species (ROS) and endoplasmic reticulum (ER) stress. This, in turn, leads to the release of danger associated molecular patterns (DAMPs) that can lead to immunogenic cell death (ICD). Key DAMPs implicated in ICD include those expressed on the cell surface (e.g. calreticulin), passively released (e.g. HMGB1) or secreted (e.g. ATP) by the dying tumour cells. These DAMPs signal through multiple pattern recognition receptors (PRRs) on innate cells such as macrophages and DCs, which in turn leads to T-cell activation and induces an anti-tumour immune response.

1.8.7.1 Calreticulin

In the pre-apoptotic stage, tumour cells are found to expose calreticulin (CRT) on the plasma membrane. CRT is a soluble protein found in the ER lumen that serves many functions, including chaperone activity, regulation of calcium homeostasis, signalling, and antigen loading on major histocompatibility complex (MHC) class I molecules. CRT serves as an “eat me” signal through its interaction with CD91 receptors expressed on phagocytes, thus allowing dead cells to be engulfed efficiently (295). CRT exposure on the cell surface allows the uptake of cancer cells by dendritic cells (DCs), thus allowing subsequent tumour antigen cross-presentation, leading to the activation of T-cell specific anti-tumour responses (297,298).

1.8.7.2 ATP

During ICD, the release of extracellular ATP (EC-ATP) from dying cells has multiple functions (293). Upon binding ATP to the purinergic metabotropic receptor P2RY2, ATP acts as a chemoattractant, resulting in the recruitment of antigen-presenting cells (APCs), which aids in the activation of the anti-tumour immune response (299). In parallel, ATP interacts with the P2RX7 receptor expressed on APCs, resulting in the activation of these innate myeloid cells and the promotion of a pro-inflammatory innate immune response by activation of the NLRP3 inflammasome and, in turn, secretion of the pro-inflammatory cytokine IL-1β (300).

It has been noted that the effects of ATP through P2RY2 and P2RX7 receptors can be compromised in the presence of overexpression of ectonucleotides CD39 and CD73, which degrade EC-ATP (301). As the immunogenicity of ATP is dependent on the induction of autophagy, followed by its release during apoptosis, the depletion of autophagy factors, such as ATG5 and ATG7, can become limiting factors for ATP's immune-mediated effects in ICD (302,303).

1.8.7.3 HMGB1

The passive release of the non-histone chromatin-binding nuclear protein, high mobility group box 1 (HMGB1), is also a key hallmark of ICD. The post-apoptotic release of HMGB1 has been found to have various immunostimulatory effects through its binding to innate Toll-like receptors (TLRs). HMGB1 binding to TLR4 expressed on DCs stimulates efficient antigen processing and cross-presentation of tumour antigens from dying cancer cells (300,304). Using HMGB1-depleted tumour cells or HMGB1 depletion by antibodies in a tumour vaccination mouse model compromised the ability of the mice to resist tumourigenesis. Moreover, breast cancer patients with the TLR4 loss-of-function allele, which prevents HMGB1 from binding to TLR4, are more prone to relapse after radiotherapy or chemotherapy (304). HMGB1 may also potentially synergise with ATP to induce the release of the pro-inflammatory cytokine IL-1β by DCs, and depletion of HMGB1 by antibody treatment abrogates the ability of DCs to produce IL-1β in response to dying tumour cells (300).

1.8.7.4 Other Notable DAMPs

Other DAMPs have also been implicated in ICD, including exposure to Heat Shock Proteins (HSPs) and Type I IFN production by dying cells. HSPs are highly conserved proteins that function as chaperones for other cellular proteins (305). Exposure to HSPs, such as HSP90 and HSP70, during cell death has been found to increase tumour cell immunogenicity and aid tumour clearance *in vivo* (295,306). In RT-induced ICD, type I Interferons (IFNs) released by dying cancer cells have been reported to occur via the cGAS/STING pathway in response to mitochondrial DNA (mtDNA) release (307,308). This release of Type I IFNs was found to aid in DC maturation and upregulation of MHC-I molecules on DCs for subsequent cross-presentation of tumour antigens for T-cell activation for the anti-tumour response (309,310). Type I IFNs also have additional broad immunostimulatory effects, such as stimulating the expression and release of IFN-stimulated genes and signalling through its cognate IFN-α and IFN-β receptors on cancer cells (311).

1.8.8 Radiotherapy's effect on the TME

The TME of solid tumours, such as neuroblastoma, is known to aid immune evasion of cancer cells due to the development of immunosuppressive mechanisms. These features of immunosuppression occur in response to adaptations to genomic stressors, such as reactive oxygen species (ROS) generated by RT. This, in turn, allows for the inhibition of anti-tumour immunity within the TME. Below are just a few examples of the effects of RT on the TME.

Immunosuppressive TMEs are found to exhibit hypoxia. This is a condition in which the oxygen demand is greater than its availability within the TME and is considered a key hallmark of cancer. Although hypoxia is detrimental to both normal and cancer cells, cancer cells have evolved through genetic changes and adaptations to survive and thrive in such an environment. Radiation exposure induces the expression of transcription factor hypoxia-inducible factor-1 alpha (HIF-1α), which is critical for regulating hypoxic responses in cells (312). Under normal oxygen conditions, HIF-1α is degraded. However, under hypoxic conditions, it translocates to the nucleus and induces gene expression, which promotes angiogenesis, metabolic adaptation, and cell survival (313,314). Additionally, HIF-1α has been found to promote the production of immunosuppressive cells such as Tregs, MDSCs, and disabled DCs within the TME (315–317). HIF-1α also inhibits the intracellular adenosine kinase, which prevents the rephosphorylation of adenosine to AMP, leading to increased

levels of intracellular adenosine. Hypoxic tumours are characterised by increased levels of adenosine and the expression of ectonucleotidases CD39 and CD73, which are involved in the conversion of adenosine from ATP/ADP (318,319). This adenosine accumulation within the TME leads to negative regulation of the anti-tumour immune response (301,318–320). Adenosine induction by RT may not be performed through HIF-1α but also directly, as shown in preclinical breast cancer models (321).

Within the TME, a major cell type is CAFs, which can influence the treatment response of the tumour due to their crosstalk with both cancer and immune cells. These interactions between CAFs and tumour cells have been shown to drive tumour progression, whereas interactions with immune cells, such as NK cells, have been found to reduce NK-mediated killing of cancer cells (322,323). CAFs are radioresistant and express FAP in response to RT (324). FAP expression is not limited to CAFs but can also be found in tumour cells and is a membrane peptidase that is involved in extracellular matrix remodelling (325). FAP-expressing CAFs have been found to promote immunosuppression, which may inhibit T cell-mediated cytotoxicity within the TME (326).

Transforming growth factor beta (TGF-β), a member of the TGF-β superfamily, is a well-characterised cytokine that acts as both a tumour suppressor and promoter in the TME (327). TGF-β is an important immunosuppressive cytokine secreted into the TME in its inactive form, which is transformed into its active form via proteolytic processing, thereby enabling its effects upon binding to its cognate receptor (328). RT-induced ROS production has been reported to result in the activation of TGF-β from its inactive form and to mediate immunosuppression, which diminishes the anti-tumour immune response and thus contributes to tumour progression (329–331). The combination of RT and TGF-β blockade has been shown to reverse immunosuppression and bolster systemic immunity at both irradiated and distant metastatic sites in preclinical breast cancer models (332).

1.9 Irradiation and Immunotherapy

While RT has been found to induce ICD, it is important to note that the occurrence of ICD and its corresponding immunogenicity based on released DAMPs can differ greatly owing to differences in radiation modality and dosing schedule, including both the dose and occurrence of fractionation (333). Additionally, the type and progression stage of the tumour being treated impacts the TME and thus the immunogenicity of the anti-tumour response that may occur following RT, with reports of both immunosuppressive and immunostimulatory

effects induced by RT on the TME (334). Therefore, one strategy for enhancing RT's immunostimulatory effects of RT is to use it in combination with other therapeutic modalities such as immunotherapy (IT), which has been of great interest. Additionally, the immunostimulatory effects induced by RT aid in more effective T-cell infiltration into the TME, which is required for the optimal efficacy of immunotherapeutic agents.

1.9.1 ICB-RT Combination

One of the first experimentally tested IT-RT combinations was the use of anti-cytotoxic T-lymphocyte associated protein 4 (anti-CTLA-4) in combination with RT in a 4T1 mouse mammary carcinoma model (335). A single 12Gy dose was found to delay tumour growth in the presence or absence of the anti-CTLA4 antibody 9H10 (335). However, RT in combination with 9H10 significantly increased survival by inhibiting $CD8^+$ T cell-mediated lung metastasis (335). Clinical translation of anti-CTLA4 in combination with RT in patients with melanoma and NSCLC has shown clinical benefits (336,337). It is important to note that the synergistic effect of IT and RT is influenced by the optimisation of the radiation regimen used. The use of fractionated (8Gy x 3) and not a single dose (20Gy x 1) RT was found to optimally synergise with immune checkpoint blockade (ICB) to enhance the anti-tumour response and induce an immune-mediated abscopal effect in a TS/A mouse breast carcinoma model (338). A combination of RT with other ICB agents, including PD-1 or PD-L1, has also been assessed and shown preclinical and clinical efficacy (339–342). Additionally, multiple IT agents have been clinically investigated in combination with RT for various types of cancers (343).

1.9.2 ACT-RT Combination

The potential of using RT in combination with ACT is that RT can help promote a pro-inflammatory TME that may enhance ACT infiltration into the TME and allow it to function and persist. ACT therapy options include tumour-infiltrating lymphocytes (TILs), engineered T cell receptors (TCR-T), and CAR-T cells.

Preclinical and clinical studies have shown that preconditioning regimens encompassing chemotherapy and/or RT increase engraftment, persistence, and functionality of TILs (344–346). TBI before treatment with ACT has been shown to promote TME changes, such as immune cell extravasation that promotes tumour recognition by naive T-cells and by tumour-specific TCR-T-cells (345,347,348). However, lymphocyte extravasation promoted by TBI

may lead to dysregulation of donor-derived T-cell trafficking, leading to potential off-target effects that promote graft-versus-host disease (GVHD) (349). It is important to note that TIL follow-up studies in patients have shown that the use of TBI as a preconditioning regimen did not increase the complete response rate or overall survival, but was found to introduce clinical toxicity compared to the use of a chemotherapeutic-based preconditioning regimen for successful adoptive transfer (345,350). Therefore, the use of TBI as a conditioning therapy before TIL therapy should be considered with caution.

1.9.3 CAR-RT Combination

The use of RT in combination with CAR-T cells is an emerging interest, and a growing number of studies have investigated this combination both preclinically and clinically (351,352). One of the earliest studies examining CAR-T cells in combination with RT against cancer was conducted by Weiss et al. in 2018 (143). The authors previously reported the upregulation of NKG2D in gliomas upon radiation and investigated the use of local RT in orthotopic glioblastoma models positive for NKG2D using anti-NKG2D mouse CAR-T cells (353,354). Seven days after tumour implantation, a single dose of 4Gy was delivered locally to the tumour, followed by anti-NKG2D CAR-T cell injections on days five, seven and ten after tumour implantation (353). RT alone did not improve the patient survival. However, in the combination treatment group, RT increased anti-NKG2D CAR-T cell activity, with prolonged survival, reduced tumour volume, and increased long-term survival (353). The proposed mechanism for this enhanced CAR activity *in vitro* is that prior irradiation of glioma cells followed by subsequent co-culture with CAR-T cells results in increased cytolysis and IFN-γ production (353). Additionally, they observed increased IFN-γ expression in tumour-infiltrating CAR-T cells *in vivo* (353).

In immunocompetent mouse glioblastoma models, the use of a single 5 Gy whole-body radiation (WBI) before treatment with anti-GD2 CAR-T cells enhanced the anti-tumour response and survival compared to CAR-T cell treatment alone (355). Subsequent tumour rechallenge in surviving mice revealed that only mice treated with WBI and GD2 CAR-T cells were able to suppress tumour growth, suggesting the formation of antigen-specific T-cell memory (355). Moreover, the use of focal 5Gy radiation at the tumour, followed by GD2 CAR-T cell infusion, resulted in a complete anti-tumour response compared to CAR-T cell treatment alone (355). This curative anti-tumour effect was not evident with CAR-T cell infusion, followed by WBI (355). Through the use of high-resolution intravital imaging (IVM),

the authors concluded that the success of this combination therapy is aided by RT inducing CAR-T cell accumulation and extravasation from the vasculature throughout the tumour stroma, thus promoting rapid CAR-T cell proliferation and sustained CAR response within the TME (355). The use of focal RT in combination with CAR-T cells showing therapeutic efficacy also suggests that potential lymphodepletion performed through WBI or chemical induction before CAR-T cell infusion may not be needed, and thus does not compromise the therapeutic effect of CAR-T cell functionality (355).

In a sialyl Lewis-A^{+} (sLeA^{+}) pancreatic mouse model, DeSelm et al. reported that the use of a single low dose of 2Gy RT was able to sensitise tumour cells to CAR therapy, and this combination therapy upregulated the sensitivity of both sLeA^{+} and sLeA^{-} tumour cells to TRAIL-mediated death (356). RNA sequencing analysis revealed that anti-sLeA CAR-T cells produce TRAIL upon engagement by sLeA^{+} tumour cells and, in turn, remove sLeA^{-} tumour cells in a TRAIL-dependent manner due to priming by RT (356). Considering that heterogeneity in antigen expression hinders CAR-T cell success, RT allows for tumour sensitisation and enables CAR-T cells to mitigate the escape of antigen-negative tumour cells (356). The mechanism by which RT promotes tumour sensitisation to CAR-T cells may involve the activation of both innate and adaptive immunity (such as CD4^{+} effector T cells), with NKG2D expressing immune cells involved in tumour control and, in turn, turning the TME more proinflammatory for CAR-T cell infiltration (357). Both the use of systemic and localised RT was found to sensitise the tumour to CAR-T cell killing and lead to an overall similar anti-tumour response. This suggests that this combination therapy may clinically provide the opportunity to use RT to sensitise local and systemic diseases that show varied antigen heterogeneity (356). However, it is important to note that the preclinical mouse model utilised NSG mice with human CAR-T cells; thus, it is unclear whether these findings are applicable in the presence of an intact immune system with the use of mouse CAR-T cells.

Clinical reports have described the use of RT as a bridging therapy before CAR-T cell infusion (351). Patients with relapsed/refractory diffuse large B-cell lymphoma (DLBCL) underwent bridging radiation treatment before receiving anti-CD19 CAR-T cells (Axicabtagene ciloleucel) (358). Bridging radiation treatment consisted of receiving 2-4Gy per session, with a median total dose of up to 20Gy (total dose range- 6-36.5Gy) (358). A subset of patients received concurrent chemotherapy (fludarabine/cyclophosphamide) (358). The results of this study suggest that RT provides sufficient disease control with no disease progression before CAR-T cell infusion (358). Moreover, RT did not reveal any obvious toxicity after CAR treatment, with 27% of the patients developing cytokine release syndrome (CRS) (358). Other clinical

studies have reported the use of RT as a bridging treatment before CAR-T cell therapy to improve clinical outcomes, including a reduction in tumour load, treatment toxicity, and improvement in the curative effect of CAR therapy (351).

The limited studies published thus far have shown that the use of RT to improve CAR-T cell efficacy in cancer treatment is promising. However, radiation dose, fractionation, and timing are important parameters to optimise to enhance CAR-T cell efficacy. Most studies published thus far have largely focused on adult cancer. Thus, there is a greater need to determine if this combination therapy is effective in childhood solid tumours, such as neuroblastoma.

1.10 RT in combination with CAR-T cell against neuroblastoma

To date, there has been limited work within the field that has looked at CAR-T cells in combination with RT against neuroblastoma.

In 2023, Sodji et al. evaluated *the in vitro* effects of radiation on the viability and functionality of anti-GD2 human CAR-T cells (359). Low doses of 1-6Gy of the radionucleotides actinium-225 (^{225}Ac) or lutetium177 (^{177}Lu) resulted in dose-dependent anti-GD2 CAR-T cell death with both radionucleotides, and ^{177}Lu was found to be less cytotoxic than ^{225}Ac (359). The radiation delivered by these radionucleotides was found to enhance the cytotoxic activity of anti-GD2 CAR-T cells against GD2 expressing human neuroblastoma line, CHLA-20, compared to non-irradiated GD2 CAR-T cells (359). Moreover, radiation-induced enhancement of GD2 CAR-T cells did not affect the expression of exhaustion (PD-1) or activation markers (CD69 and NKG2D) (359). These results suggested that targeted radiation provided by radionucleotides may enhance CAR activity in a dose-dependent manner (359).

In 2024, Sodji et al. built upon their previous work by utilising the radionucleotide ^{177}Lu to evaluate the effect of low dose radiation on anti-GD2 CAR-T cells in a model of localised neuroblastoma in immunodeficient NRG mice (360). Tumour-bearing mice received a low dose of radiation (1.8Gy or 3.6Gy) delivered by ^{177}Lu followed by anti-GD2 CAR-T cell infusions nine days later (360). A low dose of either 1.8Gy or 3.6Gy in combination with anti-GD2 CAR infusion resulted in a robust treatment response with survival greater than that seen with CAR-T or radiation treatment alone groups (360). Use of 1.8Gy within the combination treatment compared to 3.6Gy produced 100% response rate with the former dose compared to 62.5% with the latter dose (360). Their results suggest that the delivery of RT before CAR

treatment enhances T-cell infiltration, with 1.8Gy tumour irradiation improving the infiltration of anti-GD2 CAR-T cells into the TME (360). *In vitro* experiments have revealed that tumour irradiation enhances the polyfunctionality of $CD8^+$ anti-GD2 CAR-T cells, and low-dose radiation may enhance the expression of the death receptor Fas, potentially allowing CAR-T-independent killing by GD2-CAR T-cells, thus further potentiating the anti-tumour response (360). At the time of writing, this published study has not been certified by peer review, and thus findings should be approached with caution.

Ansari et al. evaluated the use of EBRT in combination with anti-B7-H3 CAR-T cells in immunodeficient NRG neuroblastoma tumour-bearing mice in 2024 (142). The mice had either local and/or disseminated disease, with tumours in the flank receiving 5Gy, while a 1.75Gy total body irradiation dose was used to target the metastatic tumours (361). B7-H3 CAR-T cells were injected one day after the radiation treatment (361). In mice with only a single flank tumour, ERBT in combination with B7-H3 CAR-T cells resulted in a disease-free survival past 130 days compared to a median survival of 82 days in the B7-H3 CAR-T treatment alone group (361). Moreover, in mice with disseminated metastases, the combination therapy of EBRT and CAR-T cells resulted in survival for 72 days, with two mice surviving until day 103, whereas in the CAR-T alone treatment group, mice did not survive past day 42 (361). This preliminary study provides encouraging results regarding the use of radiation in combination with CAR-T cells in the treatment of neuroblastoma. However, additional studies are needed to further evaluate this and its potential in the clinical setting.

It is important to note that these studies utilised immunodeficient mice bearing human neurblastoma cell-line derived tumour models (SK-NA-S, CHLA-20 and SY5Y) (199–201). As a result, it is difficult to fully evaluate the potential of radiation in combination with CAR-T cells, knowing that an intact immune system is required for the immune-mediated effects of RT, and to evaluate the toxicity associated with CAR-T cells, considering its potential off-tumour on-target effects. As a result, it is imperative to utilise murine-based neuroblastoma models such as the TH-MYCN murine allograft models that recapitulate the characteristics of human neuroblastoma and can be utilised to evaluate treatment efficacy in immunocompetent mice.

1.11 Aims and Objectives

As detailed above, RT has great potential to overcome the major obstacles that hinder CAR-T cell success in neuroblastoma. As a result, this thesis aims to investigate the effect of radiation on CAR-T cell functionality against neuroblastoma within the context of an intact immune system, using TH-MYCN models of high-risk neuroblastoma, using mouse CAR-T cells. To achieve this, I sought to address the following aims.

1) Determination of the radiosensitivity of TH-MYCN mouse models of high-risk neuroblastoma. This will be done by developing an *in vitro* radiosensitivity screen that assesses both immune- and non-immune-mediated effects of radiation to determine the presence of radiosensitivity and its range across the screened models.

2) Evaluation of a mouse CAR candidate for use in combination with RT. This will be done by assessing the parameters of mouse CAR-T cell production that allow the *in vitro* expansion of CAR with stable expression. Moreover, I will assess the *in vitro* functionality of CAR-T cells in terms of their cytotoxicity and CAR expansion in response to the antigen.

3) Evaluation of the effect of radiation on CAR-T cell functionality. This will be done by *in vitro* evaluation of CAR-T cell functionality against irradiated TH-MYCN models of high-risk neuroblastoma by assessing the parameters of cytotoxicity and CAR expansion.

Chapter 2 Materials & Methods

2.1 Materials

Media and solutions requiring sterilisation were prepared in sterile environments or autoclaved before use.

2.1.1 Reagents

Table 2.1 Buffers and growth media for molecular biology use

Reagent	Ingredients
LB Media (1L)	10g Tryptone, 5g Yeast Extract, 5g NaCl
LB Agar (1L)	10g Tryptone, 5g Yeast Extract, 5g NaCl, 15g Agar
1xTBE Buffer (1L)	0.13M Tris base (pH 7.6), 45mM boric acid (pH 8.3) and 2.5mM EDTA

Table 2.2 Buffers for ELISA and flow cytometry use

Reagent	Ingredients
Flow Cytometry Wash buffer (0.5L)	10x PBS (0.1L), Sterile dH_2O (0.9L), 0.5% BSA (2.5g)
ELISA Wash Buffer (1L)	1x PBS (1L), 0.5% Tween 20

Table 2.3 Media and buffers for tissue culture use

Cell Line Media	Reagent	Source (Catalogue Number)	Concentration
Mouse Neurosphere Media	DMEM/F12	Gibco (31331093)	-
	Foetal Bovine Serum (FBS)	Gibco (batch dependent)	15%

	β-mercaptoethanol	Gibco (21985023)	0.05mM
	Human-Epidermal Growth Factor (h-EGF)	Peprotech (AF-100-15)	0.01µg/ml
	Human Basic Fibroblast Growth Factor (hb-FGF)	Peprotech (AF-100-18B)	0.015µg/ml
	B27	Thermofisher (17504044)	1x
	Puromycin (selection pressure for hB7-H3 and mCherry subclones)	InvivoGen (ant-pr-1)	2µg/ml
9464D Media	DMEM Glutamax	Gibco (41965039)	-
	FBS	Gibco (batch dependent)	10%
	Non-Essential Amino Acids (NEAA)	Sigma-Aldrich (M7145-100ML)	1%
	Sodium Pyruvate	Hyclone (11501871)	1mM
Complete RPMI (cRPMI)	RPMI	Sigma (R8758-500ML)	-
	FBS	Gibco (batch dependent)	10%
	L-Glutamate	Sigma (G7513)	2mM
Complete IMDM (cIMDM)	IMDM	Sigma (I3390-500ML)	-
	FBS	Gibco (batch dependent)	10%
	L-Glutamate	Sigma (G7513)	2mM
	Ammonium chloride (NH_4Cl)	213330 (Sigma)	1.5M

10x Red Blood Cell (RBC) Lysis Buffer	Sodium Bicarbonate ($NaHCO_3$)	S5761 (Sigma)	0.1M
	Ethylenediaminetetraacetic acid (EDTA)	E4884 (Sigma)	0.01M
	dH_20	-	Adjust to pH 7.4 as needed with sodium hydroxide (NaOH) or hydrochloric acid (HCl).

2.2 Methods

2.2.1 Molecular Biology Techniques

2.2.1.1 Plasmid Design

All plasmids in this thesis used the established SFG γ-retroviral vector, which is a γ-retroviral vector used widely for retroviral transduction.

SFG is a double-stranded DNA vector containing a gene of interest, which can be used for the transient or stable transfection of cell lines through the co-expression of viral packaging and envelope proteins. The vectors generated for the experiments performed within this thesis were used to transfect the HEK293-based cell packaging cell line, Phoenix Ecotropic (Phoenix Eco) (362). The Phoenix Eco cell line is a second-generation retrovirus producer cell line that expresses structural and replication proteins (Gag/Pol) and an ecotropic envelope glycoprotein (Env) specific to dividing rat and mouse cells (362,363). As a result, retrovirus production only requires the addition of the transfer plasmid containing the gene of interest (364). The retrovirus produced was used for subsequent retroviral transductions of mouse splenocytes or cell lines as required.

The SFG γ-retroviral vector contains a Moloney murine leukaemia virus (MMLV) Ψ signal peptide, required for instigating cells to package the gene of interest into viral particles (365). The plasmid also encompasses an open reading frame (ORF) downstream from a EF1α promoter, which drives expression of the gene of interest. Long terminal repeats (LTRs) are also present within the plasmid, which are essential for initiating DNA synthesis and regulating viral gene transcription (365,366). Within the constructs used, the ampicillin resistance gene

was included for the positive selection of transformed colonies grown on ampicillin-positive bacterial agar plates.

A refined version of the SFG vector has been used in this project, which has been augmented with a scaffold attachment region and a chromatin insulator to improve transgene expression (366). Figure 2.1 details the constructs used within this thesis.

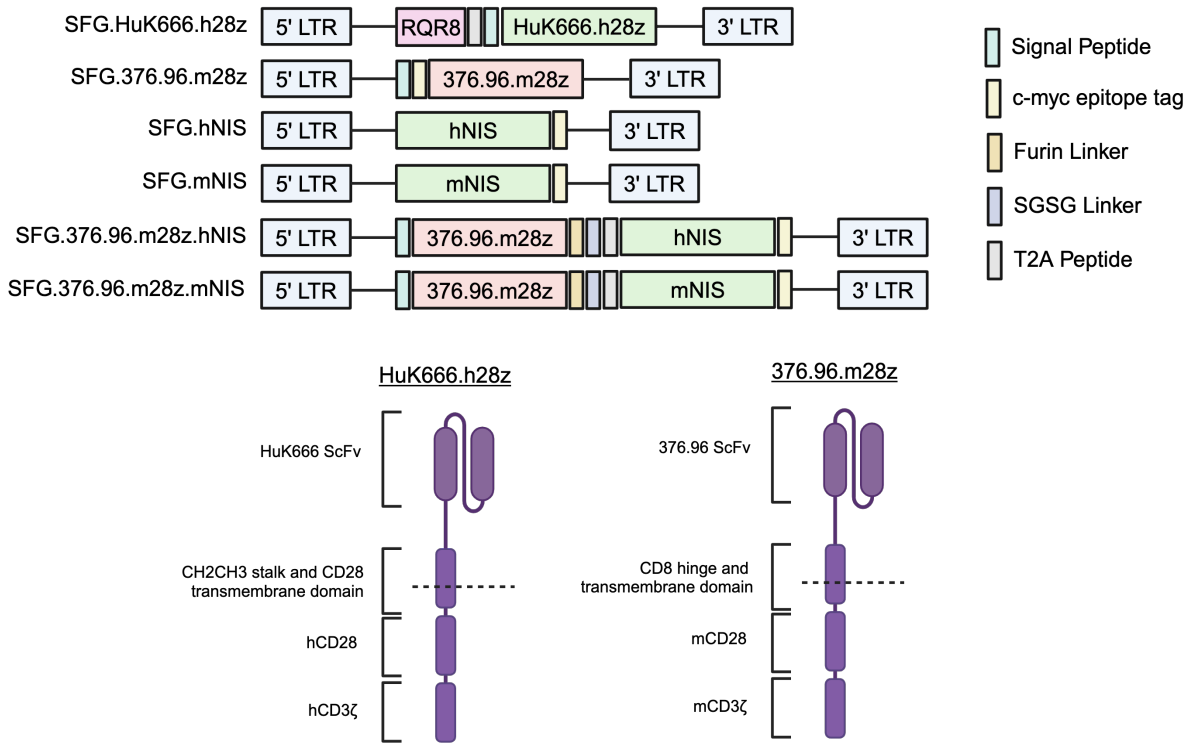

Figure 2.1 Maps of plasmid constructs

Plasmids were constructed using restriction enzymes and HiFi cloning. A schematic of the plasmid constructs and structure of the second-generation CARs, HuK666.h28z and 376.96.m28z is shown. Constructs, where shown, included signal peptide, c-myc epitope tag (EQKLISEEDL), Furin (RRKR) linker, SGSG linker and T2A peptide sequences. mNIS mouse sodium iodide symporter; hNIS human sodium iodide symporter. Figure created using Biorender.

2.2.1.1.1 GD2 CAR

The SFG.huk666GD2-hCD28tm-hCD28z (HuK666.h28z) is a second-generation CAR previously evaluated in a phase one clinical trial (NCT02761915) for patients with neuroblastoma targeting the disialoganglioside, GD2 (189) . The ORF of this construct

contains an anti-GD2 CAR and RQR8 (Figure 2.1). RQR8 is a sort/suicide gene which can be utilised to assess CAR transduction efficiency by flow cytometry (367).

2.2.1.1.2 Anti-B7H3 CAR

The SFG.376.96.mCD8STKTM.mCD28z (376.96.m28z) is a second-generation anti-B7-H3 CAR (Figure 2.1). The construct consists of the anti-B7-H3 ScFv, 376.96, with murinised CD3 and CD28 endodomains. The ScFv is derived from the anti-B7-H3 monoclonal antibody (mAb), 376.96 and has been assessed for CAR-T cell therapy within the literature and shown to be cross-reactive to human and mouse B7-H3 (1,368). A c-myc epitope tag is also within the ORF to allow CAR detection by flow cytometry.

2.2.1.1.3 NIS with a human c-myc epitope tag

An SFG γ-retroviral vector was generated encoding the CAR, the sodium iodide symporter (NIS) and a human c-myc epitope tag fused to the C-terminus sequence of the NIS (Figure 2.1).

The SFG.376.96.mCD8STKTM.mCD28z (produced by Alicia Vitali and Dr Jennifer Frosch, UCL) was used as the vector plasmid to generate these constructs. The sequence of the 376.96 CAR sequence was replaced with the human NIS (hNIS) or mouse NIS (mNIS) sequences with a c-myc epitope tag at the C-terminus end of the sequence. The intracellular epitope tag included within the constructs allows detection of the NIS, which is a type 1 transmembrane protein, resulting in the transmembrane domain on the C-terminus being intracellular (166,369).

The plasmids of mNIS and hNIS with a c-myc tag were constructed through excision of the CAR from the 376.96.m28z plasmid using MluI (ThermoFisher, #FD0564) and NcoI (ThermoFisher, #FD0574) restriction digest enzymes (see section 2.2.1.4). The larger fragment generated was then ligated with mNIS or hNIS gene blocks designed and ordered from Integrated DNA Technologies (IDT) using HiFi cloning (section 2.2.1.5).

2.2.1.1.4 anti-hB7-H3 CAR with Sodium Iodide Symporter (NIS)

The SFG.376.96.mCD8STKTM.mCD28z was also used to generate bicistronic constructs, in which the ORF contains the second generation anti-hB7-H3 CAR, 376.96.mCD28z with the mNIS or hNIS fused with an intracellular c-myc epitope tag (Figure 2.1). The two genes are separated by a furin linker, SGSG linker and 2A peptide sequence for efficient cleavage between transgenes (370).

The generation of these plasmids entailed the creation of an intermediate plasmid. This was generated through the linearisation of the 376.96.m28z plasmid with restriction digest enzymes, NcoI (ThermoFisher, #FD0574) and EcoRI (ThermoFisher, #FD0274). PCR amplification was then performed with the digested products to generate multiple amplified fragments, which were then annealed via HiFi cloning to generate this intermediate plasmid (section 2.2.1.5 for further details). This intermediate plasmid of 376.96.m28z with no c-myc tag was then digested using restriction enzymes BsgI (NEB, #R0559S) and MluI (NEB, #R3198S) (see section 2.2.1.4). The digested fragment generated was annealed with mNIS or hNIS gene blocks (IDT) using HiFi cloning (section 2.2.1.5) creating the 376.96.m28z.mNIS and 376.96.m28z.hNIS bicistronic constructs.

2.2.1.2 Cloning of the human and mouse NIS with and without 376.96.mCD28z

2.2.1.2.1 PCR amplification of SFG.376.96.mCD8STKTM.mCD28z

The SFG.376.96.mCD8STKTM.mCD28z contains a c-myc epitope tag following the signal peptide within the CAR sequence (Figure 2.1). This was removed by generating new fragments via PCR to form an intermediate plasmid, which would subsequently be used to form the 376.96 CAR with mNIS or hNIS constructs. To generate this intermediate plasmid, 376.96.m28z was linearised through the use of restriction digest enzymes, NcoI (ThermoFisher, #FD0574) and EcoRI (ThermoFisher, #FD0274) (see section 2.2.1.4). A phusion high-fidelity DNA polymerase kit (New England BioLabs, E2621S) was used for the PCR amplification reactions of SFG.376.96.mCD8STKTM.mCD28z to generate this altered vector plasmid. The PCR reactions were performed in 50µl reaction volumes containing, 2µl Phusion DNA polymerase, 10µl 5x Phusion HF buffer, 1µl 10mM dNTPs, 2.5µl 10mM forward primers, 2.5µl 10mM reverse primers, 60ng of template DNA and 29.6µl of nuclease-free

water (nf-H_20). The reaction was set up on ice and placed into the Bio-Rad T100 thermocycler. The primers and thermocycler conditions utilised are listed in Table 2.4-2.5.

Table 2.4 Primer sequences for the construction of intermediate plasmid

Template	Name	Sequences
376.96.m28z ScFv	F1	5'- GACCATCCTCTAGACTGCCAACTTC -3'
	R1	5'- CTTCCTCGAGTCCGGTACTCCCAGGCAC -3'
376.96.m28z CAR Domains	F2	5'- GAGTACCGGACTCGAGGAAGTCCAACTCGTCGAG -3'
	R2	5'- GGACTAATCCGAAACAGTATCGAACGCGTTTAGCGTG -3'
Scaffold Attachment Region to LTRs	F3	5'-CGATACTGTTTCGGATTAGTCCAATTTGTTAAAGACAGGATATCAG -3'
	R3	5'- CCCAGTCACGACGTTGTAAAACGAC -3'

Table 2.5 Phusion PCR reaction setup

PCR reaction stage	Temperature (°C)	Time (seconds)
Initial Denaturation	98	60
35 Cycles	98	10
	based on primer size	30
	72	based on PCR product size
Final extension	72	600
Hold	4	-

2.2.1.3 Purification of PCR products

PCR products were purified using a PCR and DNA clean-up kit (New England BioLabs, T1030L) under the manufacturer's instructions.

2.2.1.4 Digestion of vector plasmids and purification of digest

Vector plasmids were digested with a range of restriction enzymes at 37°C as per the manufacturer's instructions. The success of the restriction digest was confirmed by separating the digested fragments on a 1-1.5% agarose gel by gel electrophoresis to confirm expected band sizes against a 1kb DNA ladder (NEB, N3232S), or a 100bp DNA ladder (Meridian Bioscience, BIO-33056) under a UV gel imager. Required bands for downstream cloning were extracted using a scalpel and purified using Wizard SV Gel and PCR Clean-up System (Promega, A9280), following the manufacturer's instructions.

2.2.1.5 HiFi Cloning

Ligation of PCR products or digested bands with designed gene blocks (Integrated DNA Technologies) was performed using the NEBuilder HiFi DNA Assembly master mix (NEB, E2621S). The ratio of insert: vector was dependent on the number of fragments needed to assemble, and so was done following the manufacturer's guidelines for performing HiFi cloning. In line with the manufacturer's instructions, 20µl reaction volumes were used, containing digested vector and gene block as required in pmol for the reaction(s), 10µl NEBuilder HiFi DNA Assembly master mix, and nuclease-free water. The reaction tubes were then incubated in a Bio-Rad T100 thermocycler at 50°C for 15 minutes or 50 minutes for the assembly of 2-3 or 4-6 fragments, respectively.

2.2.1.6 Transformation of E.coli bacteria

Generated HiFi or plasmid DNA were used to transform competent E. coli cells through heat shock. For this process, NEB 5-alpha Competent E. coli (NEB, C2987H) stored at -70°C as single-use 50µl aliquots were

thawed on ice. To the thawed bacteria, 2µl of chilled HiFi product was added. After gently mixing, the mixture was incubated on ice for 10 minutes. The mixture was then placed in a heat block at 42°C for 30 seconds. After heat shock, a further incubation on ice was performed for 2 minutes. 250µl Super Optimal Culture (SOC) (NEB, B90205) was added to the mixture, which was then incubated for 30 minutes at 37°C and 250rpm in a bacterial shaker. After incubation, the mixture was used to streak pre-warmed ampicillin selection agar plates, which were then incubated overnight at 37°C.

2.2.1.7 Selection of bacterial colonies

The success of the bacterial transformation was confirmed by the presence of colonies on ampicillin selection agar plates. Single colonies were selected from these plates for further evaluation to confirm if the desired plasmid construct had been generated from the colonies selected.

2.2.1.8 Purification and quantification of DNA preps

Individual colonies selected from ampicillin selection plates were grown overnight in 5ml bacterial cultures containing ampicillin at 37°C and 250rpm in a bacterial shaker. Plasmid DNA was then extracted using 3ml of these overnight bacterial cultures using the miniprep plasmid purification kit (NEB, T1010S). This was done as per the manufacturer's instructions. Purified DNA was quantified using a spectrophotometer (Nanodrop ND1000) set to record dsDNA at the 260/280nm wavelength.

2.2.1.9 Plasmid Sequencing

The sequence of plasmids purified was confirmed using Sanger sequencing. Samples were prepared as required with corresponding primers and sent for sequencing to Genewiz, Azenta Life Sciences (Hope End, Takeley, Essex CM22 6TA, United Kingdom). To confirm the plasmid sequence, the sequencing files provided by Genewiz were aligned against the expected plasmid construct on SnapGene v5 (Dotmatics) to verify that the sequence of generated constructs was correct.

2.2.1.10 Large-scale plasmid preparation

Large-scale plasmid purification was performed as and when required. For midiprep, 150ml LB agar culture with ampicillin was inoculated with transformed bacteria and incubated overnight at 37°C at 250rpm in a bacterial shaker. The midiprep was purified using the NucleoBond Xtra Midi EF kit (Macherey-Ngael, 740420.50). For maxiprep, 300ml LB agar with ampicillin was inoculated with transformed bacteria and incubated overnight at 37°C at 250rpm in a bacterial shaker. The bacterial culture was purified using the NucleoBond Xtra Maxi EF kit (Macherey-Ngael, 740424.50). Both types of large-scale plasmid preparation were performed under the manufacturer's instructions. Sequences of the purified plasmids were confirmed via Sanger sequencing as detailed above in section 2.2.1.9.

2.2.2 Tissue Culture

Table 2.6 details the cell lines and culturing media used to grow the cells for subsequent *in vitro* experiments discussed within this thesis.

All mouse cell lines used except BW5 are TH-MYCN transgenic lines established from spontaneous neuroblastoma tumours cultured *ex vivo* and propagated *in vitro* to establish cell lines (213,218).

For cell culture, reagents were prewarmed to 37°C where required, before use unless otherwise stated. For *in vitro* propagation, cells were grown in appropriate volumes of cell media until the desired confluency was reached to perform subsequent passaging of cells.

Table 2.6 Cell lines used for *in vitro* experiments

Cell Line	Species Origin	Source	Culture Media
129NS1	Mouse (129/SvJ genetic background (371))	Gift from Louis Chesler (Institute of Cancer Research)	Mouse Neuropshere Media
129NS1-4B (GFP^+Luc^+)		Generated by Sophie Munnings-Tomes	

		(University College London)	
129NS1-4B hB7-H3^{+}		Generated by Farah Alam (University College London)	
TAM6		Gift from Louis Chesler (Institute of Cancer Research)	
TAM6 hB7-H3^{+} mCherry^{+}		Generated by Arika Feils & Amy Erbe-Gurel (University of Wisconsin-Madison)	
9464D WT	Mouse (C57BL/6 genetic background)	Gift from Paul Sondel (University of Wisconsin-Madison)	9464D Media
9464D hB7-H3^{+} mCherry^{+}			
9464D GD2^{+}			
BW5	Mouse (T-Cell Lymphoma on AKR/J genetic background)	ATCC (TIB-47)	cRPMI
SupT1 WT GFP^{+}Luc^{+}	Human (T-Cell Lymphoma)	Generated by Rivani Shah and Henrike Muller (University College London)	cRPMI
SupT1 hB7-H3^{+} GFP^{+}Luc^{+}			
Phoenix Eco	Human (epithelial cells)	ATCC (CRL-3214)	cIMDM
Pheonix Eco 376.96.m28z Producer Cell Line	Human (epithelial cells)	Generated by Courtney Himsworth and Carla Batiste (University College London)	

2.2.3 Preparation of cells for *in vitro* experiments

All cells were prepared as required for *in vitro* experiments into single-cell suspension. Unless otherwise stated, all centrifugation steps were performed at 300 x *g* for 5 minutes at room temperature. All dissociation steps were performed with 3-5ml of accutase or trypsin for 5 minutes at room temperature, unless otherwise stated.

2.2.3.1 129NS1 and TAM6 lines

129NS1 and TAM6 lines grow as spheroids in suspension. The cells were grown in T25-T75 cm^2 flasks until the desired confluency of 80% was reached and transferred from the flask into a 50ml falcon and centrifuged. After centrifugation, the cells underwent a PBS wash with centrifugation. After the PBS wash, cells underwent cell dissociation treatment with accutase using a p1000 single-channel pipette and then incubated as required. The accutase treatment was neutralised with neurosphere media (Table 2.3) and centrifuged. The cells were then resuspended in fresh neurosphere media using a p1000 single-channel pipette and counted via trypan blue exclusion.

2.2.3.2 9464D WT and 9464D $GD2^+$

9464D and 9464D $GD2^+$ are adherent cell lines and were grown in T175cm^2 flasks until desired 80% confluency was reached. Media was discarded from the tissue culture flasks that cells were cultured in and washed with PBS followed by cell dissociation with trypsin. 9464D media (Table 2.3) was added to neutralise trypsin, and the cell suspension was transferred into a 50ml falcon and centrifuged. After centrifugation, the cell pellet was resuspended in 9464D media and counted via trypan blue exclusion using the Countess (ThermoFisher).

2.2.3.3 9464D $hB7H3^+$ $mCherry^+$

9464D $hB7H3^+$ $mCherry^+$ was a mixed adherent cell line and grown in T175cm^2 flasks until desired 80% confluency is reached. Due to being a mxied adherent cell line, media containing the suspension cells was first transferred into a 50ml falcon. Adherent cells within the flask

underwent dissociation treatment with trypsin. The trypsin was neutralised with 9464D media. Subsequently, the cells were transferred to the same 50ml falcon containing the suspension cells and centrifuged. Post centrifugation, the cell pellet was resuspended in 9464D media and counted via a Countess flow cytometer.

2.2.3.4 SupT1 Cell lines

SupT1 cell lines are suspension cell lines and grown in T75cm^2 flasks until desired confluency of 80% is reached. Media containing the suspension cells was transferred into a 50ml falcon and centrifuged. After centrifugation, the cell pellet was resuspended in cRPMI media (Table 2.3) and counted via trypan blue using a Countess cell counter.

2.2.3.5 Pheonix Eco Lines

Pheonix Eco lines are adherent cell lines and were grown in T175cm^2 flasks until desired confluency of 80% is reached. Media was discarded from the flasks that cells were cultured in and washed with PBS. The cells underwent trypsin treatment for cell dissociation. cIMDM media (Table 2.3) was added to neutralise trypsin followed by centrifugation. After centrifugation, the cells were resuspended in fresh media and counted via trypan blue exclusion using a Countess cell counter.

2.2.4 Irradiation of cells for *in vitro* assays

Irradiation of cells was performed using a Cs^{137} sealed source irradiator (model IBL 437C) at Great Ormond Institute of Child Health. Cells requiring irradiation were prepared as a single cell suspension into 15ml falcon centrifuge tubes and placed into a centrifuge holder. The centrifuge holder containing the cells was placed into a canister and placed inside the irradiator. The calculated dose (Gy) required for irradiation, was converted to seconds; this was based on the most recent dosimetry measurements recorded for the source. The irradiator was then initiated, and cells were irradiated for the required time for the dose selected. Upon completion of irradiation treatment, cells were transported as required for downstream use for *in vitro* experiments. Sham-irradiated (0Gy) controls were treated in the same manner as irradiated controls for standardisation.

2.2.5 *In vitro* radiosensitivity screen

To assess the radiosensitivity of the cell lines in response to single dose radiation within this thesis, an *in vitro* radiosensitivity screen was performed to investigate markers of immunogenic cell death (ICD) and cell viability as indicators of radiosensitisation. The ICD markers assessed within this work were: Extracellular ATP (EC-ATP), Extracellular HMGB1 (EC-HMGB1) and calreticulin (CRT).

2.2.5.1 Extracellular ATP release time course

Cells were processed into single cell suspensions and irradiated at the required single doses ranging from 0Gy to 30Gy (see section 2.2.4 for further details). Cells were then plated at 100µl into 96-well clear flat bottom white plates at $20x10^3$ per well. Cell culture media was added as required for each timepoint to be measured, with 50ul per well for the 24 hour timepoint, and 90µl per well for the 48 and 72 hour timepoint plates, respectively. Media only wells were also included in all the timepoint plates, with 150µl and 190µl per well added to the 24 hours and 48-72 hours plates, respectively. The 48 and 72 hours timepoint plates were incubated at 37°C and 5% CO_2.

RealTime-Glo EC-ATP substrate (Promega, #GA5010) was reconstituted at 4x in neurosphere media for 20-30 minutes and protected from light. To the 24 hour timepoint plates, the substrate was added at 40µl per well. To allow the mixing of the substrate with cells, the plates were mixed for 30-60 seconds on an orbital shaker at 300-500rpm, protected from light. The plates were then incubated at 37°C and 5% CO_2 and taken out as required for luminescence readings to measure EC-ATP release on the plate reader. The readings were taken on a SpectraMax plate reader (Molecular Devices) using the luminescence settings, with the emission wavelength at 578nm.

For the 48 and 72 hour timepoints, five hours prior to readings being taken, EC-ATP substrate was constituted at 20x in neurosphere media for 20-30 minutes and protected from light. After reconstitution, to the required timepoint plate, the substrate was added at 10µl per well. The plates were mixed for 30-60 seconds on an orbital shaker at 300-500rpm, protected from light. The plates were then incubated at 37°C and 5% CO_2 and taken out as required for luminescence readings to measure EC-ATP release on the plate reader as done with the 24 hour timepoint plate(s). Results were corrected against the media only wells and plotted using GraphPad Prism v10.

2.2.5.2 Extracellular HMGB1 release time course

Target cell lines were prepared into a single-cell suspension and irradiated as outlined in section 2.2.4, at a range of doses or sham-irradiated (0Gy). Post irradiation, cells were plated at $20x10^3$ in 80µl volume per well into a 96-well clear flat bottom luminescence plate. The cells were incubated at 37°C and 5% CO_2 until 24 hours post irradiation. To quantify the concentration of EC-HMGB1 release post irradiation, an eight-point mouse HMGB1 (Abcam, ab255799) a 2.5 fold serial dilution range to make a standard curve was added to the plates at 80ul per well. The EC-HMGB1 release was performed using the Lumit HMGB1 Immunoassay kit (Promega, CS3030B01). The luminescence released was recorded using a SpectraMax plate reader (Molecular Devices) using the luminescence settings, with the emission wavelength at 578nm. The readings exported were then corrected against media only controls and interpolated against the HMGB1 standard curve. Results were plotted using GraphPad Prism v10.

2.2.5.3 Calreticulin expression time course

Target cell lines were prepared into a single cell suspension as described in section 2.2.3. After cells were in a single cell suspension, they were either irradiated at 30Gy as described in section 2.2.4, or sham-irradiated (0Gy). Post irradiation, cells were plated at $60x10^3$ in 200ul volume per well into 96-well flat bottom plate(s) to measure calreticulin expression, 18, 24, and 48 hours post irradiation. The plates were incubated at 37°C and 5% CO_2 until required for each timepoint measurement.

For flow cytometric analysis of calreticulin, cells were processed into single-cell suspension followed by treatment with mouse Fc block to prevent non-specific binding of flow cytometry antibodies via the Fc Receptors (FcR) (372). Cells were incubated with either calreticulin or isotype control antibodies followed by Annexin V staining. Viability dye DAPI was added just before samples were read on the flow cytometer, Cytoflex (Beckman Coulter). Table 2.6 details the antibodies used for these experiments.

2.2.5.4 Measurement of cell viability via MTT assay

Cells were processed into single-cell suspension and irradiated at the required single doses ranging from 0 Gy (sham-irradiated) to 30 Gy (see section 2.2.4 for further details). Cells were

then plated at 100µl per well into 96 well clear flat bottom plates at $20x10^3$ per well. Cell culture media was added to ensure that the total volume was 200µl per well, including wells for the media only controls. Plates were set up for the following time points: 24, 48, and 72 hours post irradiation. The plates were incubated at 37°C and 5% CO_2 until required for each timepoint reading.

For each timepoint reading, stock MTT (3-(4,5-dimethylthiazol-2-yl)-2,5-diphenyltetrazolium bromide)) (Sigma-Aldrich, #M2128-250MG) was diluted to a working concentration of 500µg/ml. The plate required for the time point reading was centrifuged at 800 × *g* for 2 minutes. After centrifugation, 150µl media per well was aspirated, discarded, and replaced with 150µl per well of PBS. The plate was then centrifuged as described previously. After centrifugation, the supernatant was removed from the wells. 80µl of 500µg/ml MTT was added per well and the plate was incubated for 1 hour and 15 minutes at 37°C and 5% CO_2. After incubation, the samples were centrifuged as previously described. The MTT was then aspirated from each well and discarded. 48µl DMSO was added to each well to dissolve the yellow tetrazolium salt formed, into purple formazan crystals produced by the metabolically active cells. Absorbance was measured using a SpectraMax plate reader (Molecular Devices) at 570 nm. Absorbance readings were corrected against media-only controls, normalised against the negative control (0 Gy), and plotted using GraphPad Prism v10.

2.2.5.4.1 IC_{50} calculations

The half maximal inhibitory radiation dose (IC_{50}) values were calculated for the target cell lines screened to provide a summary of the radiosensitivity of the TH-MYCN transgenic lines screened. The IC_{50} values were calculated by taking averages of the normalised cell viability results across the whole 72 hour MTT time course for each radiation dose condition. The results were then analysed using non-linear regression on GraphPad Prism v10 to calculate the IC_{50} value based on the Y-intercept.

2.2.6 Gammaretroviral production

All retroviral transductions were performed within this thesis using the SFG retroviral vector as described in section 2.2.1.1. The retrovirus was produced by transient transfection of the HEK293-based cell packaging cell line, Phoenix Eco, in which the addition of the transfer vector is only required for virus production, thus negating the need for additional helper

plasmids to generate high-titre virus (see section 2.2.1.1 for further details). The use of Phoenix Eco to transduce mouse primary lymphocytes has been cited within the literature (373), and thus utilised within this body of work.

2.2.6.1 Virus Production via Pheonix.Ecotropic

Pheonix Eco was processed into single-cell suspension as described in section 2.2.3.5. Based on the cell count, the cell concentration was adjusted to $3x10^6$/ml. On a 100mm tissue culture treated plate, 11ml of cIMDM was added with $3x10^6$ Pheonix Eco cells. The cells were left to adhere at 37°C and 5% CO_2 overnight until 70-80% cell confluency was reached.

Upon reaching the desired cell confluency, the cells were transfected as follows. 470µl of plain IMDM was gently mixed with 30µl of gene juice (Sigma Aldrich, #70967) and incubated at RT for 5 minutes. Post incubation, 4.68µg of the transfer plasmid was added to the media and gene juice mixture and incubated for 15 minutes at RT. The transfection mixture was then added to the cells drop-wise and evenly distributed. The cells were then incubated at 37°C and 5% CO_2 for collection of the 48 and 72 hour virus harvests. At 48 hours post-transfection, the supernatant was aspirated from the plate and stored at 4°C. 10ml of cIMDM was added to the plate and incubated at 37°C and 5% CO_2 for a further 24 hours for the 72 hour harvest to be collected. The 72 hour harvest was collected and combined with the 48 hour harvest. The supernatant is then centrifuged at 500 x *g* x 5 mins to remove any cellular debris. The harvest is then snap-frozen into 5ml aliquots. The aliquots are sorted at -70°C for storage until required.

2.2.6.2 Virus Concentration using Retro-X

Viral transductions were also performed with up concentrated virus to yield more high-titer virus. For this, virus production was performed in the same way as stated in the previous section 2.2.6.1. However, the 48 and 72-hour virus harvests were not snap-frozen and stored but incubated with Retro-X concentrator (Takara, #631456) overnight at 4°C per the manufacturer's instructions. After overnight incubation, the mixture underwent centrifugation at 1500 x *g* x 45 minutes at 4°C. Post centrifugation, the supernatant was slowly discarded, and the virus pellet was resuspended in 1 in 100^{th} of the original volume in cRPMI. The virus was snap-frozen into 100µl-500µl aliquots and stored at -70°C until required.

2.2.7 Generation of mouse CAR-T cells

The generation of mouse CAR-T cells for subsequent assessment of *in vitro* CAR functionality required the use of spleens from healthy 6-8 week old mice. Spleens were obtained from mice either on the inbred strains of 129/SvJ or C57BL/6. This was done through approved schedule one methods per UK Home Office guidelines under the project licence (PP5675666), and individual licence (I12957935).

All centrifugation steps were performed at 400 x *g* x 5 minutes x room temperature unless otherwise stated.

2.2.7.1 Splenocyte harvest and stimulation

Spleens were obtained from healthy 6-8 week old mice by euthanising them through CO_2 asphyxiation, followed by a confirmation of death following Home Office Guidelines. The spleens were removed from the mice and placed into 15ml falcons containing sterile PBS on ice and transported back to appropriate sterile tissue culture facilities.

To remove the PBS, the spleen was transferred in, the solution was filtered through a 40µM cell strainer. The cell strainer containing the spleen was then placed in the well of a 6-well plate. 1m of 1x ACK lysis buffer was used to macerate the spleen with a 5ml syringe plunger. The cell suspension of the macerated spleen is filtered through the strainer to get any remaining cells present on the strainer. The cell suspension was then mixed with 9ml of fresh PBS and centrifuged.

After centrifugation, the cell pellet was resuspended in 10ml PBS and centrifuged to remove any residual ACK lysis buffer. After centrifugation, the cells were resuspended in 5ml of cRPMI and counted through trypan blue exclusion. Based on the cell count, cRPMI was added to achieve a cell concentration of $1x10^6$/ml.

Splenocytes were stimulated for 24 hours with mCD3/mCD28 dynabeads (Gibco, #11452D) and human interleukin-2 (IL-2) (Proleukin) at 50U/ml. The mCD3/mCD28 dynabeads were added according to the manufacturer's instructions. Based on volume, the splenocytes were cultured in the appropriate tissue-culture treated well plate(s) or flask(s) at 37°C and 5% CO_2 for 24 hours. Where required for some experiments, splenocytes were alternatively stimulated

for 24 hours with Concanalvin-A (Sigma-Aldrich, C2010) and mouse interleukin-7 (Peprotech, 217-17) at 2µg/ml and 0.001µg/ml, respectively.

2.2.7.2 Splenocyte transduction

For splenocyte transduction, the cells were transduced with γ-gammaretrovirus that was produced as described in section 2.2.6. Splenocyte transduction required the use of retronectin-coated plates prepared the day before transduction. For each well of transduction in a non-tissue cultured treated 24-well plate, 8µg of retronectin (Takara, T100B) was required for 500µl of PBS. Once the required wells were coated, the plate was sealed with parafilm and left to coat overnight at 4°C. Before transduction, the retronectin solution was transferred into sterile 50ml conical centrifuge falcons and stored at -20°C for further reuse and then discarded.

Post 24 hour incubation of harvested splenocytes, the cells were prepared for transduction. The cells were centrifuged and resuspended in new cRPMI. After performing a cell count, the desired cell concentration of $3x10^6$/ml was achieved with cRPMI with the addition of 200U/ml of hIL-2. To each well of the retronectin coated 24 well plate, 500µl of cells were added ($1.5x10^6$ per well). To these wells, the appropriate volume of thawed retroviral supernatant was dispensed to achieve a final well volume of 2ml and 50U/ml hIL-2 concentration. For the untransduced wells, the appropriate volume of cRPMI was added to standardise the well volume. The plate was then centrifuged at 1000 x *g* x 40 minutes at 32°C with low acceleration and brake. The cells were incubated with the virus for three days and expanded as required for downstream *in vitro* use.

2.2.7.3 Mouse CAR-T Cell Expansion

72 hours post-transduction, transduced splenocytes were transferred from the retronectin-coated plates into 15ml conical centrifuge tubes. Where mCD3/mCD28 dynabeads were used for splenocyte stimulation, these were removed from the cell suspension through the use of a DynaMag Magnet (Thermofisher, #12301D). The cells were then centrifuged and resuspended in fresh cRPMI. Subsequent cell counts were performed to adjust cell concentration to $1\text{-}2x10^6$/ml for expansion with cRPMI supplemented with 50U/ml hIL-2, 5ng/ml hIL-7 (Peprotech, #200-07) and 10ng/ml hIL-15 (Peprotech, #200-15). The cells were

transferred into the appropriate plate(s) or flask(s) as required and expanded in this manner every two to three days until required for experimental use.

Where required for some experiments comparing cytokine stimulation conditions (chapter four), additional cytokine culturing conditions were used during mouse CAR-T cell expansion. These conditions included expansion with hIL-2 (50U/ml) or with hIL-7 (10ng/ml) and hIL-15 (10ng/ml).

2.2.8 Assessment of transduction efficiency

The transduction efficiency of mouse CAR-T cells was initially assessed on day four post-transduction. Subsequent checks were performed on day seven and nine in relation to assessing the stability of CAR expression during *in vitro* expansion.

Transduction efficiency was assessed by flow cytometry. The cells were processed into single-cell suspension and processed for flow cytometry as detailed in section 2.2.12. Table 2.7 details antibodies used in assessing transduction efficiencies.

2.2.8.1 The detection of 376.96.m28z CAR by flow cytometry

The detection of the 376.96.m28z CAR was done through indirect staining of the CAR itself. This involved a primary incubation with the recombinant human B7-H3, (rhB7-H3) His tagged protein (R&D Biosystems, 2318-B3) for 30 minutes at 4°C followed by surface staining with anti-histidine fluorochrome-conjugated antibody for 30 minutes at 4°C.

2.2.8.2 The detection of HuK666.h28z CAR by flow cytometry

The detection of the HuK666.h28z CAR was performed through RQR8 coexpressed with the CAR within the retroviral construct. RQR8 is a marker that combines target epitopes from both CD34 and CD20 antigens, which allows measurement of CAR transduction efficiencies where direct staining of CAR is not possible (367). RQR8 was directly stained with an anti-hCD34 fluorochrome-conjugated antibody as detailed in Table 2.7.

2.2.9 Assessment of *in vitro* CAR functionality

Assessing CAR-T cell functionality *in vitro* primarily focused on looking at tumour cell lysis and proliferation as indications of CAR-T cells causing tumour regression upon antigen stimulation. Within this thesis, *in vitro* CAR-T functionality was assessed via plate-bound antigen-based assays and co-cultures with antigen-positive target cells.

The use of antigen-positive target cells in co-cultures with CAR-T cells indicates the presence of anti-tumour activity exhibited by these T cells. These co-cultures allow additional readouts of CAR-T cell functionality, including tumour cell lysis by luciferase, cytokine release and ascertaining changes in T-cell phenotype by flow cytometry.

These assays were performed at days four to five post CAR-T cell transduction unless otherwise stated, and adjusted for transduction efficiency alongside the use of untransduced controls. These assays involved the addition of $50x10^3$ per well of CAR-T cells and targets at an effector:target ratio of 1:1 unless otherwise stated.

2.2.9.1 Plate-bound rhB7-H3 antigen-based assay

The plate-bound antigen-based assays performed used recombinant human B7-H3 tag (Anti-hB7-H3) protein (R&D systems, #2318-B3). The assay required a coating of non-tissue culture-treated 96-well flat-bottom plates with anti-histidine (anti-His) protein (Thermofisher, #PA1-983B) followed by coating with anti-hB7-H3.

The coating of wells was performed first with 100ul per well of 10µg/ml anti-His protein in PBS. The wells were left to coat overnight at 4°C. Subsequently, the wells were washed twice with PBS. The wells were then coated with 100µl per well of 25µg/ml anti-hB7-H3-His protein in PBS and left to coat overnight at 4°C.

The inclusion of anti-mCD3 as a positive control within this assay also required coating wells with anti-mCD3 (ThermoFisher, #16-0031-82 (Clone 145-2C11)). Wells were coated with 100µl per well of 1µg/ml of anti-mCD3 in PBS and left to coat overnight at 4°C.

For this assay, CAR-T cells used were at day seven post transduction and stained with Cell Trace Violet (CTV) (ThermoFisher, #C34557) following the manufacturer's instructions.

The coated wells were washed with PBS, and CAR-T cells were added in 100µl per well (adjusted for transduction efficiency). Untransduced T-cells were added at the same volume and cell number following transduction efficiency adjustment. 100µl per well of media was added to wells, and the plate(s) were incubated as required at 37°C and 5% CO_2 until defined functional endpoints to assess CAR-T functionality in response to antigen stimulation by ELISA (section 2.2.12) and flow cytometry (section 2.2.13).

2.2.9.2 Co-Culture with SupT1s

Co-cultures were performed to assess CAR-T cell functionality against SupT1 WT cell lines (see Table 2.6 for further details on these cell lines). These were performed in 96-well round bottom plates in which targets were added at 100µl per well, followed by the addition of 100µl per well of CAR-T cells (adjusted for transduction efficiency) alongside untransduced T-cell controls. The plate(s) were then incubated at 37°C and 5% CO_2. CAR-T cell functionality was determined at defined endpoints by luminescence, cytokine release and flow cytometry.

2.2.9.3 Co-Culture with adherent antigen-positive targets

Co-cultures of CAR-T cells with adherent antigen-positive targets were done so either with non-irradiated or irradiated targets at effector:target ratio of 1:1, as part of investigating the effects of single-dose radiation on CAR-T cell functionality.

For these co-cultures, antigen-positive targets were processed into a single-cell suspension and irradiated or sham-irradiated (0Gy) as described in section 2.2.4. The cells were labelled with Carboxyfluorescein succinimidyl ester (CFSE) (ThermoFisher, #C34554) under the manufacturer's instructions and plated alongside non-irradiated controls into 96-well flat bottom plates at 200µl per well at $50x10^3$ per well and incubated for 24 hours at 37°C and 5% CO_2. After this 24-hour incubation, the plates were centrifuged at 300 x *g* x 5 mins, and 100µl per well was discarded and replaced with 100µl per well of CAR T-cells labelled with CTV.

The CAR-T cells were added at $50x10^3$ per well with adjustment for transduction efficiency. Untransduced T-cell controls were also added in line with transduction efficiency adjustment. Co-cultures were incubated at 37°C and 5% CO_2, and CAR-T cell functionality was investigated at defined endpoints by cytokine release and flow cytometry.

2.2.10 Assessment of tumour cell lysis by luciferase

One way to assess tumour cell lysis as a functional readout of CAR-T cell activity was by utilising luciferase. Target cells were virally transduced to express the luciferase gene. This allowed the addition of luciferin, which generates a luminescence signal to assess tumour cell viability compared to controls in a high-throughput way.

This type of functional readout was performed as required, with co-cultures performed with luciferase^{+} target cells at effector:target ratio of 1:1. To perform this readout, D-luciferin was added to co-cultures at a concentration of 15mg/ml. This was followed by a five minute incubation at room temperature in the dark. Readings were then obtained from wells via the SpectraMax plate reader (Molecular Devices) using the luminescence settings, with the emission wavelength at 578nm.

Results were corrected against media-only controls, normalised against target-only conditions, and plotted using GraphPad Prism v10.

2.2.11 Measuring cytokine release by ELISA

Enzyme-linked immunosorption assays (ELISAs) were used to measure the concentration of the inflammatory cytokines produced by CAR-T cells in response to antigen stimulation. Mouse IL-2 and IFN-y (mIL-2 and mIFN-γ, respectively) ELISAs were performed for this.

To perform these ELISAs, 100-150µl per well of supernatant was collected from co-cultures at defined endpoints and frozen at -20°C in 96-well round bottom plates until required. The ELISAs performed used the mIL-2 (Biolegend, 431004) and mIFN-y (Biolegend, 430804) kits. The ELISAs were performed following the manufacturer's instructions.

To perform the ELISAs, supernatants were thawed at room temperature and centrifuged at 300 x *g* x 5 minutes. The supernatants were added as required for sample dilution using assay diluent. Upon completion of the ELISA using $2NH_2SO_4$, absorbance readings were read at 450nm and 540nm on a SpectraMax plate reader (Molecular Devices).

The results were analysed through absorbance reading and blank corrections. Standard curves and interpolation of the unknown samples were performed using Microsoft Excel and corrected for the sample dilution factor used.

2.2.12 Flow cytometry

Flow Cytometry is a technique that allows the detection of targets of interest through antibodies conjugated with fluorophores. The use of these flow cytometry antibodies enables measurement of the expression of cell markers of interest. As a result, a range of functional readouts can be obtained for T-cell assays, ranging from CAR expression, proliferation and T-cell memory phenotyping, alongside determining tumour cell lysis.

All flow cytometry experiments were performed using either the BD LSR II or the Beckman Coulter Cytoflex with data acquisition through FACSDiva and CytExpert software, respectively. Data Analysis was performed using FlowJo v10 (Treestar). All flow antibodies used in flow cytometry experiments are listed below in Table 2.7. Centrifugation steps were performed at 800 x *g* x 2 minutes x 4°C unless otherwise stated.

To perform flow cytometry, cells were first processed into single-cell suspension as required and transferred either into flow cytometry tubes or round bottom 96-well plate(s). Cells were washed with PBS and centrifuged. Post centrifugation, the supernatant was discarded, and cells were stained with viability dye as required in PBS for ten minutes at RT in the dark, followed by a PBS wash. Cells were then incubated with mouse Fc Block (Invitrogen, 14-0161-82) for five to ten minutes at 4°C. Surface antibody staining was performed per sample in 100µl PBS with the appropriate antibodies (see Table 2.7) and mixed before a 30 to 45 minute incubation at 4°C.

Where compensation was required, compensation beads or cells were stained individually with each fluorescently conjugated antibody of interest alongside any fluorescent minus one (FMO) controls required.

Upon completion of surface antibody staining, a final PBS wash was performed, and cells were resuspended in PBS and run through the flow cytometer. The data obtained was then analysed on the FlowJo v10 software.

Samples that could not be recorded on a cytometer upon completion of staining were resuspended in 100µl fixation buffer (Biolegend, #42080) for 10 to 15 minutes at 4°C followed by a PBS wash. Cells were then stored at 4°C in PBS for a maximum of 48 hours to be recorded on the flow cytometer during this period.

Table 2.7 Antibodies for flow cytometry experiments

Antibody	Clone	Supplier	Flurochrome	Dilution
Anti-mouse CD16/CD32	93	Invitrogen	-	1 in 500
DAPI	-	-	-	1 in 200
Fixable Viability Dye eFluor™ 780	-	Invitrogen	APC/Cy7	1 in 1000
Ghost Red e780 Viability Dye	-	Cytek Bioscience	APC/Cy7	1 in 1000
Annexin V	-	APC	Thermofisher	1 in 50
Mouse IgG2a, κ Isotype Ctrl	MOPC-173	Biolegend	APC	1 in 100
Mouse IgG1 κ Isotype Control	MOPC-21	PE	Biolegend	1 in 50
Rat IgG2a, κ Isotype Ctrl	RTK2758	Biolegend	PE	1 in 100
c-Myc	9E10	Biolegend	PE, AF647	1 in 100
Anti-His	J095G46	Biolegend	PE, APC	1 in 100
Calreticulin	FMC 75	PE	Abcam	1 in 133
Anti-human CD34	QBEnd10	Biotechne (R&D Systems)	APC	1 in 100
Anti-human GD2	14G2a	Biolegend	PE, APC	1 in 100
Anti-mouse B7-H3	MIH32	BD Biosciences	PE	1 in 100
Anti-mouse CD3	17A2	Biolegend	PE,APC,FITC, BV605, AF700	1 in 300
Anti-mouse CD4	GK1.5	Biolegend	BV510	1 in 500
Anti-mouse CD8	53-6.7	Biolegend	BV711	1 in 500
Anti-mouse CD62L	MEL-14	Biolegend	BV510-	1 in 500

Anti-mouse CD44	IM7	Biolegend	PE/Cy7	1 in 500

2.2.12.1 Determining Memory T-Cell Phenotype

Phenotyping of memory mouse T-cells was determined by the expression of mCD44 and mCD62L, which are among the markers cited in the literature for identifying memory T-cell phenotypes (374). The differential expression of mCD44 and mCD62L allows identification of T-cell populations as follows: naïve ($CD62L^{hi}CD44^{lo}$), effector ($CD62L^{lo}CD44^{lo}$), central memory ($CD62L^{hi}CD44^{hi}$), and effector memory ($CD62L^{lo}CD44^{hi}$) (374). Naïve T-cells (T_{Naive}) have not yet encountered their specific antigen, while effector T-cells ($T_{Effector}$) exert effector functions in response to antigen recognition. Effector memory ($T_{Effector\ Memory}$) cells home to tissues and can rapidly exert effector functions upon antigen rechallenge (374). Central memory ($T_{Central\ Memory}$) T-cells contribute to central immunosurveillance; upon antigen rechallenge, they differentiate into effector cells and expand, increasing the pool of effector cells available to mount an immune response (374). Table 2.8 lists the panel used to determine T-cell memory phenotype during flow cytometric analysis..

Table 2.8 Panel for determining the mouse T-cell memory phenotype

	mCD44	mCD62L
T_{Naive}	-	+
$T_{Central\ Memory}$	+	+
$T_{Effector\ Memory}$	+	-
$T_{Effector}$	-	-

2.2.13 Evaluating the *in vitro* functionality of NIS

To assess the *in vitro* functionality of the NIS^{+} mouse CAR-T cells, radionucleotide uptake assays were performed using Technetium-99m pertechnetate ($^{99m}TcO_4^-$). This is a radiotracer widely used in the clinic and compatible with NIS (166). The addition of the competitive

inhibitor, sodium perchlorate ($NaClO_4$), determines the specificity of NIS functionality observed in the presence of this inhibitor (166).

All centrifugation and incubation steps were performed at 300 x *g* x 5 minutes and 37°C and 5% CO_2, respectively, unless otherwise stated.

2.2.13.1 $99mTcO_4^-$ uptake assay

The NIS^+ Mouse CAR-T cells were evaluated for NIS functionality at days four to five post-transduction and the cell number was adjusted for transduction efficiency. Mouse CAR-T cells in culture were centrifuged, resuspended in PBS and counted via trypan blue exclusion. Based on the cell concentration, cells were prepared as required for the uptake assay. $0.5x10^6$ cells were required per mouse spleen in triplicate for conditions with and without the addition of the inhibitor, $NaClO_4$. Thus, $3x10^6$ cells were needed for these conditions per mouse spleen. The cells were then centrifuged and resuspended to a cell concentration of $1x10^6$/ml of which 500µl was added to six 1.5ml microcentrifuge tubes.

To the inhibitor controls, 50µl of 0.1M $NaClO_4$ was added, and alongside the non-inhibitor controls, incubated for 30 minutes, with samples inverted every 10 to 15 minutes. During this incubation, $^{99m}TcO_4^-$ was measured just before use using a dosimeter (Veenstra Instruments dose calibrator) and diluted as required with PBS to a final concentration of 0.02MBq/µl. Upon completion of treatment with $NaClO_4$, 0.1MBq of $^{99m}TcO_4^-$ was added per sample and incubated for 30 minutes. During this incubation, tubes were inverted every 10 to 15 minutes. After treatment with $99mTcO_4^-$, the samples were centrifuged, and the supernatant was transferred to the corresponding scintillation tubes. The cells were then washed with 1ml of ice-cold PBS and centrifuged. Post centrifugation, the supernatant was transferred into the corresponding scintillation tubes as done for the previous step. All eppendorfs and scintillation tubes containing the cell pellet and supernatant, respectively, were loaded onto the gamma counter. Overnight automated readings were obtained from the samples. Data was exported when the dead time was less than 30%. This is when stable readings are provided for further analysis (375). The results exported from the gamma counter were corrected against media controls and analysed to provide the sum percentage of Tc_{99m} uptake retained by the cells across all technical and biological replicates, in the presence or absence of $NaClO_4$.

2.2.14 Neurosphere growth assays

The TH-MYCN mouse transgenic lines, 129NS1 and TAM6 WT investigated within this thesis, propagate as spheroids *in vitro*. To utilise these models to investigate *in vitro* the effect of T-cell trafficking into the tumour spheroid, optimisations were required to determine the suitability of these *in vitro* co-cultures with these models. Seeding density growth assays were utilised to determine the seeding density and viability of the tumour spheroids.

To perform these assays, the TH-MYCN mouse transgenic luciferase$^+$ chemotherapy-naïve lines, 129NS1-4B and 129NS1-4B hB7-H3$^+$ were processed into single-cell suspensions as detailed in section 2.2.3.1. To 96-well ultra-low attachment (ULA) plate(s), cells were added at 3000, 4000 and 5000 per well in 200µl volume. Plate(s) were established in this manner for endpoint readings of 24, 48 and 72 hours post-seeding.

2.2.14.1 Neurosphere diameter measurements

To assess neurosphere growth through diameter changes for each time point, well images were taken at 4x magnification using a brightfield microscope for each seeding density. The neurosphere diameter was then measured on ImageJ. A scale bar was generated from measurements of a hemocytometer image with known measurements. The scale bar generated provided pixel-to-micron conversion, allowing neurosphere diameter measurements as required in microns.

2.2.14.2 Assessing neurosphere viability

As 129NS-14B and 129NS1-4B hB7-H3$^+$ are luciferase positive, cell viability of the cells during the spheroid forming assay was determined through the use of luciferin. For each timepoint reading, stock D-luciferin (PerkinElmer, 122799) was diluted to 30mg/ml using neurosphere media (Table 2.3) and added at 10µl per well. The plate(s) were incubated for five minutes at 37°C and 5% CO_2. Luminescence readings were then obtained from the plates using a Tecan Infinite 200Pro plate reader (Tecan Life Sciences) using the luminescence settings, with the integration time and settle time set at 1000ms and 100ms, respectively.

2.2.14.3 Determining neurosphere cell number

To estimate the cell number of the spheroids within these seeding density growth assays, eight-point standard curves were set up on day zero of the assay with known cell numbers. At the 24 hour timepoint, luminescence readings were obtained from these standard curves. In GraphPad Prism v10, Non-linear regression was used to interpolate the unknown luminescence readings for each seeding density and determine cell numbers for the neurospheres at 24-, 48- and 72 hours post seeding.

2.2.15 Statistical analysis

Statistical analysis was performed using GraphPad Prism v10. The statistical tests chosen were based on the assumption that the data showed normal distribution with parametric tests selected to evaluate statistical differences between groups. For the *in vitro* assays shown, one-way ANOVA or two-way ANOVA was used with Turkey multiple comparisons to compare between groups as all the assays performed included comparisons between three or more groups.

Chapter 3 *In vitro* radiosensitivity of TH-MYCN mouse models of neuroblastoma

3.1 Introduction

Assessing *the in vivo* treatment efficacy in preclinical mouse neuroblastoma has largely focused on the use of widely used tyrosine-hydroxylase-MYCN (TH-MYCN) transgenic models for high-risk neuroblastoma (213,376). These genetically engineered mouse models show targeted overexpression of the human MYCN gene (one of the main oncogenic drivers of neuroblastoma) within neural crest cells, under the control of the rat tyrosine hydroxylase promoter (213). This results in the spontaneous development of aggressive tumours, which have pathological and clinical features similar to those of human neuroblastoma (376). As a result, these were deemed highly suitable tumour models for evaluation in this project.

As discussed in the introduction on TH-MYCN models, the 9464D model has been the most widely characterised in the literature compared with the recently developed mouse allograft models on the 129/SvJ genetic background (129NS1 and TAM6 WT). All three models were evaluated within this thesis. To utilise these models to investigate the effect of radiation on CAR-T cell functionality, the first step was to determine the *in vitro* radiosensitivity of the cancer cells of the individual models due to limited findings published in this field. The experiments in this chapter aimed to determine which single-dose radiation should be considered further when evaluating its potential therapeutic effect on CAR-T cell functionality in subsequent *in vitro* and *in vivo* experiments. Because of the number of models considered to determine the most suitable to evaluate the treatment efficacy of radiation in combination with CAR-T cells, an *in vitro* screen was developed to determine the radiosensitivity of these models.

As discussed in the Introduction (see section 1.8.7), the immune-mediated effects of radiation are thought to depend on the occurrence of immunogenic cell death (ICD). Within the literature, multiple markers have been determined as indicators of ICD of which three are considered the main hallmarks to consider: Extracellular ATP (EC-ATP), calreticulin (CRT), and HMGB1 (298,377). The roles of these ICD hallmarks have been further explained in the Introduction (see section 1.8.7.1-1.8.7.3). An *in vitro* radiosensitivity screen was performed to evaluate the expression of the ICD markers EC-ATP, calreticulin, and EC-HMGB1 in response to a range of low (2Gy) to high (30Gy) single-dose radiation from a ^{137}Cs source.

The use of a range of single-dose radiation allows us to assess the radiosensitivity of these models, which has not yet been well defined in the literature.

The overall aim of the radiosensitivity screen was to evaluate the effect of radiation on the three TH-MYCN models in terms of the effects of immunogenic cell death and cell viability. To determine cell viability, MTT assays were utilised. The use of a range of single-dose radiation within this *in vitro* screen allows simpler evaluation than fractionated regimens and is potentially more relevant for subsequent clinical translation on the most suitable radiation doses to be considered in combination with CAR therapy. The results in this chapter describe the *in vitro* radiosensitivity of TH-MYCN models of high-risk neuroblastoma in the 129/SvJ and C57BL/6 genetic mouse backgrounds. Radiosensitivity is defined by immune (ICD markers) and non-immune mediated effects (cell viability) induced by radiation.

3.1.1 The TH-MYCN lines screened for *in vitro* radiosensitivity

As mentioned in the previous section, the TH-MYCN models of high-risk neuroblastoma evaluated in this thesis exist in two different mouse genetic strains: 129/SvJ and C57BL/6.

The TH-MYCN C57BL/6 model, 9464D, is the most characterised within the literature. The model was generated from spontaneous tumours arising in TH-MYCN transgenic mice on a C57BL/6 background and now exists as an immortalised cell line (218). This model has been characterised as akin to human neuroblastoma, with endogenous GD2 and low levels of MHC-1 (219). However, prolonged *in vitro* culturing has led to a loss of GD2 expression, thus resulting in the need for subsequent creation of 9464D models overexpressing GD2 (220).

TH-MYCN-ALK allograft lines of neuroblastoma on the 129/SvJ background were recently developed by Louis Chesler and colleagues at The Institute of Cancer Research, London, as described in the Introduction (see section 1.7.4). The generation of the chemo-naïve 129NS1 and chemo-resistance TAM6 allograft lines provides evaluation of radiation in combination with CAR therapy against both treatment-naïve and treatmen-refractory disease. This provides the potential for clinical translation of the efficacy of this combination therapy against modelling of different neuroblastoma treatment states.

Both 129NS1 and TAM6 provide certain advantages over established adherent TH-MYCN tumour cell lines, such as 9464D. These allograft neurosphere lines exist *in vitro* as spheroids (date not shown). This improves the applicability of *in vitro* and *in vivo* findings for evaluating

CAR-T cell therapy in terms of assessing tumour infiltration and antigen expression. The 129NS1 and TAM6 are also short-lived primary cell lines developed within our own labs. This provides an advantage over established cell lines like 9464D which have been transferred through multiple labs and known to acquire multiple adaptations as a result of prolonged *in vitro* culturing.

Subclones generated from the parental lines 129NS1, TAM6 WT, and 9464D WT expressing hB7-H3$^+$ were also included in this *in vitro* radiosensitivity screen. This is due to the interest in investigating CAR candidates targeting hB7-H3$^+$ within this project, because B7-H3$^+$ is a promising target for the targeted treatment of neuroblastoma, as discussed in the Introduction (see section 1.6.1). The generation of the 129NS1 expressing hB7-H3$^+$ (129NS1-4B hB7-H3$^+$) was generated by me through viral transduction of the parental 129NS1-4B line (129NS1 line expressing luciferase generated by Sophie Munnings-Tomes) with hB7-H3$^+$ retrovirus generated by the transient transfection of 293Ts. Subsequent bulk-sorting of the transduced cells yielded a 129NS1 allograft line positive for both luciferase and hB7-H3. Table 3.1 summarises the cell lines evaluated within this radiosensitivity screen.

Table 3.1 Cells lines evaluated for *in vitro* radiosensitivity screen

Cell Line	Species Origin
129NS1	Mouse (129/SvJ genetic background)
129NS1-4B (GFP$^+$Luc$^+$)	
129NS1-4B hB7-H3$^+$	
TAM6	
TAM6 hB7-H3$^+$ mCherry$^+$	
9464D WT	Mouse (C57BL/6 genetic background)
9464D hB7-H3$^+$ mCherry$^+$	

3.2 Results

3.2.1 EC-ATP levels in response to single-dose radiation

To investigate EC-ATP levels in response to radiation, TH-MYCN neuroblastoma lines were irradiated with a range of single-dose radiation. EC-ATP levels were measured by luminescence over a 72 hour time course post irradiation. The premise of this assay is that dying cells release EC-ATP, which is a substrate required for the oxidation of luciferin to oxy-luciferin by luciferase (378,379). Owing to the addition of luciferase and luciferin to these cells, luciferase^{+} lines (129NS1-4B and 129NS1-4B hB7-H3^{+}) derived from the parental line 129NS1 were excluded from these assays as endogenous expression of luciferase by these lines would create background light emission. Maximal EC-ATP levels were measured from known concentrations of ATP (Figure 8.1). However, due to the instability of ATP, the standard curve could not be utilised to determine the concentration of EC-ATP release for these timecourse assays.

In response to single-dose radiation, the TH-MYCN lines on the 129/SvJ genetic strain (129NS1 and TAM6) showed similar results with no upregulation of EC-ATP levels in response to single-dose radiation compared to the non-irradiated (0Gy) control. For both the 129NS1 and TAM6 lines, consistent EC-ATP levels were observed in the non-irradiated control, which became most apparent at 48 and 72 hours post irradiation. The reason for this high background is unknown; thus, data should be interpreted with caution. The chemo-naïve 129NS1 line showed no dose-dependent increase in EC-ATP over the 72 hour time course. The diminished EC-ATP levels seen at doses greater than 5Gy may suggest that radiation induces a protective effect in the cells, resulting in lower EC-ATP levels, as evidenced by the lower luminescence readings observed compared to the 0Gy control (Figure 3.1a). In response to radiation, the highest EC-ATP levels were observed with 2Gy from 48 hours post irradiation, followed by 5Gy. However, similar to higher radiation doses, the EC-ATP levels were still found to be no higher than 0Gy across all time points (Figure 3.1a)

The chemoresistant TAM6 WT (Figure 3.1b), similar to 129NS1, showed no upregulation of EC-ATP levels in a dose-dependent manner compared to the non-irradiated control. However, there was a trend observed with EC-ATP levels peaking at 48 hours before diminishing at 72 hours post irradiation compared to the non-irradiated control, which suggests that EC-ATP levels are time-dependent (Figure 3.1b). These results suggest that radiation has no effect on increasing EC-ATP levels and thus trends observed of EC-ATP

levels over time within the radiation group are likley not to be directly related. TAM6 hB7-H3^{+} mCherry^{+} in line with TAM6 WT showed diminished EC-ATP levels at 48 and 72 hours post irradiation compared to the non-irradiated control for doses greater than 2Gy (Figure 3.1c). EC-ATP levels were upregulated at 72 hours post irradiation with 2Gy compared to those in the non-irradiated control (Figure 3.1c).

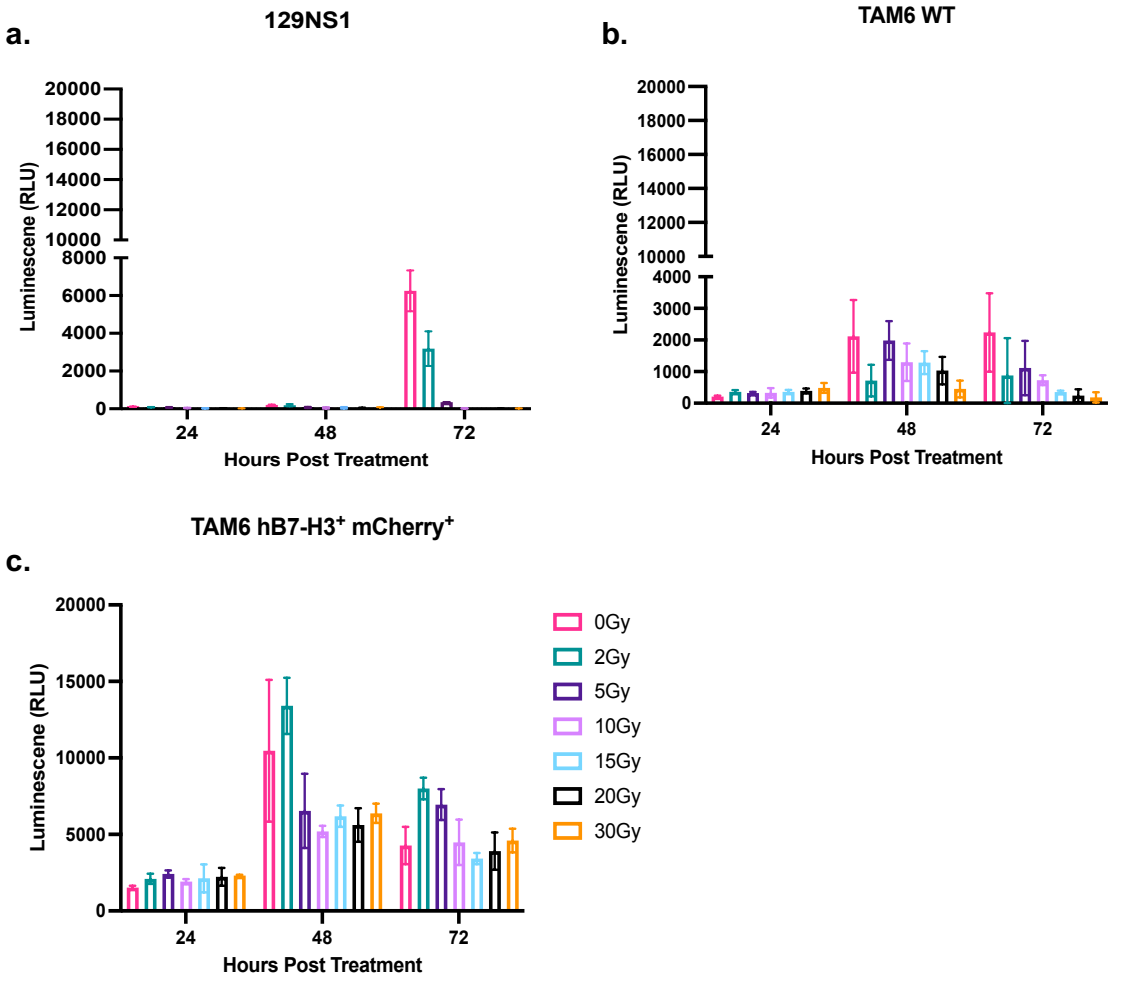

Figure 3.1 129NS1 and TAM6 lines do not show increase in EC-ATP levels in response to single-dose radiation

TH-MYCN mouse allograft lines **a**) 129NS1, **b**) TAM6 WT, and **c**) TAM6 hB7-H3^{+} mCherry^{+} were irradiated with a range of single dose of γ-radiation using a ^{137}Cs source. The irradiated single-cell suspensions were plated at 20x10^{3} per well to assess EC-ATP release in real-time over a 72-hour time course. The luminescence readings obtained at 24, 48, and 72-hour post treatment are shown. Each treatment condition included three technical replicates with the standard deviation is shown. The results are representative of two independent experiments (N=2).

The 9464D lines were also evaluated for EC-ATP levels in the same manner as the other TH-MYCN transgenic lines mentioned in the previous section. Similar to the 129NS1 and TAM6

lines, EC-ATP levels were not upregulated in response to radiation compared to the non-irradiated control for 9464D lines (Figure 3.2). For both 9464D WT (Figure 3.2a) and 9464D hB7-H3^{+} mCherry^{+} (Figure 3.2b), EC-ATP levels were relatively low at 24 hours post irradiation, before being upregulated at 48 and 72 hours post irradiation. However, this upregulation did not occur in a dose-dependent manner and was not greater than that observed in the non-irradiated control. The levels of EC-ATP levels across the investigated radiation doses were relatively comparable (Figure 3.2).

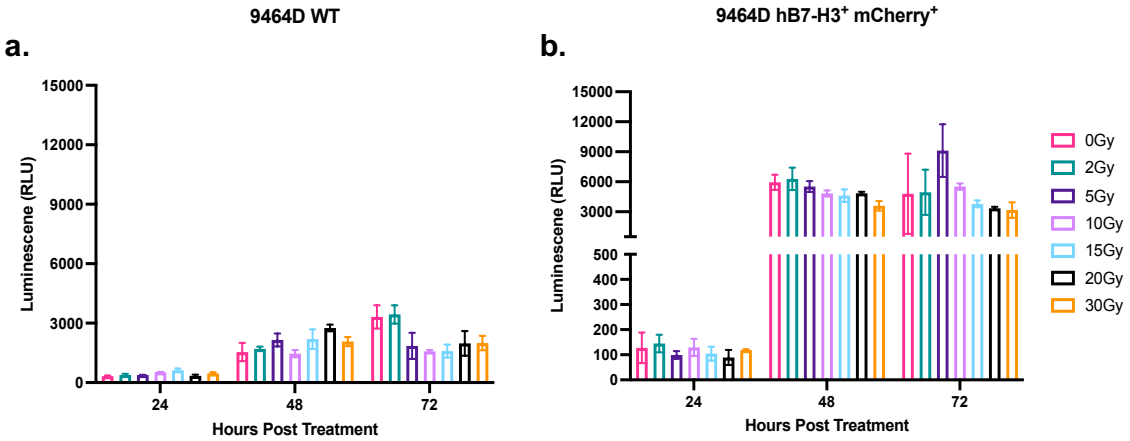

Figure 3.2 9464D cell lines do not show increase in EC-ATP levels in response to single-dose radiation

TH-MYCN cell lines: **a**) 9464D WT and **b**) 9464D hB7-H3^{+} mCherry^{+} were irradiated with a range of single-dose γ-radiation using a ^{137}Cs source. The irradiated single-cell suspensions were plated at 20x10^{3} per well to assess EC-ATP levels in real-time over a 72-hour time course. Luminescence readings obtained 24, 48, and 72 hour post treatment are shown. Each treatment condition included three technical replicates, with the standard deviation shown. The results shown are from one independent experiment (N=1).

Within the context of these luminescence-based assays, EC-ATP upregulation was not observed in response to radiation across any of the TH-MYCN lines screened, and no dose-dependent differences were observed. This may be due to technical limitations of this assay to measure EC-ATP as discussed in section 3.7 of this chapter. Alternative methods of measuring EC-ATP levels in response to radiation in a high-throughput manner may need to be considered for *in vitro* investigations of these TH-MYCN models.

3.2.2 Expression of calreticulin in response to radiation

Next, I sought to determine whether the ICD marker calreticulin was upregulated in response to radiation. The premise of the assay is that dying cells release calreticulin, which can be detected using techniques such as flow cytometry and western blotting (380). The TH-MYCN mouse neuroblastoma lines were either non-irradiated (0Gy) or irradiated with a single dose of 30Gy. Calreticulin expression was measured by flow cytometry at 18 , 48 and 72 hours post irradiation and the gating strategy used is shown in Figure 3.3.

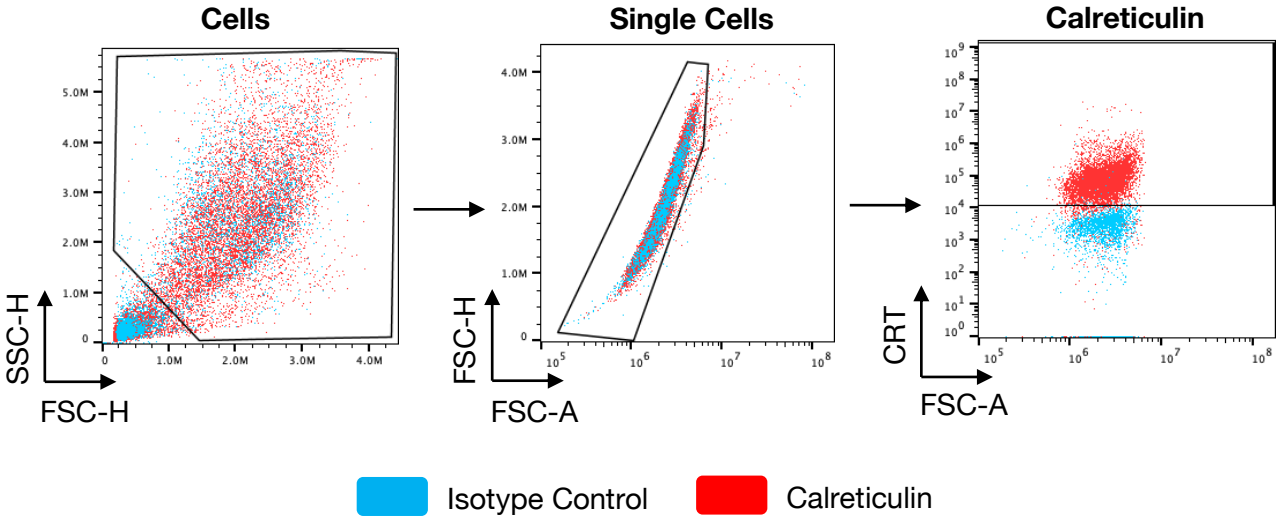

Figure 3.3 Gating strategy for measuring calreticulin expression in response to single-dose radiation

TH-MYCN mouse neuroblastoma lines of 129NS1, TAM6 and 9464D and their derivatives were either sham-irradiated (0Gy), or irradiated with a single-dose of 30Gy via a ^{137}Cs source. The irradiated single-cell suspensions were plated at 60x10^{3} per well. Ecto-calreticulin expression was measured 18, 24, and 48 hours post treatment by flow cytometry. The representative FACS plots show the gating strategy utilised to measure calreticulin (CRT) expression by flow cytometry against the isotype control on gated single cells.

3.2.2.1 Calreticulin upregulation in 129NS1 lines

In response to single-dose radiation, the chemo-naïve 129NS1 lines showed upregulation of calreticulin (Figure 3.4) compared to the non-irradiated controls. For 129NS1 (Figure 3.4a), 129NS1-4B (Figure 3.4b), and 129NS1-4B hB7-H3^{+} (Figure 3.4c), calreticulin expression was upregulated at 18 hours post irradiation. Moreover, the upregulated expression was sustained at later time points of 24 and 48 hours post irradiation across all three lines (Figure

3.4). The magnitude of calreticulin expression was found to be similar across 129NS1 and the subclone lines 129NS1-4B and 129NS1-4B hB7-H3^{+}. This suggests that the subclone behaviour in terms of radiation response for calreticulin expression is in line with that of its parental line, 129NS1.

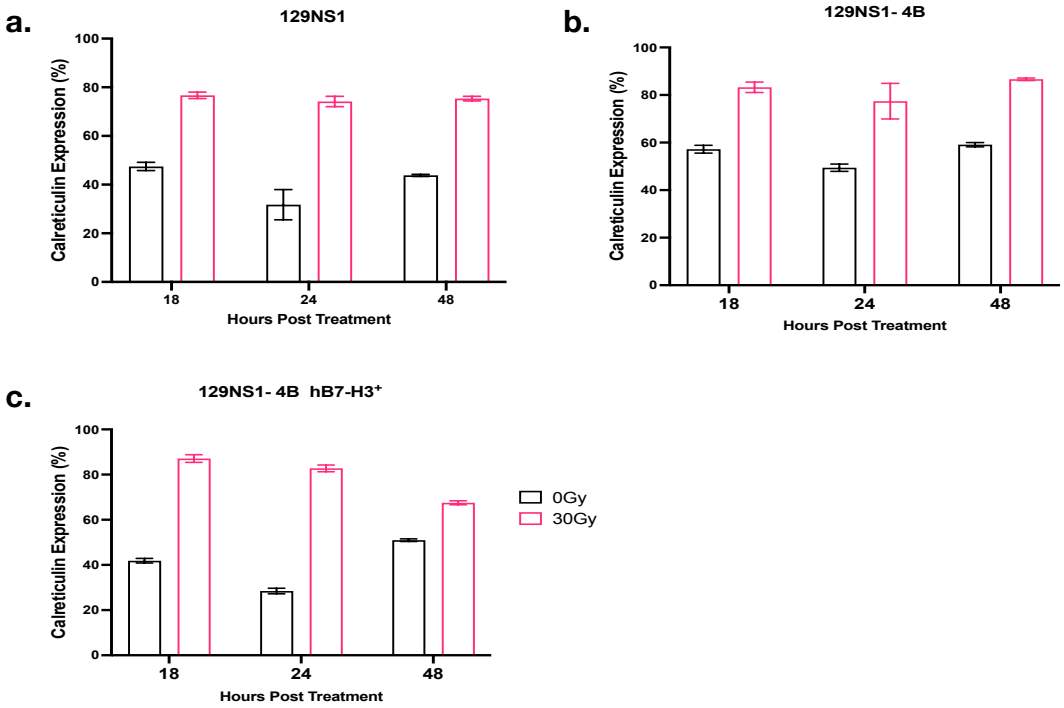

Figure 3.4 The chemo-naïve 129NS1 lines show upregulation in ecto-calreticulin expression in response to single-dose radiation

TH-MYCN mouse neuroblastoma lines, **a**) 129NS1, **b**) 129NS1–4B, and **c**) 129NS1–4B hB7-H3^{+} were either non-irradiated (0Gy), or irradiated with a single-dose of 30Gy via a ^{137}Cs source. The irradiated single-cell suspensions were plated at 60x10^{3} per well. Ecto-calreticulin expression was measured 18, 24, and 48-hr post treatment by flow cytometry. Each treatment condition includes three technical replicates, with the standard deviation shown. The results shown are from one independent experiment (N=1).

3.2.2.2 Calreticulin upregulation in TAM6 lines

In response to radiation in the TAM6 lines, variable results in the upregulation of calreticulin expression were observed. Both TAM6 WT (Figure 3.5a) and the subclone line TAM6 WT hB7-H3^{+} mCherry^{+} showed upregulation in calreticulin expression compared to the non-irradiated control at 0Gy. However, for TAM6 WT, this was most pronounced at 48 hours post irradiation compared to the non-irradiated control (Figure 3.5a). In contrast, TAM6 hB7-

H3^{+} mCherry^{+} cells showed a trend of upregulated calreticulin expression compared to the non-irradiated control cells in a time-dependent manner (Figure 3.5b). The magnitude of calreticulin expression seen between the two differed, with lower expression of calreticulin seen for TAM6 hB7-H3^{+} mCherry^{+} than for TAM6 WT (Figure 3.5). The observed differences may be due to subclone heterogeneity compared to the mixed clonal heterogeneity of TAM6 WT.

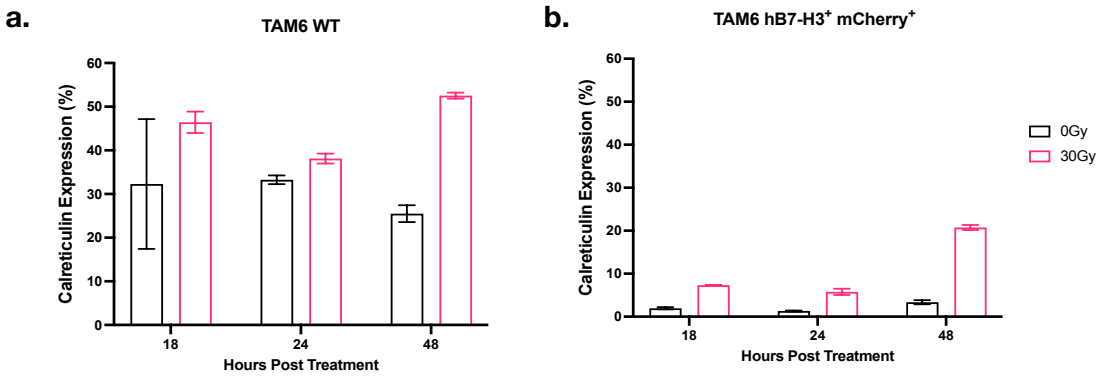

Figure 3.5 TAM6 hB7-H3^{+} mCherry^{+} shows early upregulation in ecto-calreticulin expression in response to single-dose radiation but not TAM6 WT

Mouse neuroblastoma TH-MYCN allograft lines, **a**) TAM6 WT, and **b**) TAM6 hB7-H3^{+} mCherry^{+} were either non-irradiated (0Gy) or irradiated with a single-dose of 30Gy via a ^{137}Cs source. The irradiated single-cell suspensions were plated at 60x10^{3} per well. Ecto-calreticulin expression was measured 18, 24, and 48 hours post-treatment by flow cytometry. Each treatment condition includes three technical replicates, with the standard deviation shown. The results shown are from one independent experiment (N=1).

3.2.2.3 Calreticulin upregulation in 9464D lines

When evaluating calreticulin expression in response to radiation, variable responses were observed between the 9464D WT and 9464D hB7-H3^{+} mCherry^{+} cells. 9464D WT showed minimal upregulation of calreticulin expression compared to the non-irradiated control that was not sustained in a time-dependent manner (Figure 3.6a). However, for 9464D hB7-H3^{+} mCherry^{+} cells, radiation did not upregulate calreticulin expression compared to the non-irradiated control (Figure 3.6b). This trend was sustained across all time points post-treatment (Figure 3.6b). The differences observed between 9464D WT and 9464D hB7-H3^{+} mCherry^{+} may be a result of subclone heterogeneity. Further experimental repeats will determine the significance of these results.

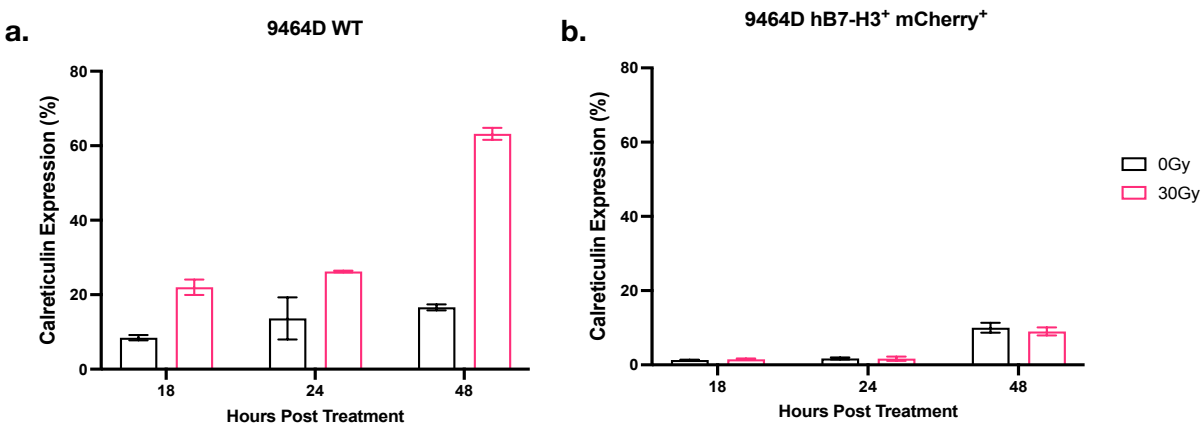

Figure 3.6 Ecto-calreticulin expression is upregulated in 9464D WT but not 9464D hB7-H3^{+} mCherry^{+} in response to single-dose radiation

TH-MYCN cell lines, **a**) 9464D WT, and **b**) 9464D hB7-H3^{+} mCherry^{+} were either non-irradiated (0Gy), or irradiated with a single-dose of 30Gy via a ^{137}Cs source. The irradiated single-cell suspensions were plated at 60x10^{3} per well. Using flow cytometry, ecto-calreticulin expression was measured 18-, 24-, and 48 hours post-treatment. Each treatment condition includes three technical replicates, with the standard deviation shown. The results shown are from one independent experiment (N=1).

3.2.3 Radiation-induced EC-HMGB1 release

To complete the screening of the main ICD markers for radiation, I looked to measure EC-HMGB1 release. To measure EC-HMGB1 release, 129NS1, TAM6 WT, and 9464D WT were irradiated in response to a range of single-dose radiation alongside a non-irradiated control and positive control of doxorubicin. EC-HMGB1 release was measured 24 hours post-treatment via luminescence, along with a standard curve of known concentrations of mouse EC-HMGB1. Luminescence readings obtained from TH-MYCN lines were extrapolated using a standard curve to quantify the concentration of EC-HMGB1 released in response to treatment.

3.2.3.1 Variable EC-HMGB1 release in response to radiation

As shown in Figure 3.7, in response to radiation, EC-HMGB1 release was found to be similar across all three cell lines compared to non-irradiated controls. The EC-HMGB1 release response did not differ in a dose-dependent manner. These results suggest that EC-HMGB1

is not found to be upregulated in response to radiation at 24 hours post treatment. The addition of additional time points would confirm whether dose-dependent differences in EC-HMGB1 would be observed at later time points.

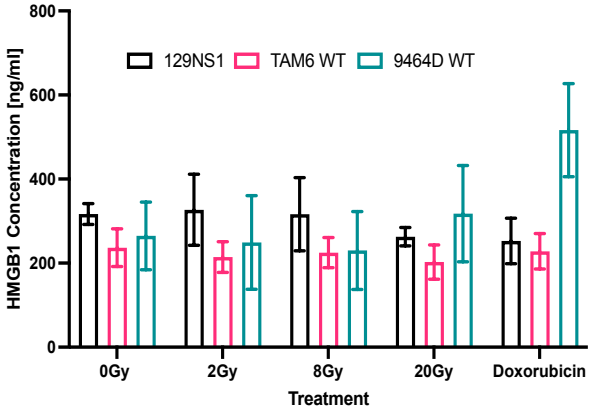

Figure 3.7 The TH-MYCN mouse cell lines did not show upregulation of EC-HMGB1 release in response to single-dose radiation

Mouse neuroblastoma TH-MYCN cell lines, 129NS1 (**black**), TAM6 WT (**pink**), and 9464D WT (**teal**) were irradiated with a range of single-dose γ-radiation using a ^{137}Cs source or treated with positive control, 25μM doxorubicin. The irradiated single-cell suspensions were plated at 20x10^{3} per well, to assess EC-HMGB1 release 24 hours post treatment by luminescence. The results shown were extrapolated using a mouse HMGB1 standard curve. Each treatment condition included four technical replicates, with the standard deviation shown. The results shown are from one independent experiment (N=1).

3.2.4 Neurosphere growth assay optimisations

Because of the variable results observed for the ICD expression dataset for these TH-MYCN mouse neuroblastoma cell lines, I also assessed the radiosensitivity of these cell lines in terms of cell viability to determine any additive effect of single-dose radiation in the absence of immune-mediated effects via ICD. However, before being able to investigate cell viability in response to radiation, I sought to perform some neurosphere growth optimisation assays (Figure 3.8) to evaluate growth characteristics and determine the viability of these TH-MYCN cell lines on the 129/SvJ background before any radiation treatment, as they were found to grow as spheroids in nature with necrotic dense centres. To perform these growth optimisation assays, chemo-naïve lines 129NS1-4B and 129NS1-4B hB7-H3^{+} were evaluated for spheroid-forming assays performed over three days. These lines also showed similar

growth characteristics to the TAM6 lines. These were also better suited for assessing cell viability by luminescence because they were luciferase-expressing.

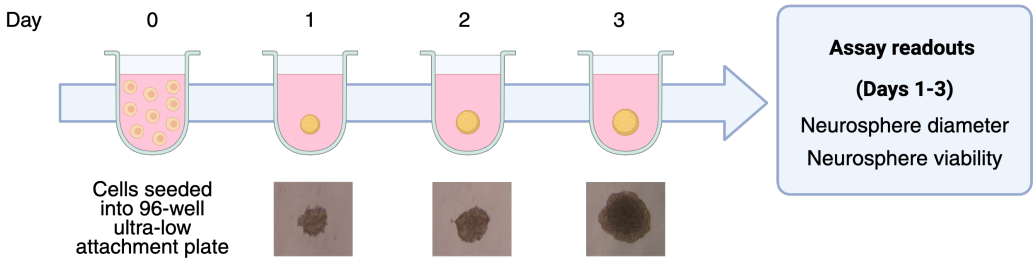

Figure 3.8 Schematic of neurosphere growth assay

Mouse neuroblastoma TH-MYCN luciferase$^+$ cell lines (129NS1-4B and 129NS1-4B hB7-H3$^+$) were plated as single-cell suspensions at varying seeding densities per well in 96-well ultra-low attachment plate(s) at day zero. The formed neurospheres were grown for three days. The formed neurosphere were assessed every 24 hours over the course of a three day spheroid forming assay for changes in neurosphere diameter and cell viability. Representative brightfield images taken at 4x magnification are shown of spheroid growth over the course of the three day spheroid forming assay. Figure created using Biorender.

3.2.4.1 Neurosphere diameter as an indicator of neurosphere growth

The first step was to determine whether neurospheres formed over a three-day spheroid forming assay were growing based on changes in neurosphere diameter. On day zero, 129NS1-4B (Figure 3.9a) and 129NS1-4B hB7-H3$^+$ (Figure 3.9b) cells were plated at densities of 3000, 4000, and 5000 per well in a 96-well plate format. Neurosphere diameters were measured from well images taken at established time points on days one–three post seeding. Neurosphere diameters were found to increase over three days in a time-dependent manner for both 129NS1-4B (Figure 3.9a) and 129NS1-4B hB7-H3$^+$ (Figure 3.9b). A general trend was seen of neuropshere diameter increasing in a manner dependent on seeding density and time.

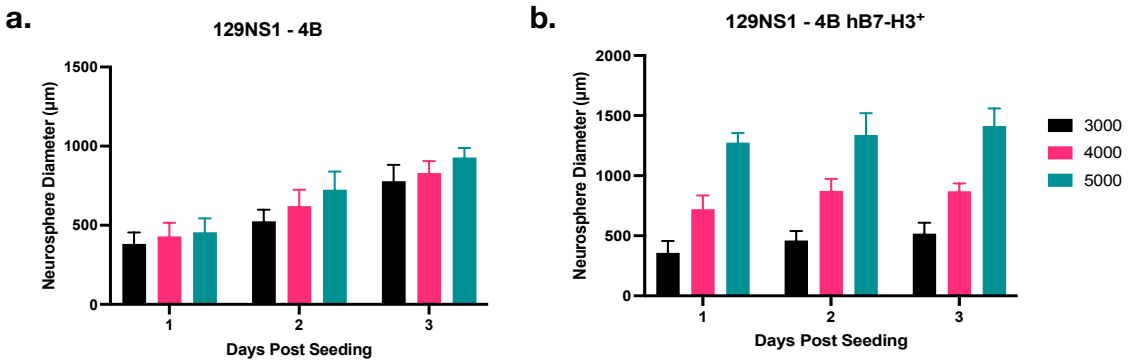

Figure 3.9 129NS1 and 129NS1-4B hB7-H3+ increase in neurosphere diameter when grown as single spheroids

Mouse neuroblastoma TH-MYCN luciferase$^+$ cell lines **a**) 129NS1-4B and **b**) 129NS1-4B hB7-H3$^+$ were plated as single-cell suspensions at 3000 (**black**), 4000 (**pink**), and 5000 (**teal**) per well in 96-well ultra-low attachment plate(s). The diameter of the spheroids was measured every 24 hours over three days post-seeding. For each 24 hour timepoint, brightfield images of the spheroids were taken and used to measure the diameter of the spheres using ImageJ. The results shown are of one independent experiment (N=1).

3.2.4.2 Neurospheres are viable as single grown spheroids

Alongside the neurosphere diameter changes, I also sought to determine the cell viability within neurospheres at each timepoint. This is important in ensuring that tumour cells are viable before the use of radiation to evaluate CAR-T cell functionality in subsequent *in vitro* co-culture experiments.

These three-day spheroid-forming assays were performed in the same way as described in the previous section (section 3.4.1) with 129NS1 and 129NS1-4B hB7-H3$^+$. Both of these lines were luciferase$^+$, and viability was assessed using luminescence via the addition of luciferin. Luminescence emitted by the viable luciferase$^+$ cells was measured as an indicator of cell viability. For the three day sphere-forming assay, 129NS1-4B (Figure 3.10a) and 129NS1 4B-hB7-H3$^+$ (Figure 3.10b) were found to be viable across the three seeding densities. The luminescence levels were found to increase across the three seeding densities in a time-dependent manner for both cell lines, suggesting cells are viable during this assay (Figure 3.10). The level of luminescence was found to be similar across all three seeding densities at the three time points evaluated (Figure 3.10). Large variability in luminescence readings, as shown by the error bars, was observed across the two cell lines on day three post seeding (Figure 3.10). The variability observed may be due to the heterogeneity of the

spheroid sizes seen. Overall, these results suggest that the neurospheres are viable throughout the three-day sphere-forming assay across the three seeding densities evaluated.

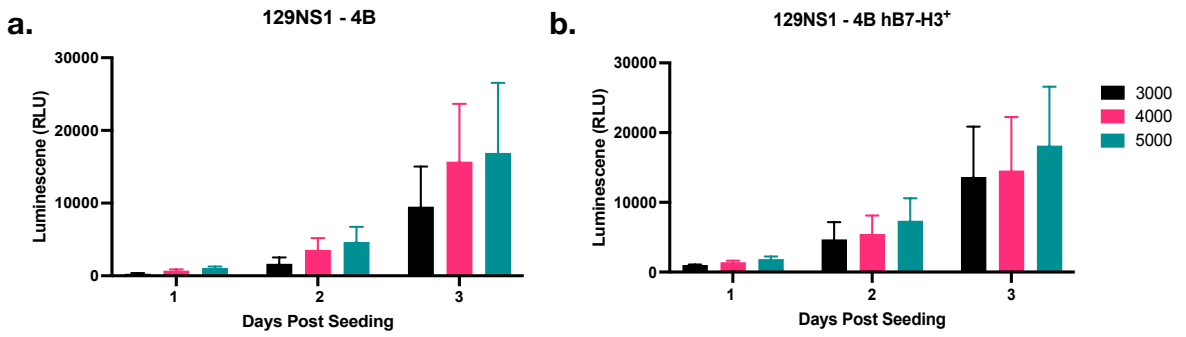

Figure 3.10 129NS1 and 129NS1-4B hB7-H3+ are viable when grown as single spheroids

Mouse neuroblastoma TH-MYCN luciferase+ cell lines, **a**) 129NS1-4B and **b**) 129NS1-4B hB7-H3^{+} were plated as single-cell suspensions at 3000 (**black**), 4000 (**pink**), and 5000 (**teal**) per well in a 96-well ultra-low attachment plate(s). The viability of the spheroids formed was measured every 24 hours for three days post-seeding. Viability was measured by luminescence using luciferin. The results shown are representative of two independent experiments (N=2).

3.2.4.3 Estimating cell number using a standard curve

Having established that the neurosphere lines are able to form spheroids which are growing and consist of viable cells based in terms of increasing neurosphere diameter and luminescence by luciferase, there is a need to determine and define the cell number of the spheroids formed during these growth-forming assays. This is important for determining the corresponding effector: target (E:T) ratio to define when performing co-cultures to assess the effect of radiation on CAR-T cell functionality against these mouse neuroblastoma lines.

To determine cell number, the sphere forming assays were performed as previously mentioned (section 3.4.1) with 129NS1-4B and 129NS1-4B hB7-H3^{+}. However, on day zero of the assay, standard curves of known cell numbers were plated and luminescence readings were measured from the plated cells one day post seeding as formed spheres. Standard curves were then used to interpolate the luminescence readings obtained from the spheres plated at different seeding densities to estimate the cell numbers throughout the assay.

Figure 3.11 shows that the results vary between the two lines. 129NS1-4B hB7-H3$^+$ (Figure 3.11b) showed the hypothesised trend of increasing cell number in line with neurosphere growth over the three days across the three seeding densities. However, on day three, there was a large variability in the results, as evidenced by the large error bars, especially for seeding densities of 4000 and 5000 (Figure 3.11b). One of the reasons for this might be the extrapolation of data points outside the range of the standard curve.

Similar to 129NS1-4B hB7-H3$^+$, 129NS1 showed a clear trend of increasing cell number in a time-dependent manner for initial seeding of 3000 to 4000 cells per well. However, great variability was seen at three days post-seeding across the three seeding densities. The lack of an expected trend of increasing cell numbers in line with the trends of neurosphere diameter and viability over time might be due to the technical difficulties in-extrapolating cell numbers based on a standard curve. Based on the results across the two lines, 3000 cells per well is the number for forming neurospheres that will be viable and with sufficient target cell numbers at three days post-seeding to perform co-cultures to ascertain the effect of radiation on CAR-T cell functionality. As these seeding densities have only been performed with 129NS1 and 129NS1-4B hB7-H3$^+$ cells, further experiments need to be performed to evaluate whether these findings are observed in other mouse neuroblastoma models of interest, such as the 9464D and TAM6 lines.

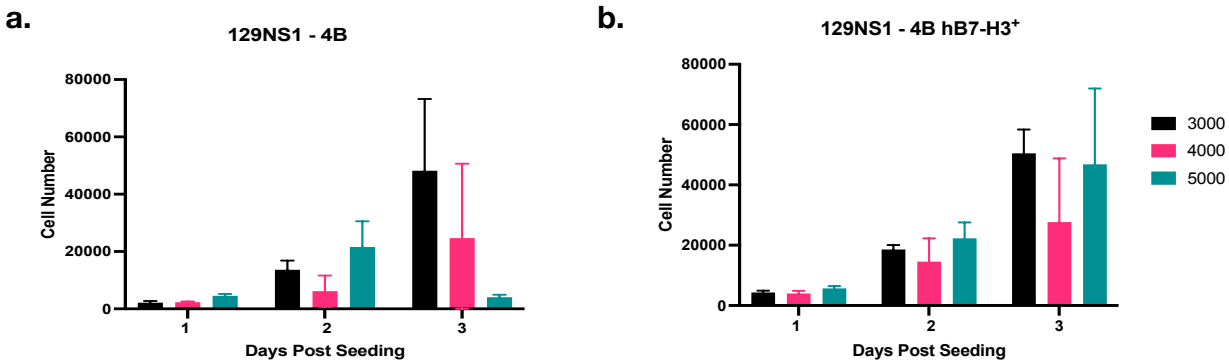

Figure 3.11 The cell number of spheroids can be extrapolated using standard curves

Mouse neuroblastoma TH-MYCN luciferase$^+$ cell lines, **a**) 129NS1-4B and **b**) 129NS1-4B hB7-H3$^+$ were plated as single-cell suspensions at 3000 (**black**), 4000 (**pink**), and 5000 (**teal**) per well in a 96-well ultra-low attachment plate(s). The viability of the spheroids formed was measured every 24 hours for three days post-seeding. Viability was measured by luminescence. The cell numbers were interpolated from a standard curve of known cell numbers. The results shown are of one independent experiment (N=1).

3.2.5 The effect of single dose radiation on *in vitro* cell viability

Assessing the radiosensitivity of TH-MYCN neuroblastoma lines was not solely based on the expression of ICD markers, as mentioned in the introduction of this chapter. It is also imperative to determine the radiosensitivity in terms of cell viability in response to single-dose radiation. This was done to ascertain whether, in the absence of ICD, single-dose radiation resulted in cell death by decreasing cell viability. To evaluate cell viability in response to radiation, I assessed cell viability using the MTT assay compared to clonogenic assays because of the limitations, as discussed further in section 3.3.

The assays were performed with cells irradiated at a range of single-dose radiation using a ^{137}Cs source, and MTT readouts were performed every 24 hours post treatment over a 72 hour time course. The MTT assay assesses mitochondrial activity as an indicator of cell viability. This is based on the conversion of MTT into insoluble formazan crystals by mitochondrial dehydrogenase in living cells, which provides a colourimetric change that can be measured using absorbance. In parallel to the MTT assays, well images were taken to ascertain if the MTT results were indicative of the phenotype of the cells. Well images are shown for 129NS1 (Figure 3.13) and TAM6 WT (Figure 3.15), but not for 9464D WT. This is because the contrast of the bright field image was not strong enough to discern changes in cell growth for 9464D WT (data not shown).

3.2.5.1 Cell viability of 129NS1 lines is affected by radiation

For the chemo-naive lines 129NSI (Figure 3.12a), 129NS1-4B (Figure 3.12b), and 129NS1-4B hB7-H3^{+} (Figure 3.12c), cell viability was reduced in response to single-dose radiation. For all three lines, all doses of radiation reduced cell viability from 24 hours to 72 hours post irradiation (Figure 3.12). Recovery of cell viability was not observed for doses greater than 10Gy at 48-72 hours post irradiation (Figure 3.12). Results at 5Gy in cell recovery differed across the three lines, with 129NS1 showing potential recovery at 72 hours, whereas subclones 129NS1-4B and 129NS1-4B hB7-H3^{+} showed little cell recovery. This may be the result of subclones being more sensitive to radiation with little cell recovery for doses higher than 5Gy compared to the parental 129NS1 line.

All three lines were sensitive to the lowest dose of 2Gy in reducing cell viability. However, this effect was sustained only until 48 hours post radiation, with recovery in cell viability observed at 72 hours post irradiation. This suggests that 2Gy induces a rapid irradiation effect;

however, a sufficient number of cells survived and proliferated within 72 hours, resulting in the recovery of cell viability (Figure 3.12). It is essential to note that the sample variation observed within this dataset (Figure 3.12) may be attributed to technical issues associated with the MTT assay, such as inconsistencies in pipetting accuracy, formazan crystal solubilisation, and variations in spectrophotometer settings (381).

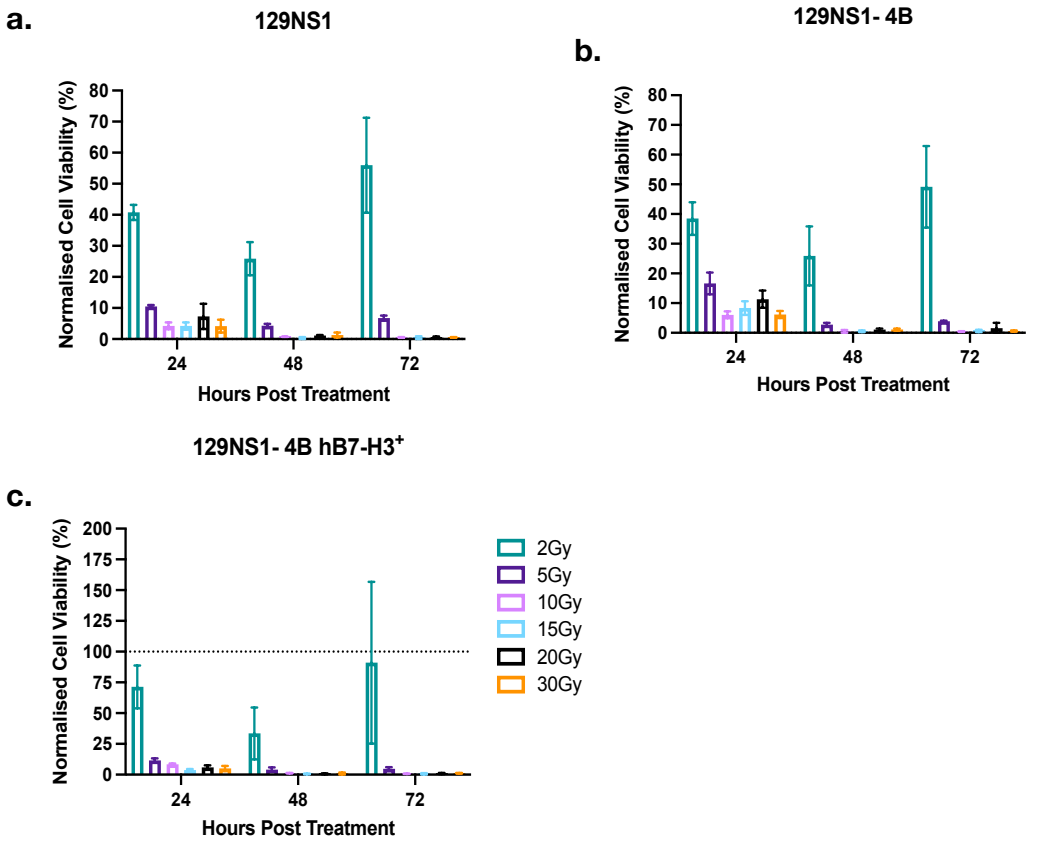

Figure 3.12 Cell viability of the 129NS1 lines is affected in response to single-dose radiation

Mouse neuroblastoma TH-MYCN allograft lines, **a**) 129NS1, **b**) 129NS1 – 4B, and **c**) 129NS1 – 4B hB7-H3^{+} were irradiated with a range of single dose γ-radiation using a ^{137}Cs source. The irradiated single-cell suspensions were plated at 20x10^{3} per well to assess cell viability using MTT every 24 hours within a 72-hour time course. The results were normalised against the negative control, 0Gy and are shown as a percentage of cell viability. Each treatment condition includes three technical replicates with the standard deviation shown. The results are representative of two independent experiments (N=2).

The well images of 129NS1 (Figure 3.13) taken in parallel with the MTT assay (Figure 3.12a) supported each other. As observed with the MTT assay, all doses of radiation caused cell death with fewer and smaller spheroids compared to the non-irradiated control at 0Gy (Figure 3.13). Moreover, this effect of cell death was sustained in a time-dependent manner at doses of 10-30Gy (Figure 3.13). As observed in the MTT assay (Figure 3.12), cell death induced by lower doses of 2-5Gy was not sustained, and recovery of cell growth was observed at 48 and 72 hours post irradiation (Figure 3.13). This suggests that the effect of doses lower than 5Gy on 129NS1 is short-lived which may be due to these lower doses leading to a cytostatic effect or being cytotoxic to a minority of cells whlist the surviving cells recover and increase over time.

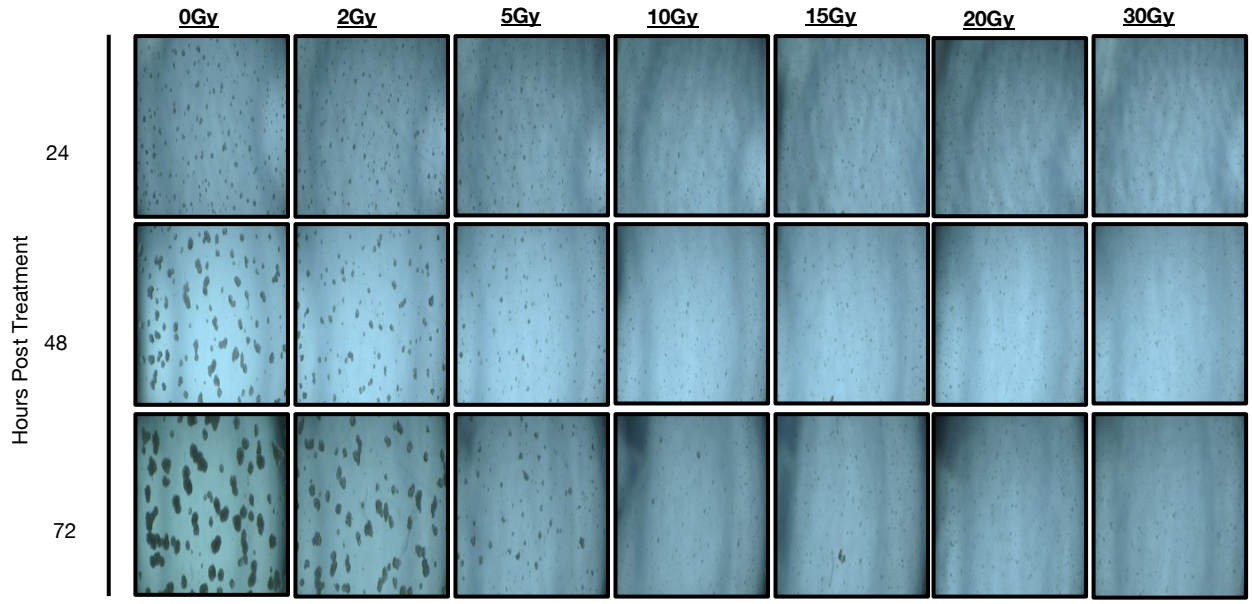

Figure 3.13 129NS1 is sensitive to radiation with evidence of cell death in response to a range of single dose radiation

The mouse neuroblastoma TH-MYCN allograft line 129NS1 was irradiated with a single dose of γ radiation using a ^{137}Cs source. The irradiated single-cell suspensions were plated at 20x10^{3} per well to assess cell viability using the MTT assay. Over the course of 72 hours, prior to the use of these plates for MTT readout every 24 hours, brightfield images were taken of wells at 4x magnification to assess the visual effect of irradiation on the cells. The results are representative of two independent experiments (N=2).

3.2.5.2 Cell viability of TAM6 lines is affected by radiation

Next, the effect of single-dose radiation on the viability of chemoresistant TAM6 lines was determined. In response to radiation, TAM6 WT (Figure 3.14a) and TAM6 hB7-H3^{+} mCherry^{+}

(Figure 3.14b) showed a decrease in cell viability in response to doses evaluated from 5-30Gy. In response to the lowest dose of 2Gy evaluated, a decrease in cell viability was observed in TAM6 WT at 72 hours post irradiation. The viability of TAM6 hB7-H3^{+} mCherry^{+} cells did not appear to be affected by 2Gy throughout the time course (Figure 3.14b). Doses above 10Gy were more effective in decreasing cell viability at 48 hours post irradiation onwards for both TAM6 lines (Figure 3.14). Compared to TAM6 WT, TAM6 hB7-H3^{+} mCherry^{+} showed an earlier onset of cell viability reduction with higher doses of 20-30Gy from 48 hours post irradiation (Figure 3.14).

Like the 129NS1 lines, TAM6 lines are susceptible to radiation in terms of decreasing cell viability, with TAM6 WT more so than the subclone line TAM6 hB7-H3^{+} mCherry^{+} (Figure 3.14). However, this effect is found to be more delayed than with the 129NS1 lines (Figure 3.12), with the effect of radiation seen on cell viability from 48 hours post irradiation onwards as opposed to 24 hours post irradiation (Figure 3.14). Doses above 5Gy were found to have an effect on decreasing cell viability (Figure 3.14). Because of the delayed effect of decreasing cell viability seen with these TAM6 lines, additional time points beyond 72 hours would be informative in determining how sustained this effect is in decreasing cell viability.

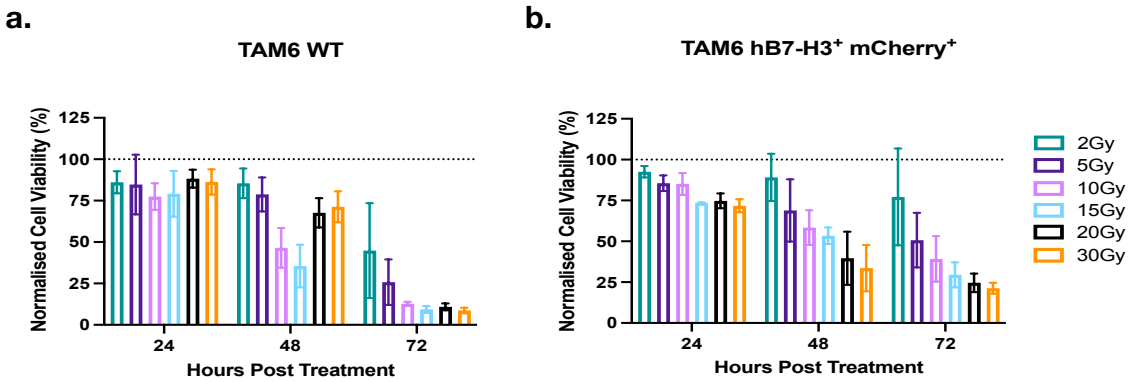

Figure 3.14 The TAM6 lines are more radioresistant, with a slower effect on cell viability seen in response to single-dose radiation

Mouse TH-MYCN allograft lines: **a**) TAM6 WT, and **b**) TAM6 hB7-H3^{+} mCherry^{+} were irradiated with a range of single dose γ-radiation using a ^{137}Cs source. The irradiated single-cell suspensions were plated at 20x10^{3} per well to assess cell viability using MTT every 24hr, within a 72-hour time course. The results were normalised against the negative control (0 Gy) and are shown as a percentage of cell viability. Each treatment condition includes three technical replicates within the same experiment, with the standard deviation shown. The results shown are representative of two independent experiments (N=2).

The well images of TAM6 WT support the findings from the MTT results (Figure 3.14), with the radiation having a delayed and reduced effect on decreasing cell viability (Figure 3.15). Moreover, with the well images, it was harder to determine any of the effects of radiation on the cells compared to the non-irradiated control, as these cells seemed to be more radioresistant than the 129NS1 lines. The clearest effect within the images is the smaller spheroid formation as seen as compared to the non-irradiated control (Figure 3.15).

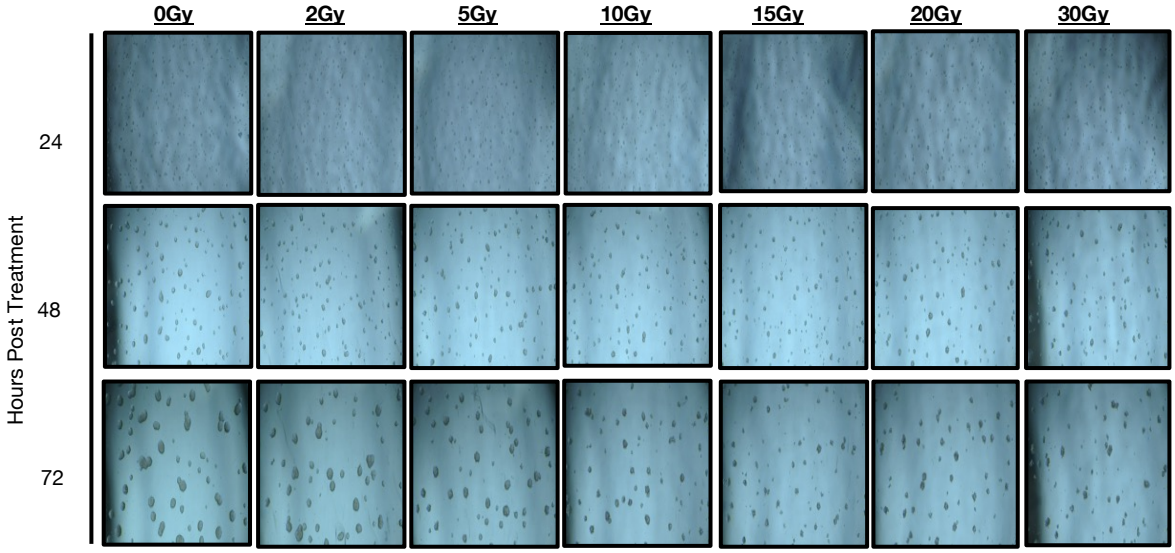

Figure 3.15 TAM6 WT appears radioresistant, with some evidence of cell death in response to radiation

TAM6 WT was irradiated with a range of single dose γ-radiation using a ^{137}Cs source. The irradiated single-cell suspensions were plated at 20x10^{3} per well to assess cell viability using the MTT assay. Over a 72 hour timecourse, brightfield images were taken at 4x magnification to assess the visual effect of irradiation on the cells. The results shown are of the same experiment and are representative of two independent experiments (N=2).

3.2.5.3 Cell viability of 9464D lines vary in response to radiation

In response to single dose radiation for the 9464D lines, the results varied between the parental 9464D WT (Figure 3.16a) and the subclone line 9464D hB7-H3^{+} mCherry^{+} (Figure 3.16b). Both 9464D WT and 9464D hB7-H3^{+} mCherry^{+} cells showed little decrease in cell viability in response to doses of 2-5Gy across the time course. Similar to the TAM6 lines, the 9464D lines showed a delayed response in decreasing cell viability in response to radiation. 9464D WT (Figure 3.16a) showed a decrease in cell viability in response to 10-30Gy from 48 hours post radiation onwards. This effect was most prominent for doses between 15-30Gy (Figure 3.16). Similar to 9464D WT cells, 9464D hB7-H3^{+} mCherry^{+} cells showed a decrease

in cell viability in response to doses greater than 5Gy. However, the reduction in cell viability was most pronounced at 72 hours post irradiation. The results show a large variation in the technical replicates shown and thus are not suitable for statistical analysis of differences between conditions to confirm the trends seen.

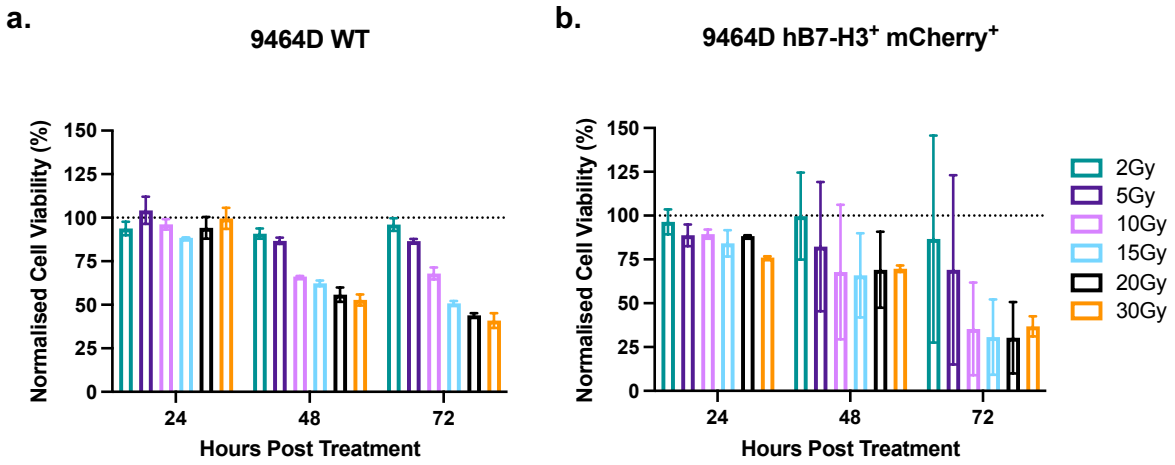

Figure 3.16 Cell viability of the 9464D lines is less affected by single-dose radiation

TH-MYCN cell lines, **a**) 9464D WT and **b**) 9464D hB7-H3^{+} mCherry^{+} were irradiated with a range of single dose γ-radiation using a ^{137}Cs source. The irradiated single-cell suspensions were plated at 20x10^{3} per well in a 96-well flat-bottom attachment plate(s) to assess cell viability using MTT every 24 hours within a 72-hour time course. The results were normalised against the negative control (0Gy) and shown as a percentage of cell viability. Each treatment condition includes three technical replicates, with the standard deviation shown. The results shown are representative of two independent experiments (N=2).

3.2.6 Cell viability of TH-MYCN lines vary in *in vitro* radiosensitivity

The results of the MTT assay, discussed in section 3.2.5 describe the effect of radiation on *in vitro* cell viability across the TH-MYCN mouse neuroblastoma models screened. Figure 3.17 provides a summary of this dataset. The half-maximal inhibitory radiation dose (IC_{50}) was determined for 24, 48 and 72 hours post treatment for all cell lines screened, using the MTT results described in section 3.2.5. The mean of those calculated IC_{50} values is shown in Figure 3.17 and shows that the screened neuroblastoma lines vary in radiosensitivity. As hypothesised, chemo-naïve lines 129NS1, 129NS1-4B, and 129NS1-4B hB7-H3^{+} seemed to be radiosensitive with an IC_{50} range of 1.7-2.4 Gy suggesting that a low dose of 2Gy will affect cell viability (Figure 3.17). The chemoresistant TAM6 WT and TAM6 hB7-H3^{+} mCherry^{+} were found to have a higher IC_{50} between 17-20Gy, indicating that, compared to the 129NS1 lines,

higher doses of radiation are required for radiation-induced cell death. The 9464D lines were found to be the most radioresistant, with IC_{50} found to be between 41-48Gy. This suggests that doses above 40Gy are required for any immediate effect of radiation-induced cell death (Figure 3.17).

TH-MYCN Lines	IC_{50} (Gy)
129NS1	1.7
129NS1 - 4B	1.5
129NS1 - 4B hB7H3$^+$	2.4
TAM6 WT	20.2
TAM6 hB7-H3$^+$ mCherry$^+$	17.5
9464D WT	47.7
9464D hB7-H3$^+$ mCherry$^+$	41.2

Figure 3.17 The TH-MYCN lines of neuroblastoma vary in radiosensitivity *in vitro*

Mouse neuroblastoma TH-MYCN lines were irradiated at a range of single dose γ-radiation using a ^{137}Cs source. The irradiated single-cell suspensions were plated at $20x10^3$ per well in a 96-well flat-bottom attachment plate(s) to assess cell viability using MTT every 24 hours within a 72-hour time course. The data were normalised against the negative control, 0Gy, and analysed through non-linear regression to ascertain the IC_{50} at 24 hour intervals throughout the 72 hour time course. The table displays the average of these calculated IC_{50} values. The results shown are from one independent experiment (N=1).

3.3 Discussion

As little is known about the radiosensitivity of TH-MYCN mouse neuroblastoma models (129NS1, TAM6, and 9464D) within the literature, an *in vitro* radiosensitivity screen was developed to ascertain the effects of single-dose radiation on these models of interest. The *in vitro* radiosensitivity screen focused on examining both the immune and non-immune mediated effects of radiation. The immune-mediated effects of radiation involved screening of the key markers of immunogenic cell death: EC-ATP, EC-HMGB1, and calreticulin. In

response to a range of single-dose radiation doses, variable results were observed for these ICD markers across the screened TH-MYCN lines.

The results of the EC-ATP time course revealed that in response to a range of single-dose radiation, no upregulation in EC-ATP was observed across all the cell lines screened except TAM6 hB7-H3^{+} mCherry^{+}; further experiments are required to ascertain the statistical significance of these findings. Within the literature, the measurement of EC-ATP in response to ICD has been mostly defined by the use of luminescence-based assays as performed above (380). However, a consideration that needs to be taken into account with the use of these assays is that EC-ATP levels may be diminished by the expression of ATP-degrading ectonucleotidases, CD39 and CD73 expressed by cancer cells (382,383). This may lead to false observations of no discernible differences in EC-ATP levels in response to radiation compared with non-irradiated controls. The expression of these ecto-nucleotidases has not been well defined in the literature within the screened mouse neuroblastoma lines; therefore, further investigation is required. If the expression of ecto-nucleotidases is confirmed in these mouse neuroblastoma lines, their confounding effect on EC-ATP levels can be confirmed by performing these luminescence-based assays in the presence of neutralising anti-CD39/CD73 antibodies. A non-luminescence-based assay can be used to measure ATP release. Intracellular staining of ATP-containing vesicles can be performed using the fluorochrome quinacrine, which turns green in the presence of ATP (384). This allows quantitative measurement of ATP release via flow cytometry or fluorescence microscopy (384,385). However, fluorochrome labelling and subsequent flow analysis of spheroids have not been optimised, and may be problematic for use in these TH-MYCN primary lines.

The results of calreticulin expression data revealed that radiation can induce upregulation of this marker in the 129NS1, TAM6, and 9464D lines. However, differences were observed in the response of subclones of TAM6 and 9464D to their corresponding parental lines, with diminished or no upregulation, respectively. This response may have been due to the subclones used to generate these lines. Both TAM6 hB7-H3^{+} mCherry^{+} and 9464D hB7-H3^{+} mCherry^{+} cells were generated via viral transduction. This could result in differences in cell biology compared to the parental lines, resulting in varied calreticulin expression in response to radiation (386,387). No discernible differences were observed in EC-HMGB1 release across the screened TH-MYCN cell lines. It may be that the release of EC-HMGB1 is time-dependent; therefore, additional work to perform the time course at later time points may allow any differences in EC-HMGB1 release in a dose- and time-dependent manner to be seen.

To ascertain the non-immune mediated effect of radiation, I evaluated this using an MTT assay. Within the field of radiation, the clonogenic assay has been established as the gold standard for assessing cell survival in response to radiation inducers *in vitro*. The assay, developed in 1956 by Theodore Puck and Philip Marcus, assesses radiosensitivity based on the ability of a tumour cell to retain the ability to form a colony, usually within two weeks (388). While the assay is considered a staple for assessing radiosensitivity, it has its disadvantages. The assay itself is quite time-consuming, as the readouts of the assay usually occur two weeks post irradiation (389,390). This makes the assay less suitable when looking for a high-throughput method for assessing multiple cancer cell lines simultaneously. Moreover, the assay has been well established for 2D-based cell culture, but less so for more biologically relevant 3D tumour spheroid lines, such as the 129NS1 and TAM6 neuroblastoma lines (390,391).

Due to the drawbacks of the clonogenic assay mentioned above, the effect of radiation on cell viability was assessed using the MTT assay. This assay assesses mitochondrial activity as an indicator of cell viability (389,392). This process is based on the conversion of MTT into insoluble formazan crystals by mitochondrial dehydrogenase in living cells (392). This can be measured using a spectrophotometer, allowing the quantification of cell viability. The MTT assay also provides the additional benefit of being adaptable to the 96-well plate format compared with the classical clonogenic assay, allowing a more desired high-throughput approach to assess multiple tumour cell lines in a short-term assay. The results of the MTT assay showed a wide range of radiosensitivity across the TH-MYCN lines screened, which provides the opportunity to evaluate CAR-T functionality against a range of treatment-sensitive neuroblastoma models when evaluating the effect of radiation on CAR-T functionality against these models.

The results of the neurosphere growth optimisation assays also provided further understanding of the use of neurosphere lines 129NS1 and TAM6 in subsequent co-cultures to evaluate CAR-T cell functionality. The results revealed that the neurospheres grew and were viable over three days. The use of standard curves allows cell numbers to be extrapolated to determine the appropriate effector: target ratios to evaluate the effect of radiation on CAR-T functionality against these models of interest.

The results of this chapter have confirmed that the screened mouse neuroblastoma models are responsive to radiation, and this is dose- and time-dependent. This suggests that these

models are suitable for evaluating the effect of radiation on CAR-T functionality in neuroblastoma.

Chapter 4 Evaluate CAR candidate for investigating the effect of radiation on antigen-specific T-cells.

4.1 Introduction

This project aimed to elucidate the impact of radiation on CAR-T cell functionality in neuroblastoma. Having established that TH-MYCN transgenic models of high-risk neuroblastoma exhibit varying degrees of radiosensitivity, thus rendering them suitable models for evaluating this combination therapy *in vitro* and *in vivo*, the next aim of this project was to identify an appropriate CAR candidate for targeting these models of high-risk neuroblastoma.

For neuroblastoma, immunotherapy has largely focused on targeting disialoganglioside GD2 with an anti-GD2 antibody therapy, dinutuximab, the only approved therapy in the clinic. Even though this has improved survival outcomes, relapse still occurs among patients with high-risk disease; thus, alternative candidates are currently being evaluated to improve survival outcomes in these patients (20). One candidate of interest is B7-H3, a cell surface protein that is highly expressed in a range of solid tumours, including neuroblastoma, with restricted expression in healthy tissues (191,393). B7-H3 belongs to the B7 family, which are cell surface ligands or receptors involved in regulating immune responses through their interaction with cognate receptors or ligands expressed on immune cells (394). B7-H3 is a highly conserved protein across different species, including mice. In humans, there are two main splicing isoforms of B7-H3 (hB7-H3): 2Ig-B7-H3 and 4Ig-B7-H3, the latter of which is more commonly expressed in human tissues and cell lines (394,395). Murine B7-H3 (mB7-H3) is expressed on chromosome 9 and exists as one isoform (2Ig-B7-H3) with 88% sequence similarity to hB7-H3 (396).

Recent advances have been made in the development of anti-B7-H3 immunotherapies. This includes the evaluation of B7-H3 in formats ranging from monoclonal antibody therapies to CAR-T cells. Regarding CAR-T cell therapies, the literature has highlighted a few anti-B7-H3 ScFvs that are being developed, showing efficacy against a range of solid tumours (1,196,397–399). However, the *in vivo* evaluation of CAR-T therapies has largely focused on the use of immunodeficient mice to evaluate against cell line-based or patient-derived xenograft models. Therefore, a thorough evaluation of the therapy cannot be performed within the immunodeficient setting, considering the potential off-target effects associated with CAR therapy.

To fully investigate the effect of radiation on CAR-T cell functionality, this project aimed to utilise a fully immunocompetent setting to effectively evaluate treatment efficacy, accounting for the immune-mediated effects of radiation and potential off-target effects of CAR-T cell therapy. This would provide a greater translation of preclinical findings compared with the use of immunodeficient models. As a result of this, I sought to identify a B7-H3 candidate reported to be cross-reactive to mouse and human B7-H3, of which 376.96 has been reported to be so (1).

4.1.1 376.96

According to the literature, the development of 376.96 dates back to 1982. Imai et al. immunised mice with the human melanoma cell line COLO 38, resulting in the secretion of an IgG2a monoclonal antibody 376.96S from a hybridoma (400). At the time, the target to which it was bound was unknown, but it was later identified as B7-H3. Since its discovery, 376.96 has been evaluated as a monotherapy or in combination with other treatments against solid tumours, such as ovarian and pancreatic cancer (368,401–403). 376.96 has also been evaluated as CAR-T cell therapy against solid tumours, showing both *in vitro* and *in vivo* efficacy (1,404–407). While most of the evaluation of 376.96 has been within human CAR-T cells, in 2019, Du et al. reported 376.96 cross-reactivity to both human and mouse B7-H3 (1). 376.96 mAb was found to be cross-reactive to both mB7-H3 overexpressed on Raji Cells and endogenously expressed mB7-H3 on bone-marrow-derived dendritic cells (BMDCs) from C57BL/6 mice (1). They subsequently generated 376.96 mouse CAR-T cells with murine CD28-CD3z and 4-1BB-CD3z endodomains and showed *in vitro* cytotoxicity, with further evaluation in immunocompetent orthotopic murine PDAC models showing transient tumour shrinkage and no evident toxicity (1). Because of these reported findings on cross-reactivity of 376.96 to mB7-H3, and its evaluation in immunocompetent mice, I was interested in evaluating the potential of this CAR candidate for use in this project.

4.2 Results

4.2.1 Structure of 376.96.m28z

The SFG.376.96.mCD8STKTM.mCD28z (376.96.m28z) is a second generation anti-B7-H3 CAR. As shown in Figure 4.1a, the CAR construct consists of the anti-B7-H3 ScFv, 376.96 with a mouse CD8α hinge and transmembrane domain, and mouse CD28-CD3ζ

endodomains. The design and molecular cloning to produce this construct were performed by Dr. Jennifer Frosch and Alice Vitali, respectively. Transduction efficiency of 376.96.m28z was initially assessed using the c-myc epitope tag included in the CAR construct. However, owing to the work that was performed in generating 376.96.m28z.NIS constructs (see section 4.3), transduction efficiency was assessed using rhB7-H3-His tag protein to indirectly stain for the CAR using an anti-His fluorophore-conjugated antibody (Figure 4.1b). Thus, indirect CAR detection by flow cytometry allowed CAR expression to be compared between the 376.96.m28z and 376.96.m28z.NIS constructs.

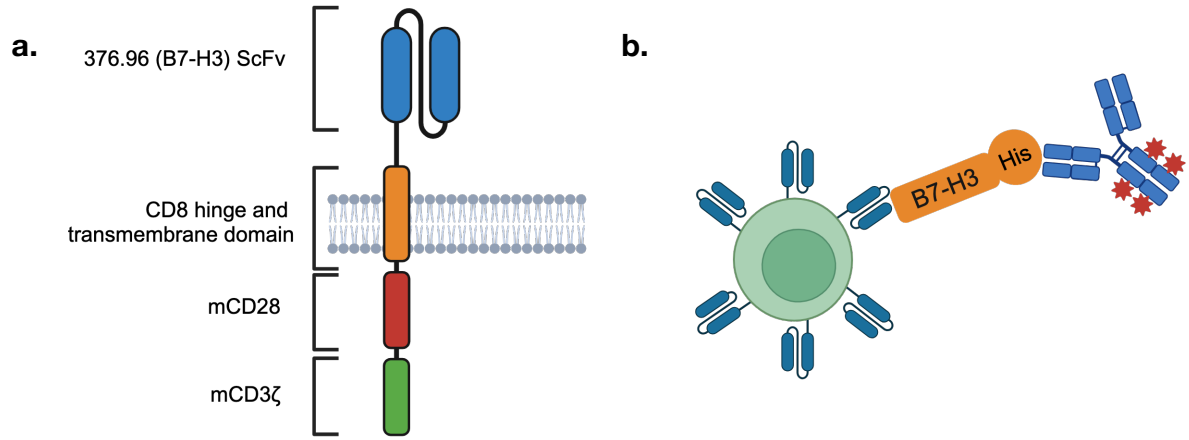

Figure 4.1 Structure of 376.96.m28z and its detection by flow cytometry

376.96.m28z is a second-generation anti-B7-H3 CAR with its structure shown in **a**). The main detection method for 376.96.m28z has been using **b**) a B7-H3-His tag recombinant protein followed by an anti-his fluorophore conjugated antibody. This allows indirect CAR detection using by flow cytometry. Figure created using Biorender.

4.2.2 Transiently produced 376.96.m28z retrovirus induces poor CAR expression

One of the established methods for CAR-T cell production is viral transduction. Human CAR-T cell production methods include both retroviral and lentiviral transduction (408). However, for mouse CAR-T cells, retroviral transduction continues to be the most commonly used method because of the incompatibility of lentiviral vectors with murine T cell biology (409).

Retrovirus generation for mouse CAR-T cell production involves transient transfection of the human epithelial cell line HEK293T with viral packaging and envelope genes to generate

retroviral particles for subsequent T-cell transduction. The viral envelope is imperative for defining the tropism required to bind to the target cells and infect them. Therefore, the packaging 293T cell line Phoenix Ecotropic (Phoenix.Eco) was used in this project. The Phoenix.Eco cell line stably expresses viral packaging genes and envelope with tropism to mouse cells via a mouse-specific ecotropic receptor. This ensures greater transduction success of mouse T-cells compared to non-specific viral envelope proteins, such as VSV-G (410). The use of a packaging cell line means that only the transfer plasmid comprising LTRs and the gene of interest is required in the transfection for retrovirus production because of their stable expression of viral packaging and envelope proteins (410). Consequently, I opted to generate 376.96.m28z mouse CAR T-cells using retrovirus produced from the Phoenix.Eco cell line.

First, I sought to determine if 376.96.m28z mouse CAR-T cells could be generated using unconcentrated (neat) and concentrated retroviruses produced by transient transfection of Phoenix.Eco cells. Splenocytes from 129/SvJ mice were transduced with neat or concentrated retroviruses at increasing multiplicity of infection (MOI). Retroviral titrations were performed on 293T cells to calculate the viral titer to determine MOI. CAR transduction success was determined by the co-expression of the c-myc epitope tag by flow cytometry. Compared to untransduced, retroviruses produced by the transient transfection of Phoenix.Eco cells yielded poor transduction efficiency, with little shift in the c-myc positive population (Figure 4.2a). This shift was not greatly improved by the use of concentrated retroviruses at increasing MOIs (Figure 4.2a). As Figure 4.2b shows, the quantified transduction efficiency seen across the three mouse spleens shows that even using concentrated retrovirus at the highest MOI of 20 yielded a negligible increase in CAR expression compared to unconcentrated retrovirus, with the expression still less than ten percent.

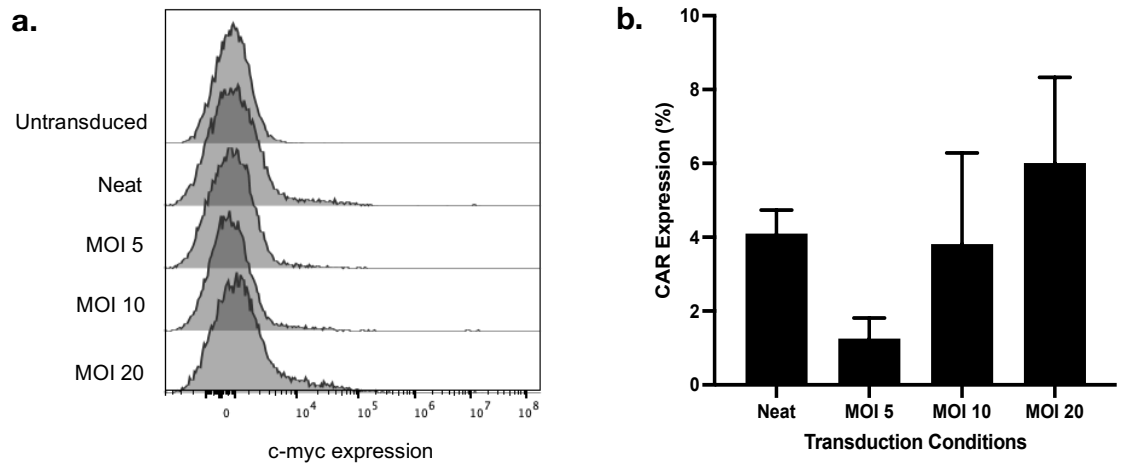

Figure 4.2 Transiently produced 376.96.m28z retrovirus induces poor CAR expression

Retrovirus produced from the transient transfection of Pheonix.Eco cells was used to generate 376.96.m28z CAR-T cells from 129/SvJ female spleens. Transduction was performed with unconcentrated (neat) or concentrated retrovirus at selected MOIs. Three days post transduction, CAR expression was assessed by flow cytometry using the c-myc epitope tag, with **a**) showing c-myc expression in a histogram plot of one mouse spleen, and **b**) showing the quantified percentage of CAR expression with n of 3 (N=3). The error bars shown represent the standard deviation.

4.2.3 A producer cell line improves CAR expression

Due to the suboptimal transduction efficiency of CAR expression observed with the use of retroviruses produced by the transient transfection of Phoenix.Eco, further investigations were conducted to evaluate methods for improving CAR expression through the generation of high-titre retroviruses using a retroviral producer cell line. A retroviral producer cell line is established through viral transduction of producer cells such as Phoenix Eco to stably integrate the transfer gene of interest, resulting in continuous production of a high-level titre of retroviral particles expressing the gene of interest. The advantage of a producer cell line is that it eliminates the need for transient transfection for retrovirus production and allows selection of clones with very high levels of expression. The retroviral titre produced through transient transfection is influenced by various factors, such as transfection method, viability of 293Ts, and quality of plasmid preparations utilised (410).

A producer cell line was generated by Courtney Himsworth and Carla Batiste through viral transduction of the Phoenix Eco cell line with 376.96.m28z retrovirus generated by the

transient transfection of 293Ts. Subsequent single-cell clonal selection of the transduced cells and evaluation of the retrovirus produced yielded a 376.96.m28z producer cell line clone that was propagated, and its retrovirus was utilised to enhance expression of generated 376.96.m28z mouse CAR-T cells.

To ascertain whether the retrovirus produced from the producer cell line enhanced CAR transduction efficiency compared to that of the transiently produced retrovirus, 376.96.m28z mouse CAR-T cells were generated via retroviral transduction using retrovirus from the transient transfection of Phoenix.Eco and 376.96.m28z producer cell line. Concurrently with the generation of mouse CAR-T cells, the retrovirus was also used to transduce the cell line BW5 as a quality control measure for the produced retrovirus. In BW5 cells, retroviruses produced from both transient transfection and the producer cell line exhibited a similar shift in CAR expression, as demonstrated in Figure 4.3a, indicating that both retroviruses can infect cells and induce CAR expression with comparable success. However, when evaluating these retroviruses for mouse CAR-T cell transduction, transient transfection resulted in a poor shift in CAR expression (Figure 4.3b). Conversely, utilising retroviruses from the producer cell line improved transduction efficiency, as evidenced by a greater shift in CAR expression (Figure 4.3b). Analysis of CAR expression across three independent mouse spleens, as illustrated in Figure 4.3c, revealed that CAR expression was significantly enhanced using retrovirus from a producer cell line compared to retrovirus generated from transient transfection, with the difference being statistically significant.

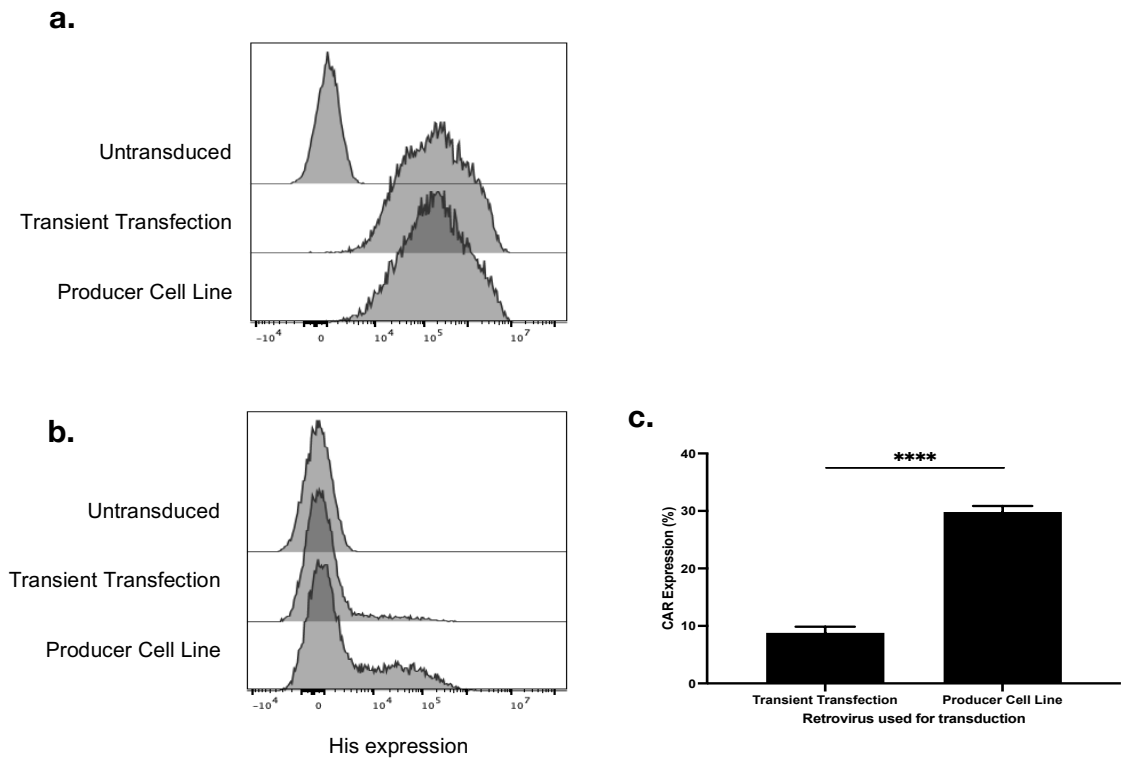

Figure 4.3 CAR expression is improved using retrovirus produced by a 376.96.m28z producer cell line

Retrovirus from the transient transfection of Phoenix.Eco cells or Phoenix.Eco producer cell line was used to generate 376.96.m28z CAR-T cells from 129/SvJ female spleens alongside the cell line control, BW5. Transduction was performed with unconcentrated (neat) retrovirus. Three days post transduction, CAR expression was assessed by flow cytometry using recombinant rhB7-H3-His followed by anti-his staining. His expression is shown as an indicator of CAR expression for **a**) BW5. CAR expression is also shown for **b**) one mouse spleen and **c**) the percentage of CAR expression shown with n of 3 (N=3). The error bars shown represent the standard deviation. Statistical analysis was performed using an unpaired t-test. ****<0.0001.

4.2.4 CAR expression is not sustained during *in vitro* expansion

Human CAR-T cell manufacturing for clinical practice typically ranges from seven to fourteen days for *in vitro* expansion to allow sufficient proliferation to provide the required therapeutic doses for infusion to patients. In line with this, I focused on evaluating this period of *in vitro* expansion for mouse CAR-T cells to be in line with human CAR-T manufacturing processes and to further expand CAR-T cell numbers for use in subsequent *in vitro* and *in vivo* CAR evaluations. For human CAR manufacturing, patient blood is obtained via leukapheresis, which is then enriched for T cells (411). However, for mouse CAR-T cell production, the

source of T cells is mainly mouse spleens; thus, a limited number is obtained after enrichment for T cells for CAR T-cell production. Therefore, it is important to improve CAR expression and the *in vitro* expansion of mouse CAR-T cells.

Within the literature, mouse CAR-T cell expansion *in vitro* has ranged from seven to fourteen days (373,412,413). As a result, an *in vitro* expansion of 376.96.m28z mouse CAR-T cells were compared to untransduced cells over a six day expansion period. Previous results showing CAR expression in sections 4.2.2 to 4.2.3 involved the use of concanavalin A and mouse IL-7 for prior stimulation before viral transduction. CAR expression is enhanced by T-cell specific mitogenic stimulation, such as anti-mouse CD3/CD28 dynabeads (373,414,415). Lanitis and colleagues reported improved proliferation in $CD3^+$ mouse T-cells using anti-CD3/CD28 compared to concanavalin A with hIL-2/IL-7 for their development of a primary murine T cell retroviral transduction and expansion protocol (412).

Prior stimulation with anti-mouse CD3/CD28 dynabeads enhanced 376.96.m28z expression in a statistically significant manner compared with stimulation with concanavalin A and mouse IL-7 (Figure 4.4a). This trend was found to be consistent at later timepoints of five and six days post transduction. However, irrespective of the stimulation method used, CAR expression was not sustained during the six days with hIL-2 expansion. Both showed a decreasing trend in CAR expression throughout the expansion period.

Aside from differences in CAR expression, neither stimulation method used yielded any statistically significant differences in total cell viability (Figure 4.4b-c). This was observed in both untransduced T cells (Figure 4.4b) and 376.96.m28z mouse CAR-T cells (Figure 4.4c), with viable cells observed, irrespective of the stimulation method used. Looking at changes in fold change for total cell expansion, both stimulation methods showed similar levels of two-fold change in total T-cell expansion at three days post transduction. This total cell count fold change was sustained at six days post transduction for 376.96.m28z CAR T-cells, but decreased for untransduced T-cells that underwent stimulation with concanavalin A and hIL-7 (Figure 4.4d).

Due to the enhancement in CAR expression with anti-CD3/CD28 dynabead stimulation, this was established as the method of T-cell stimulation for subsequent experiments performed to generate mouse CAR-T cells. However, irrespective of the stimulation method used, CAR expression decreased throughout the expansion period. Thus, it was important to determine how to improve the CAR expression stability during this expansion period by evaluating the cytokines used for mouse CAR-T cell expansion.

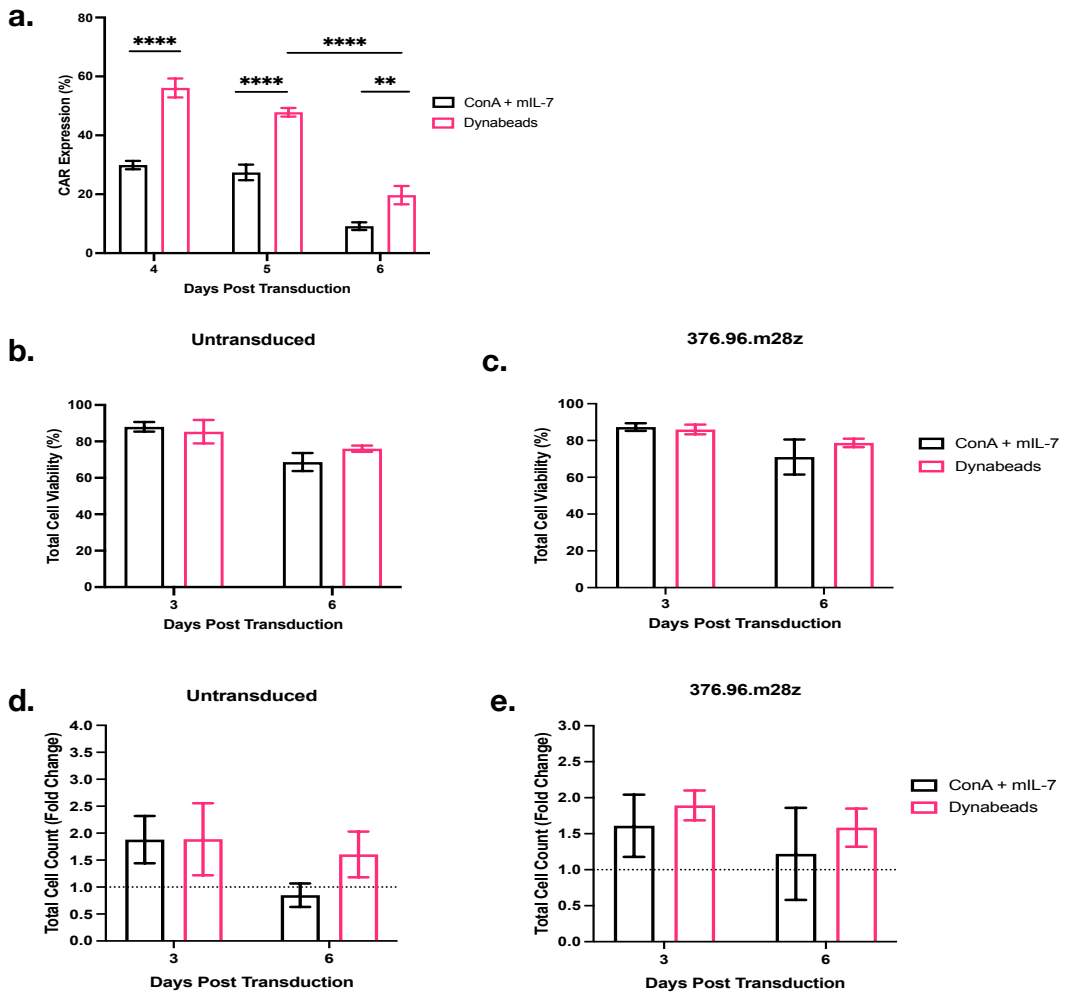

Figure 4.4 CAR expression is not sustained during *in vitro* expansion

129/SvJ spleens were used to generate 376.96.m28z mouse CAR-T cells using retrovirus produced by a P.Eco producer cell line. Splenocytes were stimulated either with concanavalin A (ConA) and mIL-7 or mCD3/mCD28 dynabeads for transduction. Cells were expanded over seven days post transduction with hIL-2. **a**) CAR expression was assessed during expansion by flow cytometry. During the expansion period, viability counts were obtained for **b**) untransduced and **c**) 376.96.m28z CAR-T cells. Cell counts are shown as fold change for **d**) untransduced and **e**) 376.96.m28z CAR-T cells. The error bars shown represent the standard deviation with an n of three (N=3). Statistical analysis was performed using two-way ANOVA. ***<0.0002, ****<0.0001.

4.2.5 The effect of hIL-2,hIL-7 and hIL-15 expansion on CAR expression

The use of hIL-2 for CAR-T cell expansion has been well established for many years because of its role in promoting the proliferation and survival of T-cells (416–418). However, expansion with hIL-2 has been reported to result in the terminal differentiation of T cells, expansion of Tregs, and T-cell exhaustion, which may inhibit the required anti-tumour response desired by CAR-T cells (416–418). Studies have been conducted to enhance CAR expansion by

replacing or combining hIL-2 with additional cytokines such as hIL-7 and hIL-15, which have been reported to improve survival, increase efficacy and preserve a more naïve/central memory phenotype (418–420). This may enhance the functional properties of mouse CAR-T cells and improve their *in vivo* persistence against tumours (412,413). Lanitis et al. reported a 26-fold expansion with anti-VEGFR-2 murine CAR-T cells expanded with hIL-2 followed by hIL-7/hIL-15, compared to a 9-fold expansion with hIL-2 alone at nine days post-expansion (412). Furthermore, expansion was sustained with hIL-7/15 for at least fourteen days, whereas hIL-2 alone resulted in a plateau after seven days of expansion (412). The use of hIL-7 and hIL-15 in mouse CAR-T cell expansion was corroborated by Hayder et al., who demonstrated that functional anti-mB7-H3 mouse CAR-T cells expand with hIL-2 combined with hIL-7 and hIL-15 (413).

Considering the importance of the cytokines used during T-cell expansion, it is imperative to determine the optimal cytokine conditions which may maintain a stable CAR population with no deleterious effects on cell viability and expansion. To evaluate the effect of various cytokine conditions utilised during *in vitro* T-cell expansion and to determine if observations are specific for particular binders in the CAR, alongside the generation of 376.96.m28z mouse CAR-T cells, eGFP mouse T cells, and ALK.h28z mouse CAR-T cells were employed as additional non-CAR and CAR controls to assess the stability of target gene expression during the expansion period under different combinations of cytokines.

eGFP^{+} T cells and CAR-T cells were generated and expanded for a ten day expansion period under three distinct cytokine growth conditions. At the point of splenocyte harvest, rest before transduction, and at the point of transduction, IL-2 was added to promote T-cell proliferation and survival. Three days post transduction, three different cytokine conditions were utilised during the expansion period of ten days (“hIL-2 alone”, “hIL-7 with hIL-15”, and “hIL-2 with hIL-7 and hIL-15”) as shown in Figure 4.5a. T-cells were supplemented on days three, six, and nine post transduction with the different cytokine conditions evaluated (Figure 4.5a). The stability of the target gene expression was subsequently measured throughout the *in vitro* expansion period using flow cytometry.

4.2.5.1 376.96.m28z Expansion

Figure 4.5b shows histogram plots of 376.96.m28z CAR expression from one independent mouse spleen compared with untransduced cells during the *in vitro* expansion period. At day

four post transduction, significant CAR expression was observed across all three cytokine growth conditions compared to the untransduced control (Figure 4.5b). However, by day seven and ten post transduction, CAR expression was greatly diminished across all cytokine growth conditions (Figure 4.5b).

Upon analysis of the percentage of CAR expression across three independent mouse spleens (Figure 4.5c), alterations in the cytokine growth conditions resulted in comparable levels of initially high CAR expression at day three post transduction, which was subsequently reduced by day seven and ten post transduction in a time dependent manner. The CAR gMFI results presented in Figure 4.5c correspond to the CAR expression percentage results shown in the same Figure, with CAR gMFI decreasing over the course of the expansion period in a time-dependent manner and without significant differences in CAR gMFI among the three different cytokine growth conditions assessed. This observation suggests that changes in cytokine conditions do not appear to lead to any improvement in the stability of 376.96.m28z CAR expression.

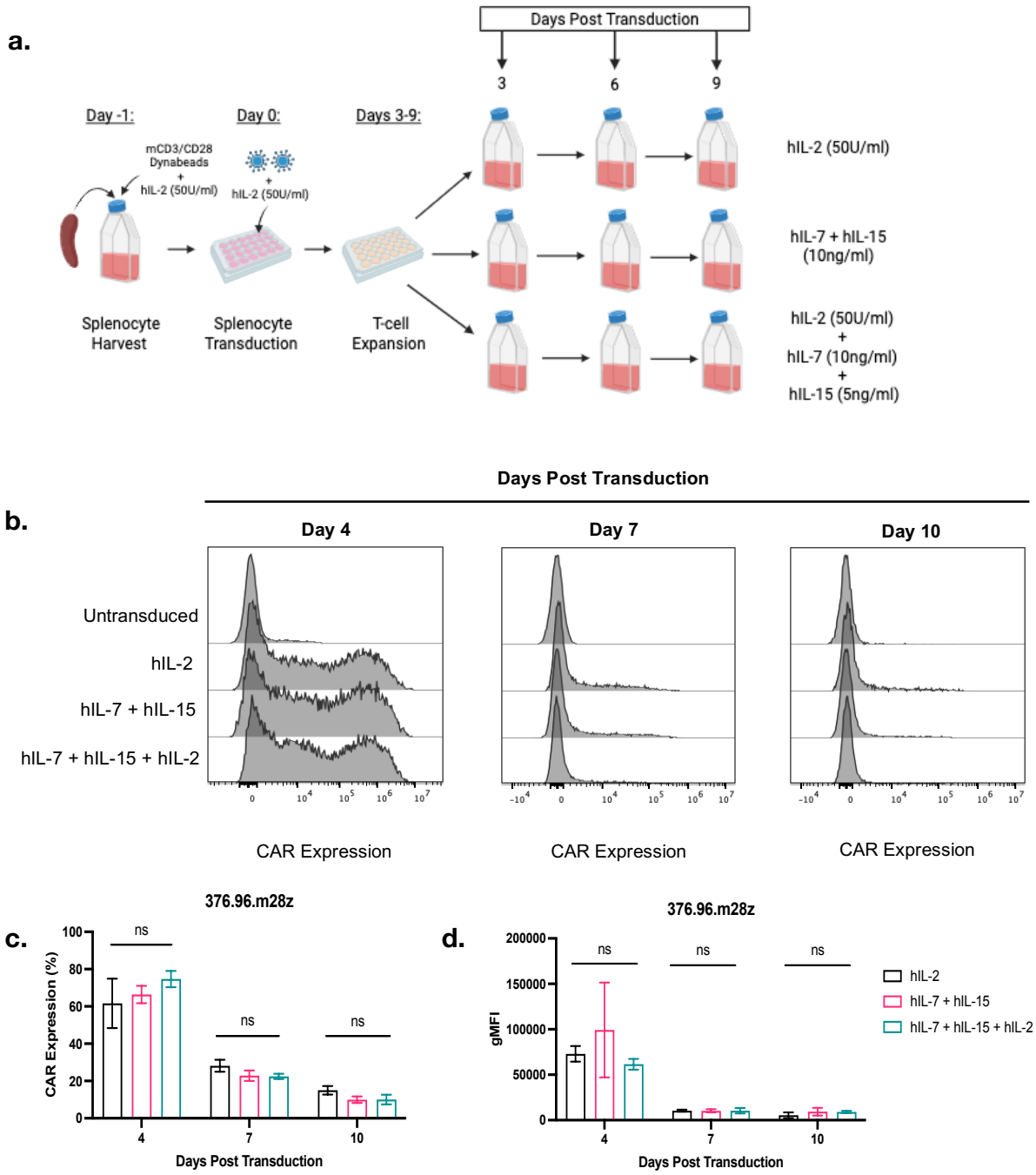

Figure 4.5 Changes in cytokine expansion conditions does not lead to stable 376.96.m28z expression

376.96.m28z CAR T-cells were generated from 129/SvJ spleens. Cells were expanded for 10 days post transduction using different cytokine combinations as shown in **a**) to improve T-cell expansion. CAR expression was evaluated by flow cytometry with **b**) histogram plots showing expression in one independent over the course of expansion. For three independent donors, **c**) CAR expression and **d**) gMFI is shown. The error bars shown in the graphs represents the standard deviation with an n of three (N=3). Statistical analysis was performed using two-way ANOVA. ns<non-significant.

4.2.5.2 ALK.h28z Expansion

To assess the stability of the CAR control, expansion of ALK.h28z (plasmid construct designed by Henrike Muller), under different cytokine conditions, as described in Section 4.2.5 was assessed. The construct includes the epitope marker RQR8 and it's co-expression was used as an indication of expression from the integrated viral expression cassette. Figure 4.6a shows histogram plots showing CAR expression across T-cells derived from one representative mouse spleen, revealing a similar shift in CAR expression across all three individual cytokine growth conditions with no discernible differences in CAR expression at days three and seven post transduction. At day ten post transduction, CAR expression was found to diminish across all three cytokine growth conditions assessed (Figure 4.6a).

Looking at the RQR8 expression across three independent mouse spleens in Figure 4.6b, expression was similar across the three cytokine conditions at days three and day seven post transduction, with expression marginally higher at day seven post transduction. However, at day ten post transduction, RQR8 expression decreased across all three cytokine conditions compared to early expansion time points, with the greatest decrease observed in CARs expanded under "hIL-7 with hIL-15" and "hIL-2 with hIL-7 and hIL-15", showing similar lower levels of RQR8 expression compared to "hIL-2 alone".

Across three independent mouse spleens, the combination of "hIL-2 with hIL-7 and hIL-15" induced a higher increase in RQR8 gMFI compared to expansion with "hIL-2 alone" or "hIL-7 with hIL-15" at day four post transduction (Figure 4.6c). By day seven post transduction, gMFI of RQR8 was greatly reduced across all three cytokine conditions, but recovered by day ten post transduction (Figure 4.6c). "hIL-2 with hIL-7 and hIL-15" showed higher recovery in gMFI than expansion with "hIL-2 alone" or "hIL-7 with hIL-15" (Figure 4.6c). However, additional studies are required to confirm the statistical significance of these results.

Compared to 376.96.m28z CAR-T cells, ALK.h28z mouse CAR-T cells showed greater stability based on expression of the co-expressed RQR8 gene in response to all cytokine conditions. This may be due to the differences in design between the two CARs. Further investigation is warranted to better understand the differences between constructs, which may explain the inherent differences in the stability of CAR expression.

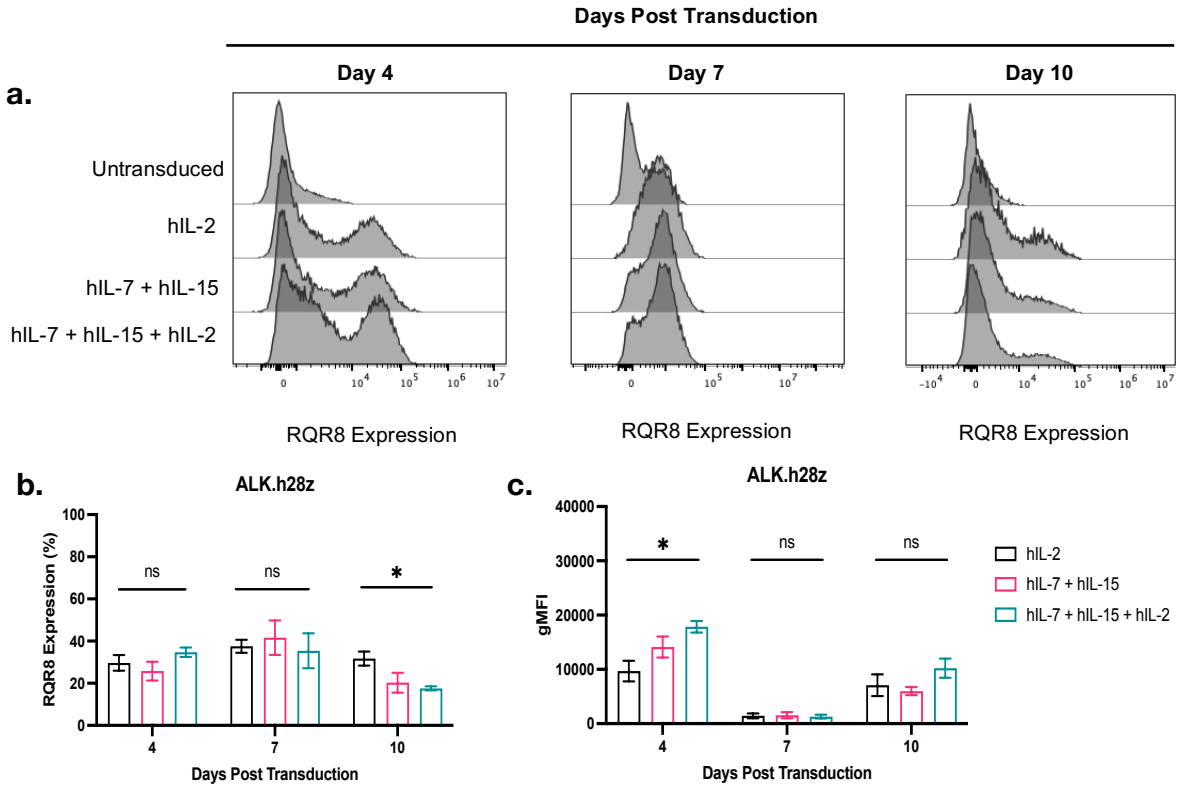

Figure 4.6 Changes in cytokine conditions does not lead to differential differences in ALK.h28z expression

ALK.h28z CAR T-cells were generated from 129/SvJ spleens. Cells were expanded for 10 days post transduction using different cytokine combinations of hIL-2, hIL-7 and hIL-15 to improve T-cell expansion. CAR marker, RQR8 expression was evaluated by flow cytometry with **a**) histogram plots showing expression in one independent donor over the course of expansion. For three independent donors, **b**) CAR expression and **c**) gMFI is shown. The error bars shown represent the standard deviation with an n of three (N=3). Statistical analysis was performed using two-way ANOVA. ns<non-significant, *<0.0332.

4.2.5.3 eGFP Expansion

The stability of the expression of the non-CAR control, eGFP^{+} T-cells, was assessed by observing GFP expression over a ten-day expansion period. A similar shift in eGFP expression was observed across the three independent cytokine expansion conditions compared with the untransduced control (Figure 4.7a). Moreover, eGFP expression remained stable at day seven and ten post transduction, with similar expression levels across all cytokine growth conditions (Figure 4.7a).

Across three independent mouse spleens in Figure 4.7b, relatively similar eGFP expression was observed across the three different cytokine growth conditions, with relatively similar and stable eGFP expression levels seen from day four to ten post transduction, suggesting no discernible differences in eGFP expression under the three different cytokine conditions evaluated. These observations appeared to be true when examining the gMFI of $eGFP^+$ T-cells over the course of the expansion period (Figure 4.7c). The gMFI was relatively similar under all three cytokine conditions over the course of the expansion period (Figure 4.7c). However, a higher eGFP gMFI was seen at day four post transduction, which was then found to drop and stabilise at days seven and ten post transduction (Figure 4.7c).

These findings suggest that changes in cytokine conditions do not seem to increase CAR or eGFP expression or the corresponding gMFI. The potential transient CAR expression seen of 376.96.m28z, compared to the relatively stable eGFP and ALK.h28z may be an inherent phenotype of this CAR, which requires further investigation to better understand its cause.

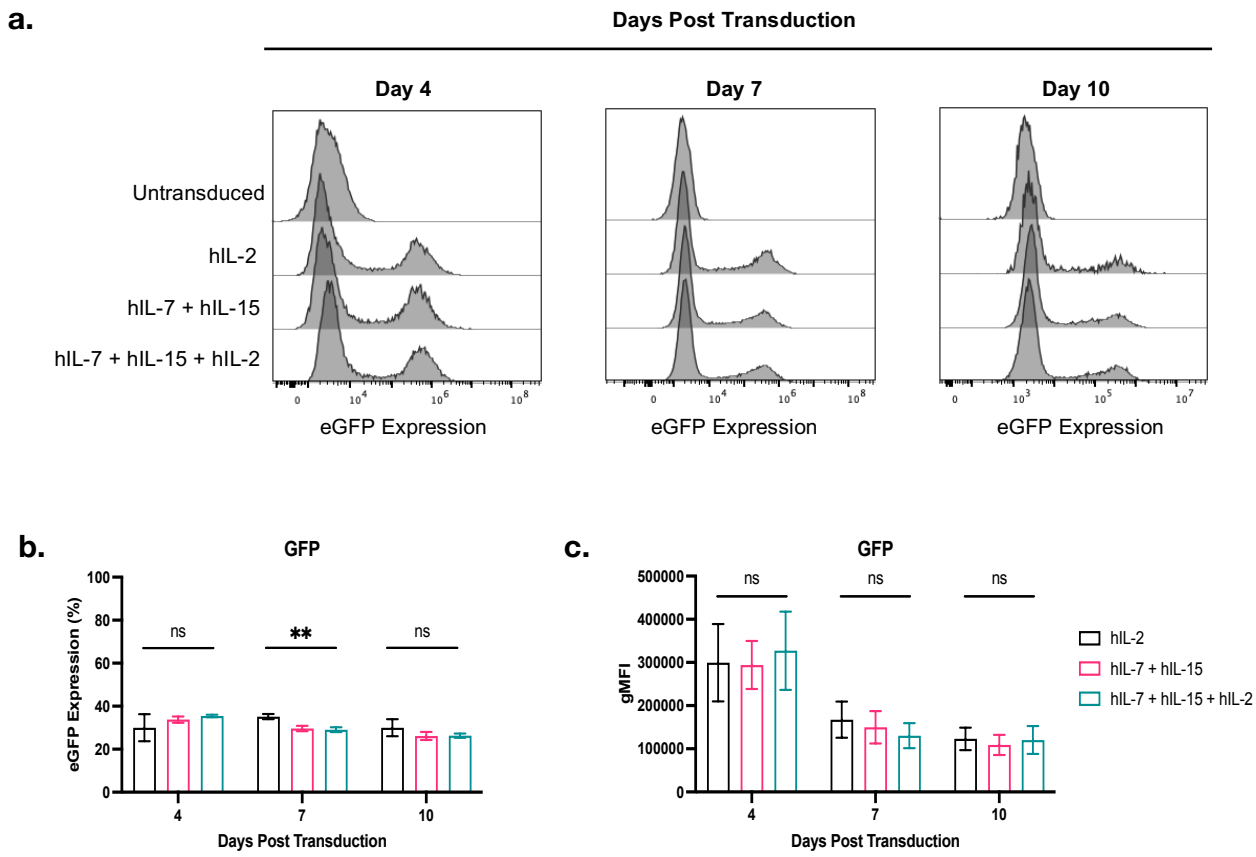

Figure 4.7 Changes in cytokine conditions does not lead to differential differences in eGFP expression

eGFP$^+$ T-cells were generated from 129/SvJ spleens. Cells were expanded for 10 days post transduction using different cytokine combinations of hIL-2, hIL-7 and hIL-15 to improve T-cell expansion. GFP expression was evaluated by flow cytometry with **a**) histogram plots showing expression in one independent donor over the course of expansion. For three independent donors, **b**) CAR expression and **c**) gMFI is shown The error bars shown represent the standard deviation with an n of three (N=3). Statistical analysis was performed using two-way ANOVA. ns<non-significant, **<0.0021.

4.2.6 Total cell viability and expansion is improved with hIL-7 and hIL-15

Assessment of the effects of different cytokine growth conditions did not yield a stable 376.96.m28z CAR$^+$ population compared with CAR and non-CAR controls of ALK.h28z and eGFP, respectively. It is also important to assess whether changes in cytokine growth conditions lead to any improvement in cell viability and cell expansion which may explain the observed changes in the CAR$^+$ population. Total cell viability and total cell fold expansion

were assessed for the generated 376.96. m28z and ALK.h28z CAR-T cells and eGFP$^+$ mouse T-cells over the ten day expansion period post transduction under these different cytokine growth conditions, as described in section 4.2.5. it is important to note that total cell viability and total cell fold expansion was assessed in response to cytokine growth conditions for these experiments and T-cell expansion would have been a more informative readout to better evaulate the effect of cytokine growth condtions on mouse CAR-T cell expansion.

As shown in Figure 4.8, the three individual cytokine growth conditions showed high total cell viability, which was stable over the course of the ten day expansion period. This was the case for both untransduced (Figure 4.8a) and eGFP$^+$ T cells (Figure 4.8d). Similar results were observed for the total cell viability with 376.96.m28z (Figure 4.8b), and ALK.h28z (Figure 4.8c) mouse CAR-T cells. However, total cell viability slightly improved with culturing under hIL-7 with hIL-15, or hIL-2 with hIL-7 and hIL-15 compared to hIL-2 alone (Figure 4.8b-c). Moreover, culturing of 376.96.m28z and ALK.h28z CAR-T cells in hIL-2 alone resulted in reduced total cell viability by day nine post transduction compared to culturing in IL-7 with hIL-15 and hIL-2 with hIL-7 and hIL-15 (Figure 4.8b-c).

Regrading total cell fold expansion, untransduced splenocytes show little discernible difference in total cell fold expansion across the three different cytokine growth conditions (Figure 4.8a). However, for eGFP$^+$ T-cells, hIL-2 alone appeared to yield marginally poorer total cell fold expansion compared to growth conditions with hIL-7 and hIL-15 alone or in combination with hIL-2, with decreasing total cell fold expansion in a time dependent manner (Figure 4.8d). This trend is mirrored with 376.96.m28z and ALK.h28z mouse CAR-T cells (Figure 4.8b-c), where culturing cells with hIL-2 alone resulted in a decrease in total cell growth over the course of the expansion period compared to culturing in hIL-7 with 15 and hIL-2 combined with hIL-7 and hIL-15.

Culturing ALK.h28z mouse CAR-T cells under either hIL-7 with hIL-15 or hIL-2 with hIL-7 and hIL-15 yielded similar total cell fold changes over the expansion period with little expansion (Figure 4.8c). However, the total cell fold change increased in a time dependent manner for 376.96.m28z mouse CAR-T cells (Figure 4.8b). Culturing under hIL-7 with hIL-15 or hIL-2 with hIL-7 and hIL-15 yielded between a two to three fold change difference, suggesting that under these two cytokine growth conditions, total cell expansion occurs (Figure 4.8b).

These results suggested that expansion with hIL-2 alone may lead to reduced total cell viability and poor total cell expansion. However, culturing under hIL-7 with hIL-15 or hIL-2 with hIL-7 and hIL-15 seemed to sustain total cell viability and maintain or increase total cell

expansion during the expansion period. Based on these results, subsequent expansion of the generated mouse CAR-T cells was performed using hIL-2 combined with hIL-7 and hIL-15.

Figure 8.2 in the appendix presents an alternative visualisation of Figure 4.8, illustrating changes in cell viability and cell counts within each expansion condition throughout the expansion period.

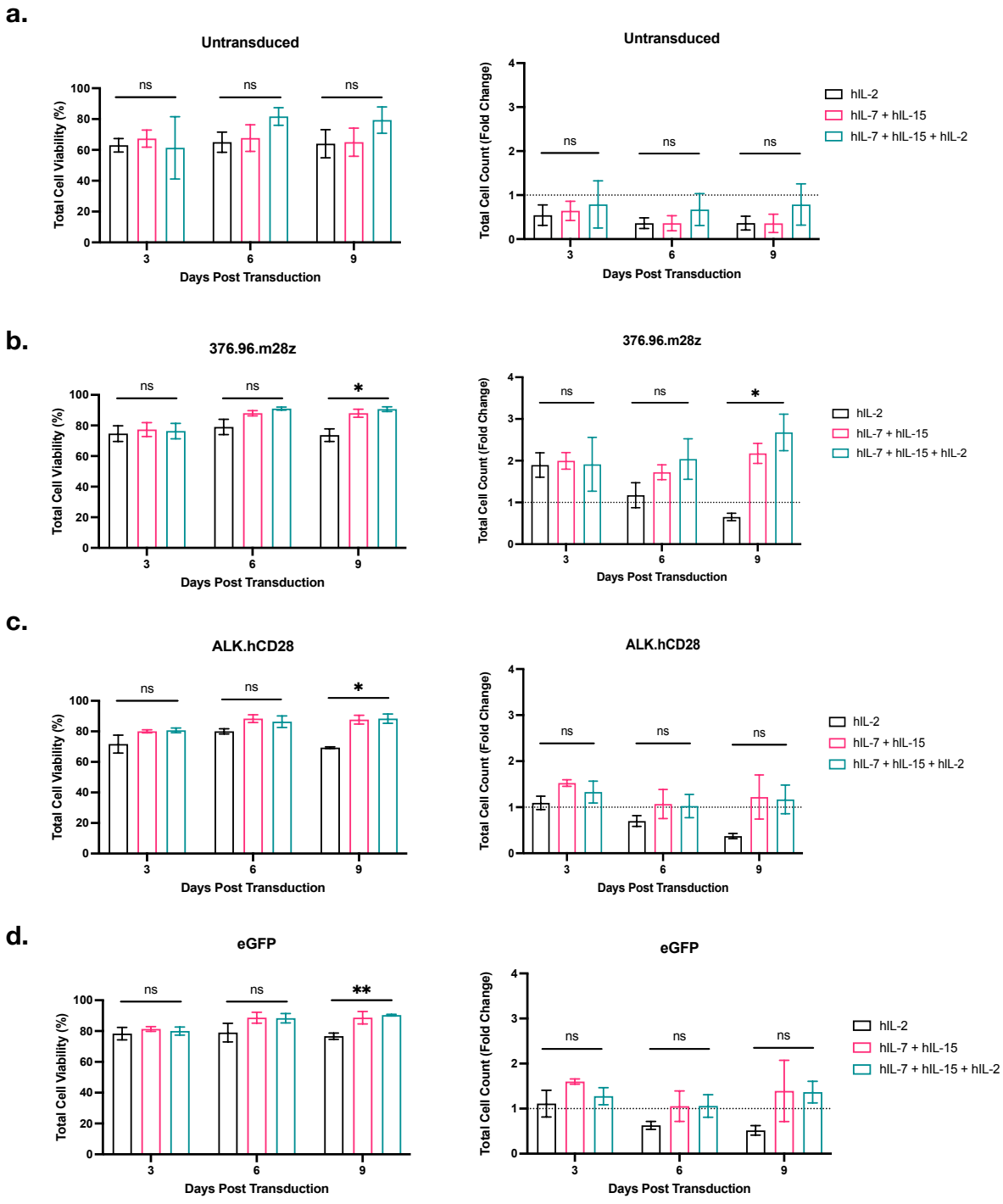

Figure 4.8 Use of hIL-7 and hIL-15 improves total cell viability and cell count

Two CARs (376.96.m28z and ALK.h28z) and eGFP^{+} T-cells were generated from 129/SvJ spleens. Cells were expanded for 10 days post transduction. Different cytokine compositions of hIL-2,hIL-7 and hIL-15 were used to improve T-cell expansion. Cell counts and viability counts were measured to evaluate expansion for **a**) untransduced **b**) 376.96.m28z **c**) ALK.h28z and **d**) GFP. The error bars shown represent the standard deviation with an n of three (N=3). Statistical analysis was performed using two-way ANOVA. ns<non-significant, *<0.0332, **<0.0021.

4.2.7 Transient CAR expression is not due to pseudotransduction

Investigating changes in cytokine growth conditions led to improved viability and expansion of generated mouse CAR-T cells. However, in CAR and non-CAR controls, ALK.h28z and eGFP showed relatively stable expression, whilst 376.96.m28z cells exhibited only transient CAR expression. Therefore, it is important to determine if this phenomenon with the 376 CAR occurs due to unstable integration of the CAR gene within the mouse T-cell genome, referred to as pseudotransduction.

Pseudotransduction involves the passive transfer of genetic material or proteins without any stable integration of the transgene within the target cell genome, resulting in transient expression of target genes and proteins. This phenomenon has been cited in the literature in the context of viral vectors. In 2004, Nash and Lever reported deficiencies when using eGFP lentiviral vectors, such as those in the absence of HIV-1 packaging signals (421). The use of such vectors could induce GFP expression within transduced 293T cells by day three post transduction, which was then found to be abrogated by day seven, compared to stable expression seen at day seven with the use of GFP vectors containing the HIV packaging signal (421). Haas et al. reported similar findings of transient GFP expression in both transduced 293Ts and $CD34^+$ cells over the course of a fourteen day expansion using lentiviral vector supernatants defective in key elements, such as integrase (422). In human CAR-T cell manufacturing, pseudotransduction has been reported by Ghassemi et al., where non-activated $CD19^+$ CARs showed no abrogation of CAR expression when treated with integrase and reverse transcriptase inhibitors during the lentiviral transduction process, compared to activated T-cells (411). Subsequent evaluation of these pseudo-transduced CAR-T cells showed no sustained effector functionality against CD19-expressing target cells, resulting in the absence of long-term persistence of the CAR-T cells (411).

To determine whether generated 376.96.m28z mouse CAR-T cells exhibited pseudotransduction, 376.96.m28z mouse CAR-T cells were generated individually from retroviral preparations derived from transient transfections of Pheonix.Eco cells, and the 376.96.m28z Pheonix.Eco producer cell line. This was to ensure that the retrovirus used accounted for all the factors which might have contributed to the transient CAR expression observed thus far. Additionally, GFP^+ mouse T-cells were generated as a control to determine whether this was a 376.96.m28z specific phenomenon. Moreover, GFP is a cytoplasmic protein and 376.96.m28z CAR is a membrane protein. As a result, if pseudotransduction occurred with 376.96.m28z CAR, then this may occur through the transfer of CAR proteins

from the vector envelope during viral fusion, as membrane proteins expressed in packaging cells are known to be incorporated into the viral envelope (411).

To determine if pseudotransduction was occurring, at the point of transduction, mouse T-cells were treated with reverse transcriptase and integrase inhibitors, saquinavir and raltegravir, respectively. These inhibitors prevent retroviral DNA from integrating into the T cell genome and generate new viral progeny for viral amplification. Moreover, additional non-treated and DMSO as treatment controls were included. After transduction, the cells were expanded for seven days during which CAR and eGFP expression were confirmed by flow cytometry.

Histogram plots for one representative spleen in Figure 4.9a show that the generated $eGFP^+$ T cells had complete abrogation in expression with saquinavir and raltegravir treatment compared to DMSO and non-treated controls at day four post transduction (Figure 4.9a). These results were also sustained by day seven post transduction, suggesting that the $eGFP^+$ transgene was stably integrated within the cell genome, thus not exhibiting pseudotransduction. Looking at the combined results of eGFP expression across three independent mouse spleens in Figure 4.9b, complete abrogation of eGFP expression was observed at day three and seven post transduction with saquinavir and raltegravir treatment. $eGFP^+$ T cells, either non-treated or treated with DMSO showed similar levels of eGFP expression at day three and seven post transduction, suggesting stable eGFP expression.

When looking at 376.96.m28z generated mouse CAR-T cells, histogram plots for one representative mouse spleen show stable integration of the transgene was occurring with complete abrogation of CAR expression with saquinavir and raltegravir treatment compared to DMSO and non-treated controls (Figure 4.9 c-f.). This was found to be the case for CAR-T cells generated using retrovirus from a producer cell line (Figure 4.9 c-d.), and the transient transfection of Phoenix.Eco cells (Figure 4.9 e-f.) This trend was also sustained on day seven post transduction using both retrovirus preparations (Figure 4.9 c and f). Looking at CAR expression across three independent mouse spleens, CAR expression was seen to be similar across both non-treated and DMSO control, suggesting DMSO was an appropriate treatment control for this experiment (Figure 4.9 d and f). However, CAR expression was found to still decrease from day four to seven post transduction across both the non-treated and DMSO controls (Figure 4.9 d and f) and across both retroviral preparations used. This suggests that the transient CAR expression observed is not due to pseudotransduction, with complete abrogation of CAR expression observed with saquinavir and raltegravir treatment.

These findings warrant further investigation to elucidate the cause of the transient *in vitro* CAR expression observed during expansion. While CAR expression during *in vitro* expansion was not stable, the intact functionality and expansion of the 376.96.m28z CAR in response to antigen exposure may circumvent this and, thus, still be a suitable CAR candidate for evaluation in combination with single dose radiation. The subsequent step was to evaluate the *in vitro* functionality of 376.96.m28z mouse CAR-T cells.

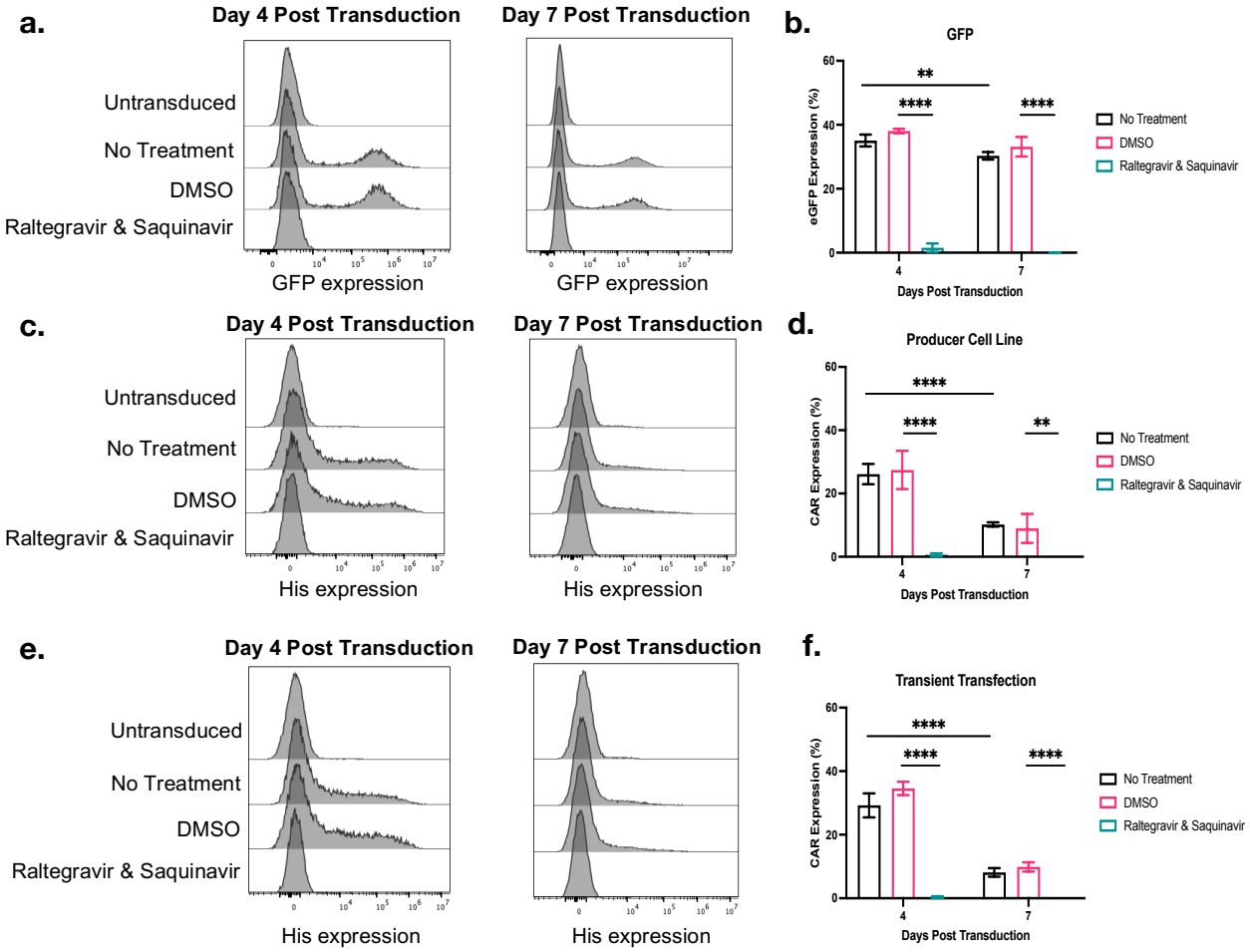

Figure 4.9 Transient *in vitro* CAR expression is not due to pseudotransduction

129/SvJ spleens were used to generate 376.96.m28z mouse CAR-T cells using retrovirus produced from transient transfection of P.Eco cells or P.Eco producer cell line alongside eGFP as a control. Transduction was performed with conditions including treatment with DMSO and Raltegravir & Saquinavir. *In vitro* expansion occurred for seven days during which CAR and eGFP expression was measured by flow cytometry. Histogram plots show **a**) GFP expression for one donor and **b**) the percentage of expression across all three donors. Histogram plots and percentage of CAR expression are also shown with transductions performed using **c**) retrovirus from producer cell line and **e**) retrovirus produced from transient transfection. The error bars shown represent the standard deviation with an n of three (N=3). Statistical analysis was performed using two-way ANOVA. **<0.0021, ****<0.0001.

4.2.8 376.96.m28z shows short term *in vitro* cytotoxicity against targets

To ascertain the functionality of mouse CAR-T cells *in vitro*, 376.96.m28z mouse CAR-T cells were generated and expanded. At day seven post transduction, CAR functionality was assessed in an antigen-bound hB7-H3^{+} stimulation assay and against GFP^{+}Luc^{+} target cells that were either negative for hB7-H3 (SupT1 WT) or positive for hB7-H3 (SupT1 hB7-H3^{+}).

During the *in vitro* expansion period, generated 376.96.m28z mouse CAR-T cells continued to show a decreasing trend in CAR expression. Figure 4.10a shows that over the course of a fourteen day expansion period, CAR expression decreased in a time-dependent manner, even though, as established in section 4.2.7, there is no evidence of pseudotransduction leading to the working assumption that the CAR transgene is stably integrated within the genome of successfully transduced cells. Figure 8.3a in the appendix shows representative flow plots for CAR expression over the fourteen day expansion period.

A key method for assessing CAR functionality is the ability to kill cells in an antigen-dependent manner. In the SupT1 co-culture performed with 376.96.m82 mouse CAR-T cells, this was assessed in two ways. First, I used a luciferase killing assay readout (Figure 4.10b-c.). Second, I examined target cell viability (Figure 4.10d-e.) by flow cytometry. For target cell vaibility assessed by flow cytometry, representative flow plots are shown in Figure 8.3b-c in the appendix. Both readouts were normalised against the target cell alone and quantified as a percentage of target cell viability.

At day one post co-culture at a 1:1 E:T ratio, 376.96.m28z CAR-T cells were found to kill SupT1 hB7-H3^{+} cells in a statistically significant manner compared to untransduced T cells. Moreover, 376.96.m28z killing was antigen-specific, with no target cell killing observed against the antigen negative control, SupT WT (Figure 4.10b). This response was sustained at day three post co-culture, with a further decrease in target cell killing by the CAR against SupT1 hB7-H3^{+} cells (Figure 4.10c).

The target cell viability results obtained from flow cytometry mirrored the same trend as that of the luciferase killing assay results. 376.96.m28z CAR-T cell activity resulted in a significant reduction in target cell viability against SupT1 hB7-H3^{+} in an antigen-dependent manner compared with untransduced T cells (Figure 4.10d). This effect was sustained at six days post co-culture in a statistically significant manner (Figure 4.10e).

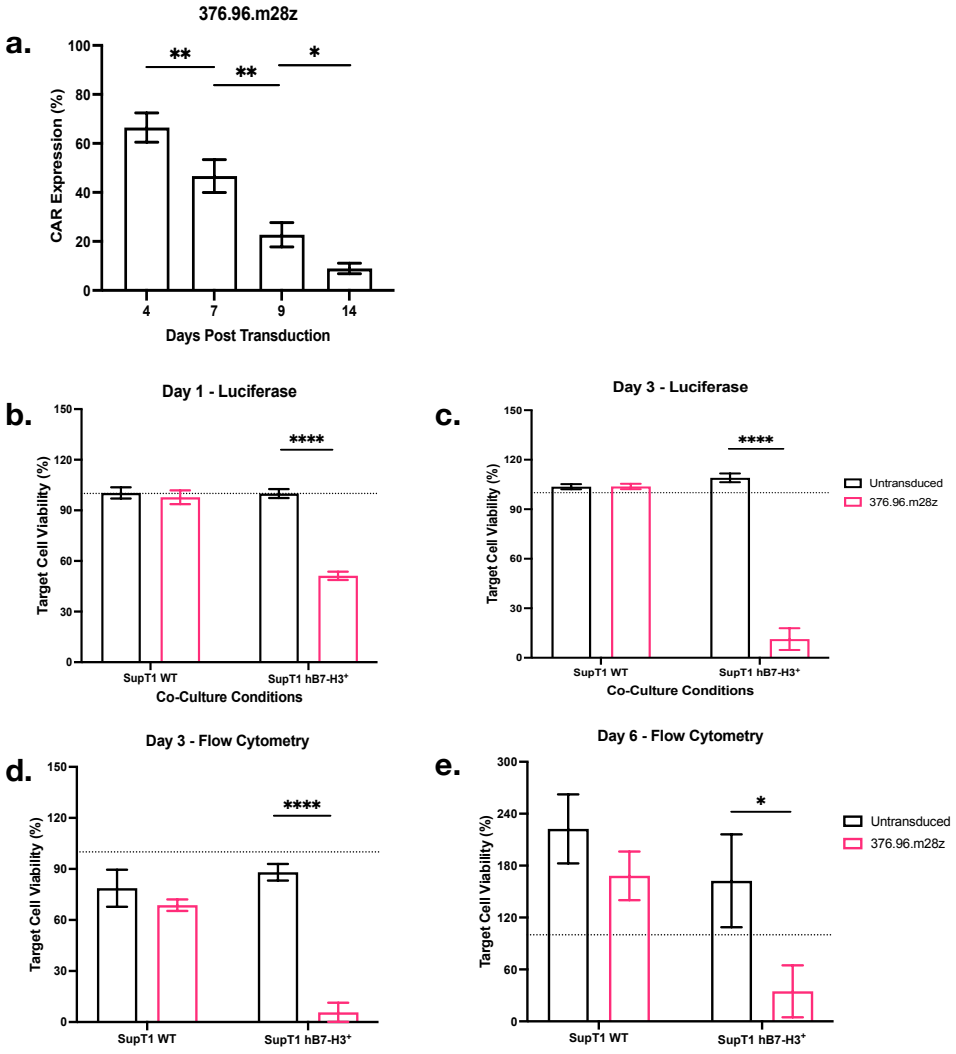

Figure 4.10 376.96.m28z shows short-term *in vitro* cytotoxicity regarding target cell killing

129/SvJ Spleens were used to generate 376.96.m28z mouse CAR-T cells and expanded *in vitro* for fourteen days. CAR expression was assessed by flow cytometry shown in **a**). At seven days post transduction, 376.96.m28z functionality was assessed in a co-culture with $GFP^{+}Luc^{+}$ target cells, SupT1 WT and SupT1 hB7-$H3^{+}$. At **b**) day one and **c**) day three post commencement of co-culture, tumour cell viability was assessed by luminescence. Target cell viability was assessed by flow cytometry as well at **d**) day three and **e**) day six post co-culture. The error bars shown represent the standard deviation with an n of three (N=3). Statistical analysis was performed using one-way ANOVA. *<0.0332, **<0.0021, ****<0.0001.

4.2.9 376.96.m28z shows short term antigen-dependent cytokine release

In vitro CAR-T functionality was also assessed by cytokine release, as it reflects activation status of the CAR and, in turn, the cytotoxicity of CAR-T cells in targeting tumour cells, as cytokine release forms part of the anti-tumour response (423). IL-2 and IFN-γ are key cytokines measured when determining CAR efficacy through cytokine release. IL-2 and IFN-γ are critical for enhancing CAR functionality through their roles in T cell activation, proliferation, and immune response mediation (423,424). Thus, both released mIL-2 and mIFN-γ were measured via ELISA as indicators of 376.96.m28z CAR functionality. Cytokine release was evaluated 24 hours after the commencement of the stimulation assay using plate bound antigen and SupT1 co-cultures, which were performed to evaluate 376.96.m28z mouse CAR-T cell functionality.

Using the antigen bound assay, 376.96.m28z cells showed antigen-dependent release of mIL-2 (Figure 4.11a) and mIFN-γ (Figure 4.11b) compared with untransduced T cells. This was found to be statistically significant compared with the unstimulated and anti-His controls, affirming the release of mIL-2 and mIFN-γ by 376.96.m28z, which occurred in response to the antigen. Similarly, in the SupT1 co-culture at an effector to target ratio of 1:1 and with supernatant collected for ELISA at 24 hours of co-culture, 376.96.m28z CARs showed mIL-2 (Figure 4.11c) and mIFN-γ (Figure 4.11d) release in an antigen-dependent manner. Release of mIL-2 and mIFN-γ was observed in response to SupT1 hB7-H3^{+} by 376.96.m28z CAR-T cells compared to untransduced controls. These results confirmed that 376.96.m28z is a functional CAR, with target cell killing and cytokine release occurring in an antigen-dependent manner, both in the format of an antigen plate-bound assay (Figure 4.11 a-b) and against antigen-expressing target cells (Figure 4.11 c-d).

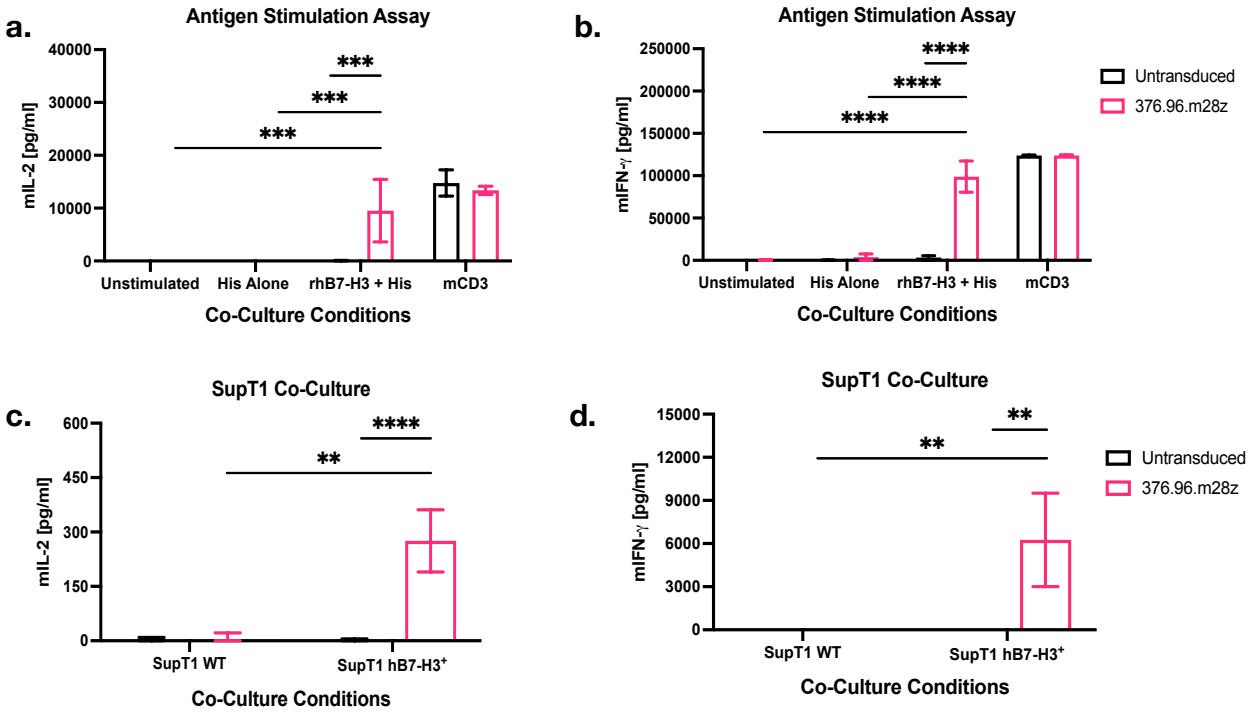

Figure 4.11 376.96.m28z shows short-term *in vitro* cytotoxicity regarding cytokine release

129/SvJ Spleens were used to generate 376.96.m28z mouse CAR-T cells and expanded *in vitro* for seven days. CAR expression was assessed by flow cytometry shown in **a**). At seven days post transduction, 376.96.m28z functionality was assessed in an antigen-bound stimulation assay and co-culture with GFP^+Luc^+ target cells, SupT1 WT and SupT1 $hB7\text{-}H3^+$. 24 hours post commencement of assays, mIL-2 and mIFN-γ cytokine release was measured for **a**-**b**) antigen stimulation assay and **c-d)** SupT1 co-culture. The error bars shown represent the standard deviation with an n of three (N=3). Statistical analysis was performed using two-way ANOVA. **<0.0021, ***<0.0002, ****<0.0001.

4.2.10 376.96.m28z does not expand in response to antigen *in vitro*

A key factor determining CAR-T cell success is the ability of the CAR to expand in response to the antigen and thus be able to show persistence against cancer cells to mount an effective anti-tumour response (425). Therefore, CAR-T cell expansion is imperative as a key factor in assessing CAR-T cell functionality. For both the plate-bound antigen stimulation assay and SupT1 co-cultures, cell expansion was evaluated for 376.96.m28z mouse CAR-T cells by flow cytometry, where the CAR fold expansion was calculated against CAR alone in both assays performed individually based on gated $mCD3^+CAR^+$ cell counts.

Histogram plots shown in Figure 4.12a of one independent mouse spleen revealed that for the plate-bound antigen stimulation assay, no shift in CAR expression was observed from day three to day six after commencement of the antigen plate bound assay, with only the positive control, mCD3 stimulation, inducing any shift in CAR expansion. This was also the case across three independent mouse spleens, as shown in Figure 4.12b. CAR fold expansion in response to the antigen was found to be similar between day three and day six post commencement of co-culture. Moreover, CAR expansion was observed between day three to day six in response to the positive control, $mCD3^+$, suggesting potential non-specific CAR activation that occurs directly through the TCR (Figure 4.12b).

Similar to the antigen plate bound assay, against the SupT1 hB7-$H3^+$ target cells, no shift in CAR expression was observed in the histogram plots shown in Figure 4.12c from day three to day six after the commencement of co-culture. CAR expression against SupT1 hB7-$H3^+$ target cells was similar to that observed with CAR alone and against antigen-negative SupT1 WT (Figure 4.12c). When examining the CAR fold expansion across three independent mouse spleens, 376.96.m28z showed no CAR expansion from day three to day six after the commencement of the co-culture (Figure 4.12d). CAR fold expansion observed on day six in response to SupT1 hB7-$H3^+$ was comparable to that of SupT1 WT, suggesting that no CAR fold expansion occurred in an antigen-dependent manner (Figure 4.12d).

In vitro evaluation of 376.96.m28z revealed that short-term CAR functionality was observed, with target cell killing and cytokine release occurring in an antigen-dependent manner. However, CAR expansion was not observed in response to either plate-bound B7-H3 or B7-$H3^+$ targets, rendering this CAR unsuitable for assessing key functional parameters for evaluating the efficacy of CAR-T cell therapy concerning CAR-T cell persistence against antigen-positive tumour cells.

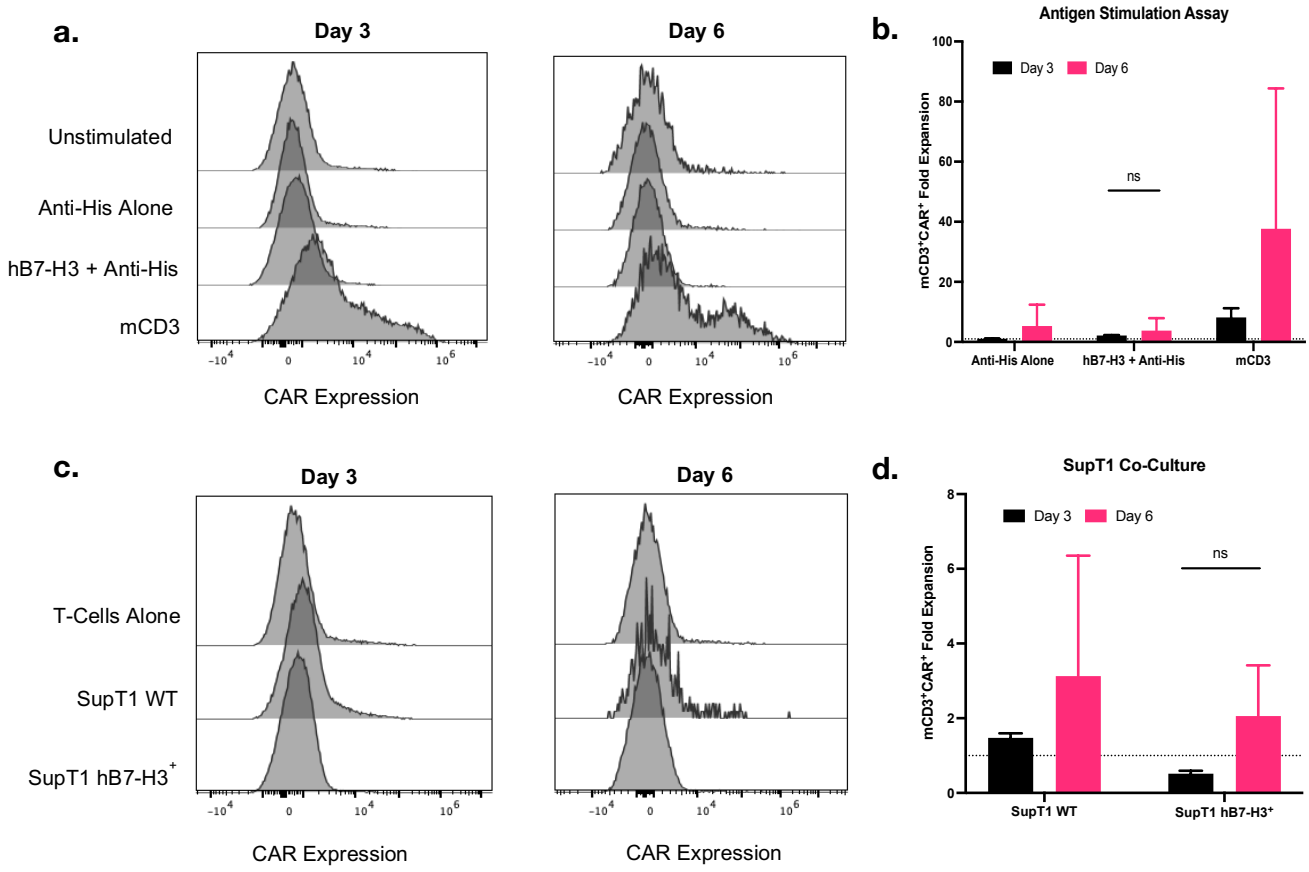

Figure 4.12 376.96.m28z does not expand in response to antigen *in vitro*

129/SvJ Spleens were used to generate 376.96.m28z mouse CAR-T cells and expanded *in vitro* for fourteen days. At seven days post-transduction, 376.96.m28z functionality was assessed in an antigen-bound stimulation assay and co-culture with $GFP^{+}Luc^{+}$ target cells, SupT1 WT and SupT1 $hB7\text{-}H3^{+}$. At days three and six post-commencement of the assays, CAR expression was assessed by flow cytometry. CAR expression is shown for one independent donor as histogram plots for **a**) antigen stimulation assay and **c**) SupT1 co-culture. $mCD3^{+}CAR^{+}$ fold expansion is shown for three independent donors for **b**) antigen stimulation assay and **d**) SupT1 co-culture. $mCD3^{+}CAR^{+}$ fold expansion was corrected against unstimulated $mCD3^{+}$CAR-T cells for **b**) and $mCD3^{+}$CAR-T cells alone for **d)**. The error bars shown represent the standard deviation with an n of three (N=3). Statistical analysis was performed using One-Way ANOVA. ns< non-significant.

4.3 Generation of 376.96.m28z.NIS mouse CAR-T cells

One of the major barriers to CAR-T efficacy in solid tumours is effective infiltration and persistence within the immunosuppressive tumour microenvironment (TME) (426–428). To effectively investigate whether radiation allows CAR-T cells to overcome this barrier in neuroblastoma, better imaging modalities are required to address this question and to allow robust *in vivo* monitoring of CAR-T cell trafficking. Of the array of imaging modalities to consider, the use of the human sodium iodide symporter (NIS) is an emerging interest for *in vivo* imaging of CAR-T cells (429,430). hNIS is a transmembrane protein part of the sodium-dependent transporter family, which is involved in the co-transport of sodium and iodide ions within the thyroid gland and has limited expression in other parts of the body, such as the stomach (431–433). Within the clinical setting, hNIS has been utilised for diagnostic and therapeutic purposes owing to its ability to mediate the uptake of commonly used radioisotopes, such as technetium-99m pertechnetate ($^{99m}TcO_4^-$) (434).

hNIS is an ideal candidate because it is non-immunogenic; it is only functional in living cells and not internalised upon substrate uptake (434). Moreover, the compatibility of hNIS with SPECT/CT imaging also provides improved image resolution in animals compared to alternatives, such as bioluminescence (BLI) based imaging using luciferase (166). Because of this, there is interest to see if hNIS can be utilised to investigate whether radiotherapy promotes CAR-T cell trafficking into the tumour. It would also allow further questions of CAR-T cell kinetics to be addressed, considering the potential of off-tumour cytotoxicity associated with CAR-T therapy (435).

The benefit of hNIS expressing CAR-T cells has only been shown in immunodeficient mice *in vivo* (166,436). However, this project aimed to use mouse CAR-T cells in conjugation with radiation in immunocompetent mice. The use of hNIS may lead to the occurrence of a non-self antigen immune response, which may confound any immune-mediated effects elicited by radiation on CAR-T cell efficacy. As a result, I evaluated both the hNIS and mNIS *in vitro* for NIS functionality. These results would indicate if mNIS functionality is comparable to that of hNIS for use in CAR-T cell imaging.

For the *in vitro* comparison of mNIS and hNIS, four types of constructs were generated using the SFG γ-retroviral vector (see section 2.2.1.1). Two of the constructs consisted of the NIS (mNIS or hNIS) with an intracellular c-myc epitope tag at the C-terminus as described in Figure 2.1 in Chapter 2. This is because hNIS has a validated detection method using flow cytometry, but not mNIS (166). There is no validated detection of mNIS by flow cytometry; detection by alternative methods such as western blotting has proved to be less robust (Dr. Gilbert

Fruhwirth, KCL, internal communication). Therefore, a c-myc epitope tag was added to standardise the detection of NIS across the two species types. Moreover, the purpose of generating these constructs was to allow *in vitro* evaluation of NIS functionality through $^{99m}TcO_4^-$ uptake assays to determine whether NIS functionality is affected by CAR co-expression.

The other two γ-retroviral constructs contained the second-generation anti-hB7-H3 murinised CAR (376.96.m28z) at the 5' end, followed by the NIS (mNIS or hNIS) sequence, and the c-myc epitope tag at the 3' end (Figure 2.1). The transgenes were separated by a furin cleavage site, SGSG linker, and T2A peptide sequence (Figure 2.1). This allows for the efficient cleavage of the expression of more than one transgene within this multicistronic construct (166,437). The use of the intracellular c-myc epitope tag resulted in difficulties in confirming NIS expression in transduced cell lines and CAR-T cells. Due to this, 376.96.m28z CAR protein expression was used as a measure of NIS transcript expression, as both transgenes are transcribed from a single transcript. NIS expression was also confirmed using $^{99m}TcO_4^-$ uptake assays to confirm NIS functionality.

4.3.1 Transiently produced retrovirus yields poor 376.96.m28z.NIS expression

Whlie NIS has been co-expressed with human CAR-T cells, this has not been done with mouse CAR-T cells thus far within the literature. Therefore, it was important to first determine the expression of 376.96.m28z.NIS mouse CAR-T cells using a retrovirus generated from the transient transfection of Pheonix.Eco cells. Expression was compared between the generated 376.96m28z.mNIS and 376.96.m28z.hNIS mouse CAR-T cells. This is because the use of hNIS within CAR-T cells has been documented in the literature; however, little is known about the use of mNIS for CAR-T tracking (166). As a result, both 376.96.m28z.mNIS and 376.96.m28z.hNIS mouse CAR-T cells were generated. The subsequent *in vitro* evaluation of NIS functionality would confirm the most appropriate one to co-express with the 376.96.m28z CAR for *in vivo* evaluation.

Using retroviral preparations from transient transfection of Pheonix.Eco cells, 376.96.m28z.mNIS and 376.96.m28z.hNIS mouse CAR-T cells were generated. BW5 cells were transduced with the retroviral preparations as a cell line control. Three days post-transduction, the transduced BW5 cells were assessed for CAR expression, as shown in the histogram plot in Figure 4.13a. Successful transduction with the retroviruses was observed

with a shift in CAR expression in BW5 cells transduced with 376.96.m28z.mNIS and 376.96.m28z.hNIS compared to untransduced. Moreover, a significant shift in CAR expression was seen with 376.96.m28z.mNIS, compared to 376.96.m28z.hNIS (Figure 4.13a).

Although BW5 showed successful transduction with the retroviral preparations, no CAR expression was observed with the transduction of mouse primary T-cells using unconcentrated neat retrovial supernatant. Figure 4.13b shows a histogram plot of CAR expression for one independent mouse spleen, with no discernible shift in CAR expression seen for both generated 376.96.m28z.mNIS and 376.96.m28z.hNIS mouse CAR-T cells compared to untransduced. Figure 4.13b shows the quantified CAR expression across three independent mouse spleens between 376.96.m28z.hNIS and 376.96.m28z.mNIS, with no CAR expression seen for 376.96.m82z.hNIS, and less than 4% CAR expression observed for 376.96.m28z.mNIS.

The results revealed that retroviruses generated from transient transfection of Pheonix.Eco cells induced poor co-expression of CAR and NIS in mouse primary T cells. Therefore, it was imperative to optimise retroviral preparations to improve the expression of 376.96.m28z.NIS mouse CAR-T cells. However, before performing these optimisations, I first determined if the functionality of mNIS and hNIS was comparable and then determined which construct is taken forward to further optimise mouse CAR-T generation for subsequent *in vivo* studies to be performed.

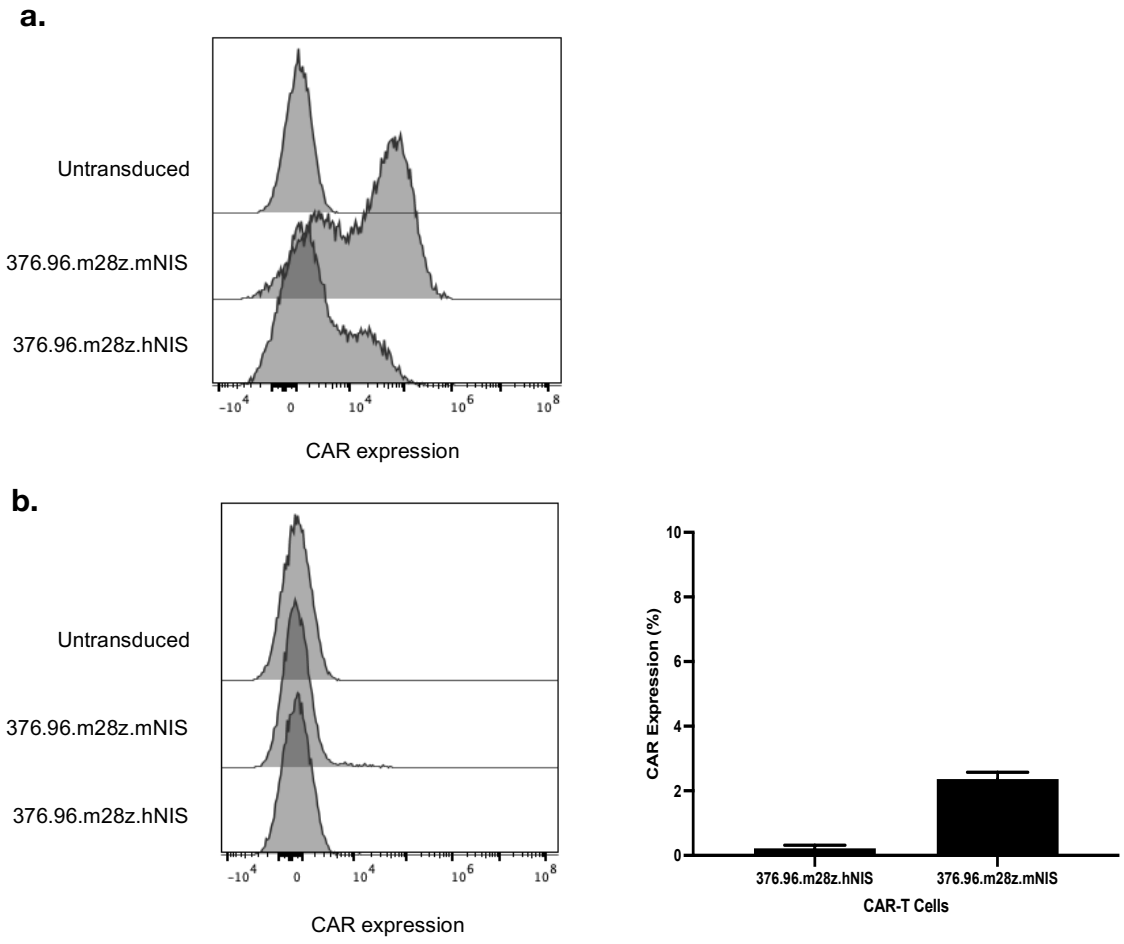

Figure 4.13 Transiently produced retrovirus yields poor 376.96.m28z.NIS expression

Retrovirus produced from transient transfection of P.Eco cells was used to generate 376.96.m28z.mNIS and 376.96.m28z.hNIS CAR-T cells from 129/SvJ female spleens. Transduction was performed with unconcentrated (neat) retrovirus. Three days post transduction, CAR expression was assessed by flow cytometry using the rhB7-H3-His tag protein, with **a**) showing CAR expression in a histogram plot on cell line control, BW5, and **b**) showing CAR expression for one donor in histogram plot and the quantified percentage of CAR expression with n of 3 (N=3). The error bars shown represent the standard deviation.

4.3.2 Similar mNIS and hNIS functionality in Tc99m uptake.

An imperative step in generating 376.96.m28z.NIS mouse CAR-T cells require *in vitro* validation of NIS function. Moreover, as literature has largely focused on the use of hNIS in mouse CAR-T cells, it is important to validate the use of mNIS, which is an ideal candidate for use in immunocompetent settings. *In vitro* validation of NIS has largely focused on the use of technetium-99m pertechnetate ($^{99m}TcO_4^-$) uptake assays. $^{99m}TcO_4^-$ is a widely used

clinical radiotracer that is compatible with NIS and is used for *in vitro* validation to confirm NIS functionality (166). Moreover, the inclusion of the competitive inhibitor, sodium perchlorate ($NaClO_4$), confirms that $^{99m}TcO_4^-$ uptake is due to NIS functionality (166).

Because of the initial poor transduction efficiencies observed in the generated 376.96.m28z.mNIS and 376.96.m28z.hNIS mouse CAR-T cells, the $^{99m}TcO_4^-$ uptake assay was performed with BW5 cells, which were successfully transduced and expressed 376.96.m8z.mNIS and 376.96.m28z.hNIS constructs as determined by staining for CAR expression, as shown in Figure 4.14a. After confirmation of expression by flow cytometry, BW5 cells were normalised for transduction efficiency based on CAR expression, and a $^{99m}TcO_4^-$ uptake assay comparing the functionality between mNIS and hNIS within these constructs was performed. Both transduced BW5 376.96.m28z.hNIS and 376.96.m28z.mNIS showed similar levels of $^{99m}TcO_4^-$ uptake in the absence of the competitive inhibitor $NaClO_4$. Moreover, complete abrogation of $^{99m}TcO_4^-$ uptake was observed in the presence of $NaClO_4$, suggesting that $^{99m}TcO_4^-$ uptake was due to the expression of hNIS and mNIS (Figure 4.14b).

These findings suggested that mNIS is similar in function to hNIS, and thus, subsequent optimisations were focused on improving the transduction efficiencies of the generated 376.96.m28z.mNIS mouse CAR-T cells.

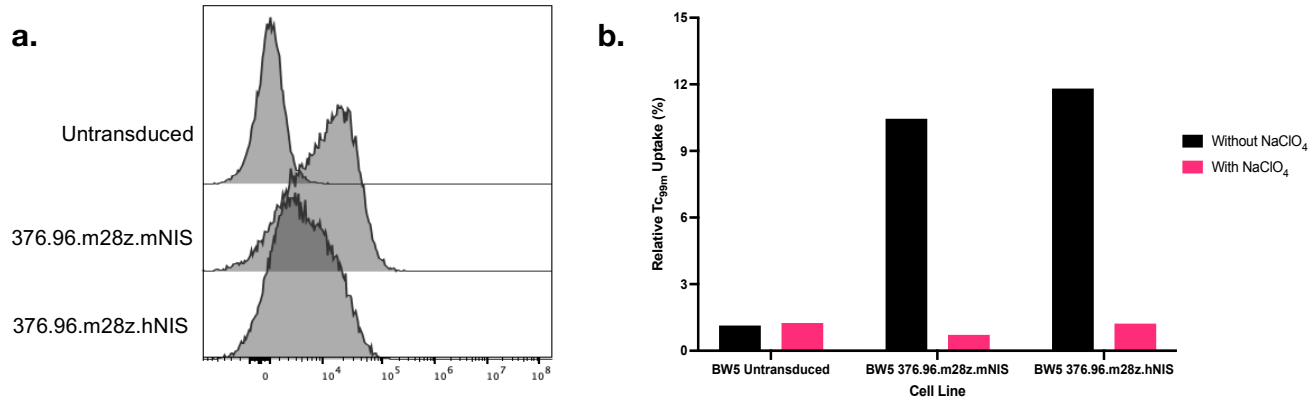

Figure 4.14 376.96.m28z.mNIS and 376.96.m28z function show Tc99m uptake

BW5 transduced with 376.96.m28z.mNIS and 376.96.m28z.hNIS were used to evaluate NIS functionality in a Tc99m uptake assay. **a**) CAR expression was confirmed by flow cytometry to determine transduction efficiency. Cell lines were adjusted for transduction efficiency and tested for NIS functionality using Tc99m in the presence and absence of inhibitor $NaClO_4$. Gamma emission was measured and analysed to determine relative Tc99m uptake as shown in **b**). The data shown is from one independent experiment (N=1).

4.3.3 Concentrating producer cell line dervied retrovirus improves transduction efficiency.

As seen with 376.96.m28z CAR-T production in section 4.2.3, the use of a producer cell line was found to improve CAR expression. Therefore, I generated a producer cell through viral transduction of Phoenix.Eco cells using 376.96.m28z.mNIS retrovirus that was generated from the transient transfection of 293Ts. The generated producer cell line was propagated *in vitro*, and the retrovirus generated in its unconcentrated (neat) and concentrated form was used to generate 376.96.m28z.mNIS mouse CAR-T cells, and CAR expression were assessed over the course of a fourteen day *in vitro* expansion period.

Figure 4.15a shows CAR expression from one independent mouse spleen as histogram plots over the course of a fourteen day expansion period. Mouse T-cell transduction with a concentrated retrovirus yielded a greater CAR expression at days four and seven post transduction compared to the use of neat retrovirus. However, from day four to day fourteen post transduction, the CAR expression was diminished, with CAR expression becoming undetectable by day fourteen post transduction. This trend was mirrored when looking at the percentage of CAR expression across three independent mouse spleens (Figure 4.15b).

Concentrated retrovirus greatly improved CAR expression compared to the use of neat retrovirus. However, both mouse CAR-T cells generated using neat or concentrated retroviruses showed a declining CAR expression trend over the course of the expansion period. Similar to the percentage of CAR expression, Figure 4.15c shows that even with gMFI, there was no stability in CAR expression with mouse CAR-T cells generated from neat or concentrated retroviruses, showing a declining trend of gMFI over the course of the expansion period.

Figure 4.15d confirmed that cell viability over the course of the expansion period was relatively stable for both mouse CAR-T cells generated using neat or concentrated retrovirus when observed at days five and seven post transduction to confirm whether T-cell viability was a factor contributing to the decreasing CAR population. No discernible differences were observed in T-cell growth when looking at fold change under both conditions of mouse CAR-T cells generated using neat or concentrated retrovirus (Figure 4.15d). Fold changes in cell expansion remained relatively similar on day four post transduction (Figure 4.15d). However, fold change in cell expansion decreased slightly for mouse CAR T- cells generated using neat retrovirus (Figure 4.15d). However, overlapping error bars across all conditions make it difficult to determine any discernible differences observed in T-cell expansion (Figure 4.15d).

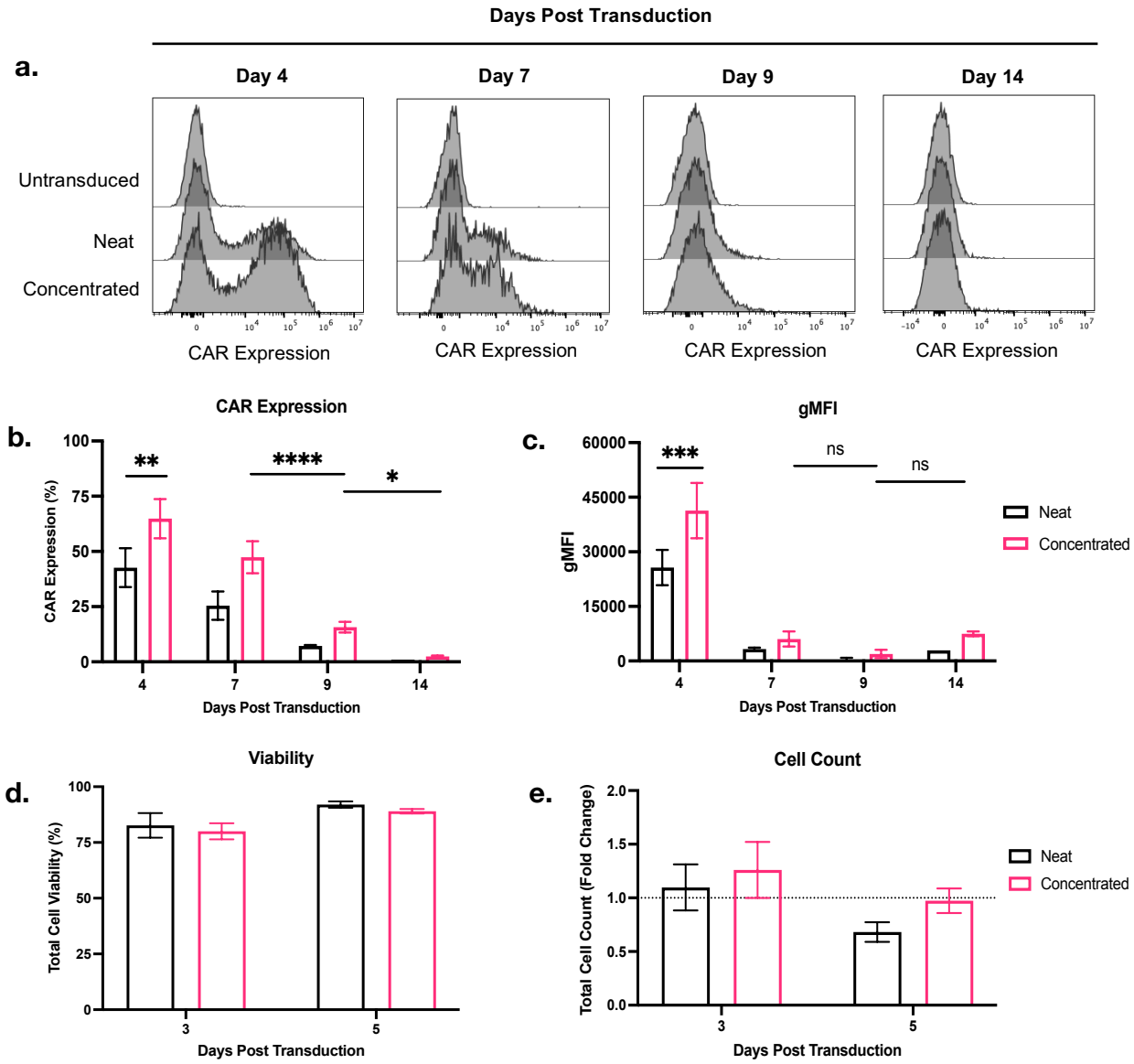

Figure 4.15 Concentrating producer cell line derived retrovirus improves transduction efficiency

129/SvJ Spleens were used to generate 376.96.m28z.mNIS mouse CAR-T cells using retrovirus produced from P.Eco producer cell line. Transductions were performed with either unconcentrated (neat) or concentrated retrovirus and **a)** histogram plots show CAR expression by flow cytometry over a 14 day *in vitro* expansion for one donor. **b**) CAR expression and **c**) gMFI shown for three independent donors, with **d**) cell viability and **e**) cell counts measured during this expansion period. The error bars shown represent the standard deviation with an n of three (N=3). Statistical analysis was performed using two-way ANOVA. ns< nonsignificant, *<0.0332,**<0.0021, ***<0.0002, ****<0.0001.

4.3.4 Transient *in vitro* 376.96.m28z.mNIS CAR expression is not due to pseudotransduction.

As described in Section 4.2.7, the trend in the transient *in vitro* expression of 376.96.m28z mouse CAR-T cells were also seen with 376.96.m28z.mNIS mouse CAR-T cells. As a result, I looked to determine that the transient expression of 376.96.m28z mouse CAR-T cells were potentially due to pseudotransduction, and I also sought to establish if this was also the case with 376.96.m28z.mNIS generated mouse CAR-T cells.

The investigation of 376.96.m28z.mNIS mouse CAR-T cells for pseudotransduction was performed in the same manner as done so with 376.96.m28z mouse CAR-T cells in section 4.2.7. 376.96.m28z.mNIS mouse CAR-T cells were generated using retroviral preparations sourced from the transient transfection of Phoenix.Eco cells and the 376.96.m28z.mNIS producer cell line. This was done to account for any differences in retroviral preparations contributing to transient CAR expression. To investigate the occurrence of pseudotransduction, T-cells were treated with integrase and reverse transcriptase inhibitors (Raltegravir & Saquinavir), along with DMSO and non-treated controls. CAR expression was measured by flow cytometry over the course of a seven day *in vitro* expansion period to determine CAR expression stability.

Figure 4.16a shows the histogram plots of CAR expression for one representative mouse spleen generated using retroviral preparations from the 376.96.m28z.mNIS producer cell line. At both day four and day seven post transduction, there was complete abrogation of CAR expression in response to Raltegravir & Saquinavir treatment compared to both DMSO and no treatment controls. This suggests that transient co-expression of 376.96.m28z and mNIS are not due to a lack of stable integration of the transgenes within the mouse T-cell genome, confirming the absence of pseudotransduction to explain this phenomenon. CAR expression was transient, with a decline in CAR expression seen between day four and seven post transduction in both DMSO and non-treated controls (Figure 4.16a).

These results were confirmed across three independent mouse spleens (Figure 4.16b), where CAR expression was measured across the different treatment conditions, showing similar CAR expression between no-treatment and DMSO control. CAR expression was highest at day four post transduction and was diminished by day seven post transduction across both controls. Complete abrogation in CAR expression was seen at both days four and seven post

transduction with Raltegravir & Saquinavir, confirming that pseudotransduction is not the cause of this transient expression of transgenes.

376.96.m28z.mNIS mouse CAR-T cells generated from retroviruses by transient transfection of Pheonix.Eco cells showed similar results (Figure 4.16c-d). Compared to the producer cell line, retrovirus derived from the transient transfection of Pheonix.Eco cells showed lower CAR expression across DMSO and no-treatment controls (Figure 4.16c). CAR expression was not sustained by day seven post transduction (Figure 4.16c). In response to Raltegravir & Saquinavir treatment, complete abrogation of CAR expression was observed across the length of the expansion period. This confirms that the transient CAR expression observed was not due to pseudotranslocation. These results were confirmed across three independent mouse spleens (Figure 4.16d). The results of these experiments confirmed that transgenes were stably integrated within the CAR-T cell genome irrespective of the retroviral preparation used, and were not the cause of this transient CAR expression. Further investigation is required to determine the cause of this transient expression phenomenon.

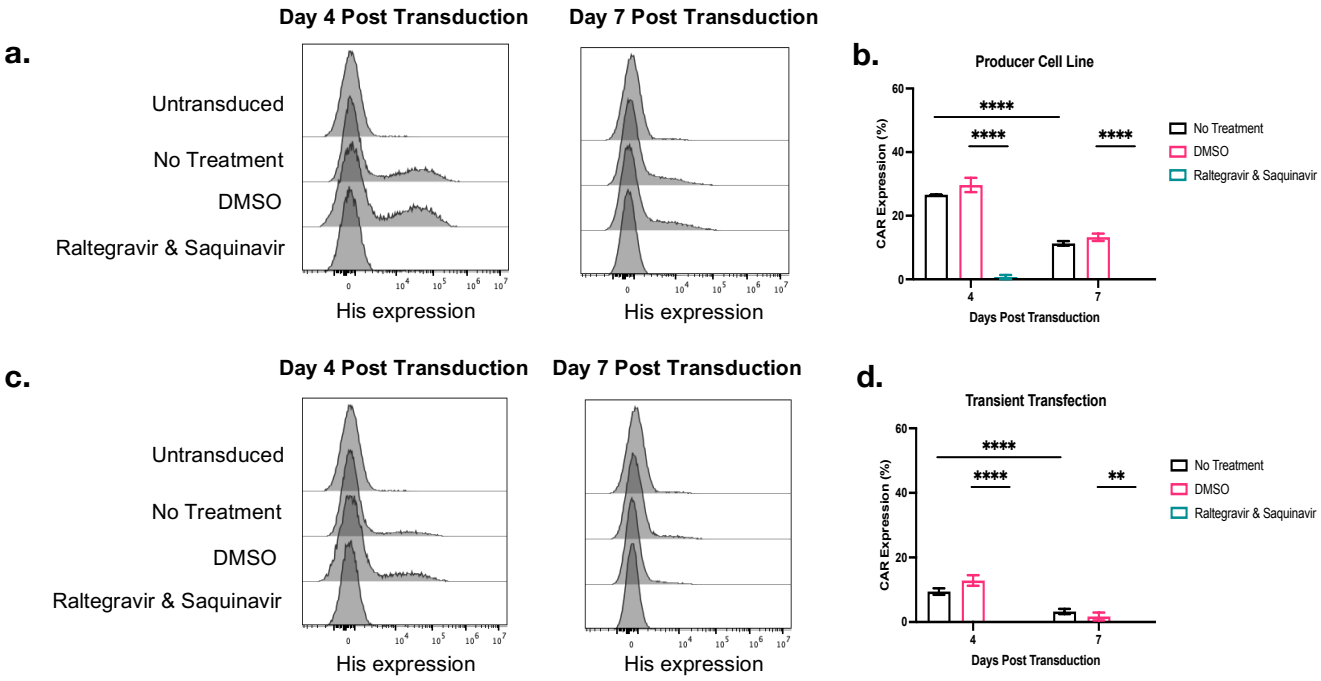

Figure 4.16 Transient *in vitro* 376.96.m28z.mNIS CAR expression is not due to pseudotransduction

129/SvJ Spleens were used to generate 376.96.m28z.mNIS mouse CAR-T cells using retrovirus produced from transient transfection of P.Eco cells or P.Eco producer cell line. Transduction was performed with treatment of DMSO and Raltegravir & Saquinavir and CAR-T cells underwent *in vitro* expansion for seven days. At days four and seven post transduction, CAR expression was assessed by flow cytometry. Histogram plots of one donor and the combined percentage of CAR expression of three donors are shown with transductions performed using **a-b**) retrovirus from producer cell line and **c-d**) retrovirus produced from transient transfection, respectively. The error bars shown represent the standard deviation with an n of three (N=3). Statistical analysis was performed using two-way ANOVA. **<0.0021, ****<0.0001.

4.3.5 376.96.m28z.mNIS CAR-T cell functionality is impaired *in vitro*

Whlist the expression of 376.96.m28z.mNIS was found to be transient during *in vitro* expansion, I sought to determine if the CAR-T cells were functional and that CAR functionality was not impacted by the co-expression of the mNIS. To determine whether the co-expression of mNIS affects 376.96.m28z CAR functionality, 376.96m28z.mNIS and 376.96.m28z mouse CAR-T cells were generated. At three days post transduction, a co-culture was performed at an E:T ratio of 1:1 with luciferase$^+$ SupT1 cells either expressing B7-H3$^+$ (SupT1 hB7-H3$^+$) or not (SupT1 WT).

CAR-T cell functionality was assessed by looking at the target cell killing by luimincense because the targets were luciferase^{+}. At day one post co-culture, both 376.96.m28z and 376.96,m28z.mNIS showed CAR-T cell killing in an antigen-specific manner against SupT1 hB7-H3^{+}. The 376.96.m28z CAR-T cells showed a significant reduction in target cell killing compared to the response to SupT1 WT (Figure 4.17a). However, 376.96.m28z.mNIS CAR-T cells showed target cell killing, but this was not statistically significant compared to its response to the antigen negative control, SupT1 WT (Figure 4.17a). The target cell viability observed between 376.96.m28z and 376.96.m28z.mNIS was not similar, suggesting that mNIS co-expression affects CAR functionality when compared to CAR alone (Figure 4.17a).

CAR-T cell functionality was also assessed on day three post co-culture, where 376.96.m28z showed antigen-specific target cell control with retained levels of target cell viability as seen at day one post co-culture compared to the antigen negative control (Figure 4.17b). However, target cell killing with the 376.69.m28z.mNIS mouse CAR-T cell killing was not comparable to that of 376.96.m28z, with levels of target cell viability comparable to the antigen negative, SupT1 (Figure 4.17b). This suggests that inclusion of mNIS within the construct inhibits CAR functionality either because of a direct effect on the CAR or through affecting levels of CAR expression. Target cell viability was also found to increase from day one post co-culture (Figure 4.17a), showing impaired CAR ability, resulting in target cell outgrowth. (Figure 4.17b).

Alongside assessing whether mNIS co-expression affected CAR function, it was also important to determine whether mNIS functionality was affected by CAR expression. 376.96.m28z.mNIS mouse CAR-T cells were generated from three independent mouse spleens and underwent a Tc99m uptake assay, four days post transduction (Figure 4.17c). The mNIS functionality was found to be affected, with Tc99m uptake being no different from that of the untransduced control (Figure 4.17c). Moreover, Tc99m uptake was not found to be specific to mNIS, with similar levels of uptake seen in the presence or absence of the competitive inhibitor, sodium percholate ($NaClO_4$) (Figure 4.17c). The results of these experiments revealed that 376.96.m28z.mNIS mouse CAR-T cells show impaired CAR and mNIS functionality and are thus unsuitable in their current iteration as a modality for monitoring the effect of single dose radiation on the long term effects of CAR-T cell therapy *in vivo*.

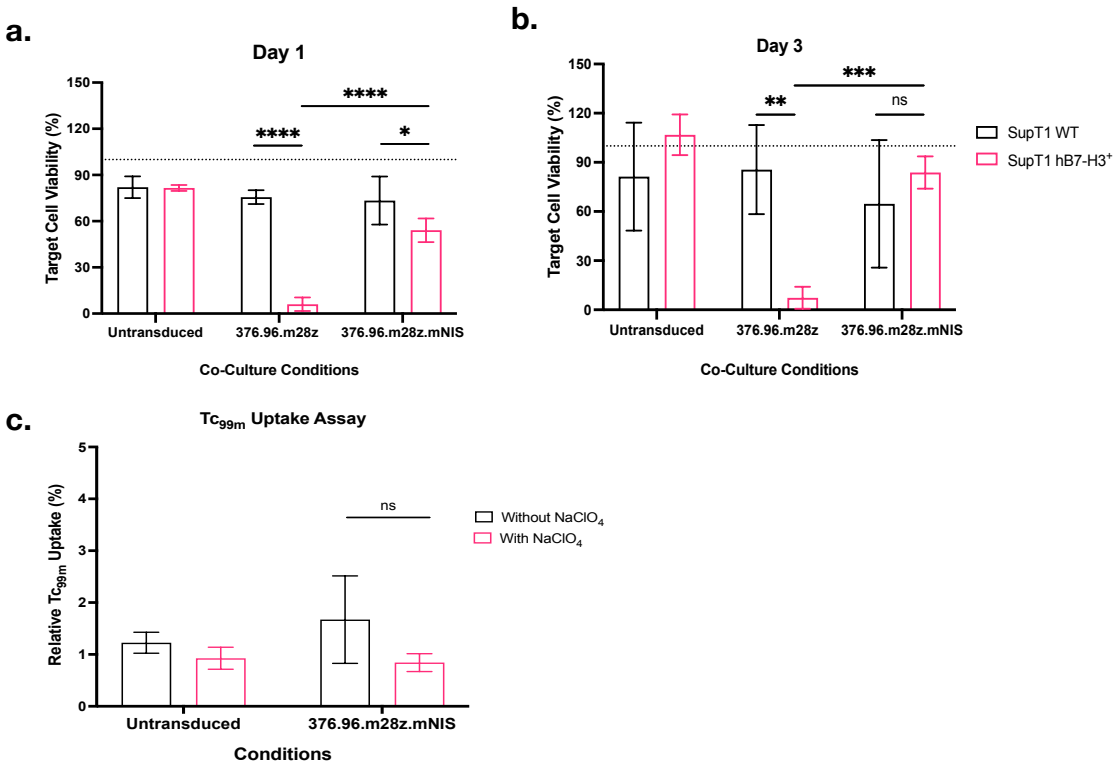

Figure 4.17 376.96.m28z.mNIS CAR-T functionality is impaired *in vitro*

129/SvJ Spleens were used to generate 376.96.m28z.mNIS mouse CAR-T cells. At three days post transduction, CAR-T cell functionality was assessed in a co-culture with luciferase+ targets, SupT1 WT and SupT1 hB7-H3^{+}. Target cell killing was assessed by luminescence at **a**) day one and **b**) day three post co-culture commencement. At day four post transduction, NIS functionality was assessed of CAR-T cells in a **c**) Tc99m uptake assay. The error bars shown represent the standard deviation with an n of three (N=3). Statistical analysis was performed using two-way ANOVA. ns<non-significant, *<0.0332,**<0.0021, ***<0.0002, ****<0.0001.

4.4 Discussion

4.4.1 Generation of 376.96.m28z mouse CAR-T cells

To assess the effect of single-dose radiation on CAR-T cell therapy within a fully immunocompetent setting, an ideal CAR candidate was required to target the TH-MYCN models of high-risk neuroblastoma of interest that were evaluated for radiosensitivity within this project. The development of CAR-T therapy for neuroblastoma has been largely focused on GD2. However, other candidates have shown to be of interest, including anti-B7-H3 ScFv, 376.96, which has shown *in vivo* efficacy as a CAR therapy in immunocompetent mice using orthotopic PDAC models (1). Thus, I was interested in further validating the use of 376.96 as

a fully murinised mouse CAR-T cell to evaluate the effect of single dose radiation on improving CAR-T cell efficacy against neuroblastoma.

The utilisation of retrovirus derived from transient transfection of Pheonix.Eco cells resulted in the production of 376.96.m28z mouse CAR-T cells, which exhibited suboptimal CAR expression levels (Figure 4.2). However, the use of high-titre retrovirus from a generated producer cell line greatly improved CAR expression (Figure 4.3). After improving CAR expression, it is important to assess the stability of CAR expression during the *in vitro* expansion period. Expansion of mouse CAR-T cells is important because of the need for a sufficient number of mouse CAR-T cells for *in vitro* and *in vivo* evaluation. Mouse spleens provide a limited source of T-cells compared with the large number of PBMCs obtained from human blood for CAR-T cell manufacturing.

Within the literature, there have been varying methods in the production of mouse CAR-T cells with varying periods of expansion that range from four to up to fourteen days of expansion (1,373,412,413). During the *in vitro* expansion, 376.96.m28z CAR expression was found to be transient, which was unexpected. Du et al. reported the use of generated anti-B7H3 (376.96) mouse CAR-T cells six to seven days post-transduction for subsequent experiments, but did not report the stability of CAR expression during this expansion period (1).

Because of this transient CAR expression, it is imperative to optimise different parameters of mouse CAR-T cell production to determine how the stability of CAR expression could be improved. Recent publications in the field have reported the use of more T-cell directed stimulation prior to retroviral transduction (373). T-cell activation is important, especially with the need for dividing cells required for successful retroviral transduction (373). The use of anti-mouse CD3 and CD28 dynabeads was found to improve CAR expression over non-specific T-cell specific activation with conA and mIL-7, with no adverse effects on cell viability and expansion observed (Figure 4.4). However, irrespective of the stimulation method used, CAR expression remained transient during the *in vitro* expansion period.

Previous *in vitro* expansion of mouse CAR-T cells focused on using hIL-2, but recent studies have highlighted improved T-cell expansion with hIL-7 and hIL-15 compared to hIL-2 alone. The choice of cytokines for mouse CAR-T cells has been highlighted in the literature as imperative for sustained T-cell proliferation, survival, and intact effector functions. Total cell viability and fold expansion were improved with hIL-7 and hIL-15 compared to hIL-2 alone for 376.96.m28z mouse CAR-T cells (Figure 4.5). However, irrespective of the cytokine

combination used for expansion, CAR expression was transient. Evaluation of these cytokine growth conditions for additional CAR and non-CAR controls (ALK.h28z and eGFP, respectively) showed relatively stable expression compared with 376.96.m28z mouse CAR-T cells (Figure 4.5-4.7), suggesting that this transient expression is an inherent phenomenon of the 376.96.m28z mouse CAR-T cells.

With improved parameters of mouse CAR-T cell production and the continued observation of transient 376.96.m28z CAR expression, I sought to determine whether stable integration of the CAR transgene occurred within the cell genome. Treatment with reverse transcriptase and integrase inhibitors (saquinavir and raltegravir) resulted in complete abrogation of CAR expression compared to DMSO and non-treated controls, confirming that pseudotransduction was not the cause of this transient CAR expression (Figure 4.9). This was found to be the case with both the use of retroviral preparations from transient transfection of Pheonix.Eco cells and from the producer cell line, confirming that differences in retroviral preparations did not contribute to the transient CAR expression observed (Figure 4.9). The reason for this transient 376.96.m28z CAR expression during *in vitro* expansion warrants further investigation of the CAR construct to determine the cause of this transient CAR expression. Even though there was a lack of stable CAR expression, I tested the 376.96.m28z CAR functionality to determine whether it is for subsequent CAR evaluation studies in conjugation with radiation. Even though there is a limited expansion period, CAR expansion upon antigen exposure may circumvent the decrease in CAR expression seen during the expansion period. Functional evaluation of 376.96.m28z mouse CAR-T cells showed short-term cytotoxicity (Figures 4.10-11) with no CAR expansion in response to both plate-bound antigen and antigen-expressing target cells (Figure 4.12). Failure of the 376.96.m28z CAR to expand in response to antigen makes it unsuitable as a CAR candidate for subsequent evaluation to assess the effect of single-dose radiation on CAR functionality. Thus, an alternative CAR candidate is required for this project.

Difficulties encountered in generating a functional 376.96.m28z mouse CAR-T cell warrant further investigation in CAR design, which may explain the failure of sustained CAR expression and functionality in response to antigen. Du et al. generated 376.96.m28z mouse CAR-T cells and reported short-term *in vitro* cytotoxicity with cytokine release and target cell killing, which I could also confirm (1). However, Du et al. have not reported long-term CAR persistence, which is imperative for CAR efficacy both *in vitro* and *in vivo* (1). *In vivo* evaluation of the 376.96.m28z CAR was based on tumour control, with no adverse toxicity. However, no findings on the CAR population within the immune compartment were reported between

the non-transduced and mB7-H3 CAR treatment groups (1). Haydar and colleagues have recently reported on the sustained *in vitro* and *in vivo* activity of fully murnised B7-H3 mouse CAR-T cells against glioma models using an ScFV derived from the mB7-H3 specific monoclonal antibody, m276 (413). A comparison between the m276 CAR and 376.96 CAR may confirm whether the 376.96 ScFv in question is the reason for the short-lived CAR functionality.

4.4.2 Evaluation of the 376.96.m28z.mNIS mouse CAR-T cells

To better evaluate the effects of single-dose radiation on CAR-T cell persistence, there is interest in generating mouse CAR-T cells co-expressing the NIS, with hNIS showing robust *in vivo* CAR-T cell tracking in immunodeficient mice (166). The compatibility of NIS with readily available radioisotopes, such as $^{99m}TcO_4^-$ with SPECT/CT also provides improved image resolution compared to other alternatives, such as bioluminescence imaging (166).To evaluate the long-term effects of single-dose radiation on CAR-T cell therapy *in vivo*, I looked to evaluate the co-expression of NIS with 376.96.m28z mouse CAR-T cells. The NIS has been assessed as a modality for monitoring human CAR-T cells in immunodeficient mice. Moreover, this evaluation has largely used the hNIS, with no published findings thus far on the use of the mNIS for CAR-T tracking *in vivo*. Thus, I wanted to incorporate the use of NIS within the immunocompetent setting to better evaluate the long-term effects of CAR-T cell therapy and determine if mNIS shows similar functionality to hNIS to co-express with the 376.96.m28z CAR.

Similar to the generation of 376.96.m28z mouse CAR-T cells, poor CAR expression was observed with the use of retrovirus from transient transfection of Phoenix.Eco cells (Figure 4.13). This was observed with both 376.96.m28z.NIS bicistronic constructs, including either the mNIS or hNIS. Thus, I sought to optimise the retroviral production method to improve CAR expression. However, before doing this, I compared the *in vitro* functionality of hNIS and mNIS and found they were comparable. To allow the evaluation of these mouse CAR-T cells within a fully immunocompetent setting, I wanted to ensure that all components were fully murinised to prevent any confounding variables on the occurrence of the results. Evaluation of these bicistronic constructs using transduced BW5 cells revealed comparable Tc99m uptake between mNIS and hNIS (Figure 4.14), and thus I opted to optimise on improving the production of 376.96.m28z.mNIS mouse CAR-T cells.

The generation of the 376.96.m28z.mNIS Phoenix.Eco producer cell improved CAR expression of the 376.96.m28z.mNIS mouse CAR-T cells (Figure 4.15). The subsequent concentration of this producer cell line derived retrovirus further enhanced CAR expression (Figure 4.15). However, the expression was transient throughout the *in vitro* expansion period and not due to pseudotransduction (Figure 4.16). No abrogation of CAR expression occurred in response to reverse transcriptase or integrase inhibitors compared to DMSO and non-treatment controls (Figure 4.16). Even with this transient expression, I wanted to determine whether CAR and mNIS functionality were affected when co-expressed on mouse CAR-T cells. I found that CAR functionality was impaired when assessed in a short term *in vitro* co-culture with B7-H3^{+} targets. Moroever, 376.96.m28z.mNIS mouse CAR-T cells also showed impaired Tc99m uptake (Figure 4.17). The Impaired functionality of both CAR and mNIS suggests the constraints of retroviral construct size in generating mouse CAR-T cells co-expressing both transgenes. Further studies are required to determine how to improve the co-expression of CAR and NIS in mouse CAR-T cells.

Chapter 5 Determine whether radiation improves the activation of antigen-specific T-cells.

5.1 Introduction

As determined in Chapter 4, the anti-B7-H3 CAR, 376.96.m28z proved to be an unsuitable CAR candidate for evaluating the effect of single dose radiation on CAR-T cell functionality due to its inability to expand in response to antigen. Thus, an alternative CAR candidate was required for evaluation, and I focused on the most studied tumour-associated antigen (TAA) in neuroblastoma, GD2.

5.1.1 GD2

GD2 is highly expressed in neuroblastoma, and its role is linked to tumour immune evasion (172,438). The success of the anti-GD2 monoclonal therapy dinituximab, based on the 14.18 monoclonal antibody, paved the way to focus on the generation of anti-GD2 CAR-T cells, with one of the first CAR-T products to be tested within children being a first-generation anti-GD2 CAR based on the 14.18 binder (438–440). Subsequent iterations in anti-GD2 CARs have been developed and evaluated within the literature, both in preclinical and clinical settings, with varying degrees of success (189,366,438,440–442).

In collaboration with Pule and colleagues, we generated a second generation humanised anti-GD2 CAR (HuK666.h28z) derived from the monoclonal anti-GD2 antibody, K666. This CAR showed effective *in vitro* cytotoxicity and sustained proliferation against GD2 expressing neuroblastoma line, LAN-1 (366). Moreover, successful elimination of GD2 expressing CT26 tumours by HuK666.h28z mouse CAR-T cells was seen in wild type Balb/c mice (366). The choice of focusing on Huk666.h28z for this project is further bolstered by the CAR being currently under clinical evaluation. Results reported by Straathof and colleagues from a phase one study in relapsed/refractory neuroblastoma patients treated with the HuK666.h28z showed disease regression without inducing on-target-off tumour toxicity (189). Thus, I looked to generate HuK666.h28z mouse CAR-T cells and evaluate *in vitro* its potential as a CAR candidate in combination with single dose radiation.

5.2 Results

5.2.1 Structure of HuK666.h28z

The SFG.RQR8.HuK666.hCD28TM.hCD28z (HuK666.h28z) is a second generation anti-GD2 CAR (366). As shown in Figure 5.1a, this CAR construct consists of the anti-GD2 ScFv, HuK666, with a human IgG1 CH2-CH3 hinge domain followed by a human CD28 transmembrane domain. The signalling endodomains of the CAR consist of the hCD28 and the hCD3ζ (Figure 5.1a). The CAR construct also includes co-expression of RQR8, an epitope-based marker used for CAR detection (Figure 5.1b). This 136 amino-acid protein consists of CD34 and CD20 antigens recognised by the anti-CD34 antibody, QBEnd10 and by mAb, Rituximab, respectively (367). Its susceptibility to rituximab provides a clinical safety switch to render lysis of CAR-T cells if required in the event of cytotxicity (367).

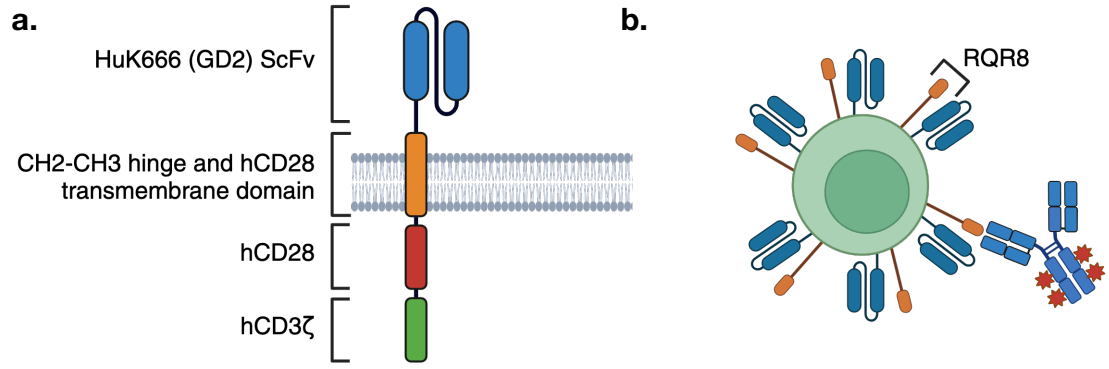

Figure 5.1 Structure of HuK666.h28z

HuK666.h28z is a second-generation anti-GD2 CAR with its structure shown in **a**). The main detection method for HuK666.h28z is through the detection of the co-expressed **b**) RQR8, an epitope-based marker composed of target antigens from CD20 and CD34 antigens. RQR8 detection using a fluorophore-conjugated anti-CD34 antibody determines the detection of the co-expressed CAR by flow cytometry. Figure created using Biorender.

HuK666.h28z *in vitro* expression in mouse T cells is stable compared to 376.96.m28z irrespective of mouse genetic strain used. To first confirm the suitability of HuK666.h28z as an alternative CAR candidate, both the HuK666.h28z and 376.96.m28z mouse CAR-T cells were generated and evaulated for expression by flow cytometry over the course of a seven day *in vitro* expansion period. Both CARs were generated on the 129/SvJ and C57BL/6 background to confirm if CAR expression is affected by differences in genetic mouse strain considering that the mouse neuroblastoma models evaulated within this project exist both

on the 129/SvJ (129N21 and TAM6) and C57BL/6 (9464D) background. Thus, it was imperative to confirm CAR transduction efficiency could be utilised for experimental use irrespective of the mouse genetic strain used to generate the CAR-T cells.

When looking at CAR expression for both CAR candidates on the 129/SvJ background across three independent mouse spleens (Figure 5.2a), CAR expression for both 376.96.m28z and HuK666.h28z is initially higher at day three post transduction, but is found to decrease by day seven post transduction in a statistically significant manner. When looking at CAR gMFI (Figure 5.2b), 376.96.m28z mirrors the same decrease in gMFI from day three to day seven post transduction as seen with CAR expression (Figure 5.2a). However, gMFI was found to be relatively stable between day three and day seven post transduction for HuK666.h28z, suggesting potentially that CAR expression is stable compared to 376.96.m28z.

Comparison on the C57BL/6 genetic background (Figure 5.2c-d) mirrored the same results as on the 129/SvJ background. CAR expression for both generated 376.96.m28z and Huk666.h28z mouse CAR-T cells decreases from day three to day four post transduction (Figure 5.2c). However, CAR gMFI for generated HuK666.h28z mouse CAR-T cells was stable over the course of the expansion period compared to the generated 376.96.m28z mouse CAR-T cells (Figure 5.2d). These results confirmed that not only were HuK666.h28z mouse CAR-T cells successfully generated, but they also showed potentially stable CAR expression based on gMFI compared to 376.96.m28z mouse CAR-T cells across two different mouse genetic strains, and thus, potentially could be evaluated further to assess the effect of single-dose radiation on CAR functionality.

Figure 8.4 in the appendix displays representative flow cytometry plots of CAR expression for 376.96.m28z and HuK666.h28z during the seven-day expansion period in both 129/SvJ and C57BL/6 mouse strains.

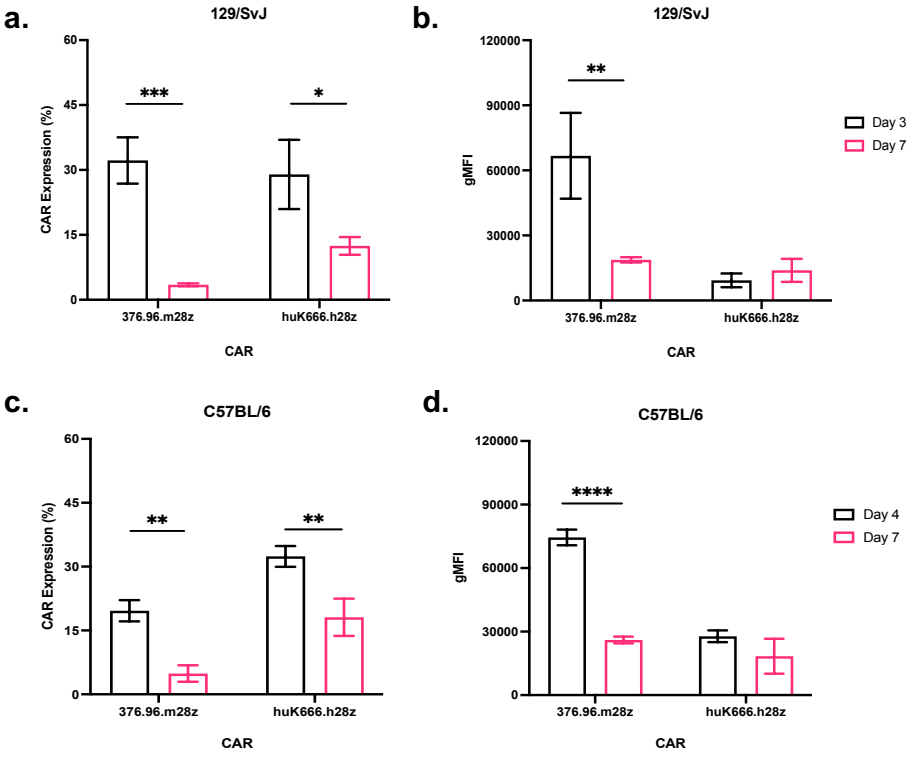

Figure 5.2 HuK666.h28z *in vitro* expression is stable compared to 376.96.m28z irrespective of mouse genetic background

376.96.m28z and huK666.h28z CAR-T cells were generated from 129/SvJ and C57BL/6 female spleens. Mouse CAR-T cells were expanded for seven days *in vitro* with CAR and RQR8 expression assessed by flow cytometry. **a**) Expression and **b**) gMFI of CARs generated on the 129/SvJ background at days three and seven post transduction. **c**) Expression and **d**) gMFI is shown of CARs generated on the C57BL/6 background at days four and seven post transduction. The error bars shown represent the standard deviation with n of three (N=3). Statistical analysis was performed using one-way ANOVA. ns<non-significant, *<0.0021, **<0.0021, ****<0.0001.

5.2.2 T-Cell subsets change during mouse CAR *in vitro* expansion.

During the *in vitro* mouse CAR-T cell expansion phase post transduction, changes in T-cell subsets were also assessed over the course of a seven day expansion period by flow cytometry across three independent mouse spleens on the C57BL/6 background. Figure 5.3a shows that from day four to day seven post transduction, the CD8:CD4 ratio increased in a statistically significant manner across both untransduced and the generated 376.96.m28z and HuK666.h28z mouse CAR-T cells. Changes in the T_{EM}:T_{CM} ratio were also determined by flow cytometry, with only 376.96.m28z and HuK666.h28z mouse CAR-T cells showing an increase in the T_{EM}:T_{CM} ratio in a time dependent manner, but not found to be a statistically

significant trend for 376.96.m28z CAR-T cells due to high biological variability (Figure 5.3b). The high biological variability seen for untransduced T-cells between day four and day seven post transduction, meant it was hard to discern if there was a statistically significant shift in the T_{EM}:T_{CM} ratio over the seven day *in vitro* expansion period (Figure 5.3b).

These results suggest that in response to the T-cell specific mitogenic stimulation (CD3/CD28 dynabeads) prior to viral transduction and subsequent T-cell expansion post transduction with hIL-2 in combination with hIL-7 and hIL-15 seems to show a shift to a more $CD8^+$ and T_{EM}^+ T-cell population for mouse CAR-T cells. These observations towards a more $CD8^+$ T-cell and T_{EM} population have been cited within the literature with the use of T-cell specific mitogenic stimulation, such as the use of CD3/CD28 dynabeads (443). However, it is important to note that the use of hIL-7 and hIL-15 has been shown to lead to a better preservation of T_{cm} compared to T-cell expansion with IL-2 alone (412,443).

Figure 8.5 in the appendix displays representative flow cytometry plots of T-cell susbet changes for 376.96.m28z and HuK666.h28z during the seven-day expansion period.

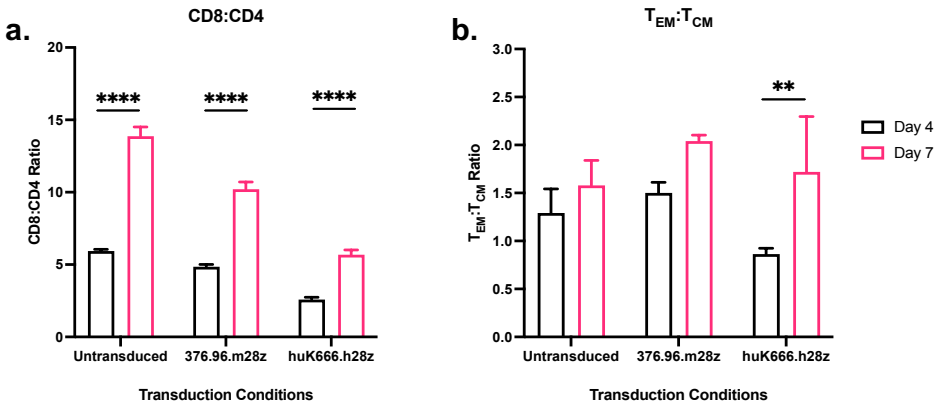

Figure 5.3 T-cell subsets change during *in vitro* expansion

Untransduced, 376.96.m28z and huK666.h28z CAR-T cells were generated from C57BL/6 female spleens. Cells were expanded for seven days *in vitro* and T-cell subsets were assessed by flow cytometry at days 4 and 7 post-transduction. Proportion of $mCD3^+mCD8^+$ and $mCD3^+mCD4^+$ is shown in **a**). Proportion of T_{EM} ($mCD3^+mCD44^+mCD62L^-$) and TCM ($mCD3^+mCD44^+mCD62L^+$) is shown in **b**). The error bars shown represent the standard deviation with n of three (N=3). Statistical analysis was performed using two-way ANOVA. ns<non-significant, **<0.0002, ****<0.0001.

5.2.3 TH-MYCN tumour models may vary in the expression of mB7-H3 and GD2.

To compare 376.96.m28z and HuK666.h28z CAR functionality against the TH-MYCN neuroblastoma models of interest within this project, it was important to determine the expression of both mB7-H3 and GD2 on these tumour models. Of the TH-MYCN models of interest evaluated, little is known about the mB7-H3 and GD2 expression, and thus it was imperative to confirm. mB7-H3 and GD2 antigen expression was assessed by flow cytometry during *in vitro* propagation of these TH-MYCN lines and corrected against the isotype control. Antigen expression was assessed on the following TH-MYCN lines of interest: 9464D WT, 9464D-GD2, 129NS1 and TAM6 WT.

Figure 5.4a shows the greatest mB7-H3 expression to be seen in 9464D WT and 9464D-GD2 lines followed by 129NS1 and TAM6 WT. Moreover, mB7-H3 gMFI was found to be the highest in 9464D WT. 9464D-GD2, 129NS1 and TAM6 WT showing relatively similarily lower levels of gMFI compared to 9464D WT. Compared to mB7-H3 expression, GD2 expression was found to vary across the lines screened. Figure 5.4b shows the greatest expression in GD2 in 9464D-GD2 and TAM6 WT followed by 129NS1. However, a complete absence of GD2 expression is seen with 9464D WT. GD2 gMFI in Figure 5.4b mirrors this trend with the highest gMFI of GD2 seen with 9464D-GD2 followed by TAM6 WT and 129NS1, with no GD2 gMFI seen with 9464D WT.

The absence of GD2 expression in 9464D WT confirms what has been reported in literature. The 9464D tumour model was generated from spontaneous tumours arising in TH-MYCN transgenic mice on the C57BL/6 background and turned into an immortalised cell line (218). Characteristics of this model were shown to be akin to human neuroblastoma, with endogenous expression of GD2 and low levels of MHC-I (219). However, prolonged *in vitro* culturing has resulted in a loss of GD2 expression (220). Thus, an 9464D line was generated to overexpress GD2 to compensate for the loss of antigen expression (216). Based on the varied expression of mB7-H3 and GD2 seen across the models, 9464D WT and 9464D-GD2 were initially chosen to assess CAR functionality due to being the highest expressing in GD2 and mB7-H3 to allow better assessment of CAR functionality in the presence of single dose radiation.

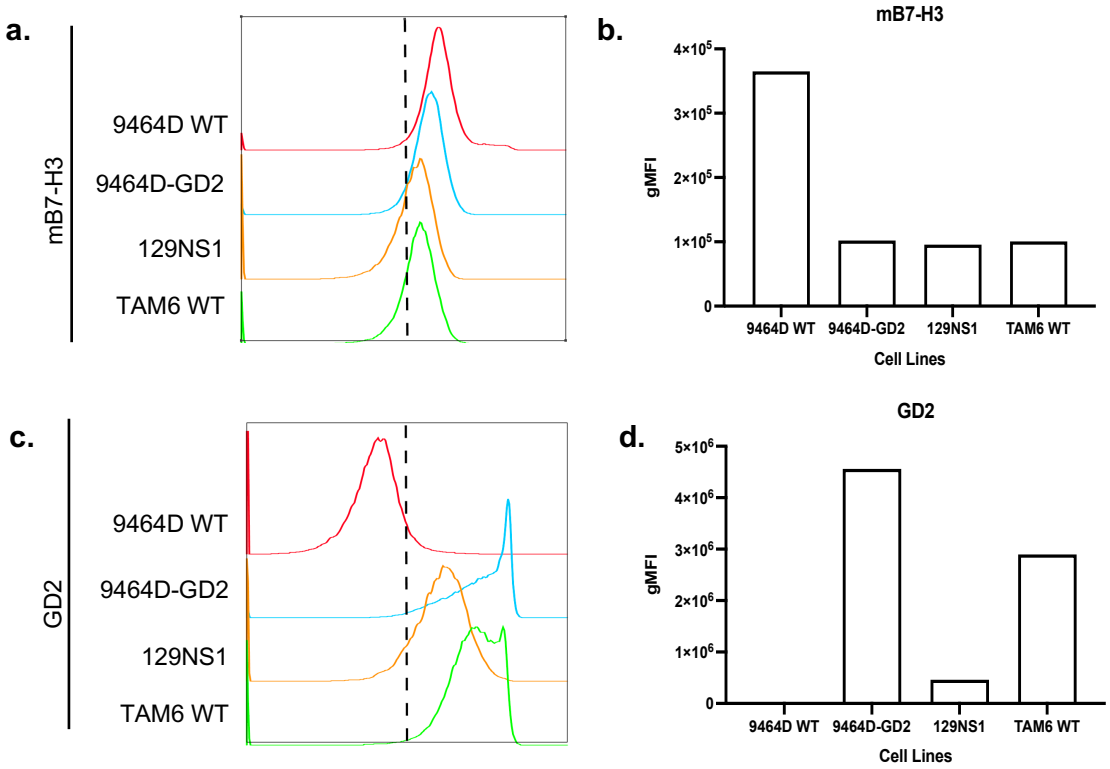

Figure 5.4 TH-MYCN tumour models may vary in expression of mB7-H3 and GD2

TH-MYCN mouse neuroblastoma cell lines were (9464D WT, 9464D-GD2, 129NS1 and TAM6 WT) were assessed for expression and gMFI quantified by flow cytometry for **a-b**) mB7-H3 and **c-d**) GD2 corrected against isotype controls (dashed black line). FACS plots and quantified gMFI represent one independent experiment (N=1).

5.2.4 The effect of single-dose radiation on *in vitro* CAR functionality

To evaulate the effect of single dose radiation on CAR functionality, target cells, 9464D-WT and 9464D-GD2 were either irradiated 24 hours prior to the start of the co-culture with a low dose of 2Gy and high dose of 8Gy alongside a non-irradated treatment control. 376.96.m28z and HuK666.h28z mouse CAR-T cells were then introduced for the commencement of the *in vitro* co-culture 24 hours post target cell irradiation at a1:1 E:T ratio.

5.2.4.1 HuK666.h28z shows greater cytokine release than 376.96.m28z

Release of mIL-2 and mIFN-γ was assessed 24 hours after the commencement of the co-culture by ELISA. In response to 9464D WT, no discernible difference was seen in mIFN-γ release between 376.96.m28z and HuK666.h28z compared to untransduced (Figure 5.5a). For 376.96.m28z, no discernible differences were seen in mIFN-γ release against non-

irradiated and 2Gy and 8Gy irradiated targets (Figure 5.5a). However, when looking at mIFN-γ release in response to 9464D-GD2, HuK666.h28z showed a statistically significant increase in cytokine release compared to untransduced and 376.96.m28z exhibiting that the cytokine release was occurring in an antigen-dependent manner (Figure 5.5b). However, no differences in mIFN-γ release were seen in a dose dependent manner, with similar levels of cytokine release between non-irradiated and 2Gy treatment. 8Gy treatment may have induced a lower mIFN-γ release based on the mean, but further experimental repeats are required to confirm this due to the large variation in results seen for this treatment condition (Figure 5.5b).

For the mIL-2 results, 9464D WT results were similar to those seen with the mIFN-γ results. No discernible differences in cytokine release were seen between 376.96.m28z and HuK666.h28z compared to untransduced (Figure 5.5c). Moreover, no discernible differences were seen between non-irradiated and irradiated conditions (Figure 5.5c). In response to 9464D-GD2, HuK666.h28z was found to release mIL-2 in an antigen dependent manner compared to untransduced and 376.96.m28z (Figure 5.5d). However, no dose-dependent differences in mIL-2 release were seen with 2Gy and 8Gy treatment compared to non-irradiated (Figure 5.5d). Additional experimental repeats may allow elucidation of any dose dependent differences in cytokine release, considering the overlapping error bars across the co-culturing conditions seen (Figure 5.5d). The cytokine results confirm HuK666.h28z cytotoxicity is occurring in terms of cytokine release in an antigen-dependent manner. However, no dose-dependent differences in cytokine release occurred with targets irradiated for 24 hours.

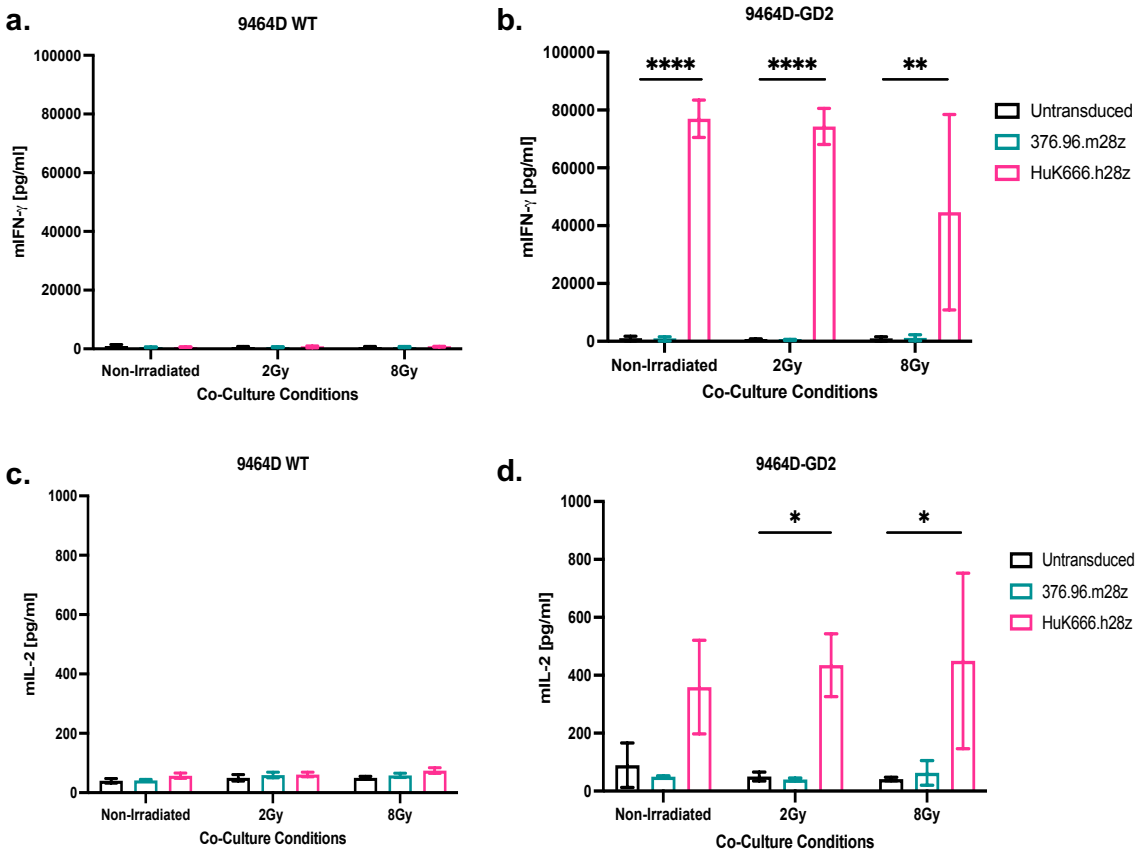

Figure 5.5 Radiation does not enhance *in vitro* Huk666.h28z CAR-T cell cytotoxicity in cytokine release

Untransduced, 376.96.m28z and huK666.h28z CAR-T cells were assessed for cytotoxicity against 9464D WT and 9464D-GD2. The co-culture was performed 24 hours post irradiation treatment of target cells. mIL-2 and mIFN-γ cytokine release was assessed by ELISA, 24 hours post commencement of co-culture. mIFN-γ release is shown for **a**) 9464D WT and **b**) 9464D-GD2. mIL-2 release is shown for **c**) 9464D WT and **d**) 9464D-GD2. The error bars shown represent the standard deviation with n of three (N=3). Statistical analysis was performed using one-way ANOVA. *<0.0332, **<0.0021, ****<0.0001.

5.2.4.2 HuK666.h28z show cytotoxicity compared to 376.96.m28z in response to target.

Alongside looking at cytokine release 24 hours post commencement of co-culture, target cell killing was also assessed at 72 hours post commencement of co-culture by flow cytometry to allow accurate determination of changes in target cell numbers (Figure 5.6). For 9464D WT, target cell killing by 376.96.m28z was not occurring in antigen-dependent manner, with the results seen across all co-culture conditions to be similar to that of the HuK666.h28z CAR and untransduced (Figure 5.6a). Target cell viability was only found to decrease in a dose

dependent manner; however, no additive antigen dependent effect on target cell viability was seen in response to 376.96.m28z compared to HuK666.h28z and untransduced (Figure 5.7a).

In response to 9464D-GD2, HuK666.h28z showed antigen-dependent killing compared to untransduced and 376.96.m8z mouse CAR-T cells. Effective tumour control by HuK666.h28z was seen with non-irradiated and 2Gy irradiated targets (Figure 5.6b). Whlist HuK666.h28z showed effective target cell killing compared to untransduced in a statistically significant manner, complete tumour control observed at non-irradiated and 2Gy was not seen at 8Gy with viable target cells still present, suggesting some radioresistant cells have survived (Figure 5.6b). HuK666.h28z shows CAR expression in response to antigen, but radiation shows no additive effect of this.

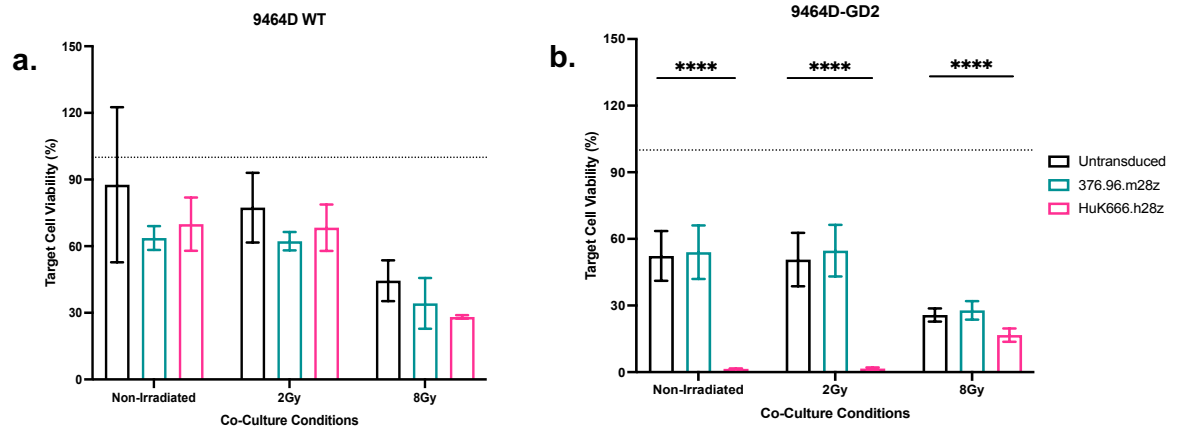

Figure 5.6 Radiation does not enhance *in vitro* huK666.h28z target cell killing against 9464D-GD2

Untransduced, 376.96.m28z and huK666.h28z CAR-T cells were assessed for cytotoxicity against 9464D WT and 9464D-GD2. The co-culture was performed 24 hours post irradiation treatment of target cells. Target cell viability was assessed by flow cytometry 72 hours post commencement of co-culture. Target cell counts were normalised against target cells alone to determine target cell viability for **a**) 9464D WT and **b**) 9464D-GD2. The error bars shown represent the standard deviation with n of three (N=3). Statistical analysis was performed using one-way ANOVA. ns<non-significant, ****<0.0001.

Given the inability of 376.96.m28z to proliferate in response to antigen, as detailed in section 4.2.10, it was crucial to confirm that Huk666.h28z did not exhibit the same limitation. This confirmation was necessary to ensure its suitability for assessing the long-term effectiveness of CAR-T cell therapy following a single dose of radiation. At 72 hours post commencement

of the co-culture with irradiated 9464D WT and 9464D-GD2, CAR expansion was assessed by flow cytometry. Fold changes in percentage of CAR expression and gMFI were analysed against CAR alone. Fold CAR expansion was determined on the normalisation of CAR^+ cell counts across co-culturing conditions against CAR^+ cell count in CAR-T cell alone conditions.

Against 9464D WT, 376.96.m28z failed to show any CAR expansion compared to CAR alone (Figure 5.7a-b). Both HuK666.h28z and 376.96.m28z showed similar levels of fold change in CAR expression and CAR gMFI across, irrespective of irradiation or not (Figure 5.7a-b). These results confirm what has been previously seen with 376.96.m28z in that it does not expand in response to antigen. Compared to 376.96.m28z, HuK666.h28z does show expansion in antigen-dependent manner (Figure 5.7c-d). In response to 9464D-GD2, Huk666.h28z was found to show up to 30 fold CAR expansion compared to 376.96.m28z, but no additive effect was seen in expansion with either 2Gy or 8Gy irradiated compared to non-irradiated targets (Figure 5.7c).

While changes were seen in CAR fold expression, no fold change was seen in CAR MFI for Huk666.h28z across all co-culture conditions compared to CAR alone (Figure 5.7d). Nonetheless, these results confirm that HuK666.h28z, compared to 376.96.m28z can successfully expand in response to the target; however, no additive effect is seen with targets irradiated at 2Gy or 8Gy for 24 hours. Thus, further work is required to optimise the radiation treatment conditions of target cells to better evaluate the effect of singe dose radiation on HuK666.h28z functionality.

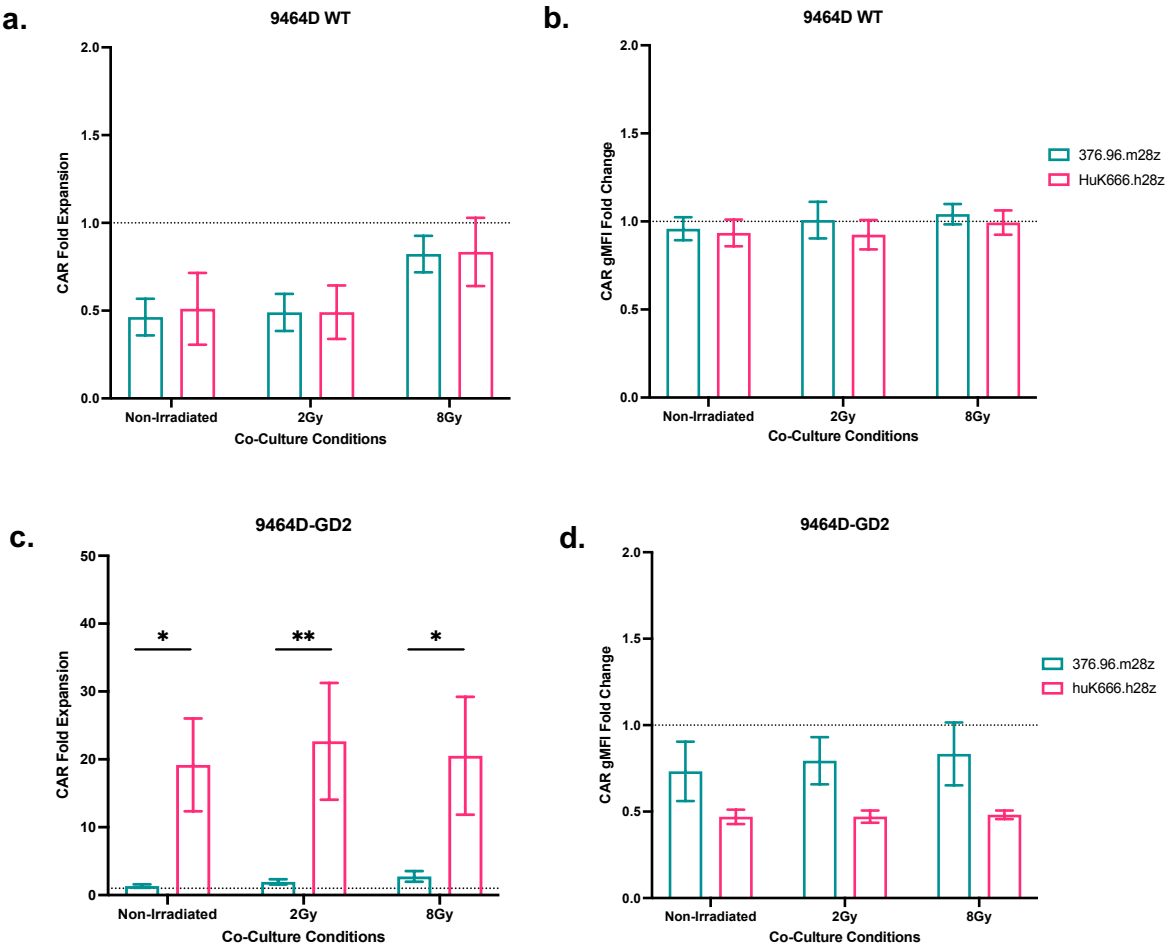

Figure 5.7 Radiation does not enhance in vitro huK666.h28z CAR expansion against 9464D-GD2

Untransduced, 376.96.m28z and huK666.h28z CAR-T cells were assessed for CAR expansion against 9464D WT and 9464D-GD2. The co-culture was performed 24 hours post irradiation treatment of target cells. CAR expression was assessed by flow cytometry 72 hours post commencement of co-culture. CAR T-cell counts were normalised against CAR T-cells alone controls to determine changes in CAR expression and gMFI. CAR expression and gMFI for co-cultures against 9464D WT and 9464D-GD2 are shown in **a**) to **b**) and **c**) to **d**), respectively. The error bars shown represent the standard deviation with n of three (N=3). Statistical analysis was performed using one-way ANOVA. ns<non-significant, *<0.0332, **<0.0021.

5.2.4.3 Radiation affects CD4:CD8 and T_{EM}:T_{CM} ratios

Alongside evaluating the effect of single dose radiation on HuK666.h28z functionality in terms of cytotoxicity and CAR expansion, I also looked to see if radiation induces any phenotypic changes in T-cell subsets within the CAR population 72 hours post commencement of co-culture by flow cytometry. Looking at changes in the CD8:CD4 ratio within the HuK666.h28z

population, CD8:CD4 ratio was found to increase in response to 9464D-GD2 compared to CAR alone (Figure 5.8a). Moreover, the changes were occurring in an antigen-dependent manner with no changes in CD8:CD4 ratio against 9464D WT compared to CAR alone observed (Figure 5.8a). CD8:CD4 ratio was found to increase in response to irradiated targets in a dose-dependent manner, suggesting that within the HuK666.h28z population, targets irradiated with a higher single dose of irradiation induce a shift towards more $CD8^+$ than $CD4^+$ T-cells (Figure 5.8a).

Changes in the T_{EM}:T_{CM} ratio were also observed within the HuK666.h28z CAR-T cell population in an antigen-dependent manner (Figure 5.8b). No changes in T_{EM}:T_{CM} ratio were observed in response to 9464D WT irrespective of target cell irradiation (Figure 5.8b). However, in response to 9464D-GD2, the T_{EM}:T_{CM} ratio was found to increase in a dose-dependent manner, with a higher dose of 8Gy irradiation treatment inducing the largest change in T_{EM}:T_{CM} compared to 2Gy irradiated and non-irradiated 9464D-GD2 (Figure 5.8b). These results seem to suggest that, potentially in response to a higher dose of 8Gy irradiation of targets, HuK666.h28z mouse CAR-T cells show a shift towards a more $CD8^+$ and T_{EM} cell subset. Further work would be required to determine the exact functional effects this has on the long term efficacy of the HuK666.h28z CAR.

Representative flow plots for the data shown in figure 5.8 can be seen in figure 8.6 in the appendix.

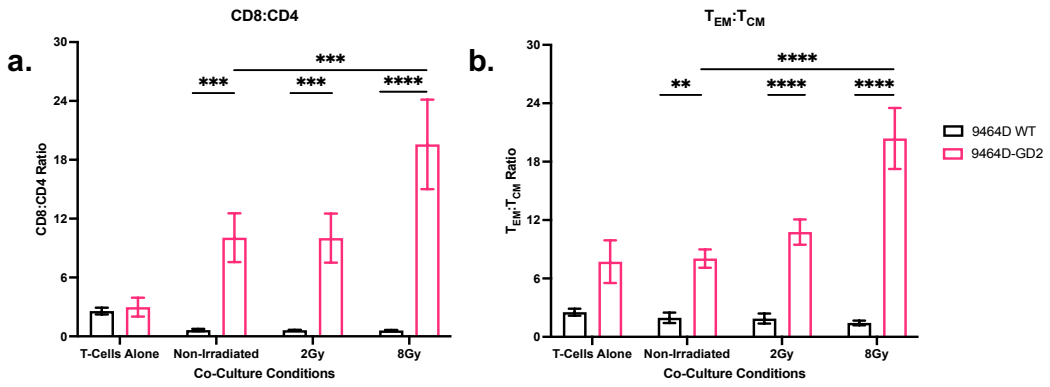

Figure 5.8 Radiation induces *in vitro* changes in HuK666.h28z CD8:CD4 and T_{EM}:T_{CM} ratios in response to antigen

Untransduced and huK666.h28z CAR-T cells were assessed for CAR expansion against 9464D WT and 9464D-GD2. The Co-culture was performed 24 hours post irradiation treatment of target cells. CAR expression was assessed by flow cytometry 72 hours post commencement of co-culture. The proportion of $mCD3^+CAR^+mCD8^+$ and $mCD3^+CAR^+mCD4^+$ is shown in **a**). Proportion of T_{EM} ($mCD3^+CAR^+mCD44^+mCD62L^-$) and T_{CM}

(mCD3$^+$CAR$^+$mCD44$^+$mCD62L$^+$) is shown in **b**). The error bars shown represent the standard deviation with n of three (N=3). Statistical analysis was performed using one-way ANOVA. **<0.0332, ***<0.002, ****<0.0001.

5.2.5 Radiation may induce changes in antigen expression

Alongside determining the effects of single dose radiation on HuK666.h28z CAR functionality, the effect of single dose radiation on the antigen expression of 9464D-GD2 was also assessed by flow cytometry, 72 hours post commencement of co-culture. GD2 and mB7-H3 expression was analysed on target cell alone conditions. The gating strategy used to measure expression of GD2 and mB7-H3 for 9464D-GD2 is shown in Figure 5.9.

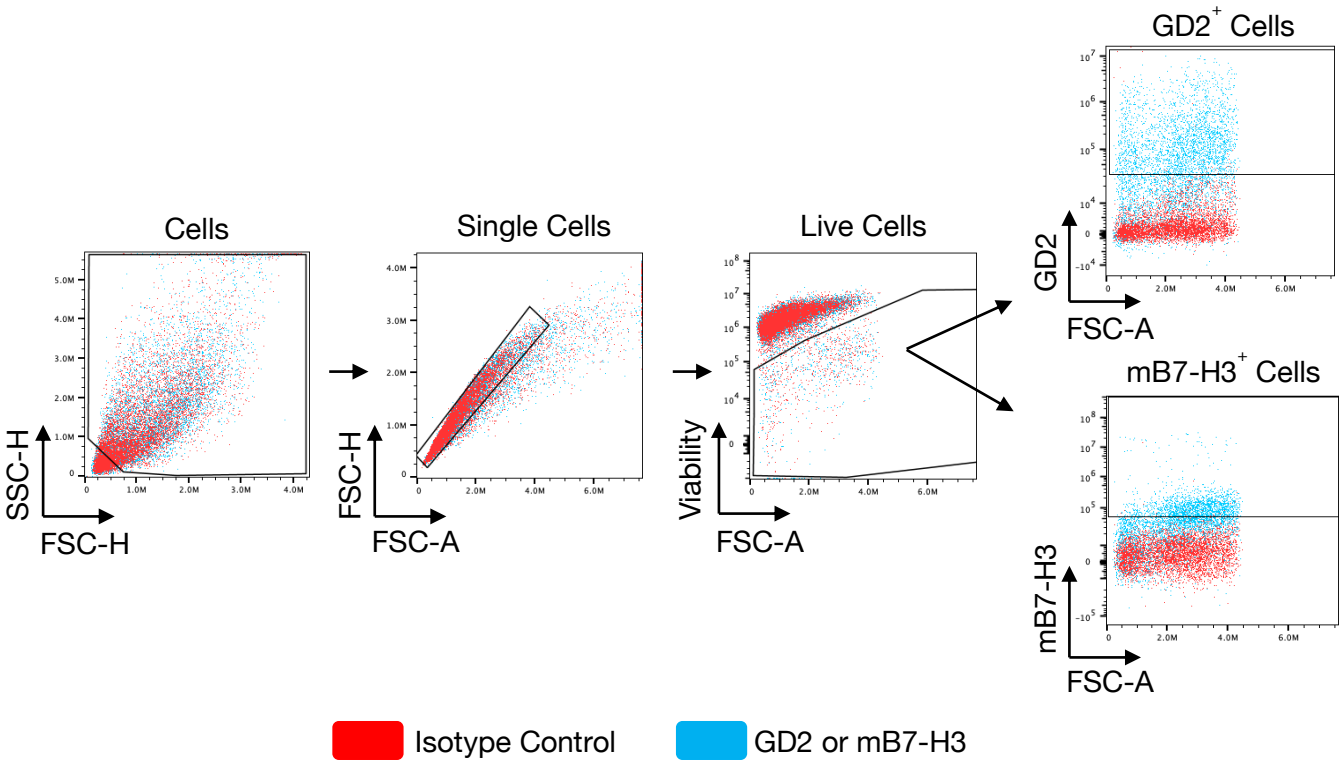

Figure 5.9 Gating strategy for measuring antigen expression in response to single-dose radiation

9464D-GD2 was non-irradiated or irradiated with single dose radiation for a co-culture with CAR-T cells performed 24 hours post irradiation. Co-culture was analysed by flow cytometry 72 hours post-culture commencement, including staining for antigen expression on conditions with target cells 9464D-GD2 alone. The representative FACS plots show the gating strategy utilised to determine GD2 and mB7-H3 expression by flow cytometry on gated viable single cells against the isotype control.

Looking at the percentage of antigen expression, mB7-H3 expression was found to decrease in response to radiation in a dose-dependent manner (Figure 5.10a). However, GD2 antigen expression was found to increase in a dose dependent manner (Figure 5.10a). Moreover, looking at changes in antigen gMFI, mB7-H3 was found similarly to the percentage of antigen expression to decrease in a dose-dependent manner (Figure 5.10b). GD2 gMFI was also found to decrease in a dose dependent manner as well (Figure 5.10b). Further experimental repeats are required to confirm the significance of these results and whether the increase in GD2 antigen expression seen provides any additive effect on Huk666.h28z functionality.

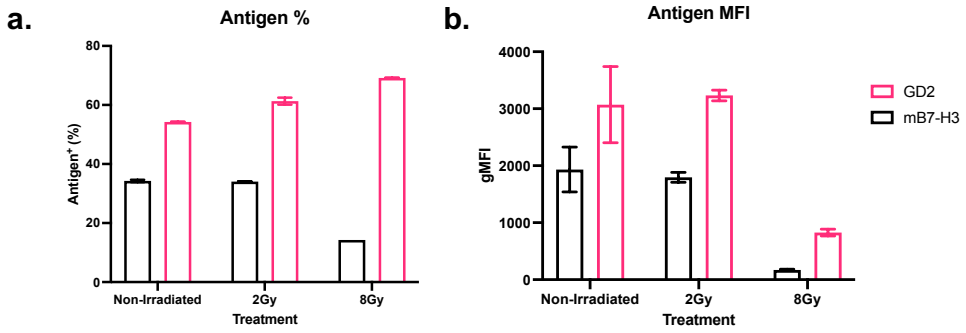

Figure 5.10 Radiation may induce changes in antigen expression *in vitro*

9464D-GD2 was non-irradiated or irradiated with single dose radiation for a co-culture with CAR-T cells performed 24 hours post irradiation. Co-culture was analysed by flow cytometry 72 hours post-culture commencement, including staining for antigen expression on conditions with target cells, 9464D-GD2 alone. Across the co-culture conditions, mB7-H3 and GD2 expression is shown as **a**) percentage and **b**) MFI on Live⁺ cells. Each condition contains three technical repeats with the errors showing the standard deviation. Results shown are of one independent experiment (N=1).

5.3 Discussion

The findings presented in this chapter provide support for the use of the anti-GD2 CAR, HuK666.h28z, as an alternative CAR candidate to utilise to investigate the effect of single dose radiation on CAR functionality. Within the literature, HuK666.h28z has been reported to show sustained *in vitro* cytotoxicity and *in vivo* efficacy within an immunocompetent mouse model (366). Moreover, its ongoing current evaluation within clinical trials against refractory neuroblastoma further bolsters the translational value in understanding if single-dose radiation can improve CAR-T cell efficacy.

Evaluation of *in vitro* production of Huk666.h28z CAR-T cells against 376.96.m28z CAR-T cells on both the 129/SvJ and C57BL/6 mouse genetic background revealed comparable levels of CAR expression, which decreased over the course of a seven day expansion period as observed previously with 376.96.m82z. While the CAR gMFI was found to decrease for 376.96.m28z CAR-T cells over the seven day expansion, HuK666.h28z CAR gMFI was found to be relatively stable over the course of the expansion period, suggesting stable CAR expression and thus potential in its ability to be evaluated *in vitro* against irradiated TH-MYCN models of neuroblastoma.

mB7-H3 and GD2 expression across the TH-MYCN models of neuroblastoma was shown to vary. Due to this, the 9464D models were selected to assess the functionality of HuK666.h28z against 376.96.m28z, with the high GD2 expression of 9464D-GD2 providing a clearer assessment of HuK666.h28z functionality. Moreover, the 9464D models propagate as a monolayer *in vitro* compared to the spheroid forming 129NS1 and TAM6 WT lines. Due to this, further technical optimisations were still required for use of 129NS1 and TAM6 WT compared to the use of 9464D lines for evaluating CAR functionality against in vitro.

For assessing CAR functionality against 9464D target lines, irradiation was performed on targets at low dose of 2Gy and high dose of 8Gy. This is due to evidence of radiation dose strength affecting CAR functionality, such as through increased tumour sensitisation to CAR-T cell killing (444). The *in vitro* evaluation of single dose radiation on CAR functionality was performed with 9464D target lines irradiated at a low dose of 2Gy and high dose of 8Gy, 24 hours prior to the addition of CAR-T cells. Both a low and high dose were chosen for this *in vitro* CAR evaluation due to dose strength and timing greatly affecting CAR functionality. Within the literature, dose strength and timing have been found to influence changes in the TME through increasing tumour sensitisation and increased tumour cell death, leading to increased CAR-T functionality (356,445). However, 9464D has not been evaluated with radiation in combination CAR-T cells within the literature, thus, we initially looked to evaluate CAR-T functionality in this manner.

In vitro assessment of HuK666.h28z mouse CAR-T cells revealed effective cytotoxicity with both mIL-2 and mIFN-γ release in an antigen-dependent manner against 9464D-GD2. Effective anti-tumour activity was also seen with antigen-dependent tumour cell killing. Moreover, Huk666.h28z showed significant CAR fold expansion, showing its ability to expand in response to antigen which 376.96.m28z failed to do. However, while Huk666.h28z showed effective CAR functionality; no dose-dependent changes were seen in response to targets

irradiated at 2Gy and 8Gy compared to non-irradiated. As the effects of radiation on CAR functionality are greatly affected by dose strength and timing, further work is required to optimise the radiation regime to further elucidate how radiation dose and timing may affect Huk666.h28z CAR functionality.

In vitro assessment of HuK666.h28z mouse CAR-T cells revealed single dose radiation induced changes in the T-cell subsets. In a dose dependent manner, an increase in both the CD8:CD4 and T_{EM}:T_{CM} ratio was observed in response to irradiated targets. These observations are supported within the literature where radiation has been found to influence dynamics of the T-cell population, with an increase in both $CD8^+$ T-cells and effector memory T-cell populations resulting in an effective anti-tumour response (446,447). Further *in vitro* and *in vivo* evaluation, looking at the long term CAR-T cell activity, would reveal if these changes in CD8:CD4 and T_{EM}:T_{CM} ratios are maintained and lead to a sustained anti-tumour response by the Huk666.h28z mouse CAR-T cells.

The ability of radiation to alter the TME is known to be imperative in the success of immunotherapy. Within this TME remodelling, there have been reports of radiation increasing antigen expression, which may further bolster antigen-mediated tumour killing (353,354,448–450) As a result, I looked to evaluate any changes in mB7-H3 and GD2 antigen expression on the irradiated 9464D-GD2 line that may aid in bolstering the CAR response. In response to single dose radiation, antigen expression of GD2 but not of mB7-H3 was found to increase in a dose-dependent manner (Figure 5.9a). These are preliminary results, and thus further work is required to elucidate HuK666.h28z CAR efficacy against irradiated targets with varying levels of GD2 expression to determine if radiation enhances antigen expression and further bolsters the CAR response.

B7-H3 expression has been noted to increase in response to radiation across a range of tumour cell lines by Wang and colleagues (448). However, this was looking at hB7-H3 antigen expression across human target cell line models. Thus, further validation of these preliminary results is required to determine if mB7-H3 antigen expression is found to increase in response to radiation or not. Previous evaluation of the 376.96.m28z CAR in chapter four showed short term effective tumour control against the hB7-H3 expressing SupT1 targets. However, evaluation of the 376.96.m28z against the mB7-H3 expressing 9464D lines showed ineffective anti-tumour control and cytotoxicity, with responses found to be similar to those of untransduced cells. These results seem to suggest that potentially 376.96.m28z mouse CAR may not be crossreactive to both mB7-H3 and hB7-H3 as has been reported by Du and

colleagues (1). Further work is required to confirm these findings with evaluation of the 376.96.m28z against overexpressing mB7-H3 and hB7-H3 targets to determine if antigen density is not a limiting factor in CAR efficacy, and thus may explain differences in responses observed.

In summary, the findings of this chapter have confirmed the use of the anti-GD2 HuK666.h28z as an alternative CAR to the 376.96.m28z to evaluate in combination with single dose radiation. Initial evaluation of the Huk666.h28z against irradiated the 9464D model showed effective CAR functionality with radiation inducing changes in T-cells subsets within the CAR population. Further *in vitro* work is required to optimise the radiation regimen in terms of use of dose and timing schedule to effectively evaluate the effect of single dose radiation on the anti-CAR response, both short term and long term, to effectively evaluate this combination therapy within an immunocompetent model.

Chapter 6 Discussion

This thesis aimed to investigate the effects of radiation on CAR-T cell function against neuroblastoma within the context of an intact immune system. I sought to address this by aiming to 1) determine the radiosensitivity of TH-MYCN models of high-risk neuroblastoma, 2) evaluate a mouse CAR candidate for use in this project, and 3) examine whether a single dose of radiation affects CAR-T cell functionality. The achievements of these aims are summarised below.

1) I confirmed that TH-MYCN mouse models of high-risk neuroblastoma (129NS1, TAM6, and 9464D) vary in radiosensitivity. The range of radiosensitivity of these models has not been previously reported in the literature. The models' responses varied in the immune-mediated effects of radiation, which focused on screening key markers of immunogenic cell death (298,377). Moreover, the use of the MTT assay to assess non-immune-mediated effects of radiation revealed that models show variation in radiosensitivity. This provides an opportunity to evaluate CAR-T functionality in various models that vary in treatment sensitivity.

2) After establishing the tumour models of interest to be radiosensitive, I evaluated the anti-B7-H3 CAR, 376.96.m28z, as a CAR candidate for use in this project because of the published literature describing its cross-reactivity between hB7-H3 and mB7-H3 and its *in vivo* efficacy against an immunocompetent model by Du et al. (1). CAR expression was found to be poor, requiring optimisation of the mouse CAR-T cell production protocol, which greatly improved CAR expression. However, *in vitro* expansion revealed that CAR expression was transient, a phenomenon inherently specific to 376.96.m28z compared to CAR and non-CAR controls, with pseudotransduction not being a cause of this. *In vitro* CAR-T functionality against B7-H3 plate-bound and B7-H3 cell targets revealed only short-term cytotoxicity mediated by CAR-T cells with no CAR-T cell expansion. As a result, 376.96.m28z was found unsuitable for evaluating CAR-T cell functionality with radiation against neuroblastoma *in vitro* and *in vivo*. Optimisations were also performed to generate mouse CAR-T cells co-expressing the reporter gene NIS with 376.96.m28z to provide a more detailed *in vivo* evaluation of this combination therapy in real time using SPECT/PET imaging (166). Protocol optimisations were performed to improve the initial poor transduction efficiency; however, *in vitro* assessment revealed that both CAR and NIS functionality are impaired when co-expressed on mouse CAR-T cells.

3) The anti-GD2 CAR, Huk666.h28z, was evaluated as an alternative to the 376.96.m28z CAR. HuK666.h28z mouse CAR-T cells showed stable CAR expression, which was sufficient for use in downstream *in vitro* and *in vivo* assessments with radiation. Evaluation of the HuK666.h28z CAR against the 9464D model revealed effective tumour control and mIL-2 and mIFN-γ release in an antigen-dependent manner compared to the 376.96.m28z CAR. Moreover, HuK666.h28z CAR showed significant expansion in an antigen-dependent manner, making this CAR suitable for assessing the long-term effects of radiation on CAR functionality. The use of targets irradiated at either a low dose of 2Gy or a high dose of 8Gy revealed no dose-dependent differences in the HuK666.h28z CAR functionality, with results similar to those of non-irradiated targets. However, T-cell subsets were found to vary in both the $CD8^+$:$CD4^+$ and T_{EM}:T_{CM} ratios within the Huk666.h28z CAR population in a dose-dependent manner, which may contribute to the observed anti-tumour response.

6.1 Determining the radiosensitivity of the TH-MYCN models of high risk neuroblastoma

This project focused on using TH-MYCN mouse models of high-risk neuroblastoma (129NS1, TAM6, and 9464D) to evaluate the efficacy of radiation in combination with CAR-T therapy. Within the field, TH-MYCN models have been used to assess *in vivo* treatment efficacy in preclinical settings (213,216,376). Moreover, these models provide the ability to evaluate CAR efficacy in an immunocompetent setting (213,376). This is imperative considering that CAR-T preclinical *in vivo* evaluation is largely performed within an immunodeficient setting (451). Thus, the current system is insufficient for assessing the on-target-off-tumour side effects associated with this therapy.

Little is known about the radiosensitivity of TH-MYCN models of high-risk neuroblastoma; therefore, I sought to develop an *in vitro* radiosensitivity screen to establish if models were susceptible to radiation in terms of assessing both immune and non-immune mediated effects of radiation. I opted to perform this screening in response to a range of single-dose radiation doses, considering that the effects of radiation are affected by dose and fractionation. The optimal radiation regimen for optimal therapeutic benefit is an important question that should be addressed in the future, after establishing radiosensitivity.

Assessing the immune-mediated effects of radiation was centred on immunogenic cell death (ICD). ICD has been implicated in anti-tumour effects elicited by modalities such as

radiotherapy, which induce cell stress (380,452). The release of DAMPs induced by this regulated form of cell death can result in the activation of $CD8^+$ T cell adaptive responses (380,452). This, in turn, would result in an enhanced anti-tumour effect when combined with CAR-T cell therapy. Multiple hallmarks of ICD have been mentioned within the field, but I looked to focus on three that have a particular emphasis in the literature: Calreticulin, EC-ATP and EC-HMGB1 (295,380). Assessing these markers *in vitro* across the TH-MYCN models of interest revealed varied levels of upregulation across the models, with calreticulin being the only marker upregulated by radiation across the three models **(Chapter 3)**.

As radiation-induced ICD is influenced by the radiation source, dose, fractionation, and exposure time, it is difficult to conclude from these results that TH-MYCN models of neuroblastoma exhibit ICD *in vitro* **(Chapter 3)**. The absence of upregulation of the other ICD markers suggests that further work is required to confirm whether these ICD markers are upregulated in response to radiation in TH-MYCN neuroblastoma models. The occurrence of ICD also depends on the timing and nature of cell death, with not all ICD inducers activating the same stress response, thus eliciting the same molecular signal (292). The mechanisms and efficacy of ICD induction can vary *in vitro* and *in vivo* due to the presence of TME, immune cell interactions, and various signalling molecules, which differ between cell-based and tumour-based models (292). To address these potential differences, it is important to translate these *in vitro* findings *in vivo* by confirming the assessment of ICD markers. It would also be prudent to determine the occurrence of cell death, considering that ICD is highly related to the detection of DNA damage and the subsequent occurrence of cell stress response, being imperative for the occurrence of this regulated form of cell death (295,380,453). Within the literature, the interest in ICD in neuroblastoma is supported by Hong et al., who recently reported on the development of a prognostic prediction tool based on the occurrence of ICD in neuroblastoma (454). Through analysis of multi-omics data from 1244 NB samples and 16 scRNA-seq datasets, they reported on an ICD-related index (ICDR-index) that can identify different neuroblastoma risk subtypes, and the identification of the ELAVL3 gene, which encodes an RNA-binding protein (HuC), was found to be overexpressed in high-risk neuroblastoma and be a potential target for ICD-based therapeutic strategies in neuroblastoma patients (454).

As mentioned above, because of the multiple factors affecting the successful measurement of ICD markers *in vitro*, I also measured the effect of radiation on cell viability using an MTT assay (**Chapter 3**). This high-throughput approach, compared with the use of traditional clonogenic assays for measuring radiotoxicity, revealed that the TH-MYCN models vary

greatly in radiosensitivity based on the IC_{50} calculated **(Chapter 3)**. This has not been previously reported in the literature; thus, it provides a framework in which models differ in treatment resistance, mirroring differences in treatment responsiveness seen within the clinical setting. As a result, this range of treatment sensitivity allows for better evaluation of the effect of radiation on CAR-T functionality against neuroblastoma.

6.2 Evaluation of the 376.96.m28z CAR

This project focused on evaluating the effect of radiation on CAR functionality within the context of an intact immune system. Hence, I sought to identify a CAR candidate targeting a known TAA of neuroblastoma that could be evaluated for CAR-T therapy in TH-MYCN tumour-bearing immunocompetent mice. The findings reported by Du et al. for anti-B7-H3 ScFv 376.96, showed cross-reactivity to both mouse and human B7-H3 with functionality in both human and mouse CAR-T cells, which led me to evaluate this CAR within the scope of this project (1).

Production of 376.96.m28z mouse CAR-T cells proved challenging. Initially, poor CAR expression was observed, which was improved through extensive protocol optimisation **(Chapter 4)**. First, CAR expression was improved using the retroviral producer cell line Phoenix.Eco. The use of producer cell lines has been well established in the literature because of their ability to develop high-titre viral supernatants and reduce the risk of contamination with helper viruses (373,412,455,455,456). This is also important not just within the preclinical setting but also in the clinical setting to reduce variability in retrovirus production as part of ensuring that the quality and safety standards of treatment are maintained for patients (457).

Second, CAR expression was found to improve further through the use of anti-CD3/CD28 Dynabeads compared to concanavalin-A and mIL-7 **(Chapter 4)**. This is important considering that retroviruses require proliferating cells; thus, the choice of the T-cell stimulation method used for mouse CAR-T cell production is an important factor to consider (373,458). The choice of anti-CD3/CD28 dynabeads for mouse CAR-T cell production is supported in the literature (373,412,459,460). Lanitis et al. reported that for their mouse CAR-T cell production protocol, mouse T-cell stimulation with anti-CD3/CD28 beads resulted in more activated and proliferating cells compared to other commonly used methods of T-cell stimulation (Concanavalin A, and plate-immobilised anti-CD3 with soluble anti-CD28 antibody) (412). Third, the evaluation of cytokine growth conditions during mouse CAR-T cell

expansion revealed that hIL-7 and hIL-15 are advantageous compared to hIL-2 expansion alone **(Chapter 4)**. The expansion of therapeutic T-cell products, including CAR-T cells, commonly uses hIL-2 (461). However, repeated hIL-2 expansion can potentially lead to T-cell exhaustion, hindering the anti-tumour response (461,462). hIL-7 and hIL-15 have been reported to promote a more central memory T-cell population, thus allowing more effective tumour control and T-cell persistence (419,420,463). This has largely been shown with human CAR-T cells; however, recent publications on mouse CAR-T cells have reported functional mouse CAR-T cells under *in vitro* expansion with IL-7 and IL-15, (1,412,413,464). Thus, the choice of IL-7 and IL-15 for mouse CAR-T cell expansion in this project is supported by the literature.

The aforementioned protocol optimisations improved the initial 376.96.m28z CAR expression post transduction. However, CAR expression was found to be transient during the *in vitro* expansion period **(Chapter 4)**. In the literature, the commonly used mouse CAR-T cell expansion period is shorter than that of human CAR-T cells. This may be due to inherent differences in T-cell biology between species; mouse T-cells have been found to be more sensitive to activation signals, and culture conditions have found to more so impact their proliferation and persistence *in vitro* compared to human T-cells (412,465). Mouse CAR-T cells have been used for downstream *in vitro* and *in vivo* analysis after four to seven days post-transduction . The authors of these papers have not reported on the stability of CAR expression throughout the *in vitro* expansion period, but only prior to their use in subsequent *in vitro* and *in vivo* experiments. Therefore, it is unclear how stable CAR expression is for these mouse CAR-T cell constructs reported in the literature. Within the studies evaulating mouse CAR-T cells, findings on the long term engraftment of mouse CAR-T cells in immune competent hosts is limited resulting in a lack of overall support in the literature for the long term effector function of mouse CAR-T cells generated using the standard retroviral apparoaches as reported in the field (366,411,412).

After confirming stable integration of the CAR transgene **(Chapter 4)**, 376.96.m28z mouse CAR-T cells revealed short-lived functionality, rendering this CAR unsuitable for use in this project **(Chapter 4)**. My findings contradict the *in vitro* efficacy of the 376.96 mouse CAR reported by Du et al. . Du et al. reported that 376.96 generated mouse CAR-T cells with both CD28ζ and 4-1BBζ murine endodomains showed effective tumour control *in vitro* against mB7-H3^{+} engineered Raji cells with IL-2 and IFN-γ release in an antigen-dependent manner . Within the co-cultures performed with SupT1 cells expressing hB7-H3, I observed the short-term functionality of the 376.96.m28z mouse CAR-T cells **(Chapter 4)** but not against the

mB7-H3^{+} endogenously expressing 9464D model **(Chapter 5)**. This suggests that 376.96 ScFV may not be cross-reactive to both hB7-H3 and mB7-H3, as reported by Du et al. . This difference may be due to the binding affinity of 376.96 ScFv, which is higher for hB7-H3 than for mB7-H3 (1). Thus, 376.96.m28z mouse CAR efficacy may only be seen against overexpressing mB7-H3 antigen on tumour cells, considering that Du et al. engineered mB7-H3^{+} Raji cells to demonstrate *in vitro* efficacy of 376.96.m28z mouse CAR-T cells compared to the range of endogenously expressed hB7-H3 human PDAC cell lines used to evaluate 376.96 human CAR-T cell *in vitro* efficacy (1). Irrespective of the use of hB7-H3^{+} or mB7-H3^{+} expressing target cells, no CAR expansion was observed in response to the antigen **(Chapters 4-5)**. Du et al. reported only 376.96 human CAR activity for proliferation and not 376.96 mouse CARs (1). Thus, it is difficult to corroborate these results due to the lack of published findings.

6.3 Coexpression of NIS with 376.96.m28z CAR

Effective infiltration and persistence within the immunosuppressive TME are imperative for CAR-T cell success in solid tumours (170,427,466). Within the preclinical *in vivo* setting, this parameter has commonly been assessed using endpoint readings, such as flow cytometry and bioluminescence-based imaging (BLI) (467,468). However, recent developments have shown improved imaging-based modalities focused on engineering T-cells to express reporter genes that allow for more robust *in vivo* monitoring of CAR-T cells, which may also provide more effective clinical monitoring of treatment efficacy and reduce the risk of adverse effects in preclinical and clinical settings (167,469). In this project, I was interested in incorporating this by focusing on the inclusion of the reporter gene, the Sodium Iodide Symporter (NIS), within mouse CAR-T cells. This would allow for more effective *in vivo* monitoring of the effect of radiation on CAR-T cell localisation and assessment of CAR-T cell viability and proliferation over prolonged periods.

NIS is an iodide transporter expressed naturally in organs, such as the stomach and salivary glands. It is a reporter gene that is non-immunogenic and compatible with multiple PET (^{124}I and ^{18}F) and SPECT (^{123}I and ^{99}Tcm) radionucleotides currently in clinical use (166,167,469,470). However, it is considered non-immunogenic and functional only within living cells, making it an ideal reporter gene for co-expression with CAR-T cells (166,167,469,470). CAR-T cells have been successfully tracked within mouse models using clinically available SPECT (Tc_{99m}) and PET (^{18}F-BF_4-) radiotracers with no effect on anti-tumour

activity (166,470). However, *the in vivo* evaluation of hNIS has been performed in immunodeficient mice using human CAR-T cells (166,470). This does not allow a thorough evaluation of CAR-T efficacy, considering the absence of an intact immune system. I evaluated the generation of NIS co-expressed with 376.96.m28z mouse CAR-T cells and determined their potential for *in vivo* assessment of the effect of radiation on CAR-T efficacy. To prevent the occurrence of non-immunogenic effects through the use of hNIS in immunocompetent mice, evaluation of 376.96.m28z co-expressing mNIS or hNIS was performed to determine whether the functionality of mNIS was comparable to that of hNIS and thus suitable for use *in vivo*.

In vitro detection of hNIS has been validated through the use of commercially available anti-hNIS fluorophore-conjugated antibodies, but not for mNIS, with alternative methods of detection, such as western blotting, providing variable results (166). Therefore, I incorporated an intracellular c-myc epitope tag to the C-terminus of mNIS and hNIS to standardise detection between the two species by flow cytometry. The inclusion of the c-myc epitope tag at the C-terminus was due to potential interference with NIS functionality, where the c-myc epitope tag was expressed at the N-terminus (471). However, unforeseen technical difficulties were encountered in detecting the intracellular c-myc epitope tag via flow cytometry. Thus, only CAR expression was measured and used as a surrogate marker for NIS expression, which was justified because the bicistronic construct was created by incorporating a 2A peptide, which is known to aid the co-expression of multiple genes with relatively equal expression (472). NIS functionality was also assessed using Tc_{99m} uptake assays to confirm the expression of the reporter gene in transduced cells.

An initial production of 376.96.m28z.NIS mouse CAR-T cells yielded poor transduction efficiency and thus required further optimisation **(Chapter 4)**. *In vitro* mNIS functionality was found to be comparable to that of hNIS in a Tc_{99m} *in vitro* uptake assay with transduced BW5 cells; thus, protocol optimisation was performed on 376.96.m28z.mNIS mouse CAR-T cells **(Chapter 4)**. The generation of the 376.96.m28z.mNIS producer cell line and concentration of retrovirus produced greatly improved the transduction efficiency of the generated mouse CAR-T cells **(Chapter 4)**. However, similar to 376.96.m28z mouse CAR-T cells, transgene expression was not stable during *in vitro* expansion, even though there was stable transgene integration within the T-cell genome **(Chapter 4)**. Subsequent *in vitro* evaluation of 376.96.m28z.mNIS mouse CAR-T cells against hB7-H3^{+} SupT1s suggested that mNIS co-expression impaired CAR-T cell functionality. Moreover, mNIS functionality was limited in 376.96.m28z.mNIS mouse CAR-T cells within a Tc_{99m} *in vitro* uptake assay **(Chapter 4)**.

The difficulty in generating functional 376.96.m28z.mNIS mouse CAR-T cells may be due to the constraints that the retroviral system poses for mouse T-cell transduction. Retroviral vectors provide a limited capacity of 8-10kb, which can restrict the inclusion of multiple transgenes within the vector design (473). The mNIS transgene is quite large, resulting in the generation of the construct size of 376.96.m28z.mNIS plasmid being 9.8Kb. Within the lentiviral system, this construct size may have circumvented the issues of the expression of these genes using a multicistronic construct. However, the incompatibility of murine T cells with HIV has led to a consistent preference for the use of γ-retroviruses in the generation of mouse CAR-T cells within the literature (474,475).

A way to overcome this issue of vector size constraints with γ-retroviruses could be to separate the mNIS and CAR onto separate plasmid constructs and generate 376.96.m28z.mNIS via double transduction using retroviruses produced separately, expressing mNIS and CAR, respectively. However, this may result in a mixed population of cells differing in the expression of mNIS and CAR, affecting transduction efficiency and downstream use in *in vitro* and *in vivo* experiments. These results reveal that the use of the γ-retroviral system limits the success of generating mNIS-co-expressing CAR-T cells owing to the vector size constraints of this system. Alternative transduction methods may potentially overcome this issue, such as CRISPR/Cas9 (476). However, these studies have largely focused on human CAR-T cells; therefore, further studies are required to determine their suitability for generating mouse CAR-T cells (477–479).

6.4 The effect of single dose radiation on CAR-T functionality

Because of the shortcomings of the 376.96.m28z CAR, it was unsuitable for use in this project, requiring an alternative CAR to be evaluated. The anti-GD2 CAR HuK666.h28z was evaluated based on previous literature showing its *in vitro* functionality and *in vivo* efficacy against an immunocompetent CT26 tumour model (366,480). Moreover, the HuK666.h28z CAR is currently under clinical evaluation, bolstering the choice of evaluating this CAR candidate in combination with radiation for this project (189). Compared to 376.96.m28z mouse CAR-T cells, HuK666.h28z mouse CAR-T cells showed stable CAR expression based on stable CAR gMFI during the *in vitro* expansion period post transduction **(Chapter 5)**. This was found in both mouse CAR-T cells generated on the 129/SvJ and C57BL/6 backgrounds **(Chapter 5)**. The reason for the comparison between the two genetic strains was imperative to confirm comparable CAR expression across the two mouse genetic backgrounds,

considering that the TH-MYCN models of neuroblastoma of interest within this project exist both on the 129/SvJ (129NS1 and TAM6 WT) and C57BL/6 (9464D) backgrounds.

The lack of stability observed in the percentage of HuK666.h28z CAR-T cell population may be due to biological and environmental factors that affect *in vitro* mouse T cell expansion. Inherent differences in the human and murine immune systems may result in mouse T-cells being more sensitive during *in vitro* culturing. Mouse T-cells may be more sensitive to activation-induced cell death via T cell-specific mitogenic stimulation, as required for successful retroviral transduction (455,481,482). Additionally, the differentiation state of T cells also plays a crucial role in their expansion capabilities. HuK666.h28z mouse CAR-T cells showed a bias towards T_{EM} cells throughout the *in vitro* expansion period **(Chapter 5)**. Changes in T cell metabolism, such as mitochondrial function and glycolytic activity, can also influence cell expansion (483,484). Considering these factors, further protocol optimisations could be considered to determine if this improves the expansion of CAR-T cells post-transduction.

Having established that Huk666.h28z mouse CAR-T cells displayed stable CAR expression, I next evaluated the effect of single-dose radiation on CAR-T cell functionality in a co-culture with irradiated target cells. GD2 and mB7-H3 expression was observed in all TH-MYCN neuroblastoma models of interest within this project **(Chapter 5)**. As 129NS1 and TAM6 WT exist as spheroids during *in vitro* propagation, they were considered more suitable for CAR-T evaluation *in vitro* because they are more representative of the tumour growth observed *in vivo*. Optimisations were performed to determine the appropriate seeding densities to form viable spheroids for use in downstream co-cultures to evaluate CAR-T functionality **(Chapter 3)**. However, further optimisations were still required for performing co-cultures with these neurosphere lines to evaluate CAR functionality; due to the time constraints of this project, I focused on performing CAR evaluation with 9464D, which has been utilised to assess immunotherapeutic agents *in vitro* and *in vivo* within the literature (215–217).

The co-culture results revealed that HuK666.h28z mouse CAR-T cells exhibited CAR functionality with sustained tumour control and mIL-2 and mIFN-γ release in an antigen-dependent manner. Moreover, HuK666.h28z mouse CAR-T cells exhibited expansion in an antigen-dependent manner, making them suitable for use in this project. CAR expansion is imperative for CAR-T cell success in the clinic, to investigate the long-term effects of CAR-T therapy in combination with radiation. In response to either 2Gy or 8Gy irradiation of 9464D targets, radiation did not lead to changes in CAR-T functionality compared to the non-

irradiated control. However, this may be due to the radiation regimen used, as dose strength, exposure time, and dose fractionation can significantly affect immunotherapeutic responses (485). Therefore, optimising the radiation regimen used to evaluate CAR-T functionality may further elucidate the *in vitro* effect of radiation on CAR-T functionality. While changes in CAR-T functionality were not observed against the irradiated targets, changes in T-cell subsets were observed within the HuK666.h28z CAR population, showing a more $CD8^+$ and T_{EM}^+ bias in a dose-dependent manner **(Chapter 5)**. These promising results indicate that examining the effect of radiation on *in vitro* CAR-T cell therapy against neuroblastoma warrants further investigation, and how this translates further in both *in vitro* and *in vivo* settings.

Within the wider literature, there is limited work published thus far evaluating the effect of radiation on immunotherapy in neuroblastoma. Within an immunocompetent setting, 9464D has been used for immunotherapy in combination with radiation. Voeller et al. reported a single dose of 12Gy either alone or in combination with hu14.18 IL-2 immunocytokine (IC), a fusion protein consisting of hu14.18. anti-GD2 mAb and IL-2 to be ineffective in inducing complete tumour regression or slowed tumour growth in 9464D-GD2 tumour-bearing mice (216). However, the addition of immunotherapeutics, anti-CTLA-4, anti-CD40, and CpG, to the radiation and hu14.18 IL-2 IC regimen resulted in significant tumour control with complete tumour regression in four out of five mice (216). The authors labelled this multi-agent innate and adaptive immunotherapy regimen as “CAIR”. Evaluation of this CAIR regimen was performed further by Zebertavage et al. to determine the translational potential of this CAIR regimen and to determine the regimen components necessary for the anti-tumour efficacy response observed against 9464D-GD2 tumour bearing mice. The results revealed that the efficacy of the CAIR regimen in exhibiting tumour control and prolonging survival in tumour-bearing mice was lost if either the single 12Gy RT dose or IC was absent, but efficacy was retained in the absence of any one of the anti-CTLA-4, anti-CD40, or CpG agents. Moreover, the CAIR regimen showed anti-tumour activity against distant small tumours in a dual-flank model, suggesting the potential of this combination in treating metastases; however, further investigation is warranted to determine its clinical potential for neuroblastoma patients. These results suggest that to harness the effectiveness of combination therapy, consideration needs to be given to appropriate immunotherapeutic approaches that engage both innate and adaptive immune responses. The work performed in this thesis builds on the use of RT against 9464D beyond the reported use of 12Gy alone and contributes to our understanding of the effect of single-dose radiation on the model and how response differs based on dose strength.

As discussed in further detail in the section 1.10, the use of radiotherapy in combination with CAR-T cells against neuroblastoma is also limited and has largely focused on the use of

immunodeficient mice, and thus does not provide information on key factors such as CAR-T toxicity. Sodji et al. reported the use of targeted radiation through 1–6 Gy of the radionucleotides actinium-225 (^{225}Ac) or lutetium177 (^{177}Lu), leading to dose-dependent anti-GD2 CAR-T cell killing and enhanced cytotoxicity with no effect on CAR-T-cell exhaustion or activation *in vitro* (359). Moreover, evaluation of low dose ^{177}Lu (1.8Gy or 3.6Gy) on anti-GD2 CAR-T cells against immunodeficient neuroblastoma tumour-bearing mice led to a robust treatment response with greater survival in the combination group compared to CAR-T or RT treatment alone groups, with 1.8Gy dose leading to a better response than 3.6Gy (360). Moreover, the authors also reported the importance of RT introduction prior to CAR-T cell treatment, which enhanced T-cell infiltration into the TME (360). However, it is important to note that this study has not been certified by peer review; thus, the findings should be interpreted with caution. The work presented in this project has not shown that radiation enhances anti-GD2 CAR-T cell-dependent killing in a dose-dependent manner, as reported by Sodji et al. This may be due to further work required to optimise the radiotherapy regimen to evaluate whether the radiation dose enhances CAR-T cell functionality, as reported by Sodji et al.

The effect of radiation on anti-B7-H3 CAR-T cells against neuroblastoma has also been reported in the field, as discussed in section 1.10. Ansari et al. evaluated ERBT in combination with anti-B7-H3 CAR-T cells in immunodeficient neuroblastoma tumour-bearing mice (361). Findings from this preliminary study revealed that RT in combination with B7-H3 CAR-T cells prolonged disease survival compared to CAR-T treatment alone in both single-flank tumours and in mice with disseminated metastases (361). These findings suggest the potential for the evaluation of RT in combination with anti-B7-H3 CAR-T cells against neuroblastoma; however, further work is warranted to determine the potential for clinical translation for neuroblastoma treatment.

6.5 Future Directions

In summary, the work presented in this project has confirmed the use of TH-MYCN mouse models of high-risk neuroblastoma to evaluate the effect of radiation on CAR-T functionality in the presence of an intact immune system. Finding a suitable CAR candidate to evaluate within the immunocompetent setting for this project has proven to be challenging while addressing the technical challenges in generating mouse CAR-T cells with stable CAR expression. However, the anti-GD2 CAR HuK666.h28z has shown promising results, with

radiation found to induce changes in the CAR population in the *in vitro* CAR functional assessment performed within this project thus far.

Further work is required to build on the findings of this project. First, the effect of radiation on CAR-T functionality is greatly affected by dose strength, fractionation, and exposure time. Thus, further work is required to optimise the radiation regimen used to evaluate CAR-T functionality against neuroblastoma *in vitro* and *in vivo*. Second, generate HuK666.h28z with murinised endodomains and evaluate its *in vitro* CAR functionality. For *in vivo* evaluation in immunocompetent tumour-bearing mice, a fully murinised CAR is optimal to prevent CAR rejection by the host immune system. Finally, evaluate the *in vivo* radiosensitivity of the TH-MYCN models of neuroblastoma with optimised radiation regimens to evaluate the effect of this combination therapy using the Small Animal Radiation Research Platform (SARRP) to provide targeted radiotherapy (486).

This project focused on the use of gamma radiation from a ^{137}Cs source. To translate this work into a clinical setting, further studies should focus on combining CAR-T therapy with MiBG (487). These preclinical findings would inform on how MiBG in combination with CAR-T cells can be utilised to improve the survival of patients with neuroblastoma.

Chapter 7 References

1. Du H, Hirabayashi K, Ahn S, Kren NP, Montgomery SA, Wang X, et al. Antitumor Responses in the Absence of Toxicity in Solid Tumors by Targeting B7-H3 via Chimeric Antigen Receptor T Cells. Cancer Cell. 2019 Feb 11;35(2):221-237.e8.

2. Scotting PJ, Walker DA, Perilongo G. Childhood solid tumours: a developmental disorder. Nat Rev Cancer. 2005 June;5(6):481–8.

3. Public Health England. Cancer survival in England for patients diagnosed between 2014 and 2018, and followed up to 2019 [Internet]. 2021 [cited 2025 Feb 26]. Available from: https://www.gov.uk/government/statistics/cancer-survival-in-england-for-patients-diagnosed-between-2014-and-2018-and-followed-up-until-2019/cancer-survival-in-england-for-patients-diagnosed-between-2014-and-2018-and-followed-up-to-2019

4. Qing T, Mohsen H, Marczyk M, Ye Y, O'Meara T, Zhao H, et al. Germline variant burden in cancer genes correlates with age at diagnosis and somatic mutation burden. Nat Commun. 2020 May 15;11(1):2438.

5. Takeshima H, Ushijima T. Accumulation of genetic and epigenetic alterations in normal cells and cancer risk. npj Precis Onc. 2019 Mar 6;3(1):1–8.

6. Sweet-Cordero EA, Biegel JA. The genomic landscape of pediatric cancers: Implications for diagnosis and treatment. Science. 2019 Mar 15;363(6432):1170–5.

7. Filbin M, Monje M. Developmental origins and emerging therapeutic opportunities for childhood cancer. Nat Med. 2019 Mar;25(3):367–76.

8. Park JA, Cheung NKV. Limitations and opportunities for immune checkpoint inhibitors in pediatric malignancies. Cancer Treatment Reviews. 2017 July 1;58:22–33.

9. Park JR, Eggert A, Caron H. Neuroblastoma: Biology, Prognosis, and Treatment. Hematology/Oncology Clinics of North America. 2010 Feb 1;24(1):65–86.

10. Lundberg KI, Treis D, Johnsen JI. Neuroblastoma Heterogeneity, Plasticity, and Emerging Therapies. Curr Oncol Rep. 2022;24(8):1053–62.

11. Mossé YP, Laudenslager M, Longo L, Cole KA, Wood A, Attiyeh EF, et al. Identification of ALK as a major familial neuroblastoma predisposition gene. Nature. 2008 Oct;455(7215):930–5.

12. Mosse YP, Laudenslager M, Khazi D, Carlisle AJ, Winter CL, Rappaport E, et al. Germline *PHOX2B* Mutation in Hereditary Neuroblastoma. The American Journal of Human Genetics. 2004 Oct 1;75(4):727–30.

13. Dang CV. *MYC* on the Path to Cancer. Cell. 2012 Mar 30;149(1):22–35.

14. Otte J, Dyberg C, Pepich A, Johnsen JI. MYCN Function in Neuroblastoma Development. Front Oncol. 2021 Jan 27;10:624079.

15. Thompson D, Vo KT, London WB, Fischer M, Ambros PF, Nakagawara A, et al. Identification of patient subgroups with markedly disparate rates of MYCN amplification

in neuroblastoma: A report from the International Neuroblastoma Risk Group project. Cancer. 2016;122(6):935–45.

16. Monclair T, Brodeur GM, Ambros PF, Brisse HJ, Cecchetto G, Holmes K, et al. The International Neuroblastoma Risk Group (INRG) Staging System: An INRG Task Force Report. JCO. 2009 Jan 10;27(2):298–303.

17. Brodeur GM, Pritchard J, Berthold F, Carlsen NL, Castel V, Castelberry RP, et al. Revisions of the international criteria for neuroblastoma diagnosis, staging, and response to treatment. JCO. 1993 Aug;11(8):1466–77.

18. Maris JM, Hogarty MD, Bagatell R, Cohn SL. Neuroblastoma. The Lancet. 2007 June 23;369(9579):2106–20.

19. Park JR, Bagatell R, London WB, Maris JM, Cohn SL, Mattay KM, et al. Children's Oncology Group's 2013 blueprint for research: Neuroblastoma. Pediatric Blood & Cancer. 2013;60(6):985–93.

20. Anderson J, Majzner RG, Sondel PM. Immunotherapy of Neuroblastoma: Facts and Hopes. Clinical Cancer Research. 2022 Aug 2;28(15):3196–206.

21. Matthay KK, Villablanca JG, Seeger RC, Stram DO, Harris RE, Ramsay NK, et al. Treatment of High-Risk Neuroblastoma with Intensive Chemotherapy, Radiotherapy, Autologous Bone Marrow Transplantation, and 13-cis-Retinoic Acid. New England Journal of Medicine. 1999 Oct 14;341(16):1165–73.

22. Podlaha O, Riester M, De S, Michor F. Evolution of the cancer genome. Trends in Genetics. 2012 Apr 1;28(4):155–63.

23. Schreiber RD, Old LJ, Smyth MJ. Cancer Immunoediting: Integrating Immunity's Roles in Cancer Suppression and Promotion. Science. 2011 Mar 25;331(6024):1565–70.

24. Vesely MD, Kershaw MH, Schreiber RD, Smyth MJ. Natural innate and adaptive immunity to cancer. Annu Rev Immunol. 2011;29:235–71.

25. Grivennikov SI, Greten FR, Karin M. Immunity, Inflammation, and Cancer. Cell. 2010 Mar 19;140(6):883–99.

26. Seager RJ, Hajal C, Spill F, Kamm RD, Zaman MH. Dynamic interplay between tumour, stroma and immune system can drive or prevent tumour progression. Converg Sci Phys Oncol. 2017;3:034002.

27. Khong HT, Restifo NP. Natural selection of tumor variants in the generation of "tumor escape" phenotypes. Nat Immunol. 2002 Nov;3(11):999–1005.

28. Rabinovich GA, Gabrilovich D, Sotomayor EM. IMMUNOSUPPRESSIVE STRATEGIES THAT ARE MEDIATED BY TUMOR CELLS. Annu Rev Immunol. 2007;25:267–96.

29. Bordon Y. The many sides of Paul Ehrlich. Nat Immunol. 2016 Dec;17(1):S6–S6.

30. Behring, Emil Von, Kitasato, Shibasaburo. Über das Zustandekommen der Diphtherie-Immunität und der Tetanus-Immunität bei Thieren. Dtsch Med Wochenschr. 1890;(16):1113–4.

31. Fagraeus A. Plasma Cellular Reaction and its Relation to the Formation of Antibodies in vitro. Nature. 1947 Apr;159(4041):499–499.

32. Tiselius A, Kabat EA. AN ELECTROPHORETIC STUDY OF IMMUNE SERA AND PURIFIED ANTIBODY PREPARATIONS. J Exp Med. 1939 Jan 1;69(1):119–31.

33. Bernard NJ. When humoral became cellular. Nat Immunol. 2016 Dec;17(1):S9–S9.

34. Nossal GJV, Lederberg J. Antibody Production by Single Cells. Nature. 1958 May;181(4620):1419–20.

35. Chiu ML, Goulet DR, Teplyakov A, Gilliland GL. Antibody Structure and Function: The Basis for Engineering Therapeutics. Antibodies (Basel). 2019 Dec 3;8(4):55.

36. Köhler G, Milstein C. Continuous cultures of fused cells secreting antibody of predefined specificity. Nature. 1975 Aug;256(5517):495–7.

37. Payne WJ, Marshall DL, Shockley RK, Martin WJ. Clinical laboratory applications of monoclonal antibodies. Clin Microbiol Rev. 1988 July;1(3):313–29.

38. Coons AH, Creech HJ, Jones RN. Immunological Properties of an Antibody Containing a Fluorescent Group.∗. Proceedings of the Society for Experimental Biology and Medicine. 1941 June 1;47(2):200–2.

39. Abdollahpour-Alitappeh M, Lotfinia M, Gharibi T, Mardaneh J, Farhadihosseinabadi B, Larki P, et al. Antibody–drug conjugates (ADCs) for cancer therapy: Strategies, challenges, and successes. Journal of Cellular Physiology. 2019;234(5):5628–42.

40. Nadler LM, Stashenko P, Hardy R, Kaplan WD, Button LN, Kufe DW, et al. Serotherapy of a patient with a monoclonal antibody directed against a human lymphoma-associated antigen. Cancer Res. 1980 Sept;40(9):3147–54.

41. Maloney DG, Grillo-López AJ, Bodkin DJ, White CA, Liles TM, Royston I, et al. IDEC-C2B8: results of a phase I multiple-dose trial in patients with relapsed non-Hodgkin's lymphoma. JCO. 1997 Oct;15(10):3266–74.

42. Maloney DG, Grillo-López AJ, White CA, Bodkin D, Schilder RJ, Neidhart JA, et al. IDEC-C2B8 (Rituximab) Anti-CD20 Monoclonal Antibody Therapy in Patients With Relapsed Low-Grade Non-Hodgkin's Lymphoma. Blood. 1997 Sept 15;90(6):2188–95.

43. McLaughlin P, Grillo-López AJ, Link BK, Levy R, Czuczman MS, Williams ME, et al. Rituximab chimeric anti-CD20 monoclonal antibody therapy for relapsed indolent lymphoma: half of patients respond to a four-dose treatment program. JCO. 1998 Aug;16(8):2825–33.

44. Salles G, Barrett M, Foà R, Maurer J, O'Brien S, Valente N, et al. Rituximab in B-Cell Hematologic Malignancies: A Review of 20 Years of Clinical Experience. Adv Ther. 2017;34(10):2232–73.

45. Merchant MS, Geller JI, Baird K, Chou AJ, Galli S, Charles A, et al. Phase I Trial and Pharmacokinetic Study of Lexatumumab in Pediatric Patients With Solid Tumors. J Clin Oncol. 2012 Nov 20;30(33):4141–7.

46. Modak S, Kushner BH, Basu E, Roberts SS, Cheung NKV. Combination of Bevacizumab, Irinotecan and Temozolomide for Refractory or Relapsed Neuroblastoma: Results of a Phase II Study. Pediatr Blood Cancer. 2017 Aug;64(8):10.1002/pbc.26448.

47. Birley K, Chester K, Anderson J. Antibody based therapy for childhood solid cancers. Current Opinion in Chemical Engineering. 2018 Mar 1;19:153–62.

48. Horta ZP, Goldberg JL, Sondel PM. Anti-GD2 MABS and Next-Generation mAb-Based Agents for Cancer Therapy. Immunotherapy. 2016 Sept 1;8(9):1097–117.

49. Piccione EC, Juarez S, Liu J, Tseng S, Ryan CE, Narayanan C, et al. A bispecific antibody targeting CD47 and CD20 selectively binds and eliminates dual antigen expressing lymphoma cells. MAbs. 2015;7(5):946–56.

50. McDonagh CF, Huhalov A, Harms BD, Adams S, Paragas V, Oyama S, et al. Antitumor Activity of a Novel Bispecific Antibody That Targets the ErbB2/ErbB3 Oncogenic Unit and Inhibits Heregulin-Induced Activation of ErbB3. Molecular Cancer Therapeutics. 2012 Mar 6;11(3):582–93.

51. Husain B, Ellerman D. Expanding the Boundaries of Biotherapeutics with Bispecific Antibodies. BioDrugs. 2018 Oct 1;32(5):441–64.

52. Campbell KS, Cohen AD, Pazina T. Mechanisms of NK Cell Activation and Clinical Activity of the Therapeutic SLAMF7 Antibody, Elotuzumab in Multiple Myeloma. Front Immunol [Internet]. 2018 Nov 5;9:2551.

53. Herrera M, Pretelli G, Desai J, Garralda E, Siu LL, Steiner TM, et al. Bispecific antibodies: advancing precision oncology. Trends in Cancer. 2024 Oct 1;10(10):893–919.

54. Couturier MA, Thomas X, Raffoux E, Huguet F, Berthon C, Simand C, et al. Blinatumomab + ponatinib for relapsed/refractory Philadelphia chromosome-positive acute lymphoblastic leukemia in adults. Leukemia & Lymphoma. 2021 Feb 23;62(3):620–9.

55. Espinosa-Cotton M, Cheung NKV. Bispecific Antibodies for the Treatment of Neuroblastoma. Pharmacol Ther. 2022 Sept;237:108241.

56. Yankelevich M, Thakur A, Modak S, Chu R, Taub J, Martin A, et al. Targeting refractory/recurrent neuroblastoma and osteosarcoma with anti-CD3×anti-GD2 bispecific antibody armed T cells. J Immunother Cancer. 2024 Mar 21;12(3):e008744.

57. Liu K, Li M, Li Y, Li Y, Chen Z, Tang Y, et al. A review of the clinical efficacy of FDA-approved antibody-drug conjugates in human cancers. Molecular Cancer. 2024 Mar 23;23(1):62.

58. Lamba JK, Chauhan L, Shin M, Loken MR, Pollard JA, Wang YC, et al. CD33 Splicing Polymorphism Determines Gemtuzumab Ozogamicin Response in De Novo Acute Myeloid Leukemia: Report From Randomized Phase III Children's Oncology Group Trial AAML0531. J Clin Oncol. 2017 Aug 10;35(23):2674–82.

59. O'Brien MM, Ji L, Shah NN, Rheingold SR, Bhojwani D, Yuan CM, et al. Phase II Trial of Inotuzumab Ozogamicin in Children and Adolescents With Relapsed or Refractory B-Cell Acute Lymphoblastic Leukemia: Children's Oncology Group Protocol AALL1621. J Clin Oncol. 2022 Mar 20;40(9):956–67.

60. Shi Z, Zhu Y, Zhang J, Chen B. Monoclonal antibodies: new chance in the management of B-cell acute lymphoblastic leukemia. Hematology. 2022 Dec;27(1):642–52.

61. Bigner DD, Brown M, Coleman RE, Friedman AH, Friedman HS, McLendon RE, et al. Phase I studies of treatment of malignant gliomas and neoplastic meningitis with131I-radiolabeled monoclonal antibodies anti-tenascin 81C6 and anti-chondroitin proteoglycan sulfate Me1-14 F (ab′)2-a preliminary report. J Neuro-Oncol. 1995 Feb 1;24(1):109–22.

62. Kramer K, Kushner BH, Modak S, Pandit-Taskar N, Smith-Jones P, Zanzonico P, et al. Compartmental intrathecal radioimmunotherapy: results for treatment for metastatic CNS neuroblastoma. J Neurooncol. 2010 May 1;97(3):409–18.

63. Cimini A, Ricci M, Chiaravalloti A, Filippi L, Schillaci O. Theragnostic Aspects and Radioimmunotherapy in Pediatric Tumors. International Journal of Molecular Sciences. 2020 Jan;21(11):3849.

64. Souweidane MM, Kramer K, Pandit-Taskar N, Zhou Z, Haque S, Zanzonico P, et al. Convection-enhanced delivery for diffuse intrinsic pontine glioma: a single-centre, dose-escalation, phase 1 trial. The Lancet Oncology. 2018 Aug 1;19(8):1040–50.

65. Shusterman S, London WB, Gillies SD, Hank JA, Voss SD, Seeger RC, et al. Antitumor Activity of Hu14.18-IL2 in Patients With Relapsed/Refractory Neuroblastoma: A Children's Oncology Group (COG) Phase II Study. JCO. 2010 Nov 20;28(33):4969–75.

66. Stanton SE, Disis ML. Clinical significance of tumor-infiltrating lymphocytes in breast cancer. J Immunother Cancer. 2016 Oct 18;4:59.

67. Hashimoto M, Kamphorst AO, Im SJ, Kissick HT, Pillai RN, Ramalingam SS, et al. CD8 T Cell Exhaustion in Chronic Infection and Cancer: Opportunities for Interventions. Annual Review of Medicine. 2018 Jan 29;69(Volume 69, 2018):301–18.

68. Blackburn SD, Shin H, Haining WN, Zou T, Workman CJ, Polley A, et al. Coregulation of CD8+ T cell exhaustion during chronic viral infection by multiple inhibitory receptors. Nat Immunol. 2009 Jan;10(1):29–37.

69. Fourcade J, Sun Z, Pagliano O, Guillaume P, Luescher IF, Sander C, et al. CD8+ T Cells Specific for Tumor Antigens Can Be Rendered Dysfunctional by the Tumor Microenvironment through Upregulation of the Inhibitory Receptors BTLA and PD-1. Cancer Research. 2012 Feb 14;72(4):887–96.

70. Ahmadzadeh M, Johnson LA, Heemskerk B, Wunderlich JR, Dudley ME, White DE, et al. Tumor antigen–specific CD8 T cells infiltrating the tumor express high levels of PD-1 and are functionally impaired. Blood. 2009 Aug 20;114(8):1537–44.

71. Arafat Hossain Md. A comprehensive review of immune checkpoint inhibitors for cancer treatment. International Immunopharmacology. 2024 Dec 25;143:113365.

72. Ishida Y, Agata Y, Shibahara K, Honjo T. Induced expression of PD-1, a novel member of the immunoglobulin gene superfamily, upon programmed cell death. The EMBO Journal. 1992 Nov;11(11):3887–95.

73. Gong J, Chehrazi-Raffle A, Reddi S, Salgia R. Development of PD-1 and PD-L1 inhibitors as a form of cancer immunotherapy: a comprehensive review of registration trials and future considerations. J Immunother Cancer. 2018 Jan 23;6:8.

74. Robert C, Ribas A, Wolchok JD, Hodi FS, Hamid O, Kefford R, et al. Anti-programmed-death-receptor-1 treatment with pembrolizumab in ipilimumab-refractory advanced melanoma: a randomised dose-comparison cohort of a phase 1 trial. The Lancet. 2014 Sept 20;384(9948):1109–17.

75. Ribas A, Wolchok JD, Robert C, Kefford R, Hamid O, Daud A, et al. P0116 Updated clinical efficacy of the anti-PD-1 monoclonal antibody pembrolizumab (MK-3475) in 411 patients with melanoma. European Journal of Cancer. 2015 July 1;51:e24.

76. van der Merwe PA, Bodian DL, Daenke S, Linsley P, Davis SJ. CD80 (B7-1) Binds Both CD28 and CTLA-4 with a Low Affinity and Very Fast Kinetics. J Exp Med. 1997 Feb 3;185(3):393–404.

77. Oderup C, Cederbom L, Makowska A, Cilio CM, Ivars F. Cytotoxic T lymphocyte antigen-4-dependent down-modulation of costimulatory molecules on dendritic cells in CD4+ CD25+ regulatory T-cell-mediated suppression. Immunology. 2006 June;118(2):240–9.

78. Qureshi OS, Zheng Y, Nakamura K, Attridge K, Manzotti C, Schmidt EM, et al. Trans-Endocytosis of CD80 and CD86: A Molecular Basis for the Cell-Extrinsic Function of CTLA-4. Science. 2011 Apr 29;332(6029):600–3.

79. Seidel JA, Otsuka A, Kabashima K. Anti-PD-1 and Anti-CTLA-4 Therapies in Cancer: Mechanisms of Action, Efficacy, and Limitations. Front Oncol. 2018 Mar 28;8:86.

80. Larkin J, Chiarion-Sileni V, Gonzalez R, Grob JJ, Cowey CL, Lao CD, et al. Combined Nivolumab and Ipilimumab or Monotherapy in Previously Untreated Melanoma. N Engl J Med. 2015 July 2;373(1):23–34.

81. Ephraim R, Fraser S, Nurgali K, Apostolopoulos V. Checkpoint Markers and Tumor Microenvironment: What Do We Know? Cancers (Basel). 2022 Aug 4;14(15):3788.

82. Ciurej A, Lewis E, Gupte A, Al-Antary E. Checkpoint Immunotherapy in Pediatric Oncology: Will We Say Checkmate Soon? Vaccines (Basel). 2023 Dec 12;11(12):1843.

83. Casey DL, Cheung NKV. Immunotherapy of Pediatric Solid Tumors: Treatments at a Crossroads, with an Emphasis on Antibodies. Cancer Immunology Research. 2020 Feb 3;8(2):161–6.

84. Pinto N, Park JR, Murphy E, Yearley J, McClanahan T, Annamalai L, et al. Patterns of PD-1, PD-L1, and PD-L2 expression in pediatric solid tumors. Pediatric Blood & Cancer. 2017;64(11):e26613.

85. Chowdhury F, Dunn S, Mitchell S, Mellows T, Ashton-Key M, Gray JC. PD-L1 and CD8+PD1+ lymphocytes exist as targets in the pediatric tumor microenvironment for immunomodulatory therapy. OncoImmunology. 2015 Oct 3;4(10):e1029701.

86. Ehlert K, Hansjuergens I, Zinke A, Otto S, Siebert N, Henze G, et al. Nivolumab and dinutuximab beta in two patients with refractory neuroblastoma. J Immunother Cancer. 2020 May 1;8(1):e000540.

87. Merchant MS, Wright M, Baird K, Wexler LH, Rodriguez-Galindo C, Bernstein D, et al. Phase 1 Clinical Trial of Ipilimumab In Pediatric Patients With Advanced Solid Tumors. Clin Cancer Res. 2016 Mar 15;22(6):1364–70.

88. Davis KL, Fox E, Isikwei E, Reid JM, Liu X, Minard CG, et al. A Phase I/II Trial of Nivolumab plus Ipilimumab in Children and Young Adults with Relapsed/Refractory Solid Tumors: A Children's Oncology Group Study ADVL1412. Clinical Cancer Research. 2022 Dec 1;28(23):5088–97.

89. Lakhani S. Early clinical pathologists: Edward Jenner (1749-1823). J Clin Pathol. 1992 Sept;45(9):756–8.

90. Le I, Dhandayuthapani S, Chacon J, Eiring AM, Gadad SS. Harnessing the Immune System with Cancer Vaccines: From Prevention to Therapeutics. Vaccines. 2022 May;10(5):816.

91. Peng M, Mo Y, Wang Y, Wu P, Zhang Y, Xiong F, et al. Neoantigen vaccine: an emerging tumor immunotherapy. Molecular Cancer. 2019 Aug 23;18(1):128.

92. Kumai T, Kobayashi H, Harabuchi Y, Celis E. Peptide vaccines in cancer — old concept revisited. Current Opinion in Immunology. 2017 Apr 1;45:1–7.

93. Beijnen EMS, van Haren SD. Vaccine-Induced CD8+ T Cell Responses in Children: A Review of Age-Specific Molecular Determinants Contributing to Antigen Cross-Presentation. Front Immunol. 2020 Dec 23;11:607977.

94. Saxena M, van der Burg SH, Melief CJM, Bhardwaj N. Therapeutic cancer vaccines. Nat Rev Cancer. 2021 June;21(6):360–78.

95. Verma C, Pawar VA, Srivastava S, Tyagi A, Kaushik G, Shukla SK, et al. Cancer Vaccines in the Immunotherapy Era: Promise and Potential. Vaccines. 2023 Dec;11(12):1783.

96. Suschak JJ, Williams JA, Schmaljohn CS. Advancements in DNA vaccine vectors, non-mechanical delivery methods, and molecular adjuvants to increase immunogenicity. Hum Vaccin Immunother. 2017 June 12;13(12):2837–48.

97. Lopes A, Vanvarenberg K, Préat V, Vandermeulen G. Codon-Optimized P1A-Encoding DNA Vaccine: Toward a Therapeutic Vaccination against P815 Mastocytoma. Mol Ther Nucleic Acids. 2017 July 13;8:404–15.

98. Wu Y, Zhai W, Sun M, Zou Z, Zhou X, Li G, et al. A Novel Recombinant Multi-Epitope Vaccine Could Induce Specific Cytotoxic T Lymphocyte Response In Vitro and In Vivo. Protein & Peptide Letters. 2017; 24(6).

99. Weide B, Carralot JP, Reese A, Scheel B, Eigentler TK, Hoerr I, et al. Results of the First Phase I/II Clinical Vaccination Trial With Direct Injection of mRNA. Journal of Immunotherapy. 2008 Mar;31(2):180.

100. Hollingsworth RE, Jansen K. Turning the corner on therapeutic cancer vaccines. npj Vaccines. 2019 Feb 8;4(1):1–10.

101. Van Tendeloo VF, Van de Velde A, Van Driessche A, Cools N, Anguille S, Ladell K, et al. Induction of complete and molecular remissions in acute myeloid leukemia by Wilms'

tumor 1 antigen-targeted dendritic cell vaccination. Proceedings of the National Academy of Sciences. 2010 Aug 3;107(31):13824–9.

102.Kantoff PW, Higano CS, Shore ND, Berger ER, Small EJ, Penson DF, et al. Sipuleucel-T Immunotherapy for Castration-Resistant Prostate Cancer. New England Journal of Medicine. 2010 July 29;363(5):411–22.

103.Zhao J, Chen Y, Ding ZY, Liu JY. Safety and Efficacy of Therapeutic Cancer Vaccines Alone or in Combination With Immune Checkpoint Inhibitors in Cancer Treatment. Front Pharmacol. 2019 Oct 11;10:1184.

104.Olsen HE, Lynn GM, Valdes PA, Cerecedo Lopez CD, Ishizuka AS, Arnaout O, et al. Therapeutic cancer vaccines for pediatric malignancies: advances, challenges, and emerging technologies. Neurooncol Adv. 2021 Feb 11;3(1):vdab027.

105.Krishnadas DK, Shusterman S, Bai F, Diller L, Sullivan JE, Cheerva AC, et al. A phase I trial combining decitabine/dendritic cell vaccine targeting MAGE-A1, MAGE-A3 and NY-ESO-1 for children with relapsed or therapy-refractory neuroblastoma and sarcoma. Cancer Immunol Immunother. 2015 Oct 1;64(10):1251–60.

106.Spiess PJ, Yang JC, Rosenberg SA. In vivo antitumor activity of tumor-infiltrating lymphocytes expanded in recombinant interleukin-2. J Natl Cancer Inst. 1987 Nov;79(5):1067–75.

107.Rosenberg SA, Spiess P, Lafreniere R. A New Approach to the Adoptive Immunotherapy of Cancer with Tumor-Infiltrating Lymphocytes. Science. 1986 Sept 19;233(4770):1318–21.

108.Rosenberg SA, Packard BS, Aebersold PM, Solomon D, Topalian SL, Toy ST, et al. Use of Tumor-Infiltrating Lymphocytes and Interleukin-2 in the Immunotherapy of Patients with Metastatic Melanoma. New England Journal of Medicine. 1988 Dec 22;319(25):1676–80.

109.Dudley ME, Wunderlich JR, Yang JC, Sherry RM, Topalian SL, Restifo NP, et al. Adoptive Cell Transfer Therapy Following Non-Myeloablative but Lymphodepleting Chemotherapy for the Treatment of Patients With Refractory Metastatic Melanoma. J Clin Oncol. 2005 Apr 1;23(10):2346–57.

110.Rosenberg SA, Yang JC, Sherry RM, Kammula US, Hughes MS, Phan GQ, et al. Durable Complete Responses in Heavily Pretreated Patients with Metastatic Melanoma Using T Cell Transfer Immunotherapy. Clin Cancer Res. 2011 July 1;17(13):4550–7.

111.Wrzesinski C, Paulos CM, Kaiser A, Muranski P, Palmer DC, Gattinoni L, et al. Increased intensity lymphodepletion enhances tumor treatment efficacy of adoptively transferred tumor-specific T cells. J Immunother. 2010 Jan;33(1):1–7.

112.Mullard A. FDA approves first tumour-infiltrating lymphocyte (TIL) therapy, bolstering hopes for cell therapies in solid cancers. Nature Reviews Drug Discovery. 2024 Feb 19;23(4):238–238.

113.Zhao Y, Deng J, Rao S, Guo S, Shen J, Du F, et al. Tumor Infiltrating Lymphocyte (TIL) Therapy for Solid Tumor Treatment: Progressions and Challenges. Cancers (Basel). 2022 Aug 27;14(17):4160.

114.Baulu E, Gardet C, Chuvin N, Depil S. TCR-engineered T cell therapy in solid tumors: State of the art and perspectives. Sci Adv. 9(7):eadf3700.

115.Morgan RA, Dudley ME, Wunderlich JR, Hughes MS, Yang JC, Sherry RM, et al. Cancer Regression in Patients After Transfer of Genetically Engineered Lymphocytes. Science. 2006 Oct 6;314(5796):126–9.

116.Rohaan MW, Gomez-Eerland R, van den Berg JH, Geukes Foppen MH, van Zon M, Raud B, et al. MART-1 TCR gene-modified peripheral blood T cells for the treatment of metastatic melanoma: a phase I/IIa clinical trial. Immunooncol Technol. 2022 June 18;15:100089.

117.Cameron BJ, Gerry AB, Dukes J, Harper JV, Kannan V, Bianchi FC, et al. Identification of a Titin-Derived HLA-A1–Presented Peptide as a Cross-Reactive Target for Engineered MAGE A3–Directed T Cells. Sci Transl Med. 2013 Aug 7;5(197):197ra103.

118.Kuwana Y, Asakura Y, Utsunomiya N, Nakanishi M, Arata Y, Itoh S, et al. Expression of chimeric receptor composed of immunoglobulin-derived V resions and T-cell receptor-derived C regions. Biochemical and Biophysical Research Communications. 1987 Dec 31;149(3):960–8.

119.Gross G, Waks T, Eshhar Z. Expression of immunoglobulin-T-cell receptor chimeric molecules as functional receptors with antibody-type specificity. Proc Natl Acad Sci U S A. 1989 Dec;86(24):10024–8.

120.Eshhar Z, Waks T, Gross G, Schindler DG. Specific activation and targeting of cytotoxic lymphocytes through chimeric single chains consisting of antibody-binding domains and the gamma or zeta subunits of the immunoglobulin and T-cell receptors. Proc Natl Acad Sci U S A. 1993 Jan 15;90(2):720–4.

121.Mitra A, Barua A, Huang L, Ganguly S, Feng Q, He B. From bench to bedside: the history and progress of CAR T cell therapy. Front Immunol. 2023 May 15;14:1188049.

122.Kershaw MH, Westwood JA, Parker LL, Wang G, Eshhar Z, Mavroukakis SA, et al. A Phase I Study on Adoptive Immunotherapy Using Gene-Modified T Cells for Ovarian Cancer. Clin Cancer Res. 2006 Oct 15;12(20 Pt 1):6106–15.

123.Brocker T. Chimeric Fv-ζ or Fv-ε receptors are not sufficient to induce activation or cytokine production in peripheral T cells. Blood. 2000 Sept 1;96(5):1999–2001.

124.Savoldo B, Ramos CA, Liu E, Mims MP, Keating MJ, Carrum G, et al. CD28 costimulation improves expansion and persistence of chimeric antigen receptor–modified T cells in lymphoma patients. J Clin Invest. 2011 May 2;121(5):1822–6.

125.Uckun FM, Jaszcz W, Ambrus JL, Fauci AS, Gajl-Peczalska K, Song CW, et al. Detailed Studies on Expression and Function of CD19 Surface Determinant by Using B43 Monoclonal Antibody and the Clinical Potential of Anti-CD19 Immunotoxins. Blood. 1988 Jan 1;71(1):13–29.

126.Brentjens RJ, Rivière I, Park JH, Davila ML, Wang X, Stefanski J, et al. Safety and persistence of adoptively transferred autologous CD19-targeted T cells in patients with relapsed or chemotherapy refractory B-cell leukemias. Blood. 2011 Nov 3;118(18):4817–28.

127.Maude SL, Laetsch TW, Buechner J, Rives S, Boyer M, Bittencourt H, et al. Tisagenlecleucel in Children and Young Adults with B-Cell Lymphoblastic Leukemia. N Engl J Med. 2018 Feb 1;378(5):439–48.

128.Schuster SJ, Bishop MR, Tam CS, Waller EK, Borchmann P, McGuirk JP, et al. Tisagenlecleucel in Adult Relapsed or Refractory Diffuse Large B-Cell Lymphoma. New England Journal of Medicine. 2019 Jan 3;380(1):45–56.

129.Locke FL, Ghobadi A, Jacobson CA, Miklos DB, Lekakis LJ, Oluwole OO, et al. Long-term safety and activity of axicabtagene ciloleucel in refractory large B-cell lymphoma (ZUMA-1): a single-arm, multicentre, phase 1–2 trial. The Lancet Oncology. 2019 Jan 1;20(1):31–42.

130.Abramson JS, Palomba ML, Gordon LI, Lunning MA, Wang M, Arnason J, et al. Lisocabtagene maraleucel for patients with relapsed or refractory large B-cell lymphomas (TRANSCEND NHL 001): a multicentre seamless design study. The Lancet. 2020 Sept 19;396(10254):839–52.

131.Wang M, Munoz J, Goy A, Locke FL, Jacobson CA, Hill BT, et al. KTE-X19 CAR T-Cell Therapy in Relapsed or Refractory Mantle-Cell Lymphoma. New England Journal of Medicine. 2020 Apr 2;382(14):1331–42.

132.Kalos M, Levine BL, Porter DL, Katz S, Grupp SA, Bagg A, et al. T Cells with Chimeric Antigen Receptors Have Potent Antitumor Effects and Can Establish Memory in Patients with Advanced Leukemia. Sci Transl Med. 2011 Aug 10;3(95):95ra73.

133.Porter DL, Levine BL, Kalos M, Bagg A, June CH. Chimeric Antigen Receptor–Modified T Cells in Chronic Lymphoid Leukemia. N Engl J Med. 2011 Aug 25;365(8):725–33.

134.Grupp SA, Kalos M, Barrett D, Aplenc R, Porter DL, Rheingold SR, et al. Chimeric Antigen Receptor–Modified T Cells for Acute Lymphoid Leukemia. N Engl J Med. 2013 Apr 18;368(16):1509–18.

135.Bhaskar ST, Dholaria B, Savani BN, Sengsayadeth S, Oluwole O. Overview of approved CAR-T products and utility in clinical practice. Clinical Hematology International. 2024 Oct 23;6(4):108–14.

136.Ferreros P, Trapero I. Interleukin Inhibitors in Cytokine Release Syndrome and Neurotoxicity Secondary to CAR-T Therapy. Diseases. 2022 July 6;10(3):41.

137.Giavridis T, van der Stegen SJC, Eyquem J, Hamieh M, Piersigilli A, Sadelain M. CAR T cell-induced cytokine release syndrome is mediated by macrophages and abated by IL-1 blockade. Nat Med. 2018 June;24(6):731–8.

138.Norelli M, Camisa B, Barbiera G, Falcone L, Purevdorj A, Genua M, et al. Monocyte-derived IL-1 and IL-6 are differentially required for cytokine-release syndrome and neurotoxicity due to CAR T cells. Nat Med. 2018 June;24(6):739–48.

139.Parker KR, Migliorini D, Perkey E, Yost KE, Bhaduri A, Bagga P, et al. Single-cell analyses identify brain mural cells expressing CD19 as potential off-tumor targets for CAR-T immunotherapies. Cell. 2020 Oct 1;183(1):126-142.e17.

140.Teachey DT, Lacey SF, Shaw PA, Melenhorst JJ, Maude SL, Frey N, et al. Identification of Predictive Biomarkers for Cytokine Release Syndrome after Chimeric Antigen

Receptor T cell Therapy for Acute Lymphoblastic Leukemia. Cancer Discov. 2016 June;6(6):664–79.

141. Balagopal S, Sasaki K, Kaur P, Nikolaidi M, Ishihara J. Emerging approaches for preventing cytokine release syndrome in CAR-T cell therapy. Journal of Materials Chemistry B. 2022;10(37):7491–511.

142. Ramakrishna S, Highfill SL, Walsh Z, Nguyen SM, Lei H, Shern JF, et al. Modulation of Target Antigen Density Improves CAR T Cell Functionality and Persistence. Clin Cancer Res. 2019 Sept 1;25(17):5329–41.

143. Walker AJ, Majzner RG, Zhang L, Wanhainen K, Long AH, Nguyen SM, et al. Tumor Antigen and Receptor Densities Regulate Efficacy of a Chimeric Antigen Receptor Targeting Anaplastic Lymphoma Kinase. Mol Ther. 2017 Sept 6;25(9):2189–201.

144. Fry TJ, Shah NN, Orentas RJ, Stetler-Stevenson M, Yuan CM, Ramakrishna S, et al. CD22-CAR T Cells Induce Remissions in CD19-CAR Naïve and Resistant B-ALL. Nat Med. 2018 Jan;24(1):20–8.

145. Xu X, Sun Q, Liang X, Chen Z, Zhang X, Zhou X, et al. Mechanisms of Relapse After CD19 CAR T-Cell Therapy for Acute Lymphoblastic Leukemia and Its Prevention and Treatment Strategies. Front Immunol. 2019 Nov 12;10:2664.

146. Gardner R, Wu D, Cherian S, Fang M, Hanafi LA, Finney O, et al. Acquisition of a CD19-negative myeloid phenotype allows immune escape of MLL-rearranged B-ALL from CD19 CAR-T-cell therapy. Blood. 2016 May 19;127(20):2406–10.

147. O'Rourke DM, Nasrallah MP, Desai A, Melenhorst JJ, Mansfield K, Morrissette JJD, et al. A single dose of peripherally infused EGFRvIII-directed CAR T cells mediates antigen loss and induces adaptive resistance in patients with recurrent glioblastoma. Sci Transl Med. 2017 July 19;9(399):eaaa0984.

148. Guzman G, Reed MR, Bielamowicz K, Koss B, Rodriguez A. CAR-T Therapies in Solid Tumors: Opportunities and Challenges. Curr Oncol Rep. 2023;25(5):479–89.

149. Muhammad N, Wang R, Li W, Zhang Z, Chang Y, Hu Y, et al. A novel TanCAR targeting IL13Rα2 and EphA2 for enhanced glioblastoma therapy. Mol Ther Oncolytics. 2022 Feb 20;24:729–41.

150. Bagley SJ, O'Rourke DM. Clinical investigation of CAR T cells for solid tumors: Lessons learned and future directions. Pharmacology & Therapeutics. 2020 Jan 1;205:107419.

151. Labanieh L, Majzner RG, Mackall CL. Programming CAR-T cells to kill cancer. Nat Biomed Eng. 2018 June;2(6):377–91.

152. Becerra CR, Hoof P, Paulson AS, Manji GA, Gardner O, Malankar A, et al. Ligand-inducible, prostate stem cell antigen (PSCA)-directed GoCAR-T cells in advanced solid tumors: Preliminary results from a dose escalation. JCO. 2019 Feb;37(4_suppl):283–283.

153. Raj D, Yang MH, Rodgers D, Hampton EN, Begum J, Mustafa A, et al. Switchable CAR-T cells mediate remission in metastatic pancreatic ductal adenocarcinoma. 2019 June 1. 68;1052-1064.

154.Wang Y, Chen ,Meixia, Wu ,Zhiqiang, Tong ,Chuan, Dai ,Hanren, Guo ,Yelei, et al. CD133-directed CAR T cells for advanced metastasis malignancies: A phase I trial. OncoImmunology. 2018 July 3;7(7):e1440169.

155.Vora P, Venugopal C, Salim SK, Tatari N, Bakhshinyan D, Singh M, et al. The Rational Development of CD133-Targeting Immunotherapies for Glioblastoma. Cell Stem Cell. 2020 June 4;26(6):832-844.e6.

156.Beatty GL, O'Hara M. Chimeric antigen receptor-modified T cells for the treatment of solid tumors: Defining the challenges and next steps. Pharmacology & Therapeutics. 2016 Oct 1;166:30–9.

157.Bernhard H, Neudorfer J, Gebhard K, Conrad H, Hermann C, Nährig J, et al. Adoptive transfer of autologous, HER2-specific, cytotoxic T lymphocytes for the treatment of HER2-overexpressing breast cancer. Cancer Immunol Immunother. 2007 July 24;57(2):271–80.

158.Weis SM, Cheresh DA. Tumor angiogenesis: molecular pathways and therapeutic targets. Nat Med. 2011 Nov;17(11):1359–70.

159.Schaaf MB, Garg AD, Agostinis P. Defining the role of the tumor vasculature in antitumor immunity and immunotherapy. Cell Death Dis. 2018 Jan 25;9(2):1–14.

160.Klein D. The Tumor Vascular Endothelium as Decision Maker in Cancer Therapy. Front Oncol. 2018 Sept 10;8:367.

161.Liu G, Rui W, Zheng H, Huang D, Yu F, Zhang Y, et al. CXCR2-modified CAR-T cells have enhanced trafficking ability that improves treatment of hepatocellular carcinoma. European Journal of Immunology. 2020;50(5):712–24.

162.Jin L, Tao H, Karachi A, Long Y, Hou AY, Na M, et al. CXCR1- or CXCR2-modified CAR T cells co-opt IL-8 for maximal antitumor efficacy in solid tumors. Nat Commun. 2019 Sept 5;10:4016.

163.Wang Y, Wang J, Yang X, Yang J, Lu P, Zhao L, et al. Chemokine Receptor CCR2b Enhanced Anti-tumor Function of Chimeric Antigen Receptor T Cells Targeting Mesothelin in a Non-small-cell Lung Carcinoma Model. Front Immunol. 2021 Mar 11;12:628906.

164.Xin L, Gao J, Zheng Z, Chen Y, Lv S, Zhao Z, et al. Fibroblast Activation Protein-α as a Target in the Bench-to-Bedside Diagnosis and Treatment of Tumors: A Narrative Review. Front Oncol. 2021 Aug 19;11:648187.

165.Bughda R, Dimou P, D'Souza RR, Klampatsa A. Fibroblast Activation Protein (FAP)-Targeted CAR-T Cells: Launching an Attack on Tumor Stroma. Immunotargets Ther. 2021 Aug 5;10:313–23.

166.Emami-Shahri N, Foster J, Kashani R, Gazinska P, Cook C, Sosabowski J, et al. Clinically compliant spatial and temporal imaging of chimeric antigen receptor T-cells. Nat Commun. 2018 Mar 14;9(1):1081.

167.Emami-Shahri N, Papa S. Dynamic imaging for CAR-T-cell therapy. Biochemical Society Transactions. 2016 Apr 11;44(2):386–90.

168.Hanahan D, Coussens LM. Accessories to the Crime: Functions of Cells Recruited to the Tumor Microenvironment. Cancer Cell. 2012 Mar 20;21(3):309–22.

169.Asgharzadeh S, Salo JA, Ji L, Oberthuer A, Fischer M, Berthold F, et al. Clinical Significance of Tumor-Associated Inflammatory Cells in Metastatic Neuroblastoma. J Clin Oncol. 2012 Oct 1;30(28):3525–32.

170.Marofi F, Motavalli R, Safonov VA, Thangavelu L, Yumashev AV, Alexander M, et al. CAR T cells in solid tumors: challenges and opportunities. Stem Cell Research & Therapy. 2021 Jan 25;12(1):81.

171.Quail D, Joyce J. Microenvironmental regulation of tumor progression and metastasis. Nat Med. 2013 Nov;19(11):1423–37.

172.Mujoo K, Cheresh DA, Yang HM, Reisfeld RA. Disialoganglioside GD2 on human neuroblastoma cells: target antigen for monoclonal antibody-mediated cytolysis and suppression of tumor growth. Cancer Res. 1987 Feb 15;47(4):1098–104.

173.Honsik CJ, Jung G, Reisfeld RA. Lymphokine-activated killer cells targeted by monoclonal antibodies to the disialogangliosides GD2 and GD3 specifically lyse human tumor cells of neuroectodermal origin. Proc Natl Acad Sci U S A. 1986 Oct;83(20):7893–7.

174.Cheung NK, Lazarus H, Miraldi FD, Abramowsky CR, Kallick S, Saarinen UM, et al. Ganglioside GD2 specific monoclonal antibody 3F8: a phase I study in patients with neuroblastoma and malignant melanoma. JCO. 1987 Sept;5(9):1430–40.

175.Yu AL, Gilman AL, Ozkaynak MF, London WB, Kreissman SG, Chen HX, et al. Anti-GD2 Antibody with GM-CSF, Interleukin-2, and Isotretinoin for Neuroblastoma. N Engl J Med. 2010 Sept 30;363(14):1324–34.

176.Yu AL, Gilman AL, Ozkaynak MF, Naranjo A, Diccianni MB, Gan J, et al. Long-term follow-up of a Phase III Study of ch14.18 (Dinutuximab) + Cytokine Immunotherapy in Children with High-risk Neuroblastoma: Children's Oncology Group Study ANBL0032. Clin Cancer Res. 2021 Apr 15;27(8):2179–89.

177.Kowalczyk A, Gil M, Horwacik I, Odrowąż Ż, Kozbor D, Rokita H. The GD2-specific 14G2a monoclonal antibody induces apoptosis and enhances cytotoxicity of chemotherapeutic drugs in IMR-32 human neuroblastoma cells. Cancer Letters. 2009 Aug 28;281(2):171–82.

178.Sorkin LS, Otto M, Baldwin WM, Vail E, Gillies SD, Handgretinger R, et al. Anti-GD2 with an FC point mutation reduces complement fixation and decreases antibody-induced allodynia. Pain. 2010 Apr;149(1):135–42.

179.Mody R, Naranjo A, Van Ryn C, Yu AL, London WB, Shulkin BL, et al. Randomised Phase II Trial of Irinotecan/Temozolomide (I/T) with Temsirolimus (TEM) or Dinutuximab (DIN) in Children with Refractory or Relapsed Neuroblastoma: A Report from The Children's Oncology Group (COG). Lancet Oncol. 2017 July;18(7):946–57.

180.Furman WL, Federico SM, McCarville MB, Shulkin BL, Davidoff AM, Krasin MJ, et al. A Phase II Trial of Hu14.18K322A in Combination with Induction Chemotherapy in Children with Newly Diagnosed High-Risk Neuroblastoma. Clinical cancer research : an official journal of the American Association for Cancer Research. 2019 Oct 10;25(21):6320.

181.Mody R, Yu AL, Naranjo A, Zhang FF, London WB, Shulkin BL, et al. Irinotecan, Temozolomide, and Dinutuximab With GM-CSF in Children With Refractory or Relapsed Neuroblastoma: A Report From the Children's Oncology Group. J Clin Oncol. 2020 July 1;38(19):2160–9.

182.Shusterman S, London WB, Hank JA, Parisi MT, Shulkin BL, Servaes SEN, et al. A feasibility and phase II study of the hu14.18-IL2 immunocytokine in combination with GM-CSF and isotretinoin in patients with recurrent or refractory neuroblastoma: A Children's Oncology Group study. JCO. 2015 May 20;33(15_suppl):10017–10017.

183.Schumacher-Kuckelkorn R, Volland R, Gradehandt A, Hero B, Simon T, Berthold F. Lack of immunocytological GD2 expression on neuroblastoma cells in bone marrow at diagnosis, during treatment, and at recurrence. Pediatric Blood & Cancer. 2017;64(1):46–56.

184.Xiao W hua, Yu AL, Sorkin LS. Electrophysiological characteristics of primary afferent fibers after systemic administration of anti-GD2 ganglioside antibody. PAIN. 1997 Jan;69(1):145.

185.Louis CU, Savoldo B, Dotti G, Pule M, Yvon E, Myers GD, et al. Antitumor activity and long-term fate of chimeric antigen receptor–positive T cells in patients with neuroblastoma. Blood. 2011 Dec 1;118(23):6050–6.

186.Pule MA, Savoldo B, Myers GD, Rossig C, Russell HV, Dotti G, et al. Virus-specific T cells engineered to coexpress tumor-specific receptors: persistence and antitumor activity in individuals with neuroblastoma. Nat Med. 2008 Nov;14(11):1264–70.

187.Long AH, Haso WM, Shern JF, Wanhainen KM, Murgai M, Ingaramo M, et al. 4-1BB Costimulation Ameliorates T Cell Exhaustion Induced by Tonic Signaling of Chimeric Antigen Receptors. Nat Med. 2015 June;21(6):581–90.

188.Heczey A, Louis CU, Savoldo B, Dakhova O, Durett A, Grilley B, et al. CAR T Cells Administered in Combination with Lymphodepletion and PD-1 Inhibition to Patients with Neuroblastoma. Mol Ther. 2017 Sept 6;25(9):2214–24.

189.Straathof K, Flutter B, Wallace R, Jain N, Loka T, Depani S, et al. Antitumor activity without on-target off-tumor toxicity of GD2–chimeric antigen receptor T cells in patients with neuroblastoma. Science Translational Medicine. 2020 Nov 25;12(571):eabd6169.

190.Bufalo FD, Angelis BD, Caruana I, Baldo GD, Ioris MAD, Serra A, et al. GD2-CART01 for Relapsed or Refractory High-Risk Neuroblastoma. New England Journal of Medicine. 2023 Apr 5;388(14):1284–95.

191.Bottino C, Vitale C, Dondero A, Castriconi R. B7-H3 in Pediatric Tumors: Far beyond Neuroblastoma. Cancers. 2023 Jan;15(13):3279.

192.Modak S, Kramer K, Gultekin SH, Guo HF, Cheung NKV. Monoclonal Antibody 8H9 Targets a Novel Cell Surface Antigen Expressed by a Wide Spectrum of Human Solid Tumors1. Cancer Research. 2001 May 1;61(10):4048–54.

193.Ahmed M, Cheng M, Zhao Q, Goldgur Y, Cheal SM, Guo HF, et al. Humanized Affinity-matured Monoclonal Antibody 8H9 Has Potent Antitumor Activity and Binds to FG Loop of Tumor Antigen B7-H3. J Biol Chem. 2015 Dec 11;290(50):30018–29.

194.Kramer K, Smith M, Souweidane MM. Safety profile of long-term intraventricular access devices in pediatric patients receiving radioimmunotherapy for central nervous system malignancies. Pediatric Blood & Cancer. 2014;61(9):1590–2.

195.Loo D, Alderson RF, Chen FZ, Huang L, Zhang W, Gorlatov S, et al. Development of an Fc-Enhanced Anti–B7-H3 Monoclonal Antibody with Potent Antitumor Activity. Clinical Cancer Research. 2012 July 15;18(14):3834–45.

196.Majzner RG, Theruvath JL, Nellan A, Heitzeneder S, Cui Y, Mount CW, et al. CAR T Cells Targeting B7-H3, a Pan-Cancer Antigen, Demonstrate Potent Preclinical Activity Against Pediatric Solid Tumors and Brain Tumors. Clinical Cancer Research. 2019 Apr 15;25(8):2560–74.

197.Sano R, Krytska K, Larmour CE, Raman P, Martinez D, Ligon GF, et al. An antibody-drug conjugate directed to the ALK receptor demonstrates efficacy in preclinical models of neuroblastoma. Sci Transl Med. 2019 Mar 13;11(483):eaau9732.

198.Bosse KR, Raman P, Zhu Z, Lane M, Martinez D, Heitzeneder S, et al. Identification of GPC2 as an oncoprotein and candidate immunotherapeutic target in high-risk neuroblastoma. Cancer Cell. 2017 Sept 11;32(3):295-309.e12.

199.Li N, Torres MB, Spetz MR, Wang R, Peng L, Tian M, et al. CAR T cells targeting tumor-associated exons of glypican 2 regress neuroblastoma in mice. Cell Rep Med. 2021 June 1;2(6):100297.

200.Ito M, Hiramatsu H, Kobayashi K, Suzue K, Kawahata M, Hioki K, et al. NOD/SCID/γcnull mouse: an excellent recipient mouse model for engraftment of human cells. Blood. 2002 Nov 1;100(9):3175–82.

201.Szadvari I, Krizanova O, Babula P. Athymic nude mice as an experimental model for cancer treatment. Physiol Res. 2016 Dec 21;65(Suppl 4):S441–53.

202.Si X, Xiao L, Brown CE, Wang D. Preclinical Evaluation of CAR T Cell Function: In Vitro and In Vivo Models. Int J Mol Sci. 2022 Mar 15;23(6):3154.

203.Masuda J, Shigehiro T, Matsumoto T, Satoh A, Mizutani A, Umemura C, et al. Cytokine Expression and Macrophage Localization in Xenograft and Allograft Tumor Models Stimulated with Lipopolysaccharide. Int J Mol Sci. 2018 Apr 23;19(4):1261.

204.Long AH, Highfill SL, Cui Y, Smith JP, Walker AJ, Ramakrishna S, et al. Reduction of MDSCs with all-trans retinoic acid improves CAR therapy efficacy for sarcomas. Cancer Immunol Res. 2016 Oct;4(10):869–80.

205.Krawczyk E, Kitlińska J. Preclinical Models of Neuroblastoma—Current Status and Perspectives. Cancers (Basel). 2023 June 23;15(13):3314.

206.Pons G, O'Dea RF, Mirkin BL. Biological Characterization of the C-1300 Murine Neuroblastoma: An in Vivo Neural Crest Tumor Model1. Cancer Research. 1982 Sept 1;42(9):3719–23.

207.Nolan JC, Frawley T, Tighe J, Soh H, Curtin C, Piskareva O. Preclinical models for neuroblastoma: Advances and challenges. Cancer Letters. 2020 Apr 1;474:53–62.

208.Lode HN, Xiang R, Dolman CS, Reisfeld RA, Varki NM, Gillies SD. Targeted Interleukin-2 Therapy for Spontaneous Neuroblastoma Metastases to Bone Marrow. JNCI: Journal of the National Cancer Institute. 1997 Nov 5;89(21):1586–94.

209.Neal ZC, Imboden M, Rakhmilevich AL, Kim KM, Hank JA, Surfus J, et al. NXS2 murine neuroblastomas express increased levels of MHC class I antigens upon recurrence following NK-dependent immunotherapy. Cancer Immunol Immunother. 2004 Jan;53(1):41–52.

210.Fowler CL, Brooks SP, Rossman JE, Cooney DR. Postoperative immunotherapy of murine C1300-neuroblastoma. J Pediatr Surg. 1990 Feb;25(2):229–37.

211.Budhu S, Wolchok J, Merghoub T. The importance of animal models in tumor immunity and immunotherapy. Curr Opin Genet Dev. 2014 Feb;24:46–51.

212.Huang M, Weiss WA. Neuroblastoma and MYCN. Cold Spring Harb Perspect Med. 2013 Oct;3(10):a014415.

213.Weiss WA, Aldape K, Mohapatra G, Feuerstein BG, Bishop JM. Targeted expression of MYCN causes neuroblastoma in transgenic mice. EMBO J. 1997 June 2;16(11):2985–95.

214.Teitz T, Stanke JJ, Federico S, Bradley CL, Brennan R, Zhang J, et al. Preclinical Models for Neuroblastoma: Establishing a Baseline for Treatment. PLOS ONE. 2011 Apr 29;6(4):e19133.

215.Aiken TJ, Erbe AK, Zebertavage L, Komjathy D, Feils AS, Rodriguez M, et al. Mechanism of effective combination radio-immunotherapy against 9464D-GD2, an immunologically cold murine neuroblastoma. J Immunother Cancer. 2022 May 1;10(5):e004834.

216.Voeller J, Erbe AK, Slowinski J, Rasmussen K, Carlson PM, Hoefges A, et al. Combined innate and adaptive immunotherapy overcomes resistance of immunologically cold syngeneic murine neuroblastoma to checkpoint inhibition. J Immunother Cancer. 2019 Dec 1;7(1):344.

217.Zebertavage L, Schopf A, Nielsen M, Matthews J, Erbe AK, Aiken TJ, et al. Evaluation of a Combinatorial Immunotherapy Regimen That Can Cure Mice Bearing MYCN-Driven High-Risk Neuroblastoma That Resists Current Clinical Therapy. Journal of Clinical Medicine. 2024 Jan;13(9):2561.

218.Kroesen M, Nierkens S, Ansems M, Wassink M, Orentas RJ, Boon L, et al. A transplantable TH-MYCN transgenic tumor model in C57Bl/6 mice for preclinical immunological studies in neuroblastoma. International Journal of Cancer. 2014;134(6):1335–45.

219.Webb ER, Lanati S, Wareham C, Easton A, Dunn SN, Inzhelevskaya T, et al. Immune characterization of pre-clinical murine models of neuroblastoma. Sci Rep. 2020 Oct 7;10(1):16695.

220.McNerney K, Karageorgos S, Ferry G, Wolpaw A, Burudpakdee C, Khurana P, et al. TH-MYCN tumors, but not tumor-derived cell lines, are adrenergic lineage, GD2+, and responsive to anti-GD2 antibody therapy. OncoImmunology. 2022 Dec 31;11(1):2075204.

221.Kroesen M, Brok IC, Reijnen D, van Hout-Kuijer MA, Zeelenberg IS, Den Brok MH, et al. Intra-adrenal murine TH-MYCN neuroblastoma tumors grow more aggressive and exhibit

a distinct tumor microenvironment relative to their subcutaneous equivalents. Cancer Immunol Immunother. 2015 May 1;64(5):563–72.

222.Dhamdhere MR, Spiegelman DV, Schneper L, Erbe AK, Sondel PM, Spiegelman VS. Generation of Novel Immunocompetent Mouse Cell Lines to Model Experimental Metastasis of High-Risk Neuroblastoma. Cancers (Basel). 2023 Sept 23;15(19):4693.

223.Molenaar JJ, Domingo-Fernández R, Ebus ME, Lindner S, Koster J, Drabek K, et al. LIN28B induces neuroblastoma and enhances MYCN levels via let-7 suppression. Nat Genet. 2012 Nov;44(11):1199–206.

224.Heukamp LC, Thor T, Schramm A, De Preter K, Kumps C, De Wilde B, et al. Targeted Expression of Mutated ALK Induces Neuroblastoma in Transgenic Mice. Science Translational Medicine. 2012 July 4;4(141):141ra91-141ra91.

225.Berry T, Luther W, Bhatnagar N, Jamin Y, Poon E, Sanda T, et al. The ALKF1174L Mutation Potentiates the Oncogenic Activity of MYCN in Neuroblastoma. Cancer Cell. 2012 July 10;22(1):117–30.

226.Ono S, Saito T, Terui K, Yoshida H, Enomoto H. Generation of conditional ALK F1174L mutant mouse models for the study of neuroblastoma pathogenesis. genesis. 2019;57(10):e23323.

227.Wienke J, Visser LL, Kholosy WM, Keller KM, Barisa M, Poon E, et al. Integrative analysis of neuroblastoma by single-cell RNA sequencing identifies the NECTIN2-TIGIT axis as a target for immunotherapy. Cancer Cell. 2024 Feb 12;42(2):283-300.e8.

228.Yogev O, Almeida GS, Barker KT, George SL, Kwok C, Campbell J, et al. In Vivo Modeling of Chemoresistant Neuroblastoma Provides New Insights into Chemorefractory Disease and Metastasis. Cancer Research. 2019 Oct 15;79(20):5382–93.

229.Yin L, Wang XJ, Chen DX, Liu XN, Wang XJ. Humanized mouse model: a review on preclinical applications for cancer immunotherapy. Am J Cancer Res. 2020 Dec 1;10(12):4568–84.

230.Cohen MA, Zhang S, Sengupta S, Ma H, Bell GW, Horton B, et al. Formation of Human Neuroblastoma in Mouse-Human Neural Crest Chimeras. Cell Stem Cell. 2020 Apr 2;26(4):579-592.e6.

231.Connell PP, Hellman S. Advances in radiotherapy and implications for the next century: a historical perspective. Cancer Res. 2009 Jan 15;69(2):383–92.

232.Delwiche FA. Mapping the literature of radiation therapy. J Med Libr Assoc. 2013 Apr;101(2):120–7.

233.Beckendorf V, Guerif S, Le Prisé E, Cosset JM, Bougnoux A, Chauvet B, et al. 70 Gy Versus 80 Gy in Localized Prostate Cancer: 5-Year Results of GETUG 06 Randomized Trial. International Journal of Radiation Oncology*Biology*Physics. 2011 July 15;80(4):1056–63.

234.Chang AR, Park W. Radiotherapy in prostate cancer treatment: results of the patterns of care study in Korea. Radiat Oncol J. 2017 Mar 17;35(1):25–31.

235.Bhatti P, Veiga LHS, Ronckers CM, Sigurdson AJ, Stovall M, Smith SA, et al. Risk of Second Primary Thyroid Cancer after Radiotherapy for a Childhood Cancer in a Large Cohort Study: An Update from the Childhood Cancer Survivor Study. rare. 2010 Oct;174(6a):741–52.

236.Lajtha LG, Oliver R, Ellis F. Rationalisation of Fractionation in Radiotherapy. British Journal of Radiology. 1960 Oct 1;33(394):634–5.

237.Fowler JF. Development of radiobiology for oncology—a personal view. Phys Med Biol. 2006 June;51(13):R263.

238.Materials NRC (US) C on E of EG for E to NOR. Radiation Quantities and Units, Definitions, Acronyms. In: Evaluation of Guidelines for Exposures to Technologically Enhanced Naturally Occurring Radioactive Materials [Internet]. National Academies Press (US);1999 [cited 2025 Mar 5]. Available from: https://www.ncbi.nlm.nih.gov/books/NBK230653/

239.Moulder JE, Seymour C. Radiation fractionation: the search for isoeffect relationships and mechanisms. International Journal of Radiation Biology. 2018 July 28;94(8):743–51.

240.Withers HR. The Four R's of Radiotherapy. Advances in Radiation Biology. Elsevier; 1975. 5, pp. 241–71.

241.Steel GG, McMillan TJ, Peacock JH. The 5Rs of Radiobiology. International Journal of Radiation Biology. 1989 Jan 1;56(6):1045–8.

242.Boustani J, Grapin M, Laurent PA, Apetoh L, Mirjolet C. The 6th R of Radiobiology: Reactivation of Anti-Tumor Immune Response. Cancers. 2019 June;11(6):860.

243.Kunschner LJ. Harvey Cushing and Medulloblastoma. Archives of Neurology. 2002 Apr 1;59(4):642–5.

244.Paterson E, Farr RF. Cerebellar medulloblastoma: treatment by irradiation of the whole central nervous system. Acta Radiol (Stockh). 1953 Apr;39(4):323–36.

245.Jairam V, Roberts KB, Yu JB. Historical Trends in the use of radiation for pediatric cancers: 1973–2008. Int J Radiat Oncol Biol Phys. 2013 Mar 1;85(3):e151–5.

246.Boterberg T, Dunlea C, Harrabi S, Janssens G, Laprie A, Whitfield G, et al. Contemporary paediatric radiation oncology. 2023 May 1;85(3):e151-5.

247.Qiu B, Matthay KK. Advancing therapy for neuroblastoma. Nat Rev Clin Oncol. 2022 Aug;19(8):515–33.

248.Ducassou A, Gambart M, Munzer C, Padovani L, Carrie C, Haas-Kogan D, et al. Long-term side effects of radiotherapy for pediatric localized neuroblastoma. Strahlenther Onkol. 2015 July 1;191(7):604–12.

249.Zhao Q, Liu Y, Zhang Y, Meng L, Wei J, Wang B, et al. Role and toxicity of radiation therapy in neuroblastoma patients: A literature review. Critical Reviews in Oncology/Hematology. 2020 May 1;149:102924.

250.Haas-Kogan DA, Swift PS, Selch M, Haase GM, Seeger RC, Gerbing RB, et al. Impact of radiotherapy for high-risk neuroblastoma: a Children's Cancer Group study. International Journal of Radiation Oncology*Biology*Physics. 2003 May 1;56(1):28–39.

251.Robbins JR, Krasin MJ, Pai Panandiker AS, Watkins A, Wu J, Santana VM, et al. Radiation therapy as part of local control of metastatic neuroblastoma: the St Jude Children's Research Hospital experience. Journal of Pediatric Surgery. 2010 Apr 1;45(4):678–86.

252.Pai Panandiker AS, Beltran C, Billups CA, McGregor LM, Furman WL, Davidoff AM. Intensity modulated radiation therapy provides excellent local control in high-risk abdominal neuroblastoma. Pediatric Blood & Cancer. 2013;60(5):761–5.

253.Gatcombe HG, Marcus RB, Katzenstein HM, Tighiouart M, Esiashvili N. Excellent Local Control From Radiation Therapy for High-Risk Neuroblastoma. International Journal of Radiation Oncology*Biology*Physics. 2009 Aug 1;74(5):1549–54.

254.Casey DL, Kushner BH, Cheung NKV, Modak S, LaQuaglia MP, Wolden SL. Local Control With 21-Gy Radiation Therapy for High-Risk Neuroblastoma. International Journal of Radiation Oncology*Biology*Physics. 2016 Oct 1;96(2):393–400.

255.Parikh NS, Howard SC, Chantada G, Israels T, Khattab M, Alcasabas P, et al. SIOP-PODC adapted risk stratification and treatment guidelines: Recommendations for neuroblastoma in low- and middle-income settings. Pediatric Blood & Cancer. 2015;62(8):1305–16.

256.Boterberg T. Radiotherapy for Neuroblastoma. In: Sarnacki S, Pio L, editors. Neuroblastoma: Clinical and Surgical Management [Internet]. Cham: Springer International Publishing; 2020 [cited 2025 Mar 6]. p. 163–70. Available from: https://doi.org/10.1007/978-3-030-18396-7_8

257.Taylor A, Powell MEB. Intensity-modulated radiotherapy—what is it? Cancer Imaging. 2004 Mar 26;4(2):68–73.

258.Beneyton V, Niederst C, Vigneron C, Meyer P, Becmeur F, Marcellin L, et al. Comparison of the dosimetries of 3-dimensions Radiotherapy (3D-RT) with linear accelerator and intensity modulated radiotherapy (IMRT) with helical tomotherapy in children irradiated for neuroblastoma. BMC Med Phys. 2012 June 28;12(1):2.

259.Merchant TE, Farr JB. Proton beam therapy: a fad or a new standard of care. Current Opinion in Pediatrics. 2014 Feb;26(1):3.

260.Hattangadi JA, Rombi B, Yock TI, Broussard G, Friedmann AM, Huang M, et al. Proton Radiotherapy for High-Risk Pediatric Neuroblastoma: Early Outcomes and Dose Comparison. International Journal of Radiation Oncology*Biology*Physics. 2012 July 1;83(3):1015–22.

261.Hill-Kayser CE, Tochner Z, Li Y, Kurtz G, Lustig RA, James P, et al. Outcomes After Proton Therapy for Treatment of Pediatric High-Risk Neuroblastoma. International Journal of Radiation Oncology*Biology*Physics. 2019 June 1;104(2):401–8.

262.Bagley AF, Grosshans DR, Philip NV, Foster J, McAleer MF, McGovern SL, et al. Efficacy of Proton Therapy in Children with High Risk and Locally Recurrent Neuroblastoma. Pediatr Blood Cancer. 2019 Aug;66(8):e27786.

263.Parisi MT, Eslamy H, Park JR, Shulkin BL, Yanik GA. 131I-Metaiodobenzylguanidine Theranostics in Neuroblastoma: Historical Perspectives; Practical Applications. Seminars in Nuclear Medicine. 2016 May 1;46(3):184–202.

264.Olecki E, Grant CN. MIBG in neuroblastoma diagnosis and treatment. Seminars in Pediatric Surgery. 2019 Dec 1;28(6):150859.

265.Hadj-Djilani NL, Lebtahi NE, Bischof Delaloye A, Laurini R, Beck D. Diagnosis and follow-up of neuroblastoma by means of iodine-123 metaiodobenzylguanidine scintigraphy and bone scan, and the influence of histology. Eur J Nucl Med. 1995 Apr 1;22(4):322–9.

266.Hattner R, Huberty J, Engelstad B, Gooding C, Ablin A. Localization of m-iodo(131I)benzylguanidine in neuroblastoma. American Journal of Roentgenology. 1984 Aug;143(2):373–4.

267.Kimmig B, Brandeis WE, Eisenhut M, Bubeck B, Hermann HJ, Winkel K zum. Scintigraphy of a Neuroblastoma with I-131 Meta-iodobenzylguanidine. Journal of Nuclear Medicine. 1984 July 1;25(7):773–5.

268.Wieland DM, Wu J long, Brown LE, Mangner TJ, Swanson DP, Beierwaltes WH. Radiolabeled Adrenergic Neuron-Blocking Agents: Adrenomedullary Imaging with [131I] Iodobenzylguanidine. Journal of Nuclear Medicine. 1980 Apr 1;21(4):349–53.

269.Wieland DM, Brown LE, Tobes MC, Rogers WL, Marsh DD, Mangner TJ, et al. Imaging the Primate Adrenal Medulla with [123I] and [131I] Meta-Iodobenzylguanidine: Concise Communication. Journal of Nuclear Medicine. 1981 Apr 1;22(4):358–64.

270.Sisson JC, Frager MS, Valk TW, Gross MD, Swanson DP, Wieland DM, et al. Scintigraphic Localization of Pheochromocytoma. New England Journal of Medicine. 1981 July 2;305(1):12–7.

271.Brisse HJ, McCarville MB, Granata C, Krug KB, Wootton-Gorges SL, Kanegawa K, et al. Guidelines for Imaging and Staging of Neuroblastic Tumors: Consensus Report from the International Neuroblastoma Risk Group Project. Radiology. 2011 Oct;261(1):243–57.

272.Matthay KK, Yanik G, Messina J, Quach A, Huberty J, Cheng SC, et al. Phase II Study on the Effect of Disease Sites, Age, and Prior Therapy on Response to Iodine-131-Metaiodobenzylguanidine Therapy in Refractory Neuroblastoma. JCO. 2007 Mar 20;25(9):1054–60.

273.Matthay KK, Quach A, Huberty J, Franc BL, Hawkins RA, Jackson H, et al. Iodine-131—Metaiodobenzylguanidine Double Infusion With Autologous Stem-Cell Rescue for Neuroblastoma: A New Approaches to Neuroblastoma Therapy Phase I Study. JCO. 2009 Mar;27(7):1020–5.

274.Howard JP, Maris JM, Kersun LS, Huberty JP, Cheng SC, Hawkins RA, et al. Tumor response and toxicity with multiple infusions of high dose 131I-MIBG for refractory neuroblastoma. Pediatric Blood & Cancer. 2005;44(3):232–9.

275.Johnson K, McGlynn B, Saggio J, Baniewicz D, Zhuang H, Maris JM, et al. Safety and efficacy of tandem 131I-metaiodobenzylguanidine infusions in relapsed/refractory neuroblastoma. Pediatric Blood & Cancer. 2011;57(7):1124–9.

276.Yanik GA, Villablanca JG, Maris JM, Weiss B, Groshen S, Marachelian A, et al. 131I-Metaiodobenzylguanidine with Intensive Chemotherapy and Autologous Stem Cell Transplantation for High-Risk Neuroblastoma. A New Approaches to Neuroblastoma Therapy (NANT) Phase II Study. Biology of Blood and Marrow Transplantation. 2015 Apr 1;21(4):673–81.

277.de Kraker J, Hoefnagel KA, Verschuur AC, van Eck B, van Santen HM, Caron HN. Iodine-131-metaiodobenzylguanidine as initial induction therapy in stage 4 neuroblastoma patients over 1 year of age. European Journal of Cancer. 2008 Mar 1;44(4):551–6.

278.Mastrangelo S, Rufini V, Ruggiero A, Di Giannatale A, Riccardi R. Treatment of advanced neuroblastoma in children over 1 year of age: The critical role of 131I-metaiodobenzylguanidine combined with chemotherapy in a rapid induction regimen. Pediatric Blood & Cancer. 2011;56(7):1032–40.

279.Baskar R, Dai J, Wenlong N, Yeo R, Yeoh KW. Biological response of cancer cells to radiation treatment. Front Mol Biosci. 2014 Nov 17;1:24.

280.Niemantsverdriet M, van Goethem MJ, Bron R, Hogewerf W, Brandenburg S, Langendijk JA, et al. High and Low LET Radiation Differentially Induce Normal Tissue Damage Signals. International Journal of Radiation Oncology*Biology*Physics. 2012 July 15;83(4):1291–7.

281.Macaeva E, Tabury K, Michaux A, Janssen A, Averbeck N, Moreels M, et al. High-LET Carbon and Iron Ions Elicit a Prolonged and Amplified p53 Signaling and Inflammatory Response Compared to low-LET X-Rays in Human Peripheral Blood Mononuclear Cells. Front Oncol. 2021 Nov 23;11:768493.

282.Barcellos-Hoff MH, Park C, Wright EG. Radiation and the microenvironment – tumorigenesis and therapy. Nat Rev Cancer. 2005 Nov;5(11):867–75.

283.Jackson SP, Bartek J. The DNA-damage response in human biology and disease. Nature. 2009 Oct;461(7267):1071–8.

284.Cosper PF, Copeland SE, Tucker JB, Weaver BA. Chromosome missegregation as a modulator of radiation sensitivity. Seminars in radiation oncology. 2022 Jan;32(1):54.

285.Golden E, Pellicciotta I, Demaria S, Barcellos-Hoff MH, Formenti SC. The convergence of radiation and immunogenic cell death signaling pathways. Front Oncol. 2012 Aug 7;2:88.

286.Slone HB, Peters LJ, Milas L. Effect of Host Immune Capability on Radiocurability and Subsequent Transplantability of a Murine Fibrosarcoma2. JNCI: Journal of the National Cancer Institute. 1979 Nov 1;63(5):1229–35.

287.Demaria S, Ng B, Devitt ML, Babb JS, Kawashima N, Liebes L, et al. Ionizing radiation inhibition of distant untreated tumors (abscopal effect) is immune mediated. International Journal of Radiation Oncology*Biology*Physics. 2004 Mar 1;58(3):862–70.

288.Demaria S, Formenti SC. The abscopal effect 67 years later: from a side story to center stage. BJR. 2020 May;93(1109):20200042.

289.Kepp O, Menger L, Vacchelli E, Locher C, Adjemian S, Yamazaki T, et al. Crosstalk between ER stress and immunogenic cell death. Cytokine & Growth Factor Reviews. 2013 Aug 1;24(4):311–8.

290.Chaurasia M, Gupta S, Das A, Dwarakanath BS, Simonsen A, Sharma K. Radiation induces EIF2AK3/PERK and ERN1/IRE1 mediated pro-survival autophagy. Autophagy. 2019 Aug 3;15(8):1391–406.

291.Azzam EI, Jay-Gerin JP, Pain D. Ionizing radiation-induced metabolic oxidative stress and prolonged cell injury. Cancer Letters. 2012 Dec 31;327(1):48–60.

292.Garg AD, Galluzzi L, Apetoh L, Baert T, Birge RB, Bravo-San Pedro JM, et al. Molecular and Translational Classifications of DAMPs in Immunogenic Cell Death. Front Immunol. 2015 Nov 20;6:588.

293.Galluzzi L, Vitale I, Aaronson SA, Abrams JM, Adam D, Agostinis P, et al. Molecular mechanisms of cell death: recommendations of the Nomenclature Committee on Cell Death 2018. Cell Death Differ. 2018 Mar;25(3):486–541.

294.Messmer MN, Snyder AG, Oberst A. Comparing the effects of different cell death programs in tumor progression and immunotherapy. Cell Death Differ. 2019 Jan;26(1):115–29.

295.Ahmed A, Tait SWG. Targeting immunogenic cell death in cancer. Molecular Oncology. 2020;14(12):2994–3006.

296.Obeid M, Panaretakis T, Joza N, Tufi R, Tesniere A, van Endert P, et al. Calreticulin exposure is required for the immunogenicity of γ-irradiation and UVC light-induced apoptosis. Cell Death Differ. 2007 Oct;14(10):1848–50.

297.Obeid M, Tesniere A, Ghiringhelli F, Fimia GM, Apetoh L, Perfettini JL, et al. Calreticulin exposure dictates the immunogenicity of cancer cell death. Nat Med. 2007 Jan;13(1):54–61.

298.Krysko DV, Garg AD, Kaczmarek A, Krysko O, Agostinis P, Vandenabeele P. Immunogenic cell death and DAMPs in cancer therapy. Nat Rev Cancer. 2012 Dec;12(12):860–75.

299.Elliott MR, Chekeni FB, Trampont PC, Lazarowski ER, Kadl A, Walk SF, et al. Nucleotides released by apoptotic cells act as a find-me signal to promote phagocytic clearance. Nature. 2009 Sept;461(7261):282–6.

300.Ghiringhelli F, Apetoh L, Tesniere A, Aymeric L, Ma Y, Ortiz C, et al. Activation of the NLRP3 inflammasome in dendritic cells induces IL-1β–dependent adaptive immunity against tumors. Nat Med. 2009 Oct;15(10):1170–8.

301.Antonioli L, Blandizzi C, Pacher P, Haskó G. Immunity, inflammation and cancer: a leading role for adenosine. Nat Rev Cancer. 2013 Dec;13(12):842–57.

302.Martins I, Wang Y, Michaud M, Ma Y, Sukkurwala AQ, Shen S, et al. Molecular mechanisms of ATP secretion during immunogenic cell death. Cell Death Differ. 2014 Jan;21(1):79–91.

303.Michaud M, Martins I, Sukkurwala AQ, Adjemian S, Ma Y, Pellegatti P, et al. Autophagy-Dependent Anticancer Immune Responses Induced by Chemotherapeutic Agents in Mice. Science. 2011 Dec 16;334(6062):1573–7.

304.Apetoh L, Ghiringhelli F, Tesniere A, Obeid M, Ortiz C, Criollo A, et al. Toll-like receptor 4–dependent contribution of the immune system to anticancer chemotherapy and radiotherapy. Nat Med. 2007 Sept;13(9):1050–9.

305.Lanneau D, Brunet M, Frisan E, Solary E, Fontenay M, Garrido C. Heat shock proteins: essential proteins for apoptosis regulation. J Cell Mol Med. 2008 June;12(3):743–61.

306.Melcher A, Todryk S, Hardwick N, Ford M, Jacobson M, Vile RG. Tumor immunogenicity is determined by the mechanism of cell death via induction of heat shock protein expression. Nat Med. 1998 May;4(5):581–7.

307.Yamazaki T, Kirchmair A, Sato A, Buqué A, Rybstein M, Petroni G, et al. Mitochondrial DNA drives abscopal responses to radiation that are inhibited by autophagy. Nat Immunol. 2020 Oct;21(10):1160–71.

308.Kate WD, Fanta M, Weinfeld M. Loss of the DNA repair protein, polynucleotide kinase/phosphatase, activates the type 1 interferon response independent of ionizing radiation. Nucleic Acids Research. 2024 Sept 9;52(16):9630–53.

309.Lim JYH, Gerber SA, Murphy SP, Lord EM. Type I interferons induced by radiation therapy mediate recruitment and effector function of CD8+ T cells. Cancer Immunol Immunother. 2014 Mar 1;63(3):259–71.

310.Burnette BC, Liang H, Lee Y, Chlewicki L, Khodarev NN, Weichselbaum RR, et al. The Efficacy of Radiotherapy Relies upon Induction of Type I Interferon–Dependent Innate and Adaptive Immunity. Cancer Research. 2011 Mar 31;71(7):2488–96.

311.Holicek P, Guilbaud E, Klapp V, Truxova I, Spisek R, Galluzzi L, et al. Type I interferon and cancer. Immunological Reviews. 2024;321(1):115–27.

312.Moeller BJ, Cao Y, Li CY, Dewhirst MW. Radiation activates HIF-1 to regulate vascular radiosensitivity in tumors: Role of reoxygenation, free radicals, and stress granules. Cancer Cell. 2004 May 1;5(5):429–41.

313.Dewhirst MW, Cao Y, Moeller B. Cycling hypoxia and free radicals regulate angiogenesis and radiotherapy response. Nat Rev Cancer. 2008 June;8(6):425–37.

314.Harris AL. Hypoxia — a key regulatory factor in tumour growth. Nat Rev Cancer. 2002 Jan;2(1):38–47.

315.Barsoum IB, Koti M, Siemens DR, Graham CH. Mechanisms of Hypoxia-Mediated Immune Escape in Cancer. Cancer Research. 2014 Dec 14;74(24):7185–90.

316.Hong J, Tobin NP, Rundqvist H, Li T, Lavergne M, García-Ibáñez Y, et al. Role of Tumor Pericytes in the Recruitment of Myeloid-Derived Suppressor Cells. J Natl Cancer Inst. 2015 Oct 1;107(10):djv209.

317.Clambey ET, McNamee EN, Westrich JA, Glover LE, Campbell EL, Jedlicka P, et al. Hypoxia-inducible factor-1 alpha–dependent induction of FoxP3 drives regulatory T-cell

abundance and function during inflammatory hypoxia of the mucosa. Proceedings of the National Academy of Sciences. 2012 Oct 9;109(41):E2784–93.

318.Allard B, Allard D, Buisseret L, Stagg J. The adenosine pathway in immuno-oncology. Nat Rev Clin Oncol. 2020 Oct;17(10):611–29.

319.Baghbani E, Noorolyai S, Shanehbandi D, Mokhtarzadeh A, Aghebati-Maleki L, Shahgoli VK, et al. Regulation of immune responses through CD39 and CD73 in cancer: Novel checkpoints. Life Sciences. 2021 Oct 1;282:119826.

320.Deaglio S, Dwyer KM, Gao W, Friedman D, Usheva A, Erat A, et al. Adenosine generation catalyzed by CD39 and CD73 expressed on regulatory T cells mediates immune suppression. J Exp Med. 2007 June 11;204(6):1257–65.

321.Wennerberg E, Spada S, Rudqvist NP, Lhuillier C, Gruber S, Chen Q, et al. CD73 Blockade Promotes Dendritic Cell Infiltration of Irradiated Tumors and Tumor Rejection. Cancer Immunology Research. 2020 Apr 1;8(4):465–78.

322.Inoue T, Adachi K, Kawana K, Taguchi A, Nagamatsu T, Fujimoto A, et al. Cancer-associated fibroblast suppresses killing activity of natural killer cells through downregulation of poliovirus receptor (PVR/CD155), a ligand of activating NK receptor. International Journal of Oncology. 2016 Oct 1;49(4):1297–304.

323.Ansems M, Span PN. The tumor microenvironment and radiotherapy response; a central role for cancer-associated fibroblasts. Clinical and Translational Radiation Oncology. 2020 May 1;22:90–7.

324.Wang Z, Tang Y, Tan Y, Wei Q, Yu W. Cancer-associated fibroblasts in radiotherapy: challenges and new opportunities. Cell Communication and Signaling. 2019 May 17;17(1):47.

325.Busek P, Balaziova E, Matrasova I, Hilser M, Tomas R, Syrucek M, et al. Fibroblast activation protein alpha is expressed by transformed and stromal cells and is associated with mesenchymal features in glioblastoma. Tumor Biol. 2016 Oct 1;37(10):13961–71.

326.Yang X, Lin Y, Shi Y, Li B, Liu W, Yin W, et al. FAP Promotes Immunosuppression by Cancer-Associated Fibroblasts in the Tumor Microenvironment via STAT3–CCL2 Signaling. Cancer Research. 2016 July 14;76(14):4124–35.

327.Bachman KE, Park BH. Duel nature of TGF-β signaling: tumor suppressor vs. tumor promoter. Current Opinion in Oncology. 2005 Jan;17(1):49.

328.Wrzesinski SH, Wan YY, Flavell RA. Transforming Growth Factor-β and the Immune Response: Implications for Anticancer Therapy. Clinical Cancer Research. 2007 Sept 17;13(18):5262–70.

329.Barcellos-Hoff MH. Radiation-induced transforming growth factor beta and subsequent extracellular matrix reorganization in murine mammary gland. Cancer Res. 1993 Sept 1;53(17):3880–6.

330.Barcellos-Hoff MH, Derynck R, Tsang ML, Weatherbee JA. Transforming growth factor-beta activation in irradiated murine mammary gland. J Clin Invest. 1994 Feb;93(2):892–9.

331.Jobling MF, Mott JD, Finnegan MT, Jurukovski V, Erickson AC, Walian PJ, et al. Isoform-Specific Activation of Latent Transforming Growth Factor β (LTGF-β) by Reactive Oxygen Species. rare. 2006 Dec;166(6):839–48.

332.Vanpouille-Box C, Diamond JM, Pilones KA, Zavadil J, Babb JS, Formenti SC, et al. TGFβ Is a Master Regulator of Radiation Therapy-Induced Antitumor Immunity. Cancer Research. 2015 May 31;75(11):2232–42.

333.Golden EB, Frances D, Pellicciotta I, Demaria S, Helen Barcellos-Hoff M, Formenti SC. Radiation fosters dose-dependent and chemotherapy-induced immunogenic cell death. OncoImmunology. 2014 Apr 1;3(4):e28518.

334.De Martino M, Daviaud C, Vanpouille-Box C. Radiotherapy: An immune response modifier for immuno-oncology. Seminars in Immunology. 2021 Feb 1;52:101474.

335.Demaria S, Kawashima N, Yang AM, Devitt ML, Babb JS, Allison JP, et al. Immune-Mediated Inhibition of Metastases after Treatment with Local Radiation and CTLA-4 Blockade in a Mouse Model of Breast Cancer. Clinical Cancer Research. 2005 Feb 8;11(2):728–34.

336.Twyman-Saint Victor C, Rech AJ, Maity A, Rengan R, Pauken KE, Stelekati E, et al. Radiation and dual checkpoint blockade activate non-redundant immune mechanisms in cancer. Nature. 2015 Apr;520(7547):373–7.

337.Formenti SC, Rudqvist NP, Golden E, Cooper B, Wennerberg E, Lhuillier C, et al. Radiotherapy induces responses of lung cancer to CTLA-4 blockade. Nat Med. 2018 Dec;24(12):1845–51.

338.Dewan MZ, Galloway AE, Kawashima N, Dewyngaert JK, Babb JS, Formenti SC, et al. Fractionated but Not Single-Dose Radiotherapy Induces an Immune-Mediated Abscopal Effect when Combined with Anti–CTLA-4 Antibody. Clinical Cancer Research. 2009 Aug 31;15(17):5379–88.

339.Philippou Y, Sjoberg HT, Murphy E, Alyacoubi S, Jones KI, Gordon-Weeks AN, et al. Impacts of combining anti-PD-L1 immunotherapy and radiotherapy on the tumour immune microenvironment in a murine prostate cancer model. Br J Cancer. 2020 Sept;123(7):1089–100.

340.Callaghan CM, Seyedin SN, Mohiuddin IH, Hawkes KL, Petronek MS, Anderson CM, et al. The Effect of Concurrent Stereotactic Body Radiation and Anti-PD-1 Therapy for Recurrent Metastatic Sarcoma. rare. 2020 June;194(2):124–32.

341.Dovedi SJ, Cheadle EJ, Popple AL, Poon E, Morrow M, Stewart R, et al. Fractionated Radiation Therapy Stimulates Antitumor Immunity Mediated by Both Resident and Infiltrating Polyclonal T-cell Populations when Combined with PD-1 Blockade. Clinical Cancer Research. 2017 Sept 14;23(18):5514–26.

342.Kordbacheh T, Honeychurch J, Blackhall F, Faivre-Finn C, Illidge T. Radiotherapy and anti-PD-1/PD-L1 combinations in lung cancer: building better translational research platforms. Annals of Oncology. 2018 Feb 1;29(2):301–10.

343.Vacchelli E, Bloy N, Aranda F, Buqué A, Cremer I, Demaria S, et al. Trial Watch: Immunotherapy plus radiation therapy for oncological indications. Oncoimmunology. 2016 July 25;5(9):e1214790.

344.Gattinoni L, Finkelstein SE, Klebanoff CA, Antony PA, Palmer DC, Spiess PJ, et al. Removal of homeostatic cytokine sinks by lymphodepletion enhances the efficacy of adoptively transferred tumor-specific CD8+ T cells. J Exp Med. 2005 Oct 3;202(7):907–12.

345.Pocaterra A, Catucci M, Mondino A. Adoptive T cell therapy of solid tumors: time to team up with immunogenic chemo/radiotherapy. Current Opinion in Immunology. 2022 Feb 1;74:53–9.

346.Lai JZ, Zhu YY, Ruan M, Chen L, Zhang QY. Local Irradiation Sensitized Tumors to Adoptive T Cell Therapy via Enhancing the Cross-Priming, Homing, and Cytotoxicity of Antigen-Specific CD8 T Cells. Front Immunol. 2019 Dec 11;10:2857.

347.Ward-Kavanagh LK, Zhu J, Cooper TK, Schell TD. Whole-body irradiation increases the magnitude and persistence of adoptively transferred T cells associated with tumor regression in a mouse model of prostate cancer. Cancer Immunol Res. 2014 Aug;2(8):777–88.

348.Manzo T, Sturmheit T, Basso V, Petrozziello E, Hess Michelini R, Riba M, et al. T Cells Redirected to a Minor Histocompatibility Antigen Instruct Intratumoral TNFα Expression and Empower Adoptive Cell Therapy for Solid Tumors. Cancer Research. 2017 Jan 31;77(3):658–71.

349.Vianello F, Cannella L, Coe D, Chai JG, Golshayan D, Marelli-Berg FM, et al. Enhanced and aberrant T cell trafficking following total body irradiation: a gateway to graft-versus-host disease? British Journal of Haematology. 2013;162(6):808–18.

350.Goff SL, Dudley ME, Citrin DE, Somerville RP, Wunderlich JR, Danforth DN, et al. Randomized, Prospective Evaluation Comparing Intensity of Lymphodepletion Before Adoptive Transfer of Tumor-Infiltrating Lymphocytes for Patients With Metastatic Melanoma. JCO. 2016 July 10;34(20):2389–97.

351.Zhong L, Li Y, Muluh TA, Wang Y. Combination of CAR-T cell therapy and radiotherapy: Opportunities and challenges in solid tumors (Review). Oncology Letters. 2023 July 1;26(1):1–10.

352.Zhou Z, Mai Y, Zhang G, Wang Y, Sun P, Jing Z, et al. Emerging role of immunogenic cell death in cancer immunotherapy: Advancing next-generation CAR-T cell immunotherapy by combination. Cancer Letters. 2024 Aug 28;598:217079.

353.Weiss T, Weller M, Guckenberger M, Sentman CL, Roth P. NKG2D-Based CAR T Cells and Radiotherapy Exert Synergistic Efficacy in Glioblastoma. Cancer Research. 2018 Feb 14;78(4):1031–43.

354.Weiss T, Schneider H, Silginer M, Steinle A, Pruschy M, Polić B, et al. NKG2D-Dependent Antitumor Effects of Chemotherapy and Radiotherapy against Glioblastoma. Clinical Cancer Research. 2018 Feb 14;24(4):882–95.

355.Murty S, Haile ST, Beinat C, Aalipour A, Alam IS, Murty T, et al. Intravital imaging reveals synergistic effect of CAR T-cells and radiation therapy in a preclinical immunocompetent glioblastoma model. Oncoimmunology. 9(1):1757360.

356.DeSelm C, Palomba ML, Yahalom J, Hamieh M, Eyquem J, Rajasekhar VK, et al. Low-Dose Radiation Conditioning Enables CAR T Cells to Mitigate Antigen Escape. Molecular Therapy. 2018 Nov 7;26(11):2542–52.

357.Herrera FG, Ronet C, Ochoa de Olza M, Barras D, Crespo I, Andreatta M, et al. Low-Dose Radiotherapy Reverses Tumor Immune Desertification and Resistance to Immunotherapy. Cancer Discovery. 2022 Jan 1;12(1):108–33.

358.Sim AJ, Jain MD, Figura NB, Chavez JC, Shah BD, Khimani F, et al. Radiation Therapy as a Bridging Strategy for CAR T Cell Therapy With Axicabtagene Ciloleucel in Diffuse Large B-Cell Lymphoma. International Journal of Radiation Oncology*Biology*Physics. 2019 Dec 1;105(5):1012–21.

359.Sodji QH, Forsberg MH, Cappabianca D, Kerr CP, Sarko L, Shea A, et al. Comparative Study of the Effect of Radiation Delivered by Lutetium-177 or Actinium-225 on Anti-GD2 Chimeric Antigen Receptor T Cell Viability and Functions. Cancers. 2024 Jan;16(1):191.

360.Sodji QH, Shea A, Cappabianca D, Forsberg MH, Eickhoff JC, Idrissou MB, et al. Low Dose Radiation by Radiopharmaceutical Therapy Enhances GD2 TRAC-CAR T Cells Efficacy in Localized Neuroblastoma. bioRxiv; 2024. p. 2024.11.02.621668.

361.Ansari IH, Shi LX, Erbe-Gurel AK, Rakhmilevich AL, Matthews JA, Sodji QH, et al. 315 Improving pediatric neuroblastoma immunotherapy outcome by using B7-H3 CAR-T cells in combination with low-dose external beam radiation therapy (EBRT): preclinical development in murine models. J Immunother Cancer. 2024 Nov 1; 12.

362.Swift S, Lorens J, Achacoso P, Nolan GP. Rapid Production of Retroviruses for Efficient Gene Delivery to Mammalian Cells Using 293T Cell–Based Systems. Current Protocols in Immunology. 1999;31(1):10.17.14-10.17.29.

363.Wang H, Kavanaugh MP, North RA, Kabat D. Cell-surface receptor for ecotropic murine retroviruses is a basic amino-acid transporter. Nature. 1991 Aug;352(6337):729–31.

364.Pear WS, Nolan GP, Scott ML, Baltimore D. Production of high-titer helper-free retroviruses by transient transfection. Proceedings of the National Academy of Sciences. 1993 Sept 15;90(18):8392–6.

365.Vargas JE, Chicaybam L, Stein RT, Tanuri A, Delgado-Cañedo A, Bonamino MH. Retroviral vectors and transposons for stable gene therapy: advances, current challenges and perspectives. Journal of Translational Medicine. 2016 Oct 12;14(1):288.

366.Thomas S, Straathof K, Himoudi N, Anderson J, Pule M. An Optimized GD2-Targeting Retroviral Cassette for More Potent and Safer Cellular Therapy of Neuroblastoma and Other Cancers. PLOS ONE. 2016 Mar 31;11(3):e0152196.

367.Philip B, Kokalaki E, Mekkaoui L, Thomas S, Straathof K, Flutter B, et al. A highly compact epitope-based marker/suicide gene for easier and safer T-cell therapy. Blood. 2014 Aug 21;124(8):1277–87.

368.Fauci JM, Sabbatino F, Wang Y, Londoño-Joshi AI, Straughn JM, Landen CN, et al. Monoclonal antibody-based immunotherapy of ovarian cancer: Targeting ovarian cancer cells with the B7-H3-specific mAb 376.96. Gynecologic Oncology. 2014 Jan 1;132(1):203–10.

369.Chou KC, Elrod DW. Prediction of membrane protein types and subcellular locations. Proteins: Structure, Function, and Bioinformatics. 1999;34(1):137–53.

370.Wälchli S, Løset GÅ, Kumari S, Johansen JN, Yang W, Sandlie I, et al. A Practical Approach to T-Cell Receptor Cloning and Expression. PLOS ONE. 2011 Nov 21;6(11):e27930.

371.Threadgill DW, Yee D, Matin A, Nadeau JH, Magnuson T. Genealogy of the 129 inbred strains: 129/SvJ is a contaminated inbred strain. Mammalian Genome. 1997 June 1;8(6):390–3.

372.Hulspas R, O'Gorman MRG, Wood BL, Gratama JW, Sutherland DR. Considerations for the control of background fluorescence in clinical flow cytometry. Cytometry Part B: Clinical Cytometry. 2009;76B(6):355–64.

373.Lee J, Sadelain M, Brentjens R. Retroviral Transduction of Murine Primary T Lymphocytes. In: Baum C, editor. Genetic Modification of Hematopoietic Stem Cells: Methods and Protocols. Methods In Molecular Biology; 2009 506:83-96.

374.Samji T, Khanna KM. Understanding Memory CD8+ T cells. Immunol Lett. 2017 May;185:32–9.

375.Karabıdak SM. Dead Time in the Gamma-Ray Spectrometry. In: New Insights on Gamma Rays. IntechOpen; 2017.

376.Chesler L, Weiss WA. Genetically engineered murine models – Contribution to our understanding of the genetics, molecular pathology and therapeutic targeting of neuroblastoma. Seminars in Cancer Biology. 2011 Oct 1;21(4):245–55.

377.Zhu M, Yang M, Zhang J, Yin Y, Fan X, Zhang Y, et al. Immunogenic Cell Death Induction by Ionizing Radiation. Frontiers in Immunology. 2021;12:705361.

378.Branchini BR, Southworth TL. Chapter Twelve - A Highly Sensitive Biosensor for ATP Using a Chimeric Firefly Luciferase. In: Thompson RB, Fierke CA, editors. Methods in Enzymology. 2017;589:351-64.

379.Dubyak GR. Chapter Six - Luciferase-assisted detection of extracellular ATP and ATP metabolites during immunogenic death of cancer cells. In: Galluzzi L, Rudqvist NP, editors. Methods in Enzymology. 2019;629:81-102.

380.Fucikova J, Kepp O, Kasikova L, Petroni G, Yamazaki T, Liu P, et al. Detection of immunogenic cell death and its relevance for cancer therapy. Cell Death Dis. 2020 Nov 26;11(11):1–13.

381.Ghasemi M, Turnbull T, Sebastian S, Kempson I. The MTT Assay: Utility, Limitations, Pitfalls, and Interpretation in Bulk and Single-Cell Analysis. Int J Mol Sci. 2021 Nov 26;22(23):12827.

382.Stagg J, Smyth MJ. Extracellular adenosine triphosphate and adenosine in cancer. Oncogene. 2010 Sept;29(39):5346–58.

383.Perrot I, Michaud HA, Giraudon-Paoli M, Augier S, Docquier A, Gros L, et al. Blocking Antibodies Targeting the CD39/CD73 Immunosuppressive Pathway Unleash Immune

Responses in Combination Cancer Therapies. Cell Reports. 2019 May 21;27(8):2411-2425.e9.

384.Forveille S, Humeau J, Sauvat A, Bezu L, Kroemer G, Kepp O. Chapter Seven - Quinacrine-mediated detection of intracellular ATP. In: Galluzzi L, Rudqvist NP, editors. Methods in Enzymology 2019;629:103-13.

385.Vessey KA, Ho T, Jobling AI, Wang AY, Fletcher EL. Fluorescent Labeling and Quantification of Vesicular ATP Release Using Live Cell Imaging. Methods Mol Bio 2020;2041:209-21.

386.Gambotto A, Dworacki G, Cicinnati V, Kenniston T, Steitz J, Tüting T, et al. Immunogenicity of enhanced green fluorescent protein (EGFP) in BALB/c mice: identification of an H2-Kd-restricted CTL epitope. Gene Ther. 2000 Dec;7(23):2036–40.

387.Yuzhakova DV, Shirmanova MV, Serebrovskaya EO, Lukyanov KA, Druzhkova IN, Shakhov BE, et al. CT26 murine colon carcinoma expressing the red fluorescent protein KillerRed as a highly immunogenic tumor model. JBO. 2015 Aug;20(8):088002.

388.Puck TT, Marcus PI. ACTION OF X-RAYS ON MAMMALIAN CELLS. Journal of Experimental Medicine. 1956 May 1;103(5):653–66.

389.Citrin DE. Short-Term Screening Assays for the Identification of Therapeutics for Cancer. Cancer Research. 2016 June 14;76(12):3443–5.

390.Willers H, Pan X, Borgeaud N, Korovina I, Koi L, Egan R, et al. Screening and Validation of Molecular Targeted Radiosensitizers. International Journal of Radiation Oncology, Biology, Physics. 2021 Dec 1;111(5):e63–74.

391.Brüningk SC, Ziegenhein P, Rivens I, Oelfke U, Haar G ter. A cellular automaton model for spheroid response to radiation and hyperthermia treatments. Scientific Reports [Internet]. 2019 [cited 2023 Jan 1];9(1). Available from: https://doi.org/10.1038/s41598-019-54117-x

392.van Meerloo J, Kaspers GJL, Cloos J. Cell Sensitivity Assays: The MTT Assay. Cancer Cell Culture. Methods in Molecular Biology 2011;731:237-45.

393.Flem-Karlsen K, Fodstad Ø, Tan M, Nunes-Xavier CE. B7-H3 in Cancer – Beyond Immune Regulation. Trends in Cancer. 2018 June 1;4(6):401–4.

394.Li G, Quan Y, Che F, Wang L. B7-H3 in tumors: friend or foe for tumor immunity? Cancer Chemother Pharmacol. 2018 Feb 1;81(2):245–53.

395.Picarda E, Ohaegbulam KC, Zang X. Molecular Pathways: Targeting B7-H3 (CD276) for Human Cancer Immunotherapy. Clinical Cancer Research. 2016 July 14;22(14):3425–31.

396.Vigdorovich V, Ramagopal UA, Lázár-Molnár E, Sylvestre E, Lee JS, Hofmeyer KA, et al. Structure and T Cell Inhibition Properties of B7 Family Member, B7-H3. Structure. 2013 May 7;21(5):707–17.

397.Nehama D, Di Ianni N, Musio S, Du H, Patané M, Pollo B, et al. B7-H3-redirected chimeric antigen receptor T cells target glioblastoma and neurospheres. EBioMedicine. 2019 Sept 1;47:33–43.

398.Theruvath J, Sotillo E, Mount CW, Graef CM, Delaidelli A, Heitzeneder S, et al. Locoregionally administered B7-H3-targeted CAR T cells for treatment of atypical teratoid/rhabdoid tumors. Nat Med. 2020 May;26(5):712–9.

399.Tang X, Zhao S, Zhang Y, Wang Y, Zhang Z, Yang M, et al. B7-H3 as a Novel CAR-T Therapeutic Target for Glioblastoma. Molecular Therapy - Oncolytics. 2019 Sept 27;14:279–87.

400.Imai K, Wilson BS, Bigotti A, Natali PG, Ferrone S. A 94,OOO-Dalton Glycoprotein Expressed by Human Melanoma and Carcinoma Cells2. JNCI: Journal of the National Cancer Institute. 1982 May 1;68(5):761–9.

401.Sabbatino F, Wang Y, Wang X, Schwab JH, Ferrone S, Ferrone CR. Novel Tumor Antigen-Specific Monoclonal Antibody-Based Immunotherapy to Eradicate Both Differentiated Cancer Cells and Cancer-Initiating Cells in Solid Tumors. Seminars in Oncology. 2014 Oct 1;41(5):685–99.

402.Kasten BB, Gangrade A, Kim H, Fan J, Ferrone S, Ferrone CR, et al. 212Pb-labeled B7-H3-targeting antibody for pancreatic cancer therapy in mouse models. Nucl Med Biol. 2018 Mar;58:67–73.

403.Kasten BB, Arend RC, Katre AA, Kim H, Fan J, Ferrone S, et al. B7-H3-targeted 212Pb radioimmunotherapy of ovarian cancer in preclinical models. Nucl Med Biol. 2017 Apr;47:23–30.

404.Li D, Wang R, Liang T, Ren H, Park C, Tai CH, et al. Camel nanobody-based B7-H3 CAR-T cells show high efficacy against large solid tumours. Nat Commun. 2023 Sept 22;14(1):5920.

405.Hirabayashi K, Du H, Xu Y, Shou P, Zhou X, Fucá G, et al. Dual-targeting CAR-T cells with optimal co-stimulation and metabolic fitness enhance antitumor activity and prevent escape in solid tumors. Nat Cancer. 2021 Sept;2(9):904–18.

406.Li H, Harrison EB, Li H, Hirabayashi K, Chen J, Li QX, et al. Targeting brain lesions of non-small cell lung cancer by enhancing CCL2-mediated CAR-T cell migration. Nat Commun. 2022 Apr 20;13(1):2154.

407.Zhang Y, He L, Sadagopan A, Ma T, Dotti G, Wang Y, et al. Targeting Radiation-Resistant Prostate Cancer Stem Cells by B7-H3 CAR T Cells. Molecular Cancer Therapeutics. 2021 Mar 2;20(3):577–88.

408.Wagner DL, Koehl U, Chmielewski M, Scheid C, Stripecke R. Review: Sustainable Clinical Development of CAR-T Cells – Switching From Viral Transduction Towards CRISPR-Cas Gene Editing. Front Immunol. 2022 Jun 17;13.

409.Michels A, Frank AM, Günther DM, Mataei M, Börner K, Grimm D, et al. Lentiviral and adeno-associated vectors efficiently transduce mouse T lymphocytes when targeted to murine CD8. Molecular Therapy - Methods & Clinical Development. 2021 Dec 10;23:334–47.

410.Cepko C, Pear W. Overview of the Retrovirus Transduction System. Current Protocols in Molecular Biology. 1996;36(1):9.9.1-9.9.16.

411.Ghassemi S, Durgin JS, Nunez-Cruz S, Patel J, Leferovich J, Pinzone M, et al. Rapid manufacturing of non-activated potent CAR T cells. Nat Biomed Eng. 2022 Feb;6(2):118–28.

412.Lanitis E, Rota G, Kosti P, Ronet C, Spill A, Seijo B, et al. Optimized gene engineering of murine CAR-T cells reveals the beneficial effects of IL-15 coexpression. J Exp Med. 2020 Nov 6;218(2):e20192203.

413.Haydar D, Ibañez-Vega J, Crawford JC, Chou CH, Guy CS, Meehl M, et al. CAR T-cell Design-dependent Remodeling of the Brain Tumor Immune Microenvironment Modulates Tumor-associated Macrophages and Anti-glioma Activity. Cancer Research Communications. 2023 Dec 1;3(12):2430–46.

414.Ando Y, Yasuoka C, Mishima T, Ikematsu T, Uede T, Matsunaga T, et al. Concanavalin A-mediated T cell proliferation is regulated by herpes virus entry mediator costimulatory molecule. In Vitro CellDevBiol-Animal. 2014 Apr 1;50(4):313–20.

415.Lee JH, Lee BH, Jeong S, Joh CSY, Nam HJ, Choi HS, et al. Single-cell RNA sequencing identifies distinct transcriptomic signatures between PMA/ionomycin- and αCD3/αCD28-activated primary human T cells. Genomics Inform. 2023 Jun 30;21(2):18.

416.Kalia V, Sarkar S. Regulation of Effector and Memory CD8 T Cell Differentiation by IL-2—A Balancing Act. Front Immunol. 2018 Dec 20;9.

417.Liu Y, Zhou N, Zhou L, Wang J, Zhou Y, Zhang T, et al. IL-2 regulates tumor-reactive CD8+ T cell exhaustion by activating the aryl hydrocarbon receptor. Nat Immunol. 2021 Mar;22(3):358–69.

418.Battram AM, Bachiller M, Lopez V, Fernández de Larrea C, Urbano-Ispizua A, Martín-Antonio B. IL-15 Enhances the Persistence and Function of BCMA-Targeting CAR-T Cells Compared to IL-2 or IL-15/IL-7 by Limiting CAR-T Cell Dysfunction and Differentiation. Cancers. 2021 Jan;13(14):3534.

419.Xu Y, Zhang M, Ramos CA, Durett A, Liu E, Dakhova O, et al. Closely related T-memory stem cells correlate with in vivo expansion of CAR.CD19-T cells and are preserved by IL-7 and IL-15. Blood. 2014 June 12;123(24):3750–9.

420.Alizadeh D, Wong RA, Yang X, Wang D, Pecoraro JR, Kuo CF, et al. IL15 Enhances CAR-T Cell Antitumor Activity by Reducing mTORC1 Activity and Preserving Their Stem Cell Memory Phenotype. Cancer Immunology Research. 2019 May 1;7(5):759–72.

421.Nash KL, Lever AML. Green fluorescent protein: green cells do not always indicate gene expression. Gene Ther. 2004 June;11(11):882–3.

422.Haas DL, Case SS, Crooks GM, Kohn DB. Critical Factors Influencing Stable Transduction of Human CD34+ Cells with HIV-1-Derived Lentiviral Vectors. Molecular Therapy. 2000 July 1;2(1):71–80.

423.Mao R, Hussein MS, He Y. Chimeric antigen receptor engineered T cells and their application in the immunotherapy of solid tumours. Expert Reviews in Molecular Medicine. 2022 ed;24:e7.

424.Ross SH, Cantrell DA. Signaling and Function of Interleukin-2 in T Lymphocytes. Annual Review of Immunology. 2018;36(1):411–33.

425.Benmebarek MR, Karches CH, Cadilha BL, Lesch S, Endres S, Kobold S. Killing Mechanisms of Chimeric Antigen Receptor (CAR) T Cells. International Journal of Molecular Sciences. 2019 Jan;20(6):1283.

426.Khorasani ABS, Sanaei MJ, Pourbagheri-Sigaroodi A, Ghaffari SH, Bashash D. CAR T cell therapy in solid tumors; with an extensive focus on obstacles and strategies to overcome the challenges. International Immunopharmacology. 2021 Dec 1;101:108260.

427.Marofi F, Achmad H, Bokov D, Abdelbasset WK, Alsadoon Z, Chupradit S, et al. Hurdles to breakthrough in CAR T cell therapy of solid tumors. Stem Cell Research & Therapy. 2022 Apr 1;13(1):140.

428.Safarzadeh Kozani P, Safarzadeh Kozani P, Ahmadi Najafabadi M, Yousefi F, Mirarefin SMJ, Rahbarizadeh F. Recent Advances in Solid Tumor CAR-T Cell Therapy: Driving Tumor Cells From Hero to Zero? Front Immunol. 2022 May 11;13:795164.

429.Krebs S, Ponomarev V, Slovin S, Schöder H. Imaging of CAR T-Cells in Cancer Patients: Paving the Way to Treatment Monitoring and Outcome Prediction. Journal of Nuclear Medicine. 2019 July 1;60(7):879–81.

430.Sakemura R, Can I, Siegler EL, Kenderian SS. In vivo CART cell imaging: Paving the way for success in CART cell therapy. Molecular Therapy - Oncolytics. 2021 Mar 26;20:625–33.

431.Carrasco N. Iodide transport in the thyroid gland. Biochimica et Biophysica Acta (BBA) - Reviews on Biomembranes. 1993 June 8;1154(1):65–82.

432.Smanik PA, Liu Q, Furminger TL, Ryu K, Xing S, Mazzaferri EL, et al. Cloning of the Human Sodium Iodide Symporter. Biochemical and Biophysical Research Communciations. 1996;226:339–45.

433.Bruno R, Giannasio P, Ronga G, Baudin E, Travagli JP, Russo D, et al. Sodium iodide symporter expression and radioiodine distribution in extrathyroidal tissues. J Endocrinol Invest. 2004 Dec;27(11):1010–4.

434.Penheiter AR, Russell SJ, Carlson SK. The Sodium Iodide Symporter (NIS) as an Imaging Reporter for Gene, Viral, and Cell-based Therapies. Curr Gene Ther. 2012 Feb;12(1):33–47.

435.Hansen DK, Dam M, Faramand RG. Toxicities associated with adoptive cellular therapies. Best Practice & Research Clinical Haematology. 2021 Sept 1;34(3):101287.

436.Sakemura R, Bansal A, Siegler EL, Hefazi M, Yang N, Khadka RH, et al. Development of a Clinically Relevant Reporter for Chimeric Antigen Receptor T-cell Expansion, Trafficking, and Toxicity. Cancer Immunol Res. 2021 Sept 1;9(9):1035–46.

437.Szymczak AL, Workman CJ, Wang Y, Vignali KM, Dilioglou S, Vanin EF, et al. Correction of multi-gene deficiency in vivo using a single ‘self-cleaving’ 2A peptide–based retroviral vector. Nat Biotechnol. 2004 May;22(5):589–94.

438.Richards RM, Sotillo E, Majzner RG. CAR T Cell Therapy for Neuroblastoma. Front Immunol. 2018 Oct 16;9.

439.Nazha B, Inal C, Owonikoko TK. Disialoganglioside GD2 Expression in Solid Tumors and Role as a Target for Cancer Therapy. Front Oncol. 2020 Jul 7;10.

440.Handgretinger R, Anderson K, Lang P, Dopfer R, Klingebiel T, Schrappe M, et al. A phase I study of human/mouse chimeric antiganglioside GD2 antibody ch14.18 in patients with neuroblastoma. European Journal of Cancer. 1995 Jan 1;31(2):261–7.

441.Prapa M, Caldrer S, Spano C, Bestagno M, Golinelli G, Grisendi G, et al. A novel anti-GD2/4-1BB chimeric antigen receptor triggers neuroblastoma cell killing. Oncotarget. 2015 July 20;6(28):24884–94.

442.ji C, You F, Zhang T, Fan S, Han Z, Xiang S, et al. Novel anti-GD2 CAR-T cells exhibit superior cytotoxicity against neuroblastoma. Eur J Inflamm. 2020 Jan 1;18:2058739220961193.

443.Li Y, Kurlander RJ. Comparison of anti-CD3 and anti-CD28-coated beads with soluble anti-CD3 for expanding human T cells: Differing impact on CD8 T cell phenotype and responsiveness to restimulation. J Transl Med. 2010 Oct 26;8:104.

444.Hauth F, Ho AY, Ferrone S, Duda DG. Radiotherapy to Enhance Chimeric Antigen Receptor T-Cell Therapeutic Efficacy in Solid Tumors. JAMA Oncol. 2021 July 1;7(7):1051–9.

445.Sugita M, Yamazaki T, Alhomoud M, Martinet J, Latouche JB, Golden E, et al. Radiation therapy improves CAR T cell activity in acute lymphoblastic leukemia. Cell Death Dis. 2023 May 4;14(5):1–8.

446.Kim KJ, Lee HW, Seong J. Combination therapy with anti-T-cell immunoglobulin and mucin-domain containing molecule 3 and radiation improves antitumor efficacy in murine hepatocellular carcinoma. Journal of Gastroenterology and Hepatology. 2021;36(5):1357–65.

447.Takeshima T, Chamoto K, Wakita D, Ohkuri T, Togashi Y, Shirato H, et al. Local Radiation Therapy Inhibits Tumor Growth through the Generation of Tumor-Specific CTL: Its Potentiation by Combination with Th1 Cell Therapy. Cancer Research. 2010 Mar 31;70(7):2697–706.

448.Wang T, Zhang K, You F, Ma R, Yang N, Tian S, et al. Preconditioning of radiotherapy enhances efficacy of B7-H3-CAR-T in treating solid tumor models. Life Sciences. 2023 Aug 12;122024.

449.Charpentier M, Spada S, Van Nest SJ, Demaria S. Radiation therapy-induced remodeling of the tumor immune microenvironment. Seminars in Cancer Biology. 2022 Nov 1;86:737–47.

450.Hovhannisyan L, Riether C, Aebersold DM, Medová M, Zimmer Y. CAR T cell-based immunotherapy and radiation therapy: potential, promises and risks. Molecular Cancer. 2023 May 12;22(1):82.

451.Duncan BB, Dunbar CE, Ishii K. Applying a clinical lens to animal models of CAR-T cell therapies. Molecular Therapy Methods & Clinical Development. 2022 Dec 8;27:17–31.

452.Zhou J, Wang G, Chen Y, Wang H, Hua Y, Cai Z. Immunogenic cell death in cancer therapy: Present and emerging inducers. J Cell Mol Med. 2019 Aug;23(8):4854–65.

453.Garg AD, Dudek-Peric AM, Romano E, Agostinis P. Immunogenic cell death. The International Journal of Developmental Biology. 2015 Sept 2;59(1-2–3):131–40.

454.Hong P, Hu Z, Lin J, Cui K, Gao Z, Tian X, et al. Multi-omics revealed that ELAVL3 regulates MYCN in neuroblastoma via immunogenic cell death: Risk stratification and experimental research. International Journal of Biological Macromolecules. 2024 Dec 1;282:137045.

455.Hagani AB, Rivière I, Tan C, Krause A, Sadelain M. Activation conditions determine susceptibility of murine primary T-lymphocytes to retroviral infection. The Journal of Gene Medicine. 1999;1(5):341–51.

456.Haydar D, Houke H, Chiang J, Yi Z, Odé Z, Caldwell K, et al. Cell-surface antigen profiling of pediatric brain tumors: B7-H3 is consistently expressed and can be targeted via local or systemic CAR T-cell delivery. Neuro Oncol. 2020 Dec 15;23(6):999–1011.

457.Amini L, Silbert SK, Maude SL, Nastoupil LJ, Ramos CA, Brentjens RJ, et al. Preparing for CAR T cell therapy: patient selection, bridging therapies and lymphodepletion. Nat Rev Clin Oncol. 2022 May;19(5):342–55.

458.Kusabuka H, Fujiwara K, Tokunaga Y, Hirobe S, Nakagawa S, Okada N. Highly efficient gene transfer using a retroviral vector into murine T cells for preclinical chimeric antigen receptor-expressing T cell therapy. Biochemical and Biophysical Research Communications. 2016 Apr 22;473(1):73–9.

459.Wijewarnasuriya D, Bebernitz C, Lopez AV, Rafiq S, Brentjens RJ. Excessive Costimulation Leads to Dysfunction of Adoptively Transferred T Cells. Cancer Immunology Research. 2020 June 1;8(6):732–42.

460.Symes JC, Siatskas C, Fowler DH, Medin JA. Retrovirally transduced murine T lymphocytes expressing FasL mediate effective killing of prostate cancer cells. Cancer Gene Ther. 2009 May;16(5):439–52.

461.Rosenberg SA. IL-2: The First Effective Immunotherapy for Human Cancer. J Immunol. 2014 June 15;192(12):5451–8.

462.Gattinoni L, Klebanoff CA, Palmer DC, Wrzesinski C, Kerstann K, Yu Z, et al. Acquisition of full effector function in vitro paradoxically impairs the in vivo antitumor efficacy of adoptively transferred $CD8^+$ T cells. J Clin Invest. 2005 June 1;115(6):1616–26.

463.Klebanoff CA, Gattinoni L, Torabi-Parizi P, Kerstann K, Cardones AR, Finkelstein SE, et al. Central memory self/tumor-reactive CD8+ T cells confer superior antitumor immunity compared with effector memory T cells. Proceedings of the National Academy of Sciences. 2005 July 5;102(27):9571–6.

464.Loos P, Short L, Savage G, Evgin L. Expansion and Retroviral Transduction of Primary Murine T Cells for CAR T-Cell Therapy. In: Siciliano V, Ceroni F, editors. Cancer Immunotherapy: Methods in Molecular Biology. 2024;2748:41-53.

465.Sudarsanam H, Buhmann R, Henschler R. Influence of Culture Conditions on Ex Vivo Expansion of T Lymphocytes and Their Function for Therapy: Current Insights and Open Questions. Front Bioeng Biotechnol. 2022 Jun 29;10.

466.Qin Y, Xu G. Enhancing CAR T-cell therapies against solid tumors: Mechanisms and reversion of resistance. Front Immunol. 2022 Dec 8;13:1053120.

467.Schanda N, Sauer T, Kunz A, Hückelhoven-Krauss A, Neuber B, Wang L, et al. Sensitivity and Specificity of CD19.CAR-T Cell Detection by Flow Cytometry and PCR. Cells. 2021 Nov;10(11):3208.

468.Kircher MF, Gambhir SS, Grimm J. Noninvasive cell-tracking methods. Nat Rev Clin Oncol. 2011 Nov;8(11):677–88.

469.Van Hoeck J, Vanhove C, De Smedt SC, Raemdonck K. Non-invasive cell-tracking methods for adoptive T cell therapies. Drug Discovery Today. 2022 Mar 1;27(3):793–807.

470.Sakemura R, Suksanpaisan L, Khadka RH, Newsom AN, Hansen MJ, Cox MJ, et al. Development of a Sensitive and Efficient Reporter Platform for the Detection of Chimeric Antigen Receptor T Cell Expansion, Trafficking, and Toxicity. Blood. 2019 Nov 13;134:53.

471.Thompson RJ, Fletcher A, Brookes K, Nieto H, Alshahrani MM, Mueller JW, et al. Dimerization of the Sodium/Iodide Symporter. Thyroid. 2019 Oct 1;29(10):1485–98.

472.Liu Z, Chen O, Wall JBJ, Zheng M, Zhou Y, Wang L, et al. Systematic comparison of 2A peptides for cloning multi-genes in a polycistronic vector. Sci Rep. 2017 May 19;7(1):2193.

473.Kerkar SP, Sanchez-Perez L, Yang S, Borman ZA, Muranski P, Ji Y, et al. Genetic Engineering of Murine CD8+ and CD4+ T Cells for Preclinical Adoptive Immunotherapy Studies. Journal of Immunotherapy. 2011 May;34(4):343–52.

474.Baumann JG, Unutmaz D, Miller MD, Breun SKJ, Grill SM, Mirro J, et al. Murine T Cells Potently Restrict Human Immunodeficiency Virus Infection. Journal of Virology. 2004 Nov 15;78(22):12537–47.

475.Tsurutani N, Yasuda J, Yamamoto N, Choi BI, Kadoki M, Iwakura Y. Nuclear Import of the Preintegration Complex Is Blocked upon Infection by Human Immunodeficiency Virus Type 1 in Mouse Cells. Journal of Virology. 2007 Jan 15;81(2):677–88.

476.Chen X, Zhong S, Zhan Y, Zhang X. CRISPR–Cas9 applications in T cells and adoptive T cell therapies. Cellular & Molecular Biology Letters. 2024 Apr 12;29(1):52.

477.Cappabianca D, Li J, Zheng Y, Tran C, Kasparek K, Mendez P, et al. Non-viral expression of chimeric antigen receptors with multiplex gene editing in primary T cells. Front Bioeng Biotechnol 2024 May 31;12:1379900.

478.Mueller KP, Piscopo NJ, Forsberg MH, Saraspe LA, Das A, Russell B, et al. Production and characterization of virus-free, CRISPR-CAR T cells capable of inducing solid tumor regression. J Immunother Cancer. 2022 Sept 1;10(9):e004446.

479.Pfenninger P, Yerly L, Abe J. Naïve Primary Mouse CD8+ T Cells Retain In Vivo Immune Responsiveness After Electroporation-Based CRISPR/Cas9 Genetic Engineering. Frontiers in Immunology 2022;13.

480.Hurtado MO, Wolbert J, Fisher J, Flutter B, Stafford S, Barton J, et al. Tumor infiltrating lymphocytes expanded from pediatric neuroblastoma display heterogeneity of phenotype and function. PLOS ONE. 2019 Aug 9;14(8):e0216373.

481.Zhan Y, Carrington EM, Zhang Y, Heinzel S, Lew AM. Life and Death of Activated T Cells: How Are They Different from Naïve T Cells? Front Immunol. 2017 Dec 13;8.

482.Gatzka M, Walsh CM. Apoptotic signal transduction and T cell tolerance. Autoimmunity. 2007 Jan 1;40(6):442–52.

483.Ma S, Ming Y, Wu J, Cui G. Cellular metabolism regulates the differentiation and function of T-cell subsets. Cell Mol Immunol. 2024 May;21(5):419–35.

484.Pearce EL. Metabolism in T cell activation and differentiation. Curr Opin Immunol. 2010 June;22(3):314–20.

485.Demaria S, Guha C, Schoenfeld J, Morris Z, Monjazeb A, Sikora A, et al. Radiation dose and fraction in immunotherapy: one-size regimen does not fit all settings, so how does one choose? J Immunother Cancer. 2021 Apr 1;9(4):e002038.

486.Ghita M, Brown KH, Kelada OJ, Graves EE, Butterworth KT. Integrating Small Animal Irradiators with Functional Imaging for Advanced Preclinical Radiotherapy Research. Cancers. 2019 Feb;11(2):170.

487.Kayano D, Kinuya S. Current Consensus on I-131 MIBG Therapy. Nucl Med Mol Imaging. 2018 Aug;52(4):254–65.

Chapter 8 Appendix

The ORF sequences of plasmids generated for this project were expressed in the SFG vector. Listed below is the ORF sequences for each plasmid from 5' to 3' end.

8.1 SFG.hNIS_Myc Tag

SFG_5'-

ATGGAAGCAGTAGAGACAGGAGAGAGACCCACCTTTGGCGCCTGGGATTATGGAGTGTTCGCACT
GATGCTCCTCGTTAGCACCGGGATTGGGCTGTGGGTTGGCTTGGCCAGGGGTGGCCAACGCAGC
GCTGAAGACTTCTTTACTGGCGGTAGGCGCCTTGCGGCTCTCCCTGTTGGGCTGTCTCTGAGCGCT
TCCTTCATGTCCGCTGTGCAAGTGCTCGGCGTGCCATCAGAGGCATATAGATACGGACTTAAATTC
CTGTGGATGTGTCTTGGCCAGCTGCTCAATTCCGTTTTGACCGCTTTGCTGTTCATGCCAGTGTTTT
ATCGGCTTGGTCTGACCAGCACATACGAATACCTCGAAATGCGGTTCTCAAGAGCGGTTCGCCTTT
GCGGTACACTTCAGTATATCGTAGCCACTATGCTGTATACTGGTATAGTGATTTATGCCCCCGCGCT
CATTCTGAATCAAGTGACAGGTTTGGATATTTGGGCTAGTCTGCTGTCTACCGGTATTATCTGTACCT
TCTATACCGCAGTCGGTGGCATGAAGGCCGTGGTGTGGACTGATGTCTTTCAAGTCGTAGTGATGC
TTTCTGGTTTCTGGGTGGTCCTGGCAAGGGGTGTCATGTTGGTGGGCGGACCCCGTCAAGTCCTCA
CGCTTGCGCAGAATCATTCACGCATTAACCTGATGGACTTTAATCCTGATCCCCGGTCCCGTTATAC
ATTTTGGACCTTCGTGGTTGGCGGAACACTGGTGTGGTTGAGTATGTATGGAGTTAATCAAGCCCAA
GTCCAACGATATGTTGCCTGCAGAACCGAGAAACAGGCTAAACTGGCCCTGCTTATTAACCAAGTA
GGCCTGTTTCTGATAGTCTCAAGTGCAGCCTGTTGTGGAATTGTCATGTTTGTATTTTACACCGATTG
TGATCCATTGCTCCTGGGGCGAATTTCCGCTCCAGACCAATACATGCCCCTGCTCGTTCTGGACAT
TTTCGAGGATCTGCCAGGTGTTCCAGGGCTGTTCCTGGCCTGTGCCTACTCTGGAACCCTCTCCAC
AGCCTCTACATCAATCAACGCTATGGCGGCTGTGACAGTCGAGGATCTGATAAAACCCCGACTGCG
TAGCCTGGCACCTAGAAAACTTGTAATAATTTCTAAGGGCCTTTCACTCATATATGGCAGTGCGTGC
CTGACCGTAGCTGCGCTGAGTAGTCTCCTGGGTGGTGGGGTGCTGCAAGGAAGTTTCACAGTGAT
GGGAGTTATCAGCGGGCCTCTGCTCGGCGCTTTTATTCTCGGCATGTTCCTTCCGGCCTGCAATAC
ACCCGGCGTTCTGGCAGGATTGGGTGCTGGCCTGGCCCTGTCACTTTGGGTGGCGCTGGGTGCTA
CACTGTACCCACCCTCTGAGCAAACCATGCGGGTATTGCCAAGTAGTGCTGCTAGATGCGTGGCC
CTGAGCGTAAACGCCAGCGGTCTTCTCGATCCTGCACTCTTGCCTGCTAACGACTCAAGCAGGGC
CCCATCATCCGGGATGGATGCGTCTCGCCCCGCACTTGCTGACTCATTTTACGCAATATCATACCT
GTATTACGGAGCTCTGGGCACGCTCACTACCGTACTGTGTGGCGCTCTGATCAGTTGCCTCACAGG
TCCTACTAAGAGAAGTACCCTTGCTCCCGGTCTGCTTTGGTGGGATCTGGCTCGGCAGACCGCGTC
TGTGGCACCTAAGGAAGAAGTGGCAATACTTGACGACAACCTGGTGAAGGGACCTGAGGAACTCC
CCACTGGCAACAAGAAACCCCCAGGGTTCCTGCCAACCAACGAGGATAGGCTCTTCTTTCTGGGTC

AGAAGGAACTTGAAGGTGCCGGTTCCTGGACTCCCTGTGTGGGTCATGACGGCGGCAGAGACCAA
CAGGAGACCAATCTCGAGCAAAAACTTATCTCTGAAGAGGACCTCTAA – SFG_3’

8.2 SFG.mNIS_Myc Tag

SFG_5’–
ATGGAGGGAGCTGAGGCCGGGGCTAGGGCCACCTTTGGTCCTTGGGACTACGGAGTATTTGCCAC
TATGCTTCTGGTTTCTACCGGAATTGGACTCTGGGTTGGACTCGCTCGAGGCGGTCAACGATCCGC
TGACGATTTCTTCACCGGGGGCCGACAGTTGGCTGCAGTGCCCGTCGGGCTTTCTCTCGCAGCTA
GTTTCATGAGTGCAGTTCAGGTGCTTGGCGTGCCCGCTGAAGCTGCTCGATACGGGCTCAAATTCC
TGTGGATGTGCGTGGGGCAACTGCTGAATTCTCTGCTCACAGCATTGCTGTTTCTTCCAATTTTTTAC
AGACTCGGGCTTACCTCAACATATCAGTATTTGGAACTGAGATTTTCTCGCGCTGTTAGATTGTGCG
GGACACTTCAATACCTTGTTGCTACTATGTTGTACACAGGCATTGTTATTTACGCACCTGCCCTGATT
TTGAATCAAGTCACAGGACTGGATATTTGGGCATCACTGCTTTCTACAGGGATAATATGCACCCTGT
ACACAACAGTAGGCGGCATGAAGGCTGTAGTTTGGACCGACGTTTTCCAGGTGGTAGTAATGCTCG
TTGGCTTTTGGGTAATACTGGCCAGAGGCGTTATGTTGATGGGTGGGCCTTGGAACGTGCTTTCACT
CGCCCAAAACCATAGCCGGATAAACCTCATGGATTTTGACCCCGACCCTCGCAGCCGGTATACATT
CTGGACATTTGTTGTTGGTGGTTCTCTTGTTTGGCTTTCCATGTATGGTGTGAATCAGGCACAGGTC
CAGAGATACGTGGCATGTCATACCGAGAGAAAAGCAAAACTTGCCCTCCTTGTAAACCAACTGGGT
CTCTTCCTGATTGTTGCAAGCGCAGCTTGTTGCGGAATCGTCATGTTTGTGTACTATAAAGACTGCG
ACCCCCTTTTGACAGGGCGAATTGCTGCTCCCGACCAATACATGCCCCTTCTTGTATTGGATATCTT
TGAAGATTTGCCTGGCGTACCAGGCCTGTTTCTTGCTTGTGCTTATAGCGGAACCCTGTCCACAGC
CTCAACTAGCATTAATGCTATGGCAGCTGTAACCGTTGAGGATCTTATTAAACCCCGCATGCCTTCT
CTTGCTCCCCGAAAACTTGTTTTTATTTCAAAGGGGCTTAGCTTCATTTACGGGTCCACCTGCCTGA
CAGTGGCCGCCCTCTCATCTTTGTTGGGCGGTGGGGTTTTGCAGGGGTCCTTCACAGTAATGGGC
GTCATATCAGGTCCTCTCCTGGGCGCCTTCACCCTTGGCATGCTTCTTCCCGCATGCAATACCCCT
GGGGTCCTCAGTGGGTTGACCGCCGGTTTGGCTGTGAGTCTCTGGGTCGCTGTCGGGGCTACCTT
GTATCCACCTGGGGAACAAACAATGGGGGTTCTTCCTACCAGTGCTGCTGGATGCACTAATGCCTC
CGTCCTTCCCTCTCCCCCTGGCGCAGCCAATACCAGCCGAGGGATTCCAAGTAGTGGTATGGACT
CAGGACGCCCTGCTTTTGCCGACACCTTTTACGCTGTGTCCTACCTGTACTATGGAGCTCTTGGGA
CCCTGACCACTATGCTGTGTGGGGCCCTTATCTCCTACTTGACTGGACCAACCAAGCGCTCAAGCT
TGGGGCCCGGACTGTTGTGGTGGGACTTGGCCAGGCAGACAGCCAGTGTGGCACCCAAAGAGGA
CACCACTACTTTGGAGGACTCACTCGTCAAAGGGCCTGAAGACATCCCCGCCGCCACAAAAAAAC
CCCCAGGCTTTCGGCCTGAGGCAGAGACACACCCACTGTACCTTGGACACGATGTGGAAACCAAC
CTGGAGCAAAAACTTATCTCTGAAGAGGACCTCTA - SFG 3’

8.3 376.96.m28z.hNIS

SFG_5’-

ATGGAGACCGACACACTGCTTCTGTGGGTGCTTCTGCTCTGGGTGCCTGGGAGTACCGGACTCGA
GGAAGTCCAACTCGTCGAGTCAGGGGGAGGTTTGGTCAAGCCCGGGGGTAGCCTCAAGCTCTCAT
GCGAAGCATCCCGATTCACTTTTAGCTCCTACGCTATGAGCTGGGTTAGGCAGACTCCTGAGAAGA
GATTGGAATGGGTTGCAGCAATTAGCGGGGGTGGTCGGTATACCTACTATCCTGATAGTATGAAGG
GAAGATTTACGATCTCCCGAGACAATGCCAAGAACTTTCTGTATCTGCAAATGAGCTCTCTGCGGTC
TGAGGATACGGCTATGTATTACTGCGCTCGACATTACGATGGGTATTTGGACTATTGGGGTCAAGGG
ACAACGCTTACAGTCTCAAGTGGTGGGGGAGGTTCTGGGGGCGGCGGTTCAGGGGGAGGGGGCT
CCGACATCGTCATGACGCAGAGTCACAAGTTTATGTCAACCAGCATTGGTGCTCGGGTTTCCATCA
CATGCAAAGCCTCTCAAGACGTAAGGACTGCCGTCGCCTGGTATCAGCAAAAACCTGGCCAAAGC
CCCAAACTTCTGATATACAGTGCTAGTTACCGATACACGGGTGTCCCTGACCGATTTACCGGTAGC
GGGTCCGGTACTGATTTTACTTTTACCATCTCTAGCGTACAGGCCGAGGATCTTGCGGTGTATTATT
GTCAGCAACATTATGGAACTCCTCCTTGGACATTCGGAGGAGGCACAAAACTTGAAATTAAATgcGG
CCGCTCAACTACCACAAAACCAGTCTTGCGAACACCTAGTCCTGTGCACCCCACAGGAACATCTCA
ACCCCAACGACCTGAAGACTGTAGGCCAAGGGGGAGCGTGAAAGGAACAGGTCTCGACTTCGCAT
GTGACATTTATATTTGGGCCCCACTTGCCGGAATCTGTGTTGCCCTGCTCCTTTCACTCATCATCAC
CTTGATTTGTTACAATTCACGCAGAAACCGGCTTCTCCAGTCCGACTACATGAATATGACTCCCAGG
CGCCCCGGACTGACCCGGAAGCCCTATCAACCATACGCACCTGCTCGCGACTTTGCCGCATACCG
CCCTAGAGCAAAATTTTCTCGATCTGCTGAGACTGCCGCAAACCTTCAAGATCCTAATCAACTTTAC
AATGAGCTCAACCTTGGACGCCGAGAAGAGTACGACGTCCTGGAGAAGAAACGCGCTAGAGACCC
TGAAATGGGAGGCAAACAACAGCGAAGACGGAATCCACAGGAAGGGGTATATAATGCACTTCAAAA
GGACAAAATGGCTGAGGCCTATAGCGAAATAGGCACAAAAGGTGAACGCAGGCGAGGAAAAGGAC
ATGACGGGCTTTATCAAGGGCTGAGCACCGCCACAAAGGACACATACGATGCTCTGCACATGCAAA
CCCTTGCACCACGCCGCAGGAAGCGCAGTGGATCCGGCGAGGGAAGGGGAAGCTTGTTGACATG
TGGTGACGTAGAGGAGAACCCAGGTCCTATGGAAGCAGTAGAGACAGGAGAGAGACCCACCTTTG
GCGCCTGGGATTATGGAGTGTTCGCACTGATGCTCCTCGTTAGCACCGGGATTGGGCTGTGGGTT
GGCTTGGCCAGGGGTGGCCAACGCAGCGCTGAAGACTTCTTTACTGGCGGTAGGCGCCTTGCGG
CTCTCCCTGTTGGGCTGTCTCTGAGCGCTTCCTTCATGTCCGCTGTGCAAGTGCTCGGCGTGCCAT
CAGAGGCATATAGATACGGACTTAAATTCCTGTGGATGTGTCTTGGCCAGCTGCTCAATTCCGTTTT
GACCGCTTTGCTGTTCATGCCAGTGTTTTATCGGCTTGGTCTGACCAGCACATACGAATACCTCGAA
ATGCGGTTCTCAAGAGCGGTTCGCCTTTGCGGTACACTTCAGTATATCGTAGCCACTATGCTGTATA
CTGGTATAGTGATTTATGCCCCCGCGCTCATTCTGAATCAAGTGACAGGTTTGGATATTTGGGCTAG
TCTGCTGTCTACCGGTATTATCTGTACCTTCTATACCGCAGTCGGTGGCATGAAGGCCGTGGTGTG
GACTGATGTCTTTCAAGTCGTAGTGATGCTTTCTGGTTTCTGGGTGGTCCTGGCAAGGGGTGTCATG
TTGGTGGGCGGACCCCGTCAAGTCCTCACGCTTGCGCAGAATCATTCACGCATTAACCTGATGGAC
TTTAATCCTGATCCCCGGTCCCGTTATACATTTTGGACCTTCGTGGTTGGCGGAACACTGGTGTGGT
TGAGTATGTATGGAGTTAATCAAGCCCAAGTCCAACGATATGTTGCCTGCAGAACCGAGAAACAGG

CTAAACTGGCCCTGCTTATTAACCAAGTAGGCCTGTTTCTGATAGTCTCAAGTGCAGCCTGTTGTGG
AATTGTCATGTTTGTATTTTACACCGATTGTGATCCATTGCTCCTGGGGCGAATTTCCGCTCCAGACC
AATACATGCCCCTGCTCGTTCTGGACATTTTCGAGGATCTGCCAGGTGTTCCAGGGCTGTTCCTGG
CCTGTGCCTACTCTGGAACCCTCTCCACAGCCTCTACATCAATCAACGCTATGGCGGCTGTGACAG
TCGAGGATCTGATAAAACCCCGACTGCGTAGCCTGGCACCTAGAAAACTTGTAATAATTTCTAAGGG
CCTTTCACTCATATATGGCAGTGCGTGCCTGACCGTAGCTGCGCTGAGTAGTCTCCTGGGTGGTGG
GGTGCTGCAAGGAAGTTTCACAGTGATGGGAGTTATCAGCGGGCCTCTGCTCGGCGCTTTTATTCT
CGGCATGTTCCTTCCGGCCTGCAATACACCCGGCGTTCTGGCAGGATTGGGTGCTGGCCTGGCCC
TGTCACTTTGGGTGGCGCTGGGTGCTACACTGTACCCACCCTCTGAGCAAACCATGCGGGTATTGC
CAAGTAGTGCTGCTAGATGCGTGGCCCTGAGCGTAAACGCCAGCGGTCTTCTCGATCCTGCACTCT
TGCCTGCTAACGACTCAAGCAGGGCCCCATCATCCGGGATGGATGCGTCTCGCCCCGCACTTGCT
GACTCATTTTACGCAATATCATACCTGTATTACGGAGCTCTGGGCACGCTCACTACCGTACTGTGTG
GCGCTCTGATCAGTTGCCTCACAGGTCCTACTAAGAGAAGTACCCTTGCTCCCGGTCTGCTTTGGT
GGGATCTGGCTCGGCAGACCGCGTCTGTGGCACCTAAGGAAGAAGTGGCAATACTTGACGACAAC
CTGGTGAAGGGACCTGAGGAACTCCCCACTGGCAACAAGAAACCCCCAGGGTTCCTGCCAACCAA
CGAGGATAGGCTCTTCTTTCTGGGTCAGAAGGAACTTGAAGGTGCCGGTTCCTGGACTCCCTGTGT
GGGTCATGACGGCGGCAGAGACCAACAGGAGACCAATCTCGAGCAAAAACTTATCTCTGAAGAGG
ACCTCTAA - SFG_3’

8.4 376.96.m28z.mNIS

SFG_5’-
ATGGAGACCGACACACTGCTTCTGTGGGTGCTTCTGCTCTGGGTGCCTGGGAGTACCGGACTCGA
GGAAGTCCAACTCGTCGAGTCAGGGGGAGGTTTGGTCAAGCCCGGGGGTAGCCTCAAGCTCTCAT
GCGAAGCATCCCGATTCACTTTTAGCTCCTACGCTATGAGCTGGGTTAGGCAGACTCCTGAGAAGA
GATTGGAATGGGTTGCAGCAATTAGCGGGGGTGGTCGGTATACCTACTATCCTGATAGTATGAAGG
GAAGATTTACGATCTCCCGAGACAATGCCAAGAACTTTCTGTATCTGCAAATGAGCTCTCTGCGGTC
TGAGGATACGGCTATGTATTACTGCGCTCGACATTACGATGGGTATTTGGACTATTGGGGTCAAGGG
ACAACGCTTACAGTCTCAAGTGGTGGGGGAGGTTCTGGGGGCGGCGGTTCAGGGGGAGGGGGCT
CCGACATCGTCATGACGCAGAGTCACAAGTTTATGTCAACCAGCATTGGTGCTCGGGTTTCCATCA
CATGCAAAGCCTCTCAAGACGTAAGGACTGCCGTCGCCTGGTATCAGCAAAAACCTGGCCAAAGC
CCCAAACTTCTGATATACAGTGCTAGTTACCGATACACGGGTGTCCCTGACCGATTTACCGGTAGC
GGGTCCGGTACTGATTTTACTTTTACCATCTCTAGCGTACAGGCCGAGGATCTTGCGGTGTATTATT
GTCAGCAACATTATGGAACTCCTCCTTGGACATTCGGAGGAGGCACAAAACTTGAAATTAAATgcGG
CCGCTCAACTACCACAAAACCAGTCTTGCGAACACCTAGTCCTGTGCACCCCACAGGAACATCTCA
ACCCCAACGACCTGAAGACTGTAGGCCAAGGGGGAGCGTGAAAGGAACAGGTCTCGACTTCGCAT
GTGACATTTATATTTGGGCCCCACTTGCCGGAATCTGTGTTGCCCTGCTCCTTTCACTCATCATCAC
CTTGATTTGTTACAATTCACGCAGAAACCGGCTTCTCCAGTCCGACTACATGAATATGACTCCCAGG

CGCCCCGGACTGACCCGGAAGCCCTATCAACCATACGCACCTGCTCGCGACTTTGCCGCATACCG
CCCTAGAGCAAAATTTTCTCGATCTGCTGAGACTGCCGCAAACCTTCAAGATCCTAATCAACTTTAC
AATGAGCTCAACCTTGGACGCCGAGAAGAGTACGACGTCCTGGAGAAGAAACGCGCTAGAGACCC
TGAAATGGGAGGCAAACAACAGCGAAGACGGAATCCACAGGAAGGGGTATATAATGCACTTCAAAA
GGACAAAATGGCTGAGGCCTATAGCGAAATAGGCACAAAAGGTGAACGCAGGCGAGGAAAAGGAC
ATGACGGGCTTATCAAGGGCTGAGCACCGCCACAAAGGACACATACGATGCTCTGCACATGCAAA
CCCTTGCACCACGCCGCAGGAAGCGCAGTGGATCCGGCGAGGGAAGGGGAAGCTTGTTGACATG
TGGTGACGTAGAGGAGAACCCAGGTCCTATGGAGGGAGCTGAGGCCGGGGCTAGGGCCACCTTT
GGTCCTTGGGACTACGGAGTATTTGCCACTATGCTTCTGGTTTCTACCGGAATTGGACTCTGGGTTG
GACTCGCTCGAGGCGGTCAACGATCCGCTGACGATTTCTTCACCGGGGGCCGACAGTTGGCTGCA
GTGCCCGTCGGGCTTTCTCTCGCAGCTAGTTTCATGAGTGCAGTTCAGGTGCTTGGCGTGCCCGCT
GAAGCTGCTCGATACGGGCTCAAATTCCTGTGGATGTGCGTGGGGCAACTGCTGAATTCTCTGCTC
ACAGCATTGCTGTTTCTTCCAATTTTTTACAGACTCGGGCTTACCTCAACATATCAGTATTTGGAACT
GAGATTTTCTCGCGCTGTTAGATTGTGCGGGACACTTCAATACCTTGTTGCTACTATGTTGTACACAG
GCATTGTTATTTACGCACCTGCCCTGATTTTGAATCAAGTCACAGGACTGGATATTTGGGCATCACT
GCTTTCTACAGGGATAATATGCACCCTGTACACAACAGTAGGCGGCATGAAGGCTGTAGTTTGGAC
CGACGTTTTCCAGGTGGTAGTAATGCTCGTTGGCTTTTGGGTAATACTGGCCAGAGGCGTTATGTTG
ATGGGTGGGCCTTGGAACGTGCTTTCACTCGCCCAAAACCATAGCCGGATAAACCTCATGGATTTT
GACCCCGACCCTCGCAGCCGGTATACATTCTGGACATTTGTTGTTGGTGGTTCTCTTGTTTGGCTTT
CCATGTATGGTGTGAATCAGGCACAGGTCCAGAGATACGTGGCATGTCATACCGAGAGAAAAGCAA
AACTTGCCCTCCTTGTAAACCAACTGGGTCTCTTCCTGATTGTTGCAAGCGCAGCTTGTTGCGGAAT
CGTCATGTTTGTGTACTATAAAGACTGCGACCCCCTTTTGACAGGGCGAATTGCTGCTCCCGACCA
ATACATGCCCCTTCTTGTATTGGATATCTTTGAAGATTTGCCTGGCGTACCAGGCCTGTTTCTTGCTT
GTGCTTATAGCGGAACCCTGTCCACAGCCTCAACTAGCATTAATGCTATGGCAGCTGTAACCGTTG
AGGATCTTATTAAACCCCGCATGCCTTCTCTTGCTCCCCGAAAACTTGTTTTTATTTCAAAGGGGCTT
AGCTTCATTTACGGGTCCACCTGCCTGACAGTGGCCGCCCTCTCATCTTTGTTGGGCGGTGGGGTT
TTGCAGGGGTCCTTCACAGTAATGGGCGTCATATCAGGTCCTCTCCTGGGCGCCTTCACCCTTGGC
ATGCTTCTTCCCGCATGCAATACCCCTGGGGTCCTCAGTGGGTTGACCGCCGGTTTGGCTGTGAGT
CTCTGGGTCGCTGTCGGGGCTACCTTGTATCCACCTGGGGAACAAACAATGGGGGTTCTTCCTACC
AGTGCTGCTGGATGCACTAATGCCTCCGTCCTTCCCTCTCCCCCTGGCGCAGCCAATACCAGCCG
AGGGATTCCAAGTAGTGGTATGGACTCAGGACGCCCTGCTTTTGCCGACACCTTTTACGCTGTGTC
CTACCTGTACTATGGAGCTCTTGGGACCCTGACCACTATGCTGTGTGGGGCCCTTATCTCCTACTTG
ACTGGACCAACCAAGCGCTCAAGCTTGGGGCCCGGACTGTTGTGGTGGGACTTGGCCAGGCAGA
CAGCCAGTGTGGCACCCAAAGAGGACACCACTACTTTGGAGGACTCACTCGTCAAAGGGCCTGAA
GACATCCCCGCCGCCACAAAAAAACCCCCAGGCTTTCGGCCTGAGGCAGAGACACACCCACTGTA
CCTTGGACACGATGTGGAAACCAACCTGGAGCAAAAACTTATCTCTGAAGAGGACCTCTAA -SFG_3’

8.5 Use of an ATP standard for quantifying EC-ATP release

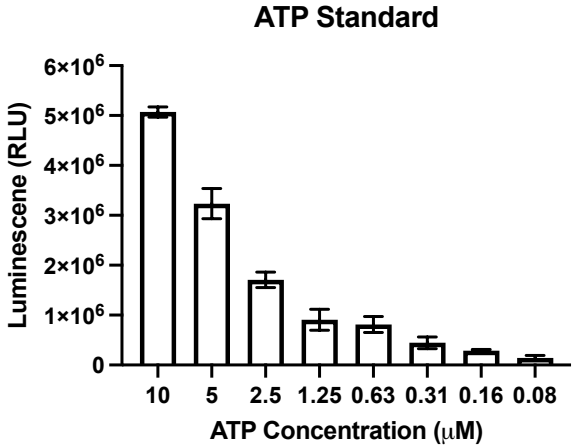

Figure 8.1 Use of ATP standard for quantifying EC-ATP release

ATP standard prepared at known concentrations was added to 96-well plates. Luminescence readings were obtained three hours post incubation of ATP standards at 37°C and 5% CO_2. Each standard curve point includes two technical replicates with the standard deviation shown. The results shown are of one independent experiment (N=1).

8.6 Use of hIL-7 and hIL-15 for T-cell expansion improves viability and cell count.

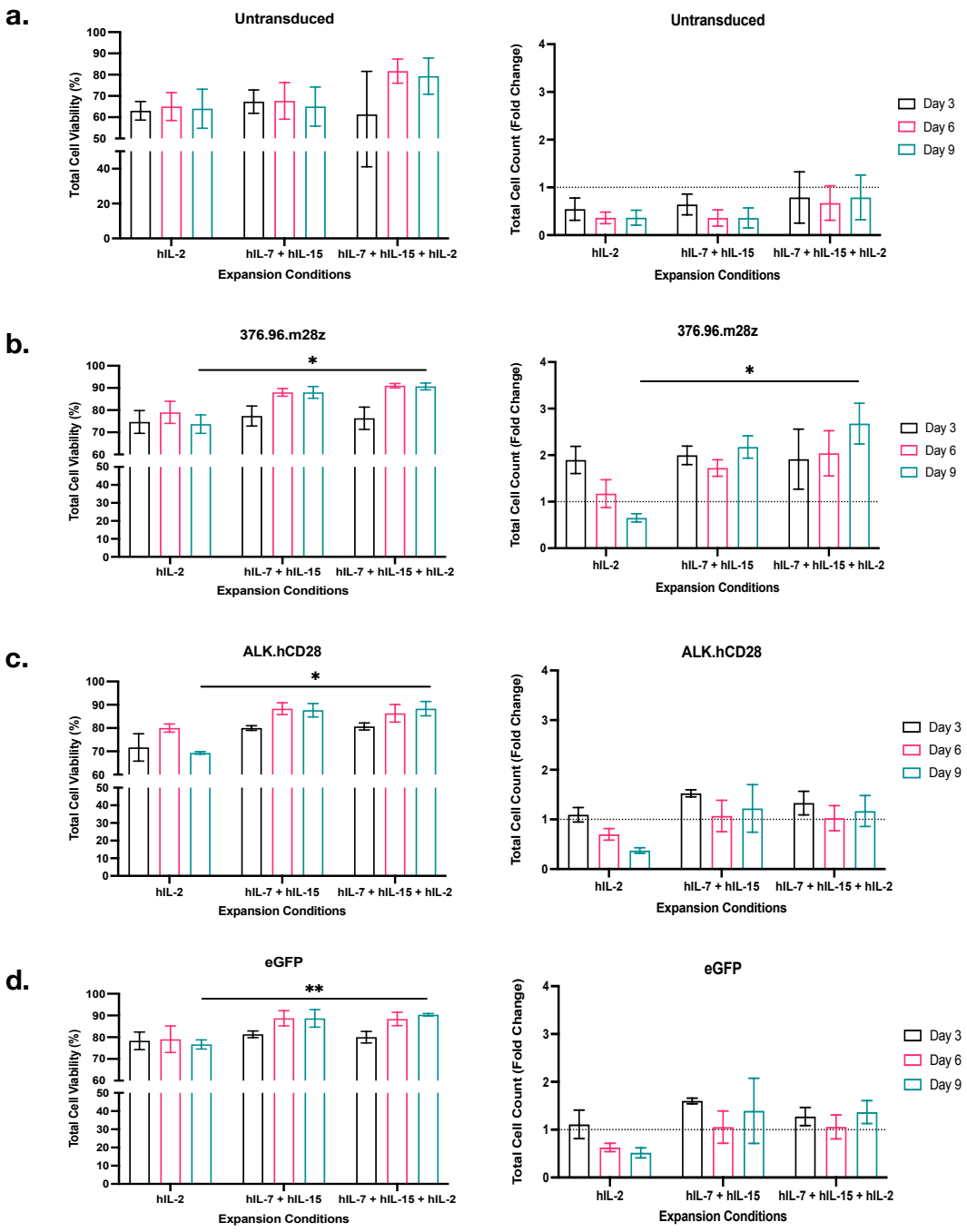

Figure 8.2 Use of hIL-7 and hIL-15 improves total cell viability and cell count

Two CARs (376.96.m28z and ALK.h28z) and eGFP^{+} T-cells were generated from 129/SvJ spleens. Cells were expanded for 10 days post transduction. Different cytokine compositions of hIL-2,hIL-7 and hIL-15 were used to improve T-cell expansion. Cell counts and viability counts were measured to evaluate T-cell expansion for **a**) untransduced **b**) 376.96.m28z **c**) ALK.h28z and **d**) eGFP. The error bars shown represent the standard deviation with an n of three (N=3). Statistical analysis was performed using two-way ANOVA. *<0.0332, **<0.0021.

8.7 376.96.m28z shows short-term target cell killing

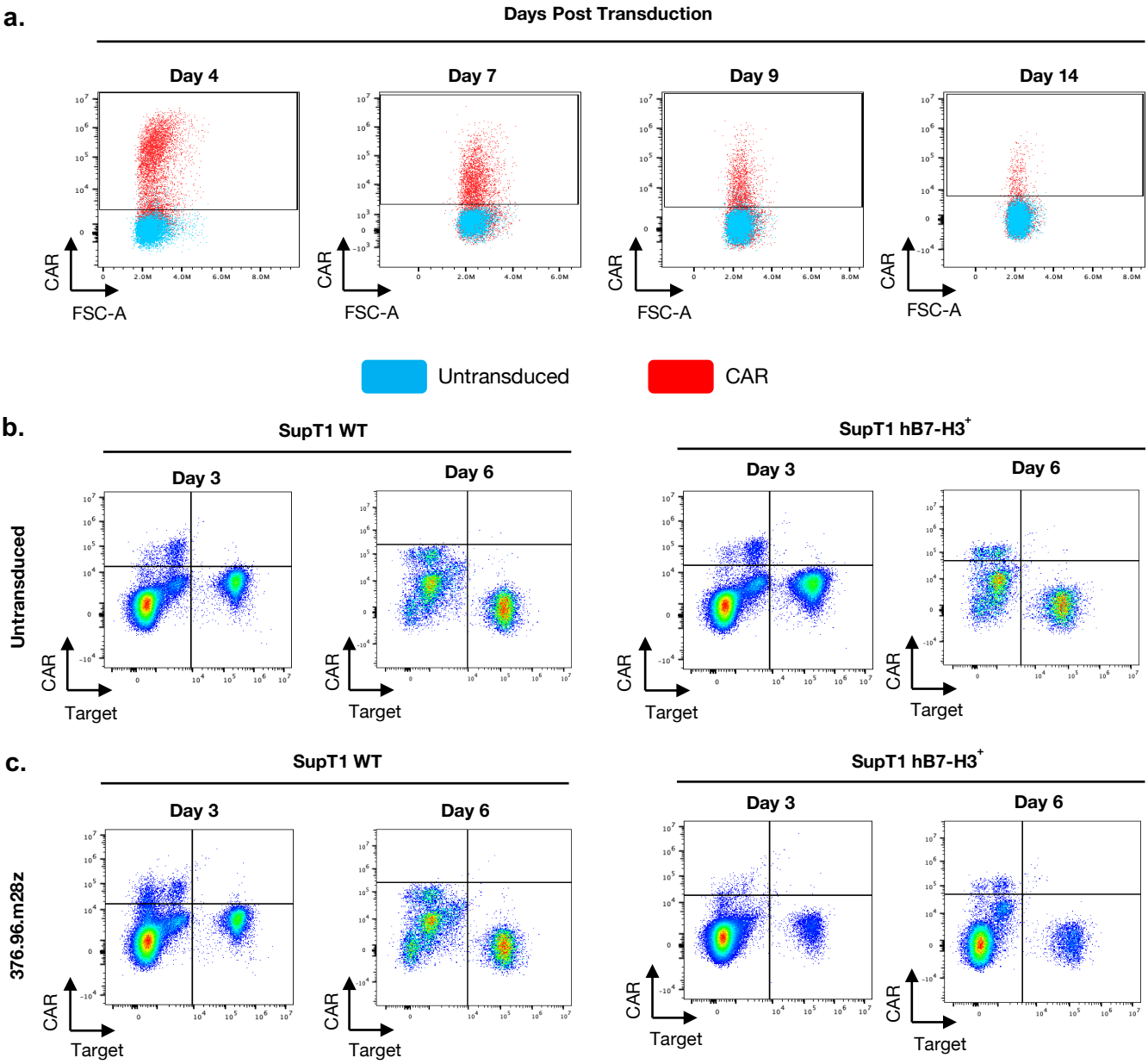

Figure 8.3 376.96.m28z shows short-term target cell killing

129/SvJ spleens were used to generate 376.96.m28z mouse CAR-T cells, which were expanded *in vitro* for fourteen days. CAR expression was evaluated by flow cytometry, with **a**) representative flow plots showing CAR expression on Live$^+$mCD3$^+$ cells. Seven days post transduction, the functionality of 376.96.m28z CAR-T cells, along with untransduced controls, was assessed in a co-culture with GFP$^+$Luc$^+$ target cells (SupT1 WT and SupT1 hB7-H3$^+$) at a 1:1 E:T ratio. On days three and six after initiating co-culture, target cell viability was determined by flow cytometry. Representative flow plots illustrate Live$^+$ cell populations of **b**) untransduced and **c**) 376.96.m28z CAR-T cells co-cultured with SupT1 WT and SupT1 hB7-H3$^+$ (N=3).

8.8 HuK666.h28z *in vitro* expression remains stable compared to 376.96.m28z regardless of mouse genetic background.

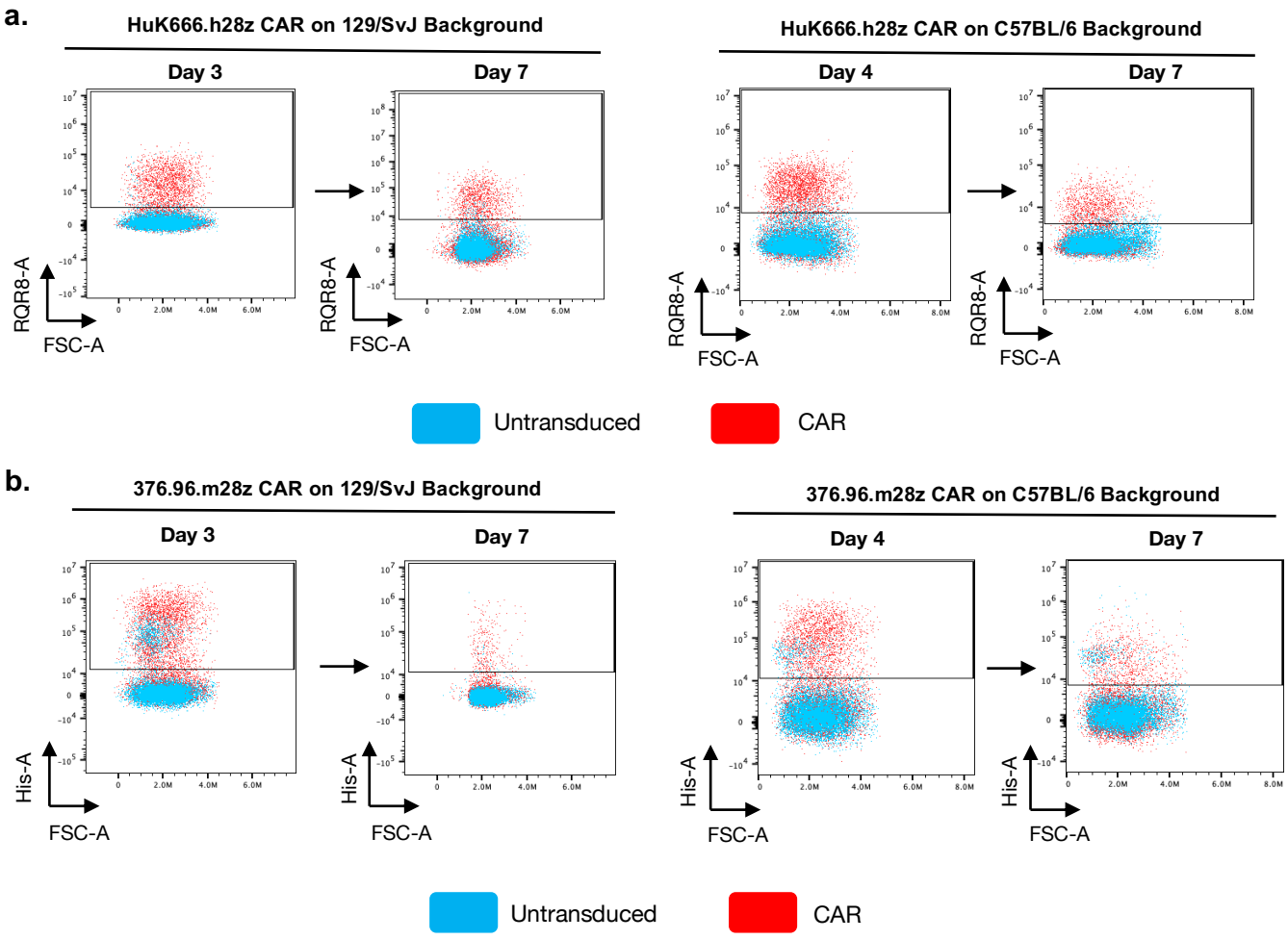

Figure 8.4 HuK666.h28z *in vitro* expression is stable compared to 376.96.m28z irrespective of mouse genetic background

376.96.m28z and huK666.h28z CAR-T cells were generated from 129/SvJ and C57BL/6 female spleens. Mouse CAR-T cells were expanded for seven days *in vitro* with CAR expression assessed by flow cytometry for 376.96.m28z and huk666.h28z, respectively. Representative flow plots are shown of expression of generated CAR-T cells on the 129/SvJ and C57BL/6 mouse genetic background for **a**) HuK666.h28z and **b**) 376.96.m28z. CAR expression on the 129/SvJ genetic mouse background is shown for days three and day seven post transduction. CAR expression on the C57BL/6 genetic mouse background is shown for days four and day seven post transduction. CAR expression is shown on Live^{+}mCD3^{+} single cells (N=3).

8.9 T-cell subsets change during *in vitro* expansion

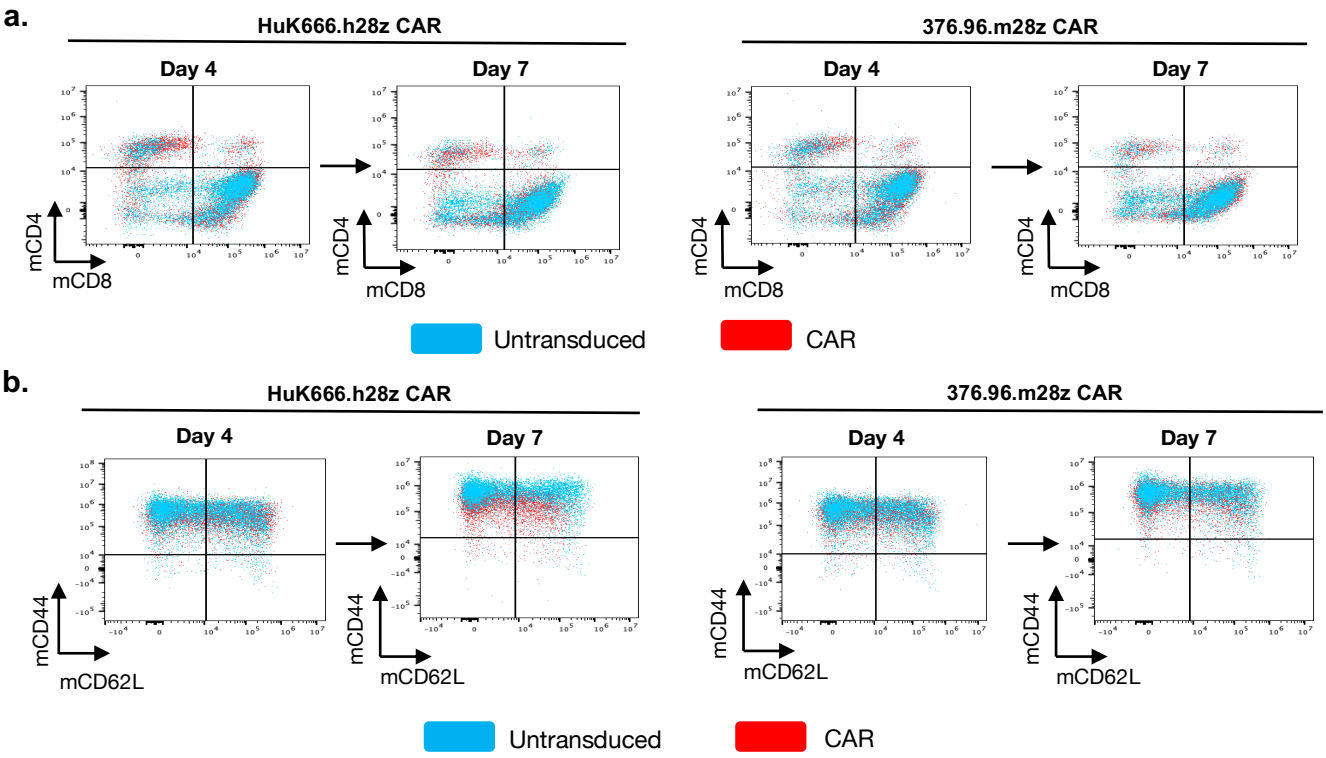

Figure 8.5 T-cell subsets change during *in vitro* expansion

Untransduced, 376.96.m28z and huK666.h28z CAR-T cells were generated from C57BL/6 female spleens. Cells were expanded for seven days *in vitro* and T-cell subsets were assessed by flow cytometry on days four and seven post-transduction. For the generated 376.96.m28z and HuK666.h28z CAR-T cells, representative flow plots are shown for **a**) the proportions of $mCD3^+mCD8^+$ and $mCD3^+mCD4^+$, and **b**) the proportion of T_{EM} ($mCD3^+mCD44^+mCD62L^-$) and T_{CM} ($mCD3^+mCD44^+mCD62L^+$) N=3.

8.10 Radiation affects CD4:CD8 and T_{EM}:T_{CM} ratio in response to radiation

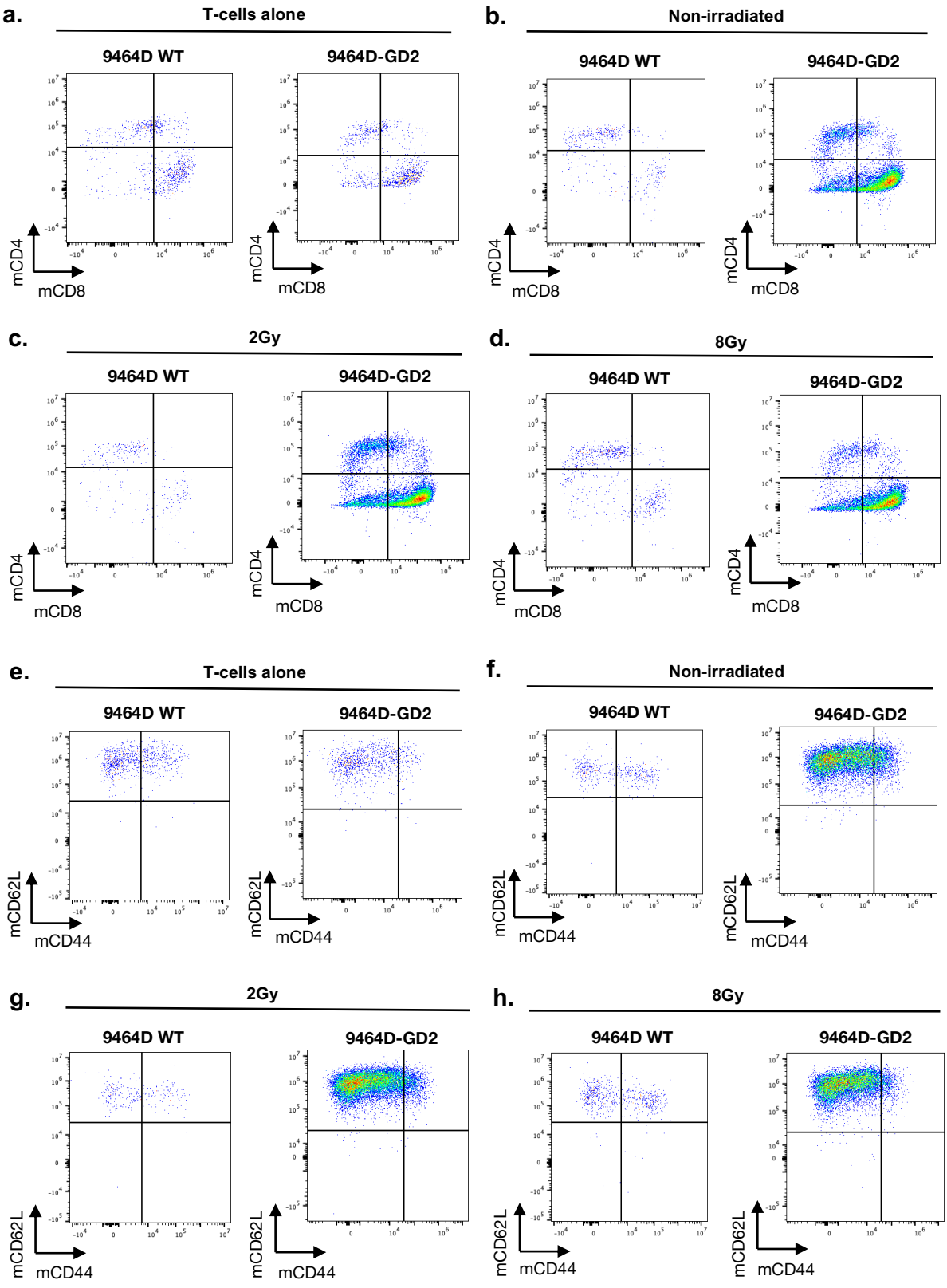

Figure 8.6 Radiation induces *in vitro* changes in HuK666.h28z CD8:CD4 and T_{EM}: T_{CM} ratios in response to antigen

Untransduced and HuK666.h28z CAR-T cells were assessed for CAR expansion against 9464D WT and 9464D-GD2. The co-culture was performed 24 hours post irradiation treatment of target cells. CAR expression was assessed by flow cytometry 72 hours post commencement of co-culture. Representative flow plots are shown of $mCD3^+CAR^+mCD8^+$ and $mCD3^+CAR^+mCD4^+$ against 9464D WT and 9464D-GD2 under co-culture conditions of **a**) T-cells alone, **b**) Non-irradiated targets, **c**) targets irradiated with 2Gy and **d**) targets irradiated with 8Gy. Representative flow plots are shown of T_{EM} ($mCD3^+CAR^+mCD44^+mCD62L^-$) and T_{CM} ($mCD3^+CAR^+mCD44^+mCD62L^+$) against 9464D WT and 9464D-GD2 under co-culture conditions of **e**) T-cells alone, **f**) Non-irradiated targets, **g**) targets irradiated with 2Gy and **h**) targets irradiated with 8Gy. N=3.